universität wien

DISSERTATION

Titel der Dissertation

TRANSITION METAL COMPLEXES WITH CARBOXYLATE LIGANDS AND THIOSEMICARBAZONE–PROLINE CONJUGATES: SYNTHESIS, CHARACTERISATION AND PROPERTIES

verfasst von

Miljan Milunović

angestrebter akademischer Grad

Doktor der Naturwissenschaften (Dr. rer. Nat.)

Wien, 2013

Studienkennzahl lt. Studienblatt:	A 091 419
Dissertationsgebiet lt. Studienblatt:	Chemie
Betreut von:	O. Univ.- Prof. Dr. Dr. Bernhard K. Keppler

universität wien

Doctoral Thesis

Transition Metal Complexes with Carboxylate Ligands and Thiosemicarbazone–proline Conjugates: Synthesis, Characterisation and Properties

written by

Miljan Milunović

Vienna, 2013

Dedicated to my beloved
parents Milica and Nenad Milunović,
brother Predrag Milunović,
aunt Svetlana Haschka,
Tanja Spasojević and
uncle Nebojša Mirović

”If you do not know how, watch the phenomena of nature,
it will give you clear answers and inspiration.”

(”Ako ne znate kako, posmatrajte pojave prirode,
ona će vam dati jasne odgovore i inspiraciju.”)

Nikola Tesla

”As the lightning in the dark night shines on the traveler’s
entire horizon in front of him, with that lightning,
in the brain of genius man, opens new views
and discoveries in new areas of science.”

(”Kao što munja u tamnoj noći obasja putniku ceo horizont pred njim,
tako se takvom munjom u mozgu genijalnog čoveka otvaraju u
nauci novi vidici i otkrivaju nove oblasti nauke.”)

Milutin Milanković

”Knowledge is the light that illuminates our path through life.”

(”Znanje je svetlost, koja osvetljava naš put kroz život.”)

Mihajlo Pupin

”Do not crash all the bridges, maybe you'll come back.
You're not a bird or a butterfly that flies along the coast,
when there are no bridges, in vain is to yearn,
in vain is to understand, in vain is to wish.”

(”Ne ruši sve mostove, možda ćeš se vratiti.
Nisi ptica ni leptir obalom što leti,
kad nema mostova uzalud je čeznuti,
uzalud je shvatiti, uzalud je hteti.”)

Ivo Andrić

”None ever yet drank of the cup of honey, who did not embitter it with
the cup of gall.”

(”Čašu meda jošt niko ne popi, što je čašom žuči ne zagrči,
čaša žuči ište čašu meda, smiješane najlakše se piju.”)

Petar II Petrović Njegoš

Acknowledgment

I would like to express my sincere thanks to:
O. Univ.-Prof. Dr. Dr. Bernhard Keppler for the opportunity to perform my PhD work at the Institute of Inorganic Chemistry, University of Vienna,
Ao. Univ.-Prof. Dr. Vladimir Arion for great supervision, constructive discussions, suggestions, reading the proofs of the publications and the thesis, refinement and description of X–ray structures of my compounds,
Ao. Univ.-Prof. Mag. Dr. Regina Krachler for financial support,
Dr. Éva Anna Enyedy and group of Prof. Dr. Tamas Kiss for a great collaboration and wonderful working atmosphere during my research stay at University of Szeged,
Mag. Dr. Michael Jakupec for supervising cytotoxicity tests and proofreading of my publication,
Dr. Robert Trondl for performing cytotoxicity tests,
Ao. Univ.-Prof. Dr. Markus Galanski and the NMR team for measurement of numerous NMR spectra,
Mag. Aliona Luganschi and Mag. Anatolie Dobrov for mass spectrometry measurements,
Alexander Roller for collection of X–ray data,
Dr. Michael Malarek for proofreading of the introduction of the thesis,
Dr. Werner Ginzinger for useful administrational and computational advice,
Mag. Elfriede Limberger for managing administrative material,
Slađana Mitić (my chemistry teacher) and O. Univ.-Prof. Dr. Danilo Popović, who awakened my interest for chemistry;
All colleagues, former and current members of Laboratory 5 and 7, especially Lukas and Paul for a great working atmosphere,
Nadine, Masha, Sarah and Hristo for interesting scientific and non-scientific discussions,
University of Vienna for financial support,
I want to express special gratitude to:
my family for their support and help through all of my studies,
my Viennese family aunt Svetlana and her husband Peter Haschka, who had initiated my arrival to Vienna and have always been there for me,
and last but not least, all Milunović in Vienna.

Abstract

Humic substances are omnipresent in the biosphere and play an important role in biological processes in soil, rivers and oceans (plant growth and respiration, metal uptake by organisms, catalytic polymerisation and aquatic redox reactions). They control the transport of organic and inorganic molecules, pollutants and metal ions throughout the biosphere. The structure of humic substances is very complex, and to understand their role as transport carriers or chelating agents, investigation has to be based on small molecules, recognised as the building blocks of humic substances. Compounds often referred to as model–humic substances include derivatives of benzoic acid, benzoic aldehyde, phenol and some heterocyclic compounds. 3,4,5-Trimethoxybenzoic acid has been chosen as a model compound because it easily builds iron(III) complexes. The later have been studied by UV–vis, IR, Mössbauer spectroscopy, magnetic susceptibility measurements and X–ray crystallography. The hexanuclear iron(III) complex has a recliner conformation of a ferric peroxido–dioxido $\{Fe_6(O_2)(O)_2\}^{12+}$ core. The undecanuclear iron(III) complex possesses a core with 9 six–coordinate and 2 five–coordinate ferric ions. A highlighted motif of the core is the distorted cubane entity $\{Fe_4(\mu_3\text{–}O)(\mu_4\text{–}O)_3\}^{4+}$. Both complexes act as catalytic precursors in oxidation of cyclohexane to cyclohexanol and cyclohexanone in the presence of aqueous H_2O_2 and pyrazinecarboxylic acid, under mild conditions. These facts, may contribute to elucidation of the role of metal complexes of humic substances in catalytic processes of terrestrial and aqueous eco–systems.

More elaborate systems, which contain carboxylic groups and tridentate thiosemicarbazone moieties have also been prepared and proven to be good chelators for iron(III). In addition, these compounds proved to be suitable for development of anticancer drugs. Cancer is one of the three most common causes of human death. In the past, cancer treatment was based on cisplatin and its derivatives, but due to increasing tumor resistance to those drugs nowadays, attention is focused on other anticancer drug candidates, and in particular on thiosemicarbazones (TSCs). Over the last decades, TSCs, praticularly α-N-heterocyclic ones, have attracted attention due to their significant cytotoxicity (e.g., Triapine). However, the low water solubility and severe side effects make their further development difficult. One way to increase the water solubility is coordination of low soluble ligands to metal ions, but usually metal

complexes show lower cytotoxic activity than the corresponding ligands. In this work, the new series of thiosemicarbazones (TSCs), based on methyl salicylaldehyde, namely, 2-hydroxy-3-methyl-(*S*)-pyrrolidine-2-carboxylate-5-methylbenzaldehyde thiosemicarbazone and 2-hydroxy-3-methyl-(*R*)-pyrrolidine-2-carboxylate-5-methylbenzaldehyde thiosemicarbazone, which were synthesized, and characterized by elemental analysis, UV–vis, IR, ^{1}H and ^{13}C NMR spectroscopy, and electrospray ionisation mass spectrometry, possess very good aqueous solubility. Their cytotoxicity was tested in ovarian (CH1) and colon (SW480) cancer cell lines by MTT assay.

Surprisingly, the complexation with copper(II) led to 5 – 13 times better cytotoxicity in the low micromolar concentration range. Additionally, the thermodynamic behaviour of ligands as well as their copper(II), zinc(II), iron(III) and iron(II) complexes was investigated in solution. Predominant species of copper(II) and zinc(II) are monoligand complexes, while for iron(III) and iron(II) bis–ligand complexes are characteristic at physiological pH. The O, N, S–coordination mode and square planar coordination geometry of the copper(II) complexes were confirmed by EPR spectroscopy and X–ray diffraction studies.

Zusammenfassung

Huminstoffe sind in der Biosphäre allgegenwärtig. Sie spielen eine wichtige Rolle in biologischen Prozessen in Böden, Flüssen und Meeren (Pflanzenwachstum und Pflanzenatmung, Metall–Aufnahme durch Organismen, katalytische Polymerisation und aquatische Redox–Reaktionen). Sie kontrollieren den Transport von organischen und anorganischen Molekülen, Schadstoffen und Metallionen in der Biosphäre. Die Struktur der Huminstoffe ist sehr komplex. Um ihre Rolle als Stoffträger oder Chelatbildner zu verstehen, muss sich die Forschung auf kleine Moleküle, die Bausteine der Huminstoffe, konzentrieren. Diese Verbindungen, die oft als Modell–Huminstoffe bezeichnet werden, sind Derivate der Benzoesäure, Benzaldehyd, Phenol, sowie einige heterocyclische Verbindungen. 3,4,5-Trimethoxybenzoesäure wurde als Modellverbindung gewählt, weil sie leicht Eisen (III)–Komplexe bildet. Diese wurden anschließend mittels UV–vis, IR, Mössbauer–Spektroskopie, Messung der magnetischen Suszeptibilität und Röntgenkristallographie untersucht. Der hexanukleare Eisen (III)–Komplex verfügt über eine sechskernige Eisen Peroxido–dioxido $\{Fe_6(O_2)(O)_2\}^{12+}$–Einheit in Sessel–Konformation. Der undecanukleare Eisen(III)–Komplex dagegen besitzt einen Kern mit 9 sechsfach koordinierten und 2 fünffach koordinierten Eisenionen. Die Besonderheit dieser Anordnung bildet die verzerrte Cuban Einheit $\{Fe_4O_4\}^{4+}$. Beide Komplexe wirken als Katalysatorvorläufer bei der Oxidation von Cyclohexan zu Cyclohexanol und Cyclohexanon in Gegenwart von wässrigem H_2O_2 und Pyrazincarbonsäure unter milden Bedingungen. Diese Tatsachen können zu Aufklärung der Rolle von Metall–komplexen der Huminstoffe in katalytischen Prozessen von terrestrischen und wässriger Ökosysteme beitragen.

Komplexere Systeme, die Carboxylgruppen und eine dreizähnige Thiosemicarbazone Einheit enthalten, wurden ebenfalls hergestellt und erwiesen sich als gute Komplexbildner für Eisen(III). Darüber hinaus erwiesen sich diese Verbindungen als geeignet für die Entwicklung von Antikrebs–Therapeutika. Krebs ist eine der drei häufigsten Todesursachen. In der Vergangenheit basierte die Krebsbehandlung auf Cisplatin und seinen Derivaten. Nachdem Tumore gegen diese Medikamente zunehmend Resistenzen entwickelten, konzentriert sich die Aufmerksamkeit der Forschung auf neue potenzielle Therapeutika, vor allem auf die Gruppe der

Thiosemicarbazone (TSC). In den letzten Jahrzehnten weckten TSCe, insbesondere, α-N-heterocyclische Thiosemicarbazone das Interesse der Wissenschaft aufgrund ihrer signifikanten Zytotoxizität (z.B. Triapine). Die geringe Wasserlöslichkeit, sowie die schweren Nebenwirkungen standen einer Weiterentwicklung bisher im Weg. Eine Möglichkeit die Wasserlöslichkeit zu erhöhen, ist die Koordination von Liganden an Metallionen. Allerdings zeigen Metall–Komplexe häufig geringere zytotoxische Aktivität als die entsprechenden Liganden. In dieser Arbeit wird eine neue Serie von Thiosemicarbazonen mit sehr guten Wasserlöslichkeiten auf Basis von Methyl Salicylaldehyd synthetisiert. Hierzu wurden die Verbindungen 2-Hydroxy-3-Methyl-(S)-Pyrrolidin-2-carbonsäure-5-methylbenzaldehyd thiosemicarbazon und 2-Hydroxy-3-methyl-(R)-Pyrrolidin-2-carbonsäure-5-methylbenzaldehyd thiosemicarbazon synthetisiert und durch Elementaranalyse, UV–vis, IR, ^{1}H– und ^{13}C–NMR–Spektroskopie, sowie Elektrospray–Massenspektrometrie charakterisiert, sowie deren Zytotoxizität in Eierstock (CH1) und Dickdarm (SW480) Krebs–Zelllinien durch MTT–Assay getestet.

Interessanterweise führte die Komplexierung mit Kupfer(II) zu einer 5 – 13 mal höheren Zytotoxizität im niedrigen mikromolaren Konzentrationsbereich. Zusätzlich wurde das thermodynamische Verhalten von Liganden sowie deren Kupfer(II), Zink(II), Eisen(III) und Eisen(II) Komplexen in Lösung untersucht. Vorherrschende Spezies von Kupfer(II) und Zink(II) Komplexe sind monoligand, während für Eisen(III) und Eisen(II) bis–Ligand Komplexe bei physiologischem pH–Wert charakteristisch sind. Die O, N, S–Koordination und quadratisch–planare Koordinationsgeometrie der Kupfer(II) Komplexe wurden durch EPR–Spektroskopie und Röntgenstrukturanalyse bestätigt.

Table of Contents

1 Introduction

1.1 Humic substances

Humic substances (HS) are organic macromolecules, which are an important part of soil, stream and marine ecosystems. The main constituents of HS are carbon, hydrogen, oxygen, sometimes nitrogen and occasionally sulfur and phosphorus.[1] They are formed during the humification process through the influence of different factors: climate, vegetation, microorganisms, parent material and time.[2] Humification is a term used to describe biochemical, physical and microbial transformation of plant residues into stable forms characterized by an increase in number of aromatic and alkyl carbons and decrease of O–alkyl carbons.[3] HS is a generic name for the coloured material obtained on the basis of solubility characteristics after extraction of humus or soil organic matter by alkali or acidic solutions. They can be divided into three main classes: *Humin* – fraction insoluble in alkali, *humic acids* (HA) – dark coloured fraction soluble in alkaline solution but insoluble in diluted acids, and, *fulvic acids* (FA) – coloured fraction soluble in alkali, which remains in solution after removal of HA by acidification. According to older literature a light yellow fraction of FA is so called *crenic acid* and yellow–brown fraction is an *apocrenic acid*. From humic acid *hymatomelanic acid* can be further extracted using alcohol and the residue can be again dissolved in base and coagulated with addition of electrolyte yielding two fractions: soluble – *brown humic acids* and insoluble – *grey humic acids*.[2,4,5] HS are omnipresent in terrestrial and aqueous ecosystems. They have been identified as a major fraction of soil and surface water organic matter with participation of 60 – 70% and 30 – 50% in content of organic carbon, respectively.[1,6] It was suggested that river, lake and marine HS are of terrestrial origin, with note that aquatic HS have been changed *in situ* by aquatic organisms and UV–radiation.[6,7] Recently, it was suggested that HS of each ecosystem (soil, stream and marine) are unique.[8]

Genesis of HS cannot be described by simple chemical or biochemical reactions due to the lack of information related to their detailed structure and various other factors, which affect formation of HS. A few model theories concerning the formation mechanism of humic substances have been suggested. All suggested theories are comprised in one common model of HS formation (Scheme 1).

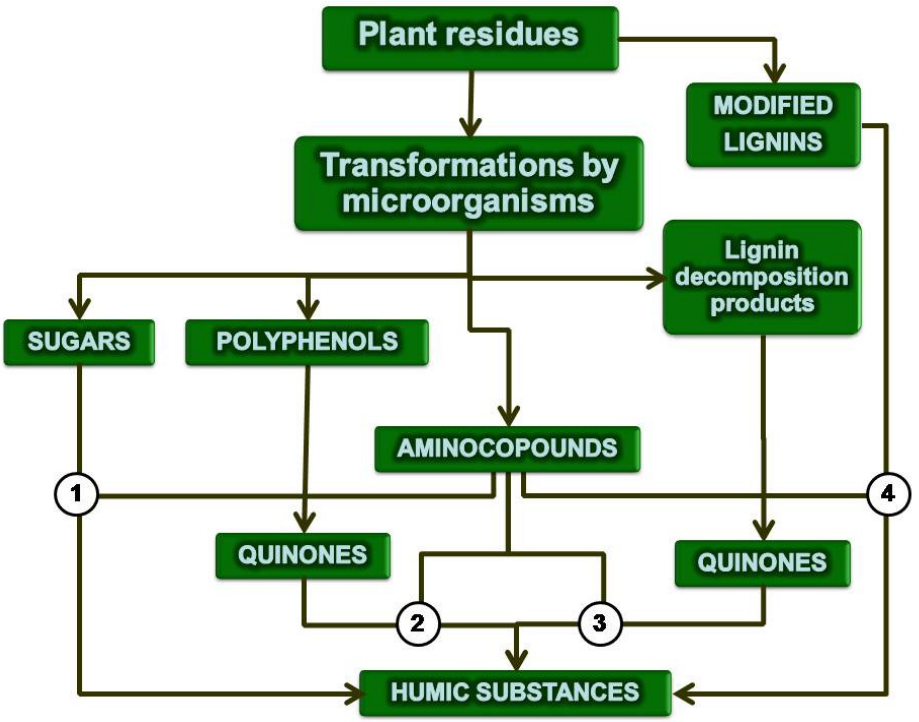

Scheme 1. Genesis of HS and different pathways of HS formation.[2]

Lignin theory developed by Selman Waxman suggests that HS are formed after microbial degradation of modified lignins, which undergo oxidation of aliphatic side chains in order to increase the content of carboxylic groups and decrease the content of methoxy groups (see pathway 4 in Scheme 1).[2]

Polyphenol theory describes formation of HS via polymerisation of quinones (originated from polyphenolic aldehydes and acids formed during enzymatic modification of lignin by microorganisms or from cellulose and other nonlignin sources) and aminoacids (see pathway 2 and 3 in Scheme 1).[2]

Melanioidine (sugar–amine) theory proposes a model, in which polymerization of sugars and amino acids leads to further formation of melanoidines, which by reorganisation, cyclisation and decarboxylation afford humic–like macromolecules (see pathway 1 in Scheme 1).[2] According to other model theories, the precursors for HS are fatty acids, or alkenones.[2]

After formation, humic substances are involved in the terrestrial and aquatic environmental pathways (Scheme 2).[2]

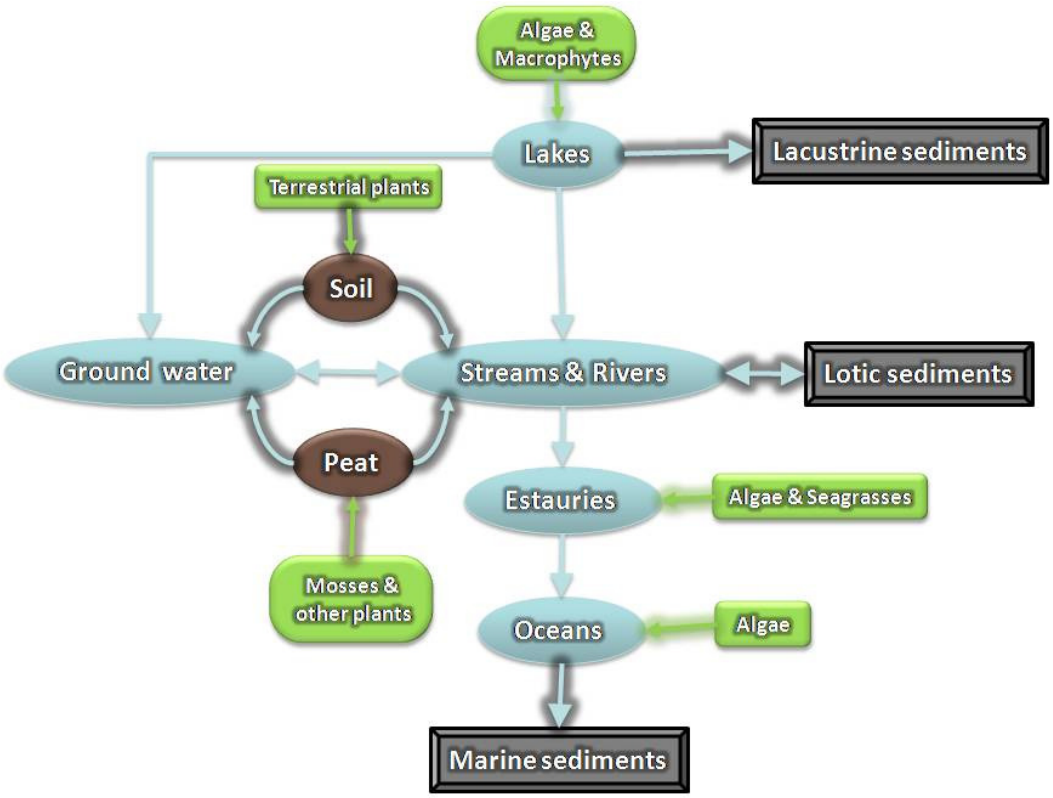

Scheme 2. The environmental flowpathways of HS.[2]

Humic substances can reach different ecosystems mostly due to water which is an important medium for their transport. HS play an important role in the interaction processes due to their good solubility in the pH range of natural waters and high chelating ability.[1–5]

Despite numerous methods which can be applied for HS determination, their characterization is one of the most difficult problems so far. Some difficulties lie in the mass distribution of HS which can be a few thousand, sometimes even higher, and, in distinguishing between intrinsic high mass molecules and aggregates of high mass. Various techniques and methods were developed for isolation and characterization of HS. Methods and techniques which are often used are: precipitation,[9] solvent extraction methods (under inert atmosphere to prevent oxidation) using different extractants, supercritical extraction, dialysis,[10] freeze–drying method[6] – for isolation of HS; gel permeation chromatography, viscometry, ultrafiltration,[9] ultracentrifugation methods (sedimentation velocity method, equilibrium sedimentation method), light scattering (photon correlation) techniques, field flow fractionation, partial specific volumes method, electron microscopy[1] – for

determination of molecular mass; elemental analysis – for determination of composition; size exclusion chromatography, radiometry, calcium acetate method, barium hydroxide method, direct titration, capillary electrophoresis[4] – for functional group determination; oxidation methods (using different oxidising agents: $KMnO_4$, HNO_3, H_2O_2, peracetic acid, hypochlorite, alkaline nitrobenzene), reduction methods (using Zn–dust distillation, Na–amalgam), acidic base hydrolysis, enzymatic degradation, UV–vis spectrophotometry, IR spectroscopy, ^1H NMR spectroscopy, ^{13}C CPMAS NMR spectroscopy (cross polarisation magic angle spinning method), thermochemolysis with tetramethylammonium hydroxide (TMAH), pyrolysis–gas chromatography/mass spectrometry, thermochemolysis–gas chromatorgaphy,[11] Field Flow Fractionation–ICP mass spectrometry – for structural characterization.

Elemental and functional group composition of HS are known but the exact structure of HS is difficult to define because of variety of factors, which are involved during their formation in ecosystems. Therefore, the physical and chemical description of HS will be presented in this chapter just in general giving an insight into the solubility, elemental composition and functional group content.

Molecular weight of HS is in the range of 0.5 – 5 kDa for FA and 5 – 1000 kDa for HA. Generally, soil HA have much higher molecular weight (50 – 500 kDa) than aquatic HA (1.5 – 5 kDa), while molecular weight of soil, stream and aquatic FA is extremely variable but still in the range of 0.1 – 5 kDa.[8]

Content of carbon, hydrogen and oxygen in HS is different for terrestrial and aquatic ecosystems. FA have lower C content and higher O content than HA (Table 1).

Table 1. C, H, O, N, S–content of soil HS.[2]

	Humic acids (%)	**Fulvic acids (%)**
Carbon	53.8 – 58.7	40.7 – 50.6
Hydrogen	3.2 – 6.2	3.8 – 7.0
Oxygen	32.8 – 38.3	39.7 – 49.8
Nitrogen	0.8 – 4.3	0.9 – 3.3
Sulfur	0.1 – 1.5	0.1 – 3.6

Elemental content (carbon, hydrogen, oxygen) in soil HS can vary from 54 – 59%, 4 – 5% and 34 – 36%, respectively, in accord with the different regions where soil samples were collected (arctic, temperate, subtropical and tropical). Also, the ratio between HA and FA can differ concerning type of the soil. For example, grassland soils contain higher quantities of HA and forest soils have higher content of FA. HA are found in soils, water, compost heaps, marine and lake sediments, peat bogs, carbonaceous shales, lignites and brown coals.[2] In river waters, carbon and hydrogen contents for HA and FA are approximately around 54 and 4%, respectively. Differences can be seen in the content of oxygen 30% for HA and 40.5% for FA and in nitrogen content 1.2% for HA and 0.7% for FA.[12] Humin is slightly less aromatic than HA, with higher polysaccharide content.[2] In general, FA are soluble in water at all pH values, HA are soluble at pH > 2 and humin is insoluble in water.[1]

The majority of functional groups in organic chemistry are found in HS. It is worth noting that the amount and type of functional groups in HS depends on the type of ecosystem in which HS are found. Some of important functional groups of HS are listed in Table 2.[2]

Table 2. Functional groups in HS.[2]

Functional groups	
Acidic groups	
Carboxyl	**R–COOH**
Enol	**R–CH=CH–OH**
Phenolic	**Ar–OH**
Quinone	**Ar=O**
Neutral groups	
Alcoholic	**R–CH_2–OH**
Ether	**R–CH_2–O–CH_2–R**
Ketone	**R– (C=O) –R**
Aldehyde	**R–CHO**
Ester	**R–C=O(–OR)**
Basic groups	
Amine	**R–CH_2–NH_2**
Amide	**R–C=O(–NH–R)**

Generally, FA possess approximately two times higher content of COOH groups than HA.[4] There are compositional differences between soil, stream and marine FA. Content of aromatic carbons of FA increases in the following order: marine, soil and stream FA. Stream FA are intermediate in carbonyl group (C=O) content and in the number of carbon atoms of C–O and C–N moieties, while soil FA are characterized by their highest content.[8]

Comparing aromaticity, phenolic content and methoxy content of marine, stream and soil HA, it has been observed that marine HA are lowest, while stream HA are higher in phenolic group content than soil or marine HA. Soil HA possess the highest content of C–O moieties.[8]

Interesting investigation concerning ^{14}C age for HS showed that marine HS from deep ocean are old (3000 – 6000 years), while stream HS are near zero carbon age and for soil HS ^{14}C age is in range from several hundreds to thousands years (see Table 3).[8]

Table 3. ^{14}C age for soil, stream and marine HS.[8]

Source	**^{14}C age (years)**
Soil	Several hundred to thousand
Stream	0
Marine	3000 – 6000

Humic substances can also contain traces of nucleic acids and their derivatives, chlorophyll and its degradation products, phospholipids and vitamins. High levels of amino acids were found in HS (Table 4).[2]

High content of stable free radicals (hydroquinone type) and variety of functional groups (carboxylic, phenolic, amine, *etc.*) render HS as good complexation agents and transporters for various transition metal ions (Fe^{3+}, Cu^{2+}, Cr^{3+}, Pb^{2+}, Ni^{2+}), small organic molecules (*e.g.* pesticides), nitrogen and carbon oxides, actinides and other pollutants. Therefore, HS have great importance in plant growth and respiration, biological processes in soil, metal uptake by organisms, catalytic polymerisation and aquatic redox reactions.[2,4,13]

Table 4. Amino acids concentrations (nmol/mg) after hydrolysis of stream, soil and marine HS.[2]

Amino acid	Soil		Stream		Marine
	FA	HA	FA	HA	FA
Alanine	50	86	5.3	24	5.7
Arginine	0.8	25	–	6.7	1.0
Aspartic acid	100	110	9.2	27	7.6
Cysteine	1.7	1.9	0.2	2.2	0.3
Glutamic acid	120	81	4.9	48	7.2
Glycine	66	100	17	49	14
Histidine	13	54	5.4	13	3.2
Isoleucine	17	28	1.7	9.6	2.3
Leucine	18	46	2.3	17	3.5
Lysine	8.7	32	1.3	5.8	1.8
Methionine	5.1	12	0.4	2.8	0.6
Phenyalanine	10	36	0.7	8.5	1.8
Proline	12	45	2.8	26	2.9
Serine	31	59	4.5	24	5.3
Threonine	31	59	4.1	19	3.9
Tyrosine	3.7	20	1.1	8.9	1.6
Valine	32	49	2.9	16	1.0
Total	520	843.9	63.8	307.5	63.7

Especially, HS under 5 kDa have shown good complexation ability for heavy metals.[14] Fulvic acids (FA) owing to their low molecular weight, better solubility, higher acidity and higher carboxylic group content can more effectively transport metal ions and interact with other molecules in the environment than humic acids (HA).[2,10] FA exhibit polyelectrolyte properties and functional group heterogeneity.[15,16] Metal–FA stability constants were investigated using ion exchange equilibrium and continuous variation methods toward some transition metal ions. Affinity of metal ions to FA decreases in the following order: $Fe^{3+} > Al^{3+} > Cu^{2+} > Ni^{2+} > Co^{2+} > Pb^{2+} > Ca^{2+} > Zn^{2+} > Mn^{2+} > Mg^{2+}$.[2] It was shown that for some ions (Fe^{3+}, Cr^{6+}, Pb^{2+}) the binding properties are strongly dependent on pH.[13] Trivalent metal ions bind to humic materials much stronger than divalent metal ions at any pH value.[13,17] Therefore,

humic substances, particularly FA, contribute to the better mobility of transition metals (Pb, Cu, Fe, Zn) in the environment, increase their uptake and inhibit their sorption onto clay particles.

Recently, possible therapeutic application of HS in order to prevent acute poisoning with Al, Pb, or Cd has been reported based on their strong chelating ability.[18] The solubility, mobility, biochemical and geochemical behaviour of a wide range of metals, particularly Fe, in soil and aquatic ecosystems, are controlled by metal–HS complexation, but the exact nature of this binding and the mechanisms involved are not well understood.[1, 19] The possible reason for this lack of knowledge is diversity of humic substances. Therefore, computational chemical modeling of HS–metal system can represent an useful tool for elucidating environmental situation.[1,20–22]

Significance of iron in the environment is enormous. On the micro–level iron is important for diverse cellular functions (nitrogen fixation, chlorophyll production, photosynthesis),[23] for nutrition of aquatic species when associated with HS. On the macro–level its importance is reflected in the global carbon cycle playing an important role in regulating atmospheric pressure of carbon dioxide.[24,25] Iron transport to the ocean is an important factor in that cycle with HS, as the main carriers for iron, through the soil, streams and marine ecosystems. Iron input to the open ocean follows different flow pathways. At the beginning, iron input originates from silicate rocks and is controlled by the sedimentation process, then the inorganic and organic river–borne iron colloids undergo flocculation in the estuarine mixing zone due to ionic strength change.[26–28]

Environmental iron can exist in two oxidation states Fe(II) and Fe(III). Fe(II) species, as very soluble, are usually oxidised in the presence of atmospheric oxygen into the more thermodynamically stable and often insoluble Fe(III) species, which are more dominant in natural waters. Fe(II) can be recovered by reduction of Fe(III) in the presence of light and microorganisms.[29] Stable oxyhydroxide species of Fe(III) in oceans, originated from chemical iron transformation, are usually insoluble. Therefore, bioavailability of iron can be scarce. Organic compounds, particularly, HS can form soluble complexes with mentioned Fe(III) species preventing their hydrolysis and increasing their bioavailability.[23]

1.2 Model compounds of humic substances

Different methods have been developed in order to establish and elucidate the structure of HS or to identify their building blocks (see above). A few proposals of the HS structure were developed by using spectroscopic, chemical, pyrolytic, oxidative/reductive degradation, electron–microscopy measurements and performing molecular mechanics and molecular dynamics calculations. With advances in analytical methods the understanding of HS structure has progressed. One of the first suggested structures of HS is based on aromatic carbon rings covalently interconnected to aliphatic carbon long–chains, which together with carboxyl, hydroxyl, keto, methoxy, ether, ester, nitrile functional groups and heterocylic rings form flexible networks (Figure 1).[30–32] Later proposals suggested other biomolecules as constitutents of HS, e.g., carbohydrates, proteins or lipids.[32,33]

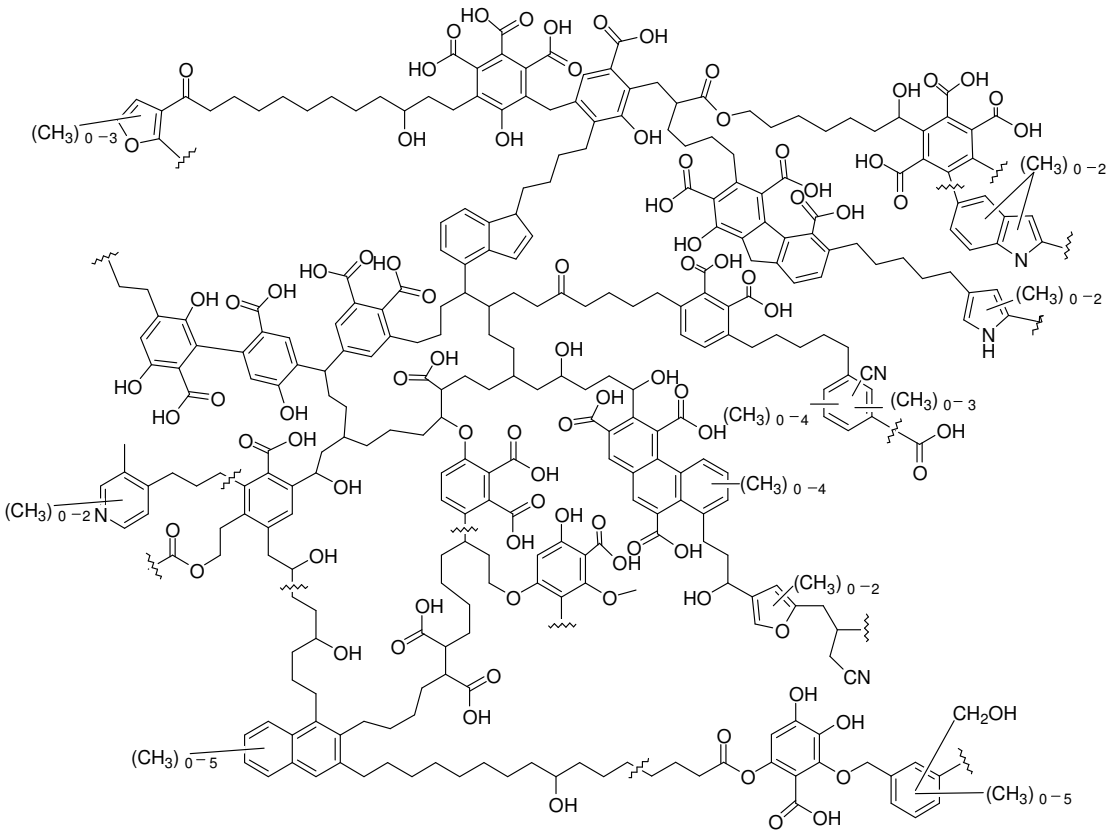

Figure 1. Proposal of HA structure.[32]

By introducing computational chemistry calculations, a better insight into the structural networks of HS models, as well mechanisms and interactions on molecular scales have been provided. An improved 3D–model of humic substances, is based on an already published 2D–model and combines shorter aliphatic links, N–heterocycles

(amines, amides, azoles, indoles, pyridines, pyroles) and oxygen–containing functional groups (Figure 2).[32]

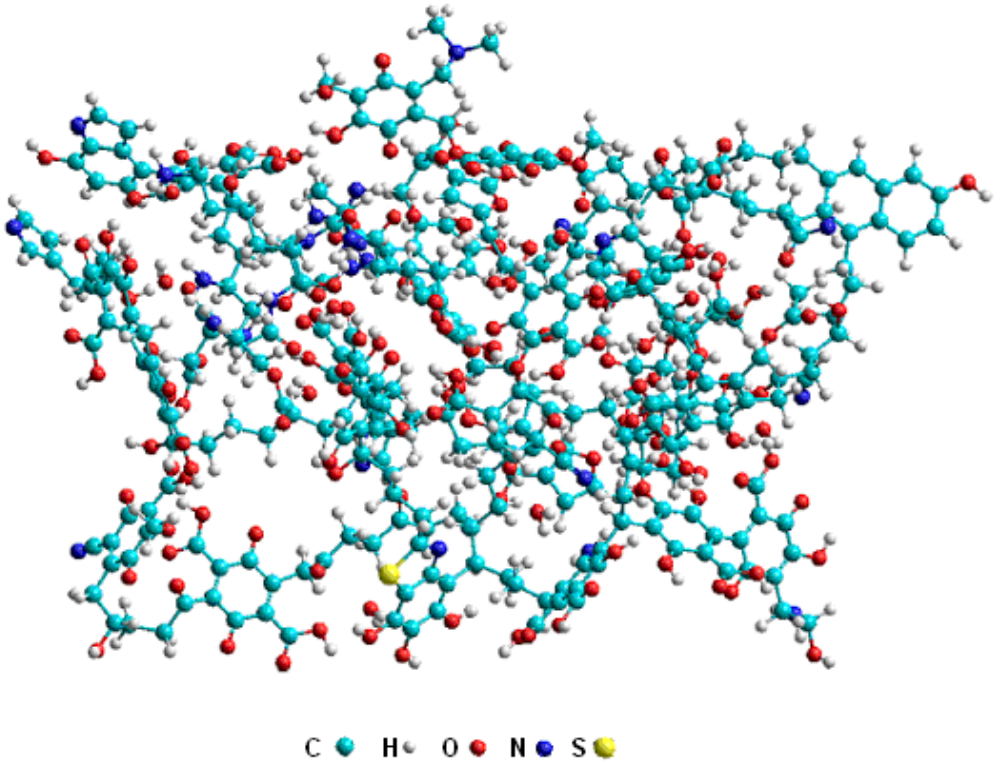

Figure 2. 3D–model of HA.[32] Reused by permission of Elsevier.

Compounds, which were identified as constituents of HS using analytical methods (freeze–drying, pyrolysis), could be divided into the following classes: lignin monomeric and dimeric derivatives, N–containing compounds (azoles, pyrimidines, pyrroles, pyridines), peptides, carbohydrates (mono–, oligo– and polysaccharides), alkylaromatic compounds, phenols, sterols and lipids (fatty acids, esters).[30,32]

A synthesis of artificial HS starts from small humic–like model molecules (*eg.* gallic acid) and via the slow oxidative polymerisation/condensation reactions using catalysts, results in products with similar properties to natural HS.[34] Starting compounds for the investigation of the binding mechanism of the HS–metal system are usually small model humic–like compounds and environmental transition metals (Fe, Al, Cu, Zn, Ni, Mo). Further UV–vis, IR, NMR, Mössbauer spectroscopic, spectrophotometric, mass spectrometric, potentiometric, X–ray diffraction investigation of metal–HS model

systems were performed in order to elucidate complexation behaviour, coordination mode, binding mechanism and possible metal mobility.
The compounds, which are identified as common building units in the structure of some HA and FA and often taken as model HS compounds, are: phenol, naphthalene, benzoic aldehyde, benzoic acid and their derivatives. Some compounds were proposed as humic–like models due to structural similarity to the building units of natural HS.[35–53]

Polyphenols form stable complexes with divalent and trivalent transition metals. Potentiometric, spectrophotometric and EPR spectroscopic studies of complexation of transition metal ions (Fe^{2+}, Fe^{3+}, Cu^{2+}, Co^{2+}, Ni^{2+}, Mn^{2+}, Mn^{3+}, Cr^{2+}, Cr^{3+}, Ti^{4+}, Mo^{5+}) with catechol and pyrogallol confirmed the formation of mono–, di– and trimeric complexes with a predicted coordination mode through the O–atoms of hydroxido groups.[35–39]

Benzoic acid derivatives have been investigated towards complexation with different transition metal ions (Fe, Cu, Al, Ni, Mo).[39–49] Gallic acid (3,4,5-trihydroxybenzoic acid) possesses a good complexation capacity due to three hydroxo and one carboxyl group, which can bind to metal, particularly, to iron via the carboxylic group or via the *catecholic* group forming dimeric and trimeric metal (iron) complexes.[36,45,48,49] 2,3-Dihydroxybenzoic acid showed a similar coordination mode with Fe and Ni, including *salycilic* or *catecholic* binding types, resulting in formation of monomeric nickel complexes and di– or trimeric mononuclear and dinuclear iron complexes.[42,44,47,53] Complexes of 2,5-dihydroxybenzoic, 2,6-dihydroxybenzoic acid and their methoxy derivatives with transition metals have been, also, spectroscopically and structurally characterised.[41,52,53] Potentiometric and UV–vis spectroscopic studies of protocatechuic (3,4-dihydroxybenzoic acid), caffeic (3,4-dihydroxycinnamic) and hydrocaffeic (3,4-dihydroxyhydrocinnamic) acid, have indicated the formation of various complexes with Fe^{3+}, Cu^{2+} and Al^{3+} via catecholic and carboxyl moieties. The introduction of an alkyl side chain between the carboxylic group and the aromatic moiety does not affect complex formation.[40,43,44]

Also, complexation of benzoic, salicylic acid and their derivatives with metal ions, especially with iron, has been studied[53–55] resulting in polynuclear metal complexes, or oxido–bridged species.[41,51,54,55]

A salient feature of humic substances is their complexation ability for a wide variety of metals, opening a possibility to apply them as detoxification agents, because they are not harmful for living organisms. Toxicity tests performed on rats, showed that HS are not toxic up to a concentration of 512 mg kg^{-1}.[18]

Interestingly, syringic acid has not shown a significant scission effect on DNA, but its complexation with metal ions (Fe^{3+}, Cu^{2+}) leads to DNA scission at pH 7.8.[56]

1.3 Iron oxido–bridged carboxylates

1.3.1 Dinuclear iron oxido complexes

In polynuclear iron oxido–carboxylate chemistry, a small diiron oxido–bridged unit, $\{Fe_2O\}^{4+}$, plays a significant role due to its occurance in biologically important catalytic enzymes and metaloproteins (ribonucleotide reductase, purple phosphatases, methane monooxygenase, hemerythrin, uteroferrin).[57,58] The stability of the $\{Fe_2O\}^{4+}$ unit, its magnetic behaviour, and occurrence at the active site in enzymes, awakened the interest for synthesis of model iron compounds.[59] Since carboxylates are common bridging ligands in the active centers of enzymes, a large number of model oxido–diiron carboxylate complexes have been synthesised in order to elucidate catalytic mechanisms of these enzymes.[59,60] The $\{Fe_2O_2\}^{2+}$ core is important for stabilizing high oxidation states in nonheme enzymes.[61] The same manganese unit has already been found in the photosynthetic oxygen evolving complex (OEC).[62] A model dinuclear iron complex with ''diamond'' $\{Fe_2O_2\}^{2+}$ core has been structurally and spectroscopically characterised.[61] The $\{Fe_2O_2\}^{2+}$ core can change its own architecture by interaction with water ligands under acid–base conditions (Scheme 3).[61]

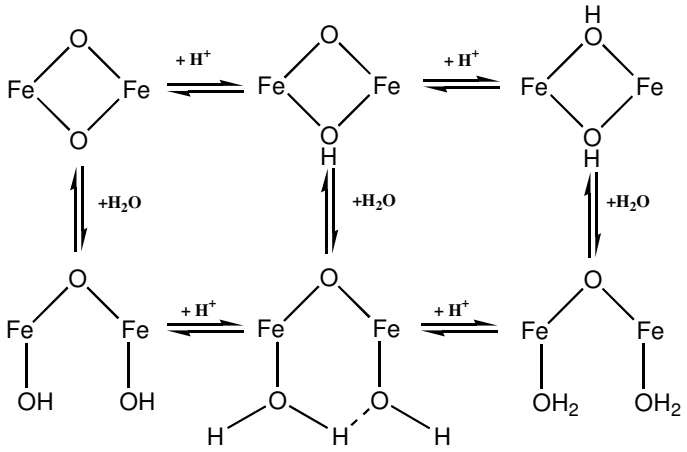

Scheme 3. Rearrangement of $\{Fe_2O_2\}^{2+}$ core unit.[61]

Moreover, a number of dinuclear iron biomimetic complexes have been found as relatively unstable.[59,63]

1.3.2 Trinuclear iron oxido complexes

Trinuclear μ_3–oxido metal carboxylates have been known since the beginning of 20th century, when they were synthesised and characterized by the german chemist Weinland.[64,65] Their triangular structure was proposed in 1928 by Welo,[66] while the exact structure was determined in 1960 by Orgel and confirmed by X–ray crystallography in 1965.[67] The general formula for oxido centered trinuclear complexes is $[M_{3-x}M_x^*O(O_2CR)_6L_3]^{n+}$, where M is a trivalent metal ion, M^* is a divalent or trivalent metal ion, $RCOO^-$ is a carboxylate bridging ligand, and L is a monodentate terminal ligand. The structure is shown in the Figure 3.

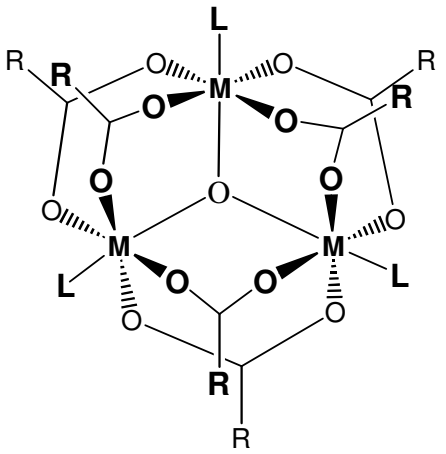

Figure 3. Trinuclear iron core.

In the case of heteronuclear complexes M^* can be a transition metal (Co, Ni). The same type of complexes are also known for other trivalent transition metals: Fe, Cr, V, Mn, Co, Ru, Rh, Ir, and divalent metals (Mg, Cr, Mn, Fe, Co, Ni, Zn, Cu), which can be involved in the formation of homo–, heteronuclear or mixed–valent complexes.[68,69] Homonuclear mixed–valent complexes are mainly characteristic for iron[70,71] and manganese,[72] but have also been observed for chromium[73] and vanadium.[74] Interestingly, a homonuclear complex with all three iron atoms in oxidation state 2+ has been reported.[75] The most often used ligands in the synthesis of these complexes are formic, acetic, picolinic, benzoic, amino, fatty acids and their methoxy and halogenated derivatives (as bridging ligands) and water, methanol, ethanol, pyridine and its derivatives (as terminal ligands).[68]

The synthetic pathways to trinuclear oxido iron carboxylates are mainly based on the methods developed by Weinland. The c*arboxylic acid method* is based on using a mixture of metal salt, carboxylic acid and potassium or sodium hydroxide. Heating this mixture at a moderate temperature results in precipitation of a trinuclear complex. A possible disadvantage of this method is formation of metal hydroxides. The *carboxylate method* involves sodium or potassium carboxylate and metal salts, which upon heating give the complex as a precipitate. The drawback of both methods is a possible co–precipitation of sodium or potasium carboxylates. The *anhydride method* possesses some advantages since it is based on using just two reactants: carboxylate anhydride and metal salts. In addition, undesirable side products are avoided.[68] The trinuclear μ–oxido iron carboxylates are well characterized by physical, electro–, magnetochemical, spectroscopical and X–ray diffraction techniques.[76–78]

1.3.3 Tetranuclear iron oxido complexes

Tetranuclear oxido iron complexes can be classified according to their core type into five subclasses: adamantane type $\{Fe_4O_6\}$, butterfly type $\{Fe_4O_2\}^{8+}$, tetragone type $\{Fe_4O_4\}^{4+}$, face–to–face type $\{Fe_4O_6\}$ and cubane type $\{Fe_4O_4\}^{4+}$ (Figure 4).[79–86]

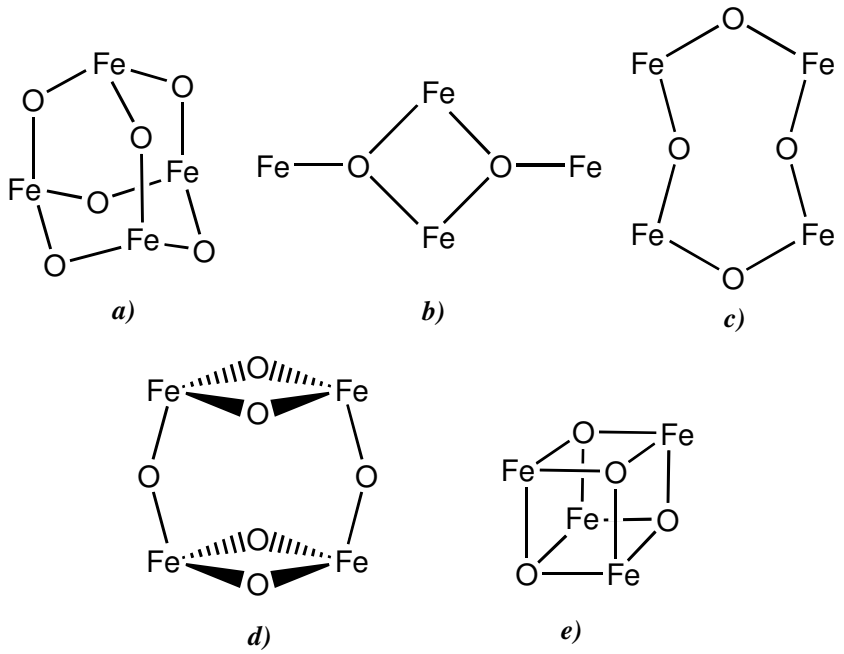

Figure 4. Different core types of the tetranuclear iron oxo complexes: a) adamantane type, b) butterfly type, c) tetragone type, d) face–to–face type, e) cubane type.

Interestingly, a tetranuclear iron oxido complex with a defective double cuban core has been reported[87] and the three conformations of butterfly core have been discussed (Figure 5).[88]

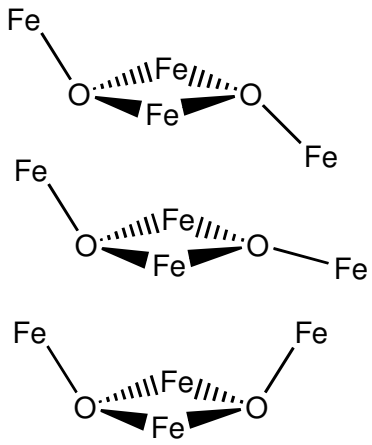

Figure 5. Conformations of ''butterfly'' tetranuclear iron core.[88]

The majority of tetranuclear iron complexes possess those mentioned structural units and their synthesis starts either with organic and inorganic iron salts (perchlorate,[79] nitrate,[80] acetate,[82] chloride[84]) or with lower nuclearity iron complexes (dinuclear, trinuclear).[81,88] The rearrangement of the initial structure, in the latter case, in appropriate solvent or with ligand exchange,[80,86,88] results in new tetranuclear iron complexes. One approach in the synthesis of tetranuclear iron complexes is self–assembly reaction, where one core can be converted into another one via oxidation with O_2 in appropriate solvents (see Figure 6).[89]

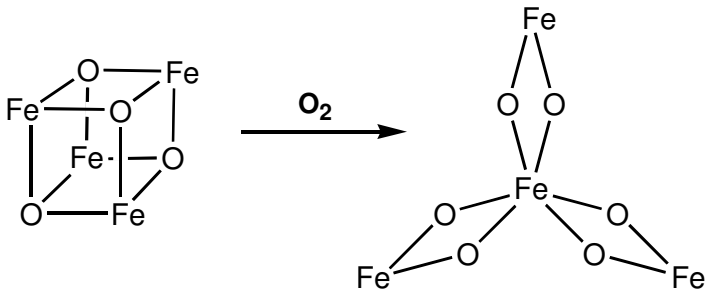

Figure 6. Self–assembly reaction of tetranuclear iron core.[89]

Tetranuclear oxido iron complexes show interesting magnetic, supramagnetic and singular molecule magnetic behaviour.[79,84,89] Some of them are used as models for polynuclear iron proteins.[90,91]

1.3.4 High nuclearity iron oxido complexes

The group of higher nuclearity iron oxido complexes is structurally different. Structural units $\{Fe_2O\}^{4+}$, $\{Fe_3O\}^{7+}$, $\{Fe_4O_2\}^{8+}$, $\{Fe_4O_4\}^{4+}$ and $\{Fe_4O_6\}$, as main units in the structure of low nuclearity complexes, have been found to be ubiquitous structural motifs in the higher nuclearity iron complexes, as described elsewhere (*vide infra*). Over the past decades high nuclearity complexes of transition metals, particularly, iron attracted attention due to their magnetic behaviour as single molecule magnets,[92,93] application in investigation of biomineralisation mechanism of iron storage proteins[94] and use as catalysts in different chemical reactions.[95] The desire to understand and model the polynuclear Fe/O core of ferritin, led to new complexes with interesting structures which showed unusual or novel magnetic characteristics.[96,97] Complexes without defined shapes are known as having a cage structure, which can be symmetrical or asymmetrical. Those with small cubic portions are known as cubane complexes. Complexes with a wheel–like structure have also been published.[68]

The most common methods explored in the synthesis of polynuclear iron carboxylates include: a high temperature method,[98] solvothermal method,[68,99] solvolysis method,[100] solid state decomposition method[101] and microwave–assisted synthesis method.[102]

In the *high temperature method*, trinuclear complexes are often used as precursors which by removing of ligand(s) at temperatures between 200 – 500 °C form new compounds.

The *solvothermal method* is based on replacing ligands from metal precursors (low nuclear complexes) with solvent at high temperature and prolonged reaction time, and afterwards, by replacing solvent molecules again with ligands upon cooling, producing higher nuclearity complexes.

The *solvolysis (hydrolysis) method* refers to treatment of polynuclear precursors with excess solvent (water, methanol, phenol) leading to formation of complexes with different nuclearity.[100] Solvolysis of polymeric iron complexes in water and nonaqueous solvents increases their nuclearity and in combination with self–assembly of their cores leads to formation of complexes with interesting structures.

The *solid state decomposition method* requires an appropriate starting material (high nuclear complexes) containing ligands that are volatile (volatile carboxylates). Ligands should be removed without destroying the metal–oxide core by heating at carefully chosen temperature and reaction time in order to avoid formation of undesirable byproducts (metal oxides).

Formation of polynuclear complexes using the *microwave–assisted synthesis method*, is based on heating iron salts and ligands or low nuclear complexes in appropriate solvents for a few minutes in a microwave oven.[102]

Easy and reproducible rearrangement, as well as, good solubility in most organic solvents render low nuclearity iron complexes (di–, tri–, tetranuclear) as important starting materials for the synthesis of higher nuclearity complexes. Recently, one new approach emerged for the synthesis of polynuclear complexes.[103] Some high nuclear iron complexes can be obtained by serendipitous assembly of cores of smaller iron complexes. Self–assembly of small complexes has been already described for other transition metals and leads to polynuclear cage complexes with new unpredictable structures. The synthesis of the compounds with most interesting physical properties is based on serendipitous assembly. Therefore, the self–assembly approach for the synthesis of iron complexes becomes very attractive for researchers.[103]

1.3.4.1 Hexanuclear iron oxido complexes

The structure of the hexanuclear oxido iron complexes is quite different. The cores of hexanuclear iron complexes $[Fe_6O_2(O_2CH_2)(O_2CH_2Bu^t)_{12}(py)_2]$, $[Fe_6O_3(O_2CMe)_9(OPh)_2(bpy)_2]ClO_4$, $[Fe_6O_2(OH)_2(OH_2)(O_2CPh)_{12}(1,4\text{-dioxane})]$ and $[Fe_6(O_2)(O)_2(O_2CCMe_3)_{12}(HO_2CCMe_3)_2]$ can be described as two triangular oxido–centered units $\{Fe_3(\mu_3\text{–}O)\}^{7+}$ connected via μ_4–carboxylato, μ_4–oxido, two μ_2–hydroxido or μ_4–peroxido bridge, respectively (Figure 7).[96,100,104,105]

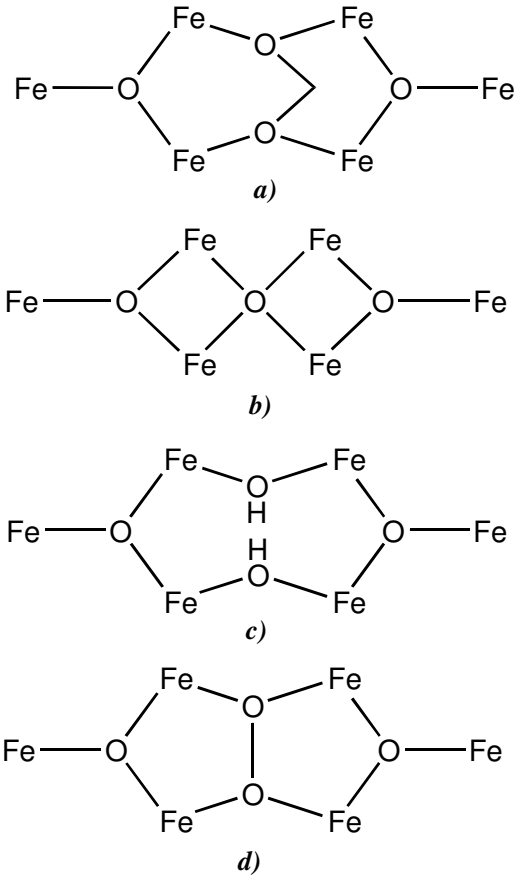

Figure 7. Different core topology of iron complexes: a) $[Fe_6O_2(O_2CH_2)(O_2CH_2Bu^t)_{12}(py)_2]$ b) $[Fe_6O_3(O_2CMe)_9(OPh)_2(bpy)_2]ClO_4$, c) $[Fe_6O_2(OH)_2(O_2CPh)_{12}(1,4\text{-dioxane})]$ and d) $[Fe_6(O_2)(O)_2(O_2CCMe_3)_{12}(HO_2CCMe_3)_2]$.

In the synthesis of hexanuclear iron complexes trinuclear iron complexes with an oxido centered $\{Fe_3O\}^{7+}$ unit are usually used as starting materials, therefore this unit is a dominant motif in their stuctures.[96,100,104,105]

The conformations of the $\{Fe_6(\mu_4\text{–}O_2)(\mu_3\text{–}O)_2\}^{6+}$ unit of the hexanuclear iron peroxido bridge complexes has already been discussed. The $\{Fe_6(\mu_4\text{–}O_2)(\mu_3\text{–}O)_2\}^{6+}$

unit possesses a ''butterfly'' like conformational differences, with an almost planar or twisted tetranuclear iron peroxido subunit $\{Fe_4(\mu_4–O_2)\}^{10+}$ (Figure 8).[105]

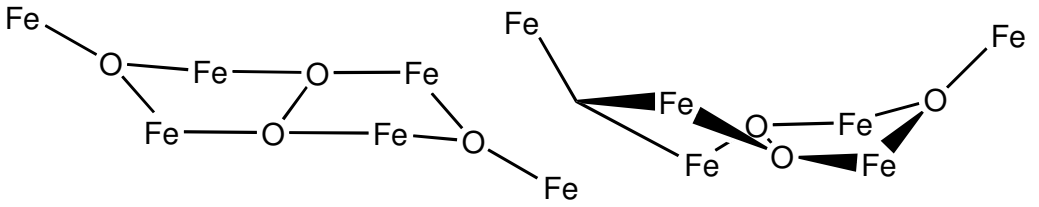

Figure 8. The conformations of $\{Fe_6(O_2)(O)_2\}^{6+}$ unit.[105]

Hexanuclear iron complexes serve as starting materials for the synthesis of both lower and higher nuclearity complexes. By reduction of a hexanuclear iron complex with $NaBH_4$ the synthesis of a tetranuclear iron complex was realised,[105] while by exploring the solvolysis method in the presence of solvent excess a hexanuclear iron complex has been rearranged into the larger octanuclear, decanuclear or, with thermal decomposition, into the undecanuclear iron complex. [100,101]

The hexanuclear iron carboxylate complex $[Fe_6O_3(OH)(p–NO_2C_4H_6COO)_{11}(dmf)_4]$, with core unit $[Fe_6(\mu_3–O)_3(\mu_2–OH)]^{11+}$, obtained by slow diffusion of diethyl ether in N,N'-dimethyformamide (dmf) solution of trinuclear iron complex $[Fe_3O(p–NO_2C_4H_6COO)_6](p–NO_2C_4O_6COO)\cdot H_2O$, showed interesting catalytic properties and a new core type (Figure 9).[95]

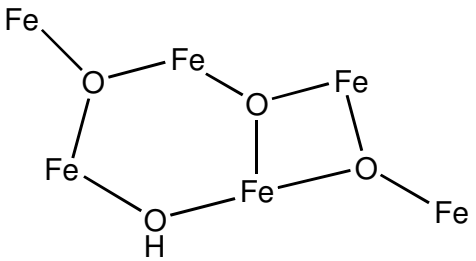

Figure 9. The hexanuclear iron core of $[Fe_6O_3(OH)(p\text{-}NO_2C_4H_6COO)_{11}(dmf)_4]$.[95]

Recently, a few other hexanuclear iron complexes with interesting core types have been synthesised.[96,106,107] The reaction of trinuclear iron carboxylate, iron(III) nitrate monohydrate and 2-**m**eth**o**xy **e**thanol (moe) in MeCN after slow diffusion of diethyl ether produced $[Fe_6O_2(OH)(O_2CCH_2Cl)_6(moe)_6](NO_3)_2$. The core contains two $\{Fe_3O\}^{7+}$ units connected in face–to–face fashion by six alkoxide and six carboxylate bridging ligands giving an Fe_6 octahedron (Figure 10).[96]

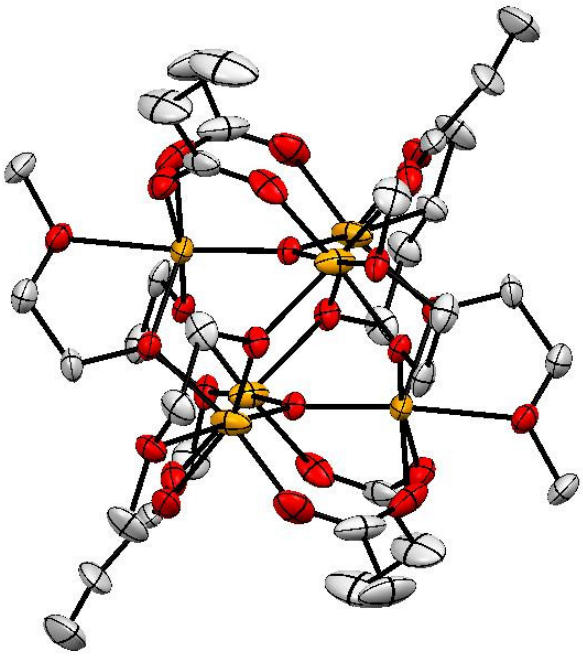

Figure 10. The structure of $[Fe_6O_2(OH)(O_2CCH_2Cl)_6(moe)_6](NO_3)_2$. The iron (yellow), oxygen (red) and carbon (gray) atoms are depicted, while H and Cl atoms are omitted for clarity.[96]

Transformation of trinuclear iron carboxylate $[Fe_3O(O_2CPh)_6(H_2O)_3](O_2CPh)$ into tetranuclear iron carboxylate $[Fe_4(O)_2(O_2CPh)_8(C_5H_5N)_2]\cdot C_6H_5CH_3$ and its reaction with aluminium isopropyl alkoxide ($AlOPr^i$) in benzene led to a new iron(III) species, $[Fe_6O_2(OPr^i)_8(O_2CPh)_6]\cdot 1.33C_6H_6$, with a hexanuclear iron core which consist of the planar tetranuclear $[Fe_4(\mu_3\text{–}O)_2]^{10+}$ unit, connected via three OR groups with two $\{Fe(OR)_4\}^-$ units one above and one below the Fe_4 plane (Figure 11).[106] Another hexanuclear iron complex with the same core type has also been reported.[108]

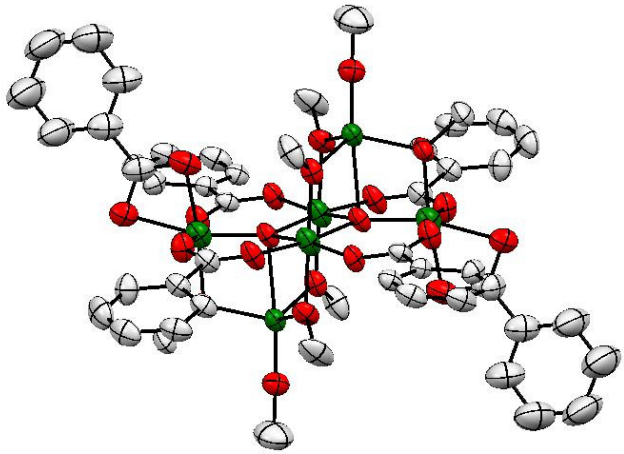

Figure 11. The core of $[Fe_6O_2(OPr^i)_8(O_2CPh)_6]\cdot 1.33C_6H_6$. The iron (green), oxygen (red), carbon (gray) atoms are depicted, while CH_3 groups of alkoxy moiety and H atoms are omitted for calrity.[106]

The product of the reaction of anhydrous $FeCl_3$, NaO_2CPh and 1,2-bis(2,2'-bipyridyl-6-yl)ethane (L) in water, is a hexanuclear iron complex $[Fe_6O_6(O_2CPh)_3L_3(H_2O)_2]Cl_3$, with a ''six–rung ladder'' core (Figure 12).[107]

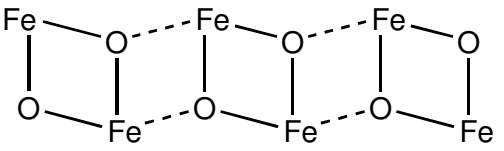

Figure 12. The core of $[Fe_6O_6(O_2CPh)_3L_3(H_2O)_2]Cl_3$.[107]

The structure of $[Fe_6O_6(O_2CPh)_3L_3(H_2O)_2]Cl_3$ can be described as three joined $\{Fe_2O_2\}^{2+}$ units giving almost planar $\{Fe_6O_6\}^{6+}$ ladder–like core.

The complex $[Fe_6O_4Cl_4(O_2CPh)_4L_2][FeCl_4]_2$, with a similar core type was discovered a few years ago (Figure 13a).[109]

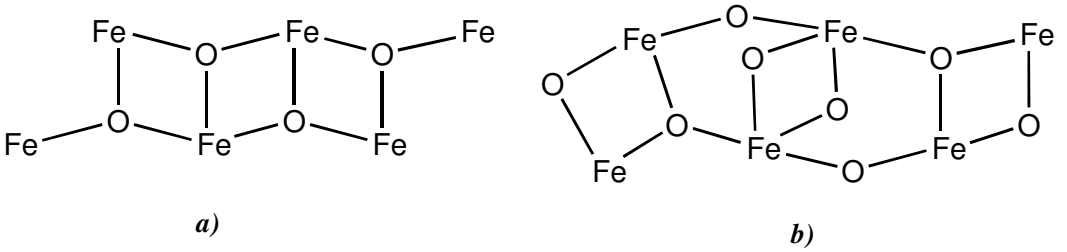

a) ***b)***

Figure 13. The core of $[Fe_6O_4Cl_4(O_2CPh)_4L_2][FeCl_4]_2$ (a) and $[Fe_6O_2(O_2CBu^t)_8(edteH)_2]$ (b).[109,110]

$[Fe_6O_2(O_2CBut)_8(edteH)_2]$, which consists of two triangular $\{Fe_3O\}^{7+}$ units, joined together via four alkoxide O atoms from $edteH_4$ ligand (Figure 13b), was obtained by reaction of N,N,N',N'-tetrakis(2-hydroxyethyl)ethylenediamine ($edteH_4$) with $Fe(ClO_4)_3 \cdot 6H_2O$ and $NaO_2CMe \cdot 3H_2O$.[110]

1.3.4.2 Heptanuclear iron oxido complexes

Heptanuclear iron complexes, with carboxylate ligands are rare and recent. Just a few complexes containing $\{Fe_7O_2\}^{17+}$, $\{Fe_7O_3\}^{15+}$, $\{Fe_7O_4\}^{13+}$ and $\{Fe_7O_6\}^{9+}$ cores are known.[111–116] In their structures, besides carboxylate ligands also phosphonate,[111,112] alkoxo[113,114] and bipyrimidine[116] ligands were found.

Treatment of trinuclear iron carboxylate $[Fe_3O(O_2CPh)_6(H_2O)_3]Cl$ with cyclohexane phosphonic acid ($C_6H_9PO_3H_3$) leads to an interesting heptanuclear iron complex, $[Fe_7O_2(O_2CPh)_9(O_3PC_6H_9)_4(py)_6]\cdot CH_3CN\cdot 3H_2O$, with the structural unit $\{Fe_7O_2\}^{17+}$ (Figure 14).[111]

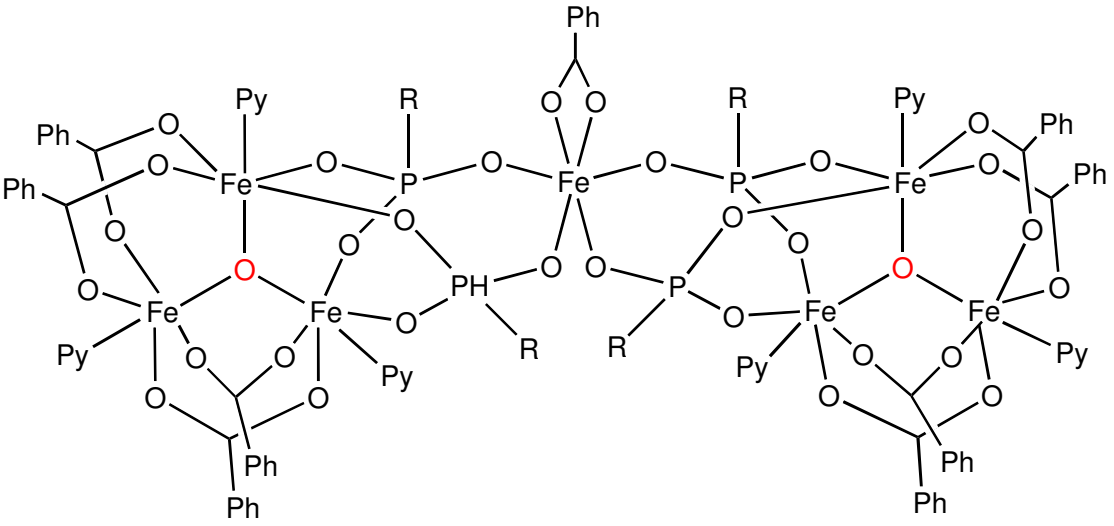

Figure 14. The core of $[Fe_7O_2(O_2CPh)_9(O_3PC_6H_9)_4(py)_6]\cdot MeCN\cdot 3H_2O$.[111]

The two isostructural heptanuclear iron complexes $[Fe_7O_3(O_2CCMe_3)_9(bheapH)_3(H_2O)_3]$ and $[Fe_7O_3(O_2CCMe_3)_9(teaH)_3(H_2O)_3]$, obtained by mixing trinuclear iron carboxylates with ligands 1-[N,N-bis(2-hydroxyethyl)-amino]-2propanol ($bheapH_3$) and triethanolamine ($teaH_3$), possess a ''millennium dome'' like core (Figure 15a).[113]

Three heptanuclear iron complexes of general formula $[Fe_7O_3(\mu_3\text{–}O_2CCMe_3)_6(L)_3(\eta^1\text{–}O_2CCMe_3)_3(H_2O)_3]$ with three different ligands: triethanolamine ($teaH_3$), butyldiethanolamine ($bdeaH_2$) and phenyldiethanolamine (phdea) have recently been reported. They comprise the same $\{Fe_7O_3\}^{15+}$ core unit (Figure 15 b), with a three–blade propeller topology, which corresponds to the theoretical model of a frustrated Heisenberg star. [114]

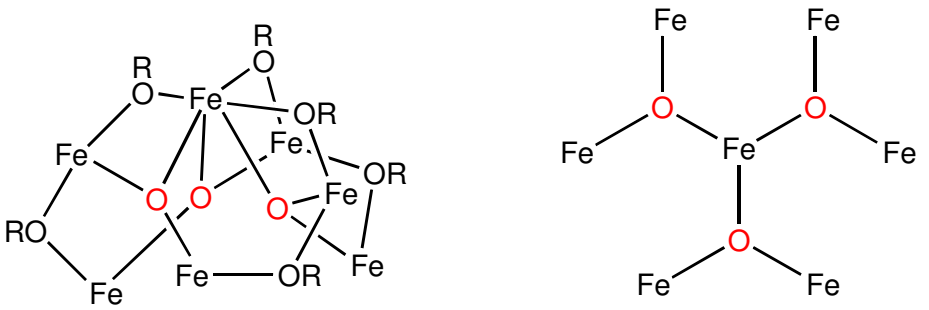

a) *b)*

Figure 15. a) The core of $[Fe_7O_3(O_2CCMe_3)_9(bheapH)_3(H_2O)_3]$ and $[Fe_7O_3(O_2CCMe_3)_9(teaH)_3(H_2O)_3]$ where R is alkyl residue of $bheapH_3$ or $teaH_3$, R= $(–CH_2–CH_2)_2NCH_2CHCH_3$ or $(–CH_2–CH_2)_3N$. b) The core of $[Fe_7O_3(\mu_3–O_2CCMe_3)_6(L)_3(\eta^1–O_2CCMe_3)_3(H_2O)_3]$ where L = teaH, bdea or phdea.[113,114]

Three different methods have been applied for the synthesis of $[Fe_7O_4(O_2CPh)_{11}(dmem)_2]$. The following starting compounds were used: in the first method, trinuclear iron carboxylate; in the second, $FeCl_3$ and NaO_2CPh and in the third, $(NEt_4)_2[Fe_2OCl_6]$ and NaO_2CPh. All starting compounds were dissolved in MeCN and treated with 2-{[2-(dimethylamino)ethyl]methylamino}-ethanol (dmemH). After stirring at room temperature with different reaction times, crystals of $[Fe_7O_4(O_2CPh)_{11}(dmem)_2]$, with a new heptanuclear core topology were obtained by slow evaporation of the solvent.[115] The same methods (first and second) were used in the synthesis of the $[Fe_7O_4(O_2CMe)_{11}(dmem)_2]$ complex. $\{Fe_3O\}^{7+}$ units of both complexes are linked differently, forming different cores (Figure 16).[115]

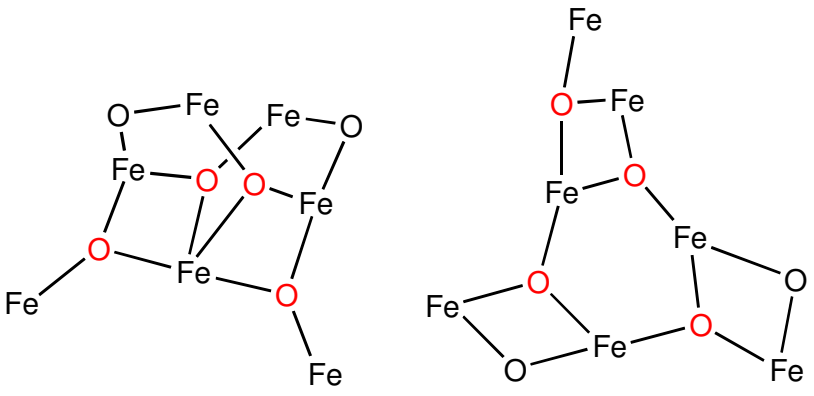

a) *b)*

Figure 16. Different types of $\{Fe_7O_4\}^{13+}$ core unit. The core units of $[Fe_7O_4(O_2CPh)_{11}(dmem)_2]$ (a) and $[Fe_7O_4(O_2CMe)_{11}(dmem)_2]$ (b).[115]

A very interesting rearrangement of the hexanuclear iron pivalate into the charge neutral heptanuclear iron complex, $[Fe_7O_4(OH)_2(O_2CCMe_3)_{11}(bmp)_2H_2O]$, containing 2,2'-bipyrimidine (bmp) as co–ligand, has been performed, starting from trinuclear iron pivalate (Figure 17).[116]

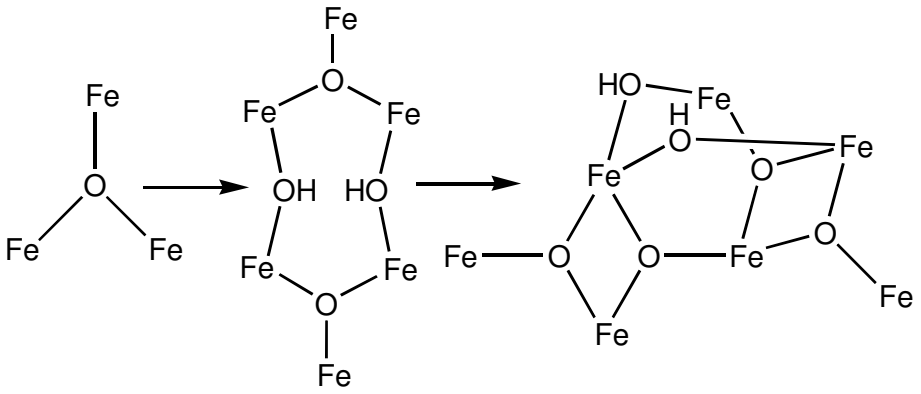

Figure 17. The core rearrangement of trinuclear iron complex into the heptanuclear one.[116]

The heptanuclear core of $[Fe_7O_4(OH)_2(O_2CCMe_3)_{11}(bmp)_2H_2O]$, in which all iron atoms are six–coordinate, can be described as two tetranuclear iron units, $\{Fe_4(\mu_3–O)_2\}^{8+}$, joined together by a common iron atom and additionally bridged by two hydoxide and eleven pivalate ligands.[116]

In the heptanuclear complex $[Fe_7O_3(OCH_3)(fdc)_6(CH_3OH)_3][FeCl_4]Cl_2$, where $fdcH_2$ = ferrocene-1,1'-dicarboxylic acid, the $[Fe_7(\mu_4–O_3)(\mu_3–OCH_3)]^{14+}$ core comprises a central cubane unit $\{Fe_4O_4\}^{4+}$ which is built up of four irons and four μ_4–oxido ligands. The cubane unit is connected to three irons and one methyl ligand via four $\mu_4–O^{2–}$ bridges (Figure 18).[117]

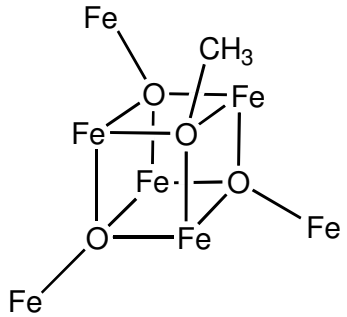

Figure 18. The core of $[Fe_7O_3(OCH_3)(fdc)_6(CH_3OH)_3][FeCl_4]Cl_2$.[117]

1.3.4.3 Octanuclear iron oxido complexes

Octanuclear iron complexes have been synthesized from the following starting materials: trinuclear iron complexes,[114,118] hexanuclear iron complexes,[100] inorganic[113] and organic[119] iron salts. Complexes with this interesting core topology are well documented in the literature. In some octanuclear iron complexes, iron atoms are connected with three μ_4–oxido ligands. The complexes $[Fe_8O_3(O_2CCH_2CH_3)_6(tea)(teaH)_3F_3]$,[113] $[Fe_8O_3(O_2CCH_2CH_3)_6(tea)(teaH)_3(N_3)_3]$, $[Fe_8O_3(O_2CCH_2CH_3)_6(tea)(teaH)_3(SCN)_3]$[114] and $[Fe_8O_3(O_2CPh)_9(tea)(teaH)_3]$[118] possess the same core unit $\{Fe_8(\mu_4\text{–}O)_3\}^{18+}$ (Figure 19).

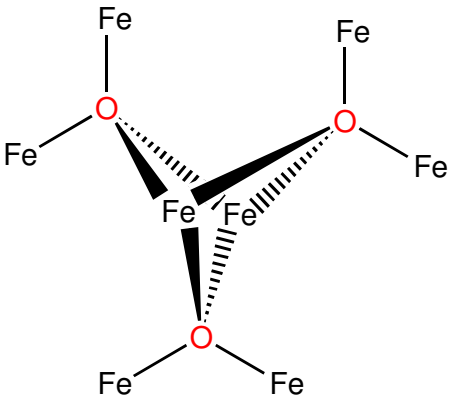

Figure 19. The core unit $\{Fe_8(\mu_4\text{–}O)_3\}^{18+}$.

The wheel–like octanuclear iron core, bridged by a combination of carboxylate and $thme^{3-}$ ligands (Figure 20), is found in $[Fe_8(O_2CPh)_{12}(thme)_4]$ and $[Fe_8(O_2CCMe_3)_{12}(thme)_4]$, where $thmeH_3$ = 1,1,1-tris(hydroxymethyl)ethane.[93]

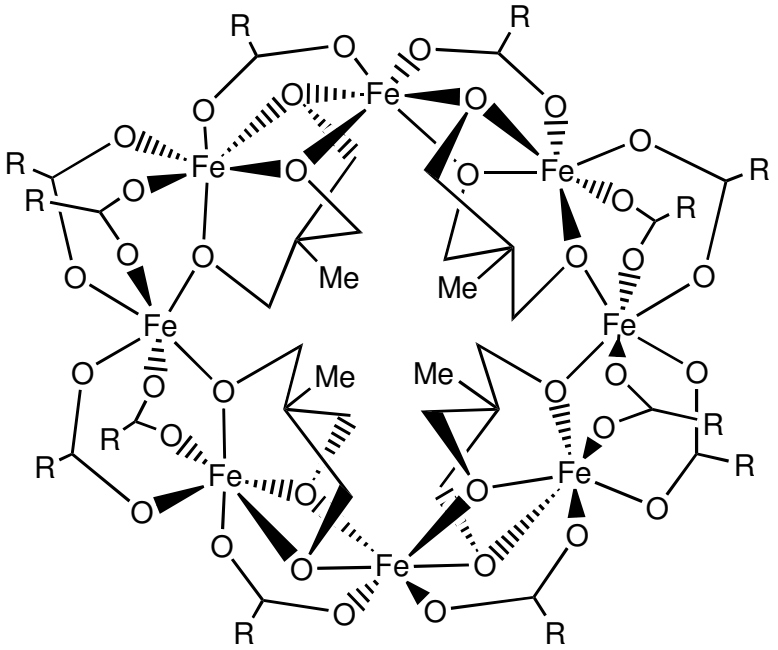

Figure 20. The wheel–like core of $[Fe_8(O_2CR)_{12}(thme)_4]$. R = Ph or CMe_3.[93]

Another complex with the same wheel–like core topology has also been found, in which iron atoms are connected via twelve *tert*-butyl carboxylate, eight phenoxido and four μ_2–hydroxido bridges.[100]

The complex $[Fe_8O_4(sao)_8(py)_4]\cdot 4py$ ($saoH_2$ = 2-hydroxybenzaldehyde oxime), with an uncommon octanuclear iron core, has been obtained employing the microwave assisted method.[119] The core consists of a cuban unit $\{Fe_4(\mu_4\text{–}O)_4\}^{4+}$, which is situated in iron edged tetrahedron (Figure 21).

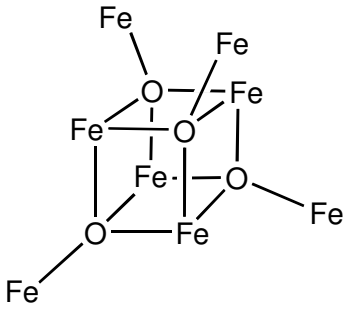

Figure 21. The ''cube in tetrahedron'' of $[Fe_8O_4(sao)_8(py)_4]\cdot 4py$.[119]

1.3.4.4 Nonanuclear iron oxido complexes

The core of the nonanuclear iron complex $[Fe_9O_4(O_2CCMe_3)_{13}(thme)_2]$, where $thmeH_3$ = 1,1,1-tris(hydroxymethyl)ethane, can be described as four $\{Fe_3O\}^{7+}$ edge or side shared units connected via three common iron atoms to the central $\{Fe_4(thme)_2\}^{6+}$ unit (Figure 22).[93] The core is additionally bridged by thirteen trimethyl carboxylate ligands via carboxylic groups.

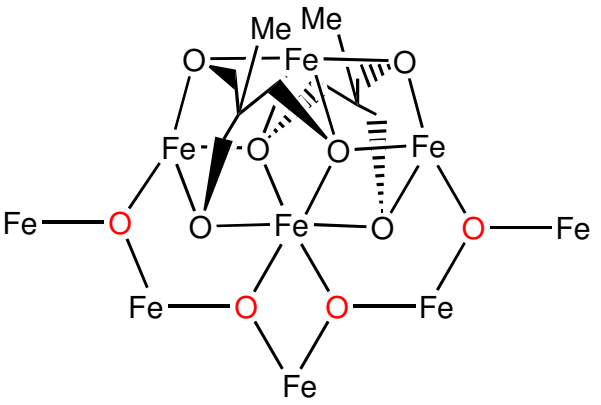

Figure 22. The core of $[Fe_9O_4(O_2CCMe_3)_{13}(thme)_2]$. Carboxylate ligands are omitted.[93]

Employing phosphonic acid derivatives; e.g., camphyl phosphonic acid ($cpaH_2$), 4-*tert*-butyl phenylphosphonic acid ($tbpaH_2$), 3,5-dimethylphenyl phosphonic acid ($dmppaH_2$) and diphenylmethylphosphonic acid ($dpmpaH_2$) nonanuclear iron complexes, with a variety of core topologies have been prepared. The reaction of $cpaH_2$ with trinuclear iron pivalate and trinuclear iron benzoate precursors resulted in two nonanuclear iron complexes with different core topologies $[Fe_9O_4(O_2CCMe_3)_{13}(cpa)_3]$, (with the same core as $[Fe_9O_4(O_2CCMe_3)_{13}(thme)_2]$) (Figure 22), and $[Fe_9O_2(OH)(O_2CPh)_{10}(cpa)_6(H_2O)_2]\cdot 7CH_3CN$ (Figure 23).[120] These complexes could be also synthesized in a one–step reaction by mixing $FeCl_3$, $cpaH_2$ and trimethylacetic or benzoic acid in the presence of triethylamine.

Two other complexes, $[Fe_9O_2(OH)(O_2CPh)_{10}(PhPO_3)_6(H_2O)_5(CH_3CN)]$ and $[Fe_9O_2(OH)(O_2CPh)_{10}(cpa)_6(H_2O)_6]$, have similar cores to the one found in $[Fe_9O_2(OH)(O_2CPh)_{10}(cpa)_6(H_2O)_2]\cdot 7CH_3CN$.[112] The core consists of three iron(III) triangles (Figure 23). Two $\{Fe_3O\}^{7+}$ units as outer planes are connected to the three remaining iron atoms via phosphonate and carboxylate ligands.[112,120]

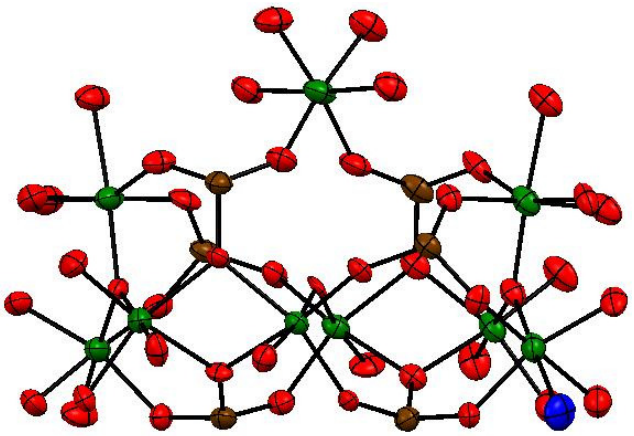

Figure 23. The $Fe_{(green)}/O_{(red)}/P_{(brown)}/N_{(blue)}$ backbone of $[Fe_9O_2(OH)(O_2CPh)_{10}(PhPO_3)_6(H_2O)_5(CH_3CN)]$ and $[Fe_9O_2(OH)(O_2CPh)_{10}(cpa)_6(H_2O)_6]$. C and H atoms are omitted for clarity.[112]

By reaction of $[Fe_3O(O_2CCMe_3)_6(H_2O)_3]Cl$ with two different ligands ($dmppaH_2$ and $dpmpaH_2$), two complexes, $[Fe_9O_4(dmppa)_3(O_2CCMe_3)_{13}]$ and $[Fe_9O_3(OH)_3(dpmpa)_6(O_2CCMe_3)_6]$ with different core topologies have been obtained (Figure 24 a and b, respectively).[121]

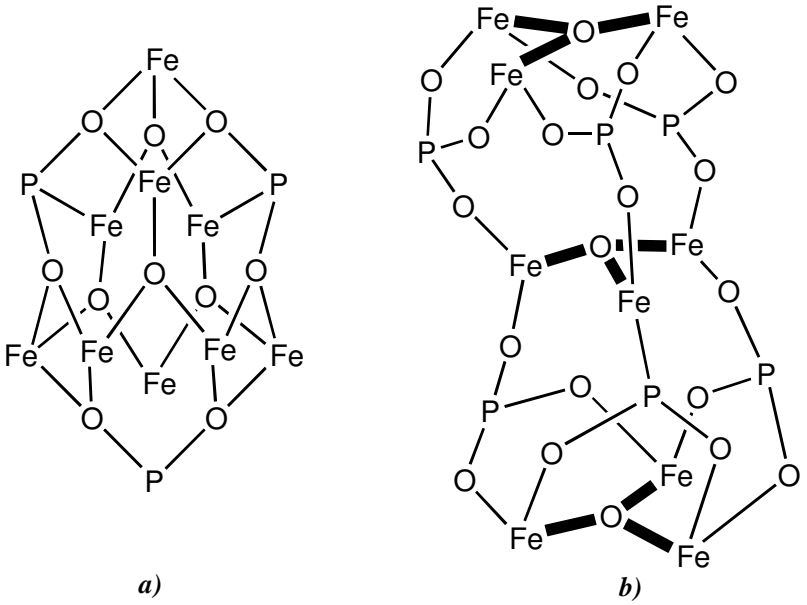

Figure 24. The cores of the structures: a) $[Fe_9O_4(dmppa)_3(O_2CCMe_3)_{13}]$ and b) $[Fe_9O_3(OH)_3(dpmpa)_6(O_2CCMe_3)_6]$.[121]

The core of the complex $[Fe_9O_4(dmppa)_3(O_2CCMe_3)_{13}]$ consists of two units: $\{Fe_6O_3\}^{12+}$ and $\{Fe_3O\}^{7+}$. Connection between the $\{Fe_6O_3\}^{12+}$ and $\{Fe_3O\}^{7+}$ units is provided by three phosphonate ligands (Figure 24a).

The structure of $[Fe_9O_3(OH)_3(dpmpa)_6(O_2CCMe_3)_6]$ consists of three iron oxido–centered $\{Fe_3O\}^{7+}$ units, which are linked via three phosphonate ligands (Figure 24b).

1.3.4.5 Decanuclear iron oxido complexes

Decanuclear iron oxido–complexes have mainly structures in the form of a wheel (Figure 25).

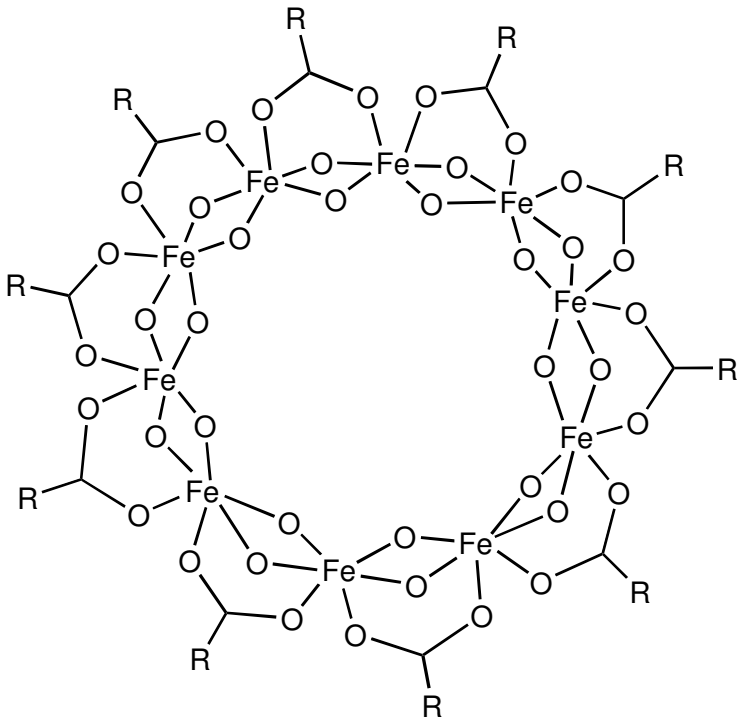

Figure 25. The core of decanuclear complexes. R = CH_3, CH_2Cl, Bu^t, CH_2CH_3, Ph.

Synthesis of decanuclear iron oxido–complexes usually starts with reaction of trinuclear or hexanuclear iron precursors with ligands (acetic, chloracetic, propionic, benzoic or *tert*-butyl carboxylic acid) in different solvents (MeCN, diethylether, MeOH, CH_2Cl_2, toluene), applying different reaction conditions (ligand substitution, prolonged reaction time).[100,122,123] Decanuclear iron complexes can be described as $[Fe(OMe)_2(O_2CR)]_{10}$ or $[Fe_{10}(OMe)_{20}(O_2CR)_{10}]$, where R = Me, CH_2Cl, ^tBu, Et or Ph. The wheel–like structure of decanuclear iron complexes consists of ten octahedral iron atoms arranged in a planar ring. Each iron atom is bridged by a neighboring iron atom via two μ_2–methoxido and one μ_2–carboxylate moieties, giving layers of oxygen atoms above and below the ferric plane (Figure 25).

A mechanism of self–assembly rearrangement of trinuclear and hexanuclear precursors into decanuclear iron complexes is still unknown. One simplified reaction was proposed to describe the formation of a decanuclear iron complex from a hexanuclear one (Reaction 1, hepH = 2-(2-hydroxyethyl)pyridine).[100]

$5[Fe_6O_2(OH)_2(O_2CBu^t)_{10}(hep)_2] + 60MeOH \rightarrow 3[Fe_{10}(OMe)_{20}(O_2CBu^t)_{10}] + 20H_2O + 10hepH + 20Bu^tCO_2H$ (Reaction 1)

Two interesting cage complexes $[NaFe_{10}O_3(OH)_4(HL)_2(O_2CCMe_3)_{13}]\cdot CH_2Cl_2\cdot H_2O$ and $[Fe_{10}O_4(OH)_2(HL)_2(O_2CCMe_3)_{12}(H_2O)_2]\cdot 2H_2O\cdot 5MeCN$ have been obtained by reaction of trinuclear iron pivalate with tetra–deprotonated ligand 2-[bis(2-hydroxyethyl)amino]-2-(hydroxymethyl)-propane-1,3-diol (H_5L) by self–assembly of trinuclear precursors, in the presence or absence of sodium cations, in appropriate solvent (Figure 26).[124]

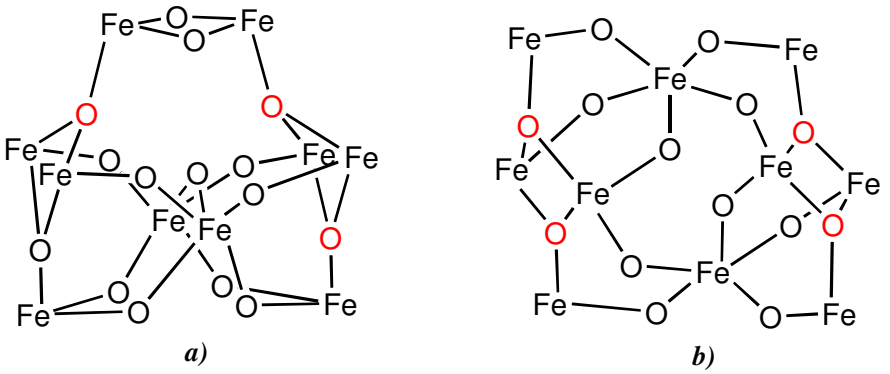

Figure 26. The cores of $[NaFe_{10}O_3(OH)_4(HL)_2(O_2CCMe_3)_{13}]\cdot CH_2Cl_2\cdot H_2O$ and $[Fe_{10}O_4(OH)_2(HL)_2(O_2CCMe_3)_{12}(H_2O)_2]\cdot 2H_2O\cdot 5MeCN$. Alkyl residues of ligands are omitted for clarity.[124]

In the structure of $[NaFe_{10}O_3(OH)_4(HL)_2(O_2CCMe_3)_{13}]\cdot CH_2Cl_2\cdot H_2O$, the central unit $\{NaFe_2O(HL)_2(O_2CCMe_3)_2\}^{5-}$ is connected to two $\{Fe_4O(OH)(O_2CCMe_3)_5\}^{4+}$ fragments (Figure 26a).

In the complex $[Fe_{10}O_4(OH)_2(HL)_2(O_2CCMe_3)_{12}(H_2O)_2]\cdot 2H_2O\cdot 5MeCN$, two $\{Fe_4O_2(O_2CCMe_3)_6\}^{2+}$ units are bridged via two separate $\{Fe(HL)(OH)\}^{2-}$ units (Figure 26b).

1.3.4.6 Undecanuclear iron oxido complexes

The first undecanuclear iron complex was obtained in 1986, by searching for a model compound of the iron storage protein ferritin.[94] Hydrolysis of $Et_4N[Fe_2OCl_6]$ in the presence of a benozoate ligand in acetonitrille followed by vapour diffusion of water or by liquid diffusion of aqueous THF, resulted in the unprecedented undecanuclear iron complex $[Fe_{11}O_6(OH)_6(O_2CPh)_{15}]$ (Figure 27). Undecanuclear iron complexes, with the same core topology, have been obtained by rearrangement of hexanuclear iron complexes at high–temperature, using different ligands: 3,3-dimethylbutanoic, 3-methylbenzoic and benzoic acids.[98,101]

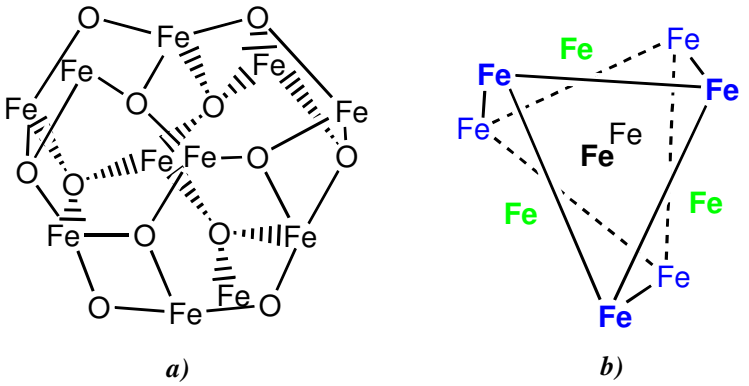

Figure 27. The core of $[Fe_{11}O_6(OH)_6(O_2CPh)_{15}]$ (a) and arrangement of iron atoms in the core as pentacapped trigonal distorted prism (b).[97,101]

The core of $[Fe_{11}O_6(OH)_6(O_2CPh)_{15}]$ (Figure 27a) can be described as a pentacapped trigonal distorted prism (Figure 27b). There are three types of iron atoms in the core of this compound. Two iron atoms (black coloured) are situated on the C_3 axis in the trigonal form, and belong to the first type. Each iron atom is connected to three benzoate oxygen atoms and three bridging μ_3–oxygens. Six iron atoms (blue coloured) of the second type define the body of the trigonal prism. Each of them is linked to the three benzoate oxygens, two μ_3–hydroxido and one μ_3–oxido bridges. Three iron atoms (green coloured) of the third type are situated on the C_2 axis in the trigonal form and each connected to two benzoate oxygen atoms, two μ_3–oxido and two μ_3–hydroxido bridges.[94,97] Another description suggests that six vertex sharing oxido–centered $\{Fe_3O\}^{7+}$ units form the Fe/O core (Figure 27).[101]

The incorporation of more than one type of ligand, which can chelate and bridge iron centers leads to undecanuclear iron complexes with core topologies containing $\{Fe_{11}O_7\}^{19+}$, $\{Fe_{11}O_4\}^{25+}$ and $\{Fe_{11}O_3(OH)\}^{26+}$ units.[92,93,125,126]

The undecanuclear iron complex $[NEt_4][Fe_{11}O_4(O_2CPh)_{10}(thme)_4(dmhp)_2Cl_4]$ has been obtained by reaction of $[NEt_4][Fe_2OCl_6]$ with sodium benzoate ($PhCO_2H$), 4,6-**dim**ethyl-2-**h**ydroxy**p**yrimidine (dmhp) and 1,1,1-**t**ris(**h**ydroxy**m**ethyl)-**e**thane (H_3thme). The core of $[NEt_4][Fe_{11}O_4(O_2CPh)_{10}(thme)_4(dmhp)_2Cl_4]$ (Figure 28) can be described as four fused butterfly motifs $\{Fe_4O_2\}^{8+}$. Two butterfly units, in the center of the structure, share one iron atom forming a planar $\{Fe_7O_4\}^{13+}$ system. Two peripheral butterfly units are nonplanar and share two iron atoms with a $\{Fe_7O_4\}^{13+}$ system. Two defective double cubane units, previously reported,[72] can be seen in the structure, which are connected to the $\{Fe_3O_4\}^{+}$ planar system. This complex has additionally been studied by density functional methods and Monte Carlo simulations.[127]

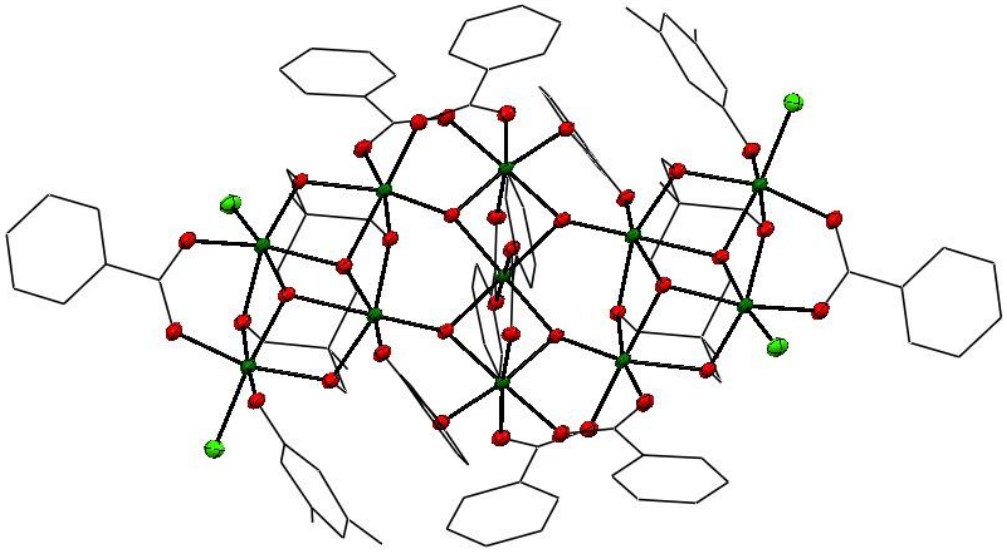

Figure 28. The core of $[NEt_4][Fe_{11}O_4(O_2CPh)_{10}(thme)_4(dmhp)_2Cl_4]$. Fe (green), O (red), Cl (light green).[125]

The complex $[Fe_{11}O_7(\mu\text{–}O_2CCMe_3)_{12}(dea)_3]Cl\cdot 5MeCN$ has been obtained by reaction of $FeCl_3\cdot 6H_2O$ with pivalic acid (Me_3CCO_2H) and **die**thanol**a**mine ($deaH_2$) in MeCN and characterized by X–ray crystallography.[92] The structure consists of an $\{Fe_{11}O_7\}^{19+}$ core, in which eleven iron atoms are linked with three μ_4–O and four μ_3–O bridges

and peripheral coordination is provided by twelve pivalates and three dea^{2-} ligands (Figure 29).

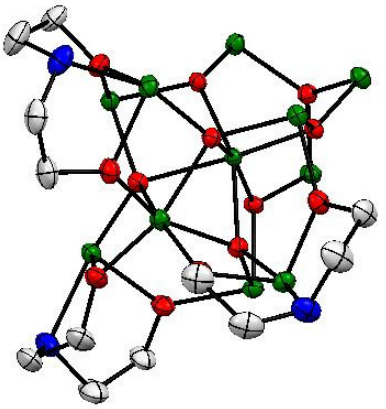

Figure 29. The core of $[Fe_{11}O_7(\mu\text{–}O_2CCMe_3)_{12}(dea)_3]Cl\cdot 5MeCN$. The Fe (green), O (red) atoms and dea^{2-} ligands (N (blue) and C (gray) are depicted, while pivalate ligands are omitted for clarity.[92]

The core possesses eight atoms with an octahedral coordination environment and three with a trigonal bipyramidal geometry. The trigonal bipyramidal coordination is provided by three different pivalates and two μ_3–O ligands.[92]

Both complexes $[NEt_4][Fe_{11}O_4(O_2CPh)_{10}(thme)_4(dmhp)_2Cl_4]$[125], (Figure 28) and $[Fe_{11}O_7(\mu\text{–}O_2CCMe_3)_{12}(dea)_3]Cl\cdot 5MeCN$[92] (Figure 29) showed single–molecule magnet behaviour.

The complex $[Fe_{11}O_3(OH)(O_2CMe)_8(thme)_2L_6]$, where L = salicyliden-2-ethanolamine, was prepared by structural agglomeration and rearrangement of trinuclear iron complex, associated with ligand substitution.[126]

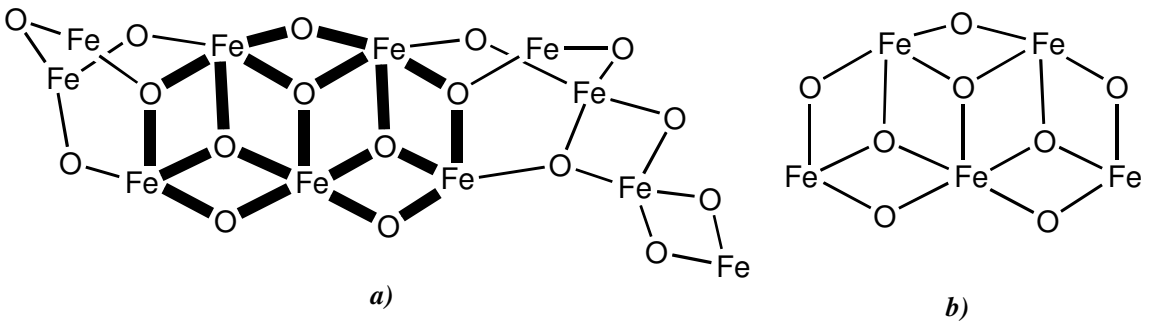

Figure 30. The $\{Fe_{11}(\mu_3\text{–}O)_6(\mu_2\text{–}O)_{11}\}^-$ core of the complex $[Fe_{11}O_3(OH)(O_2CMe)_8(thme)_2L_6]$.[126]

The structure consists of an $\{Fe_{11}(\mu_3\text{–}O)_6(\mu_2\text{–}O)_{11}\}^{-}$ core (Figure 30a), where O atoms originate from oxido, hydroxido, L^{2-} or $thme^{2-}$ ligands. The central core unit is $\{Fe_5O_8\}^{-}$ (Figure 30b), which contains three deformed cuboidal $\{Fe_3O_4\}^{+}$ units.

1.3.4.7 Dodecanuclear iron oxido complexes

The family of dodecanuclear iron complexes is numerous. Thus, complexes with a wheel–like structure,[128] those with cubane units[129] or hexanuclear iron butterfly units[121] inside a dodecanuclear iron cage have been reported. The complex $[Fe_{12}(pd)_{12}(O_2CEt)_{12}]$, with a wheel–like core (Figure 31a) resulted from the reaction of trinuclear iron carboxylates with excess 1,3-**p**ropane**d**iol (pdH_2).[128] The complex is a member of a large family of ferric wheel complexes with general formula $[Fe_x(OR)_{2x}(O_2CR)_x]$, where x = 10 or 12.[100,122,123, 130] Rearrangement of $[Fe_{12}(pd)_{12}(O_2CEt)_{12}]$ in MeCN upon addition of 2,2':6,2''-terpyridine (tpy) and $NaOCl_4$ yielded a molecular square complex $[Fe_{12}O_4(pd)_8(O_2CEt)_4(tpy)_8](ClO_4)_8$. The core consists of $\{Fe_2O(tpy)_2\}^{4+}$ ''side'' units and $\{Fe(\eta^2{:}\eta^2{:}\mu_3\text{–}pd)_2(\eta^2\text{–}O_2CEt)\}^{2-}$ ''corner'' units (Figure 31b).[128]

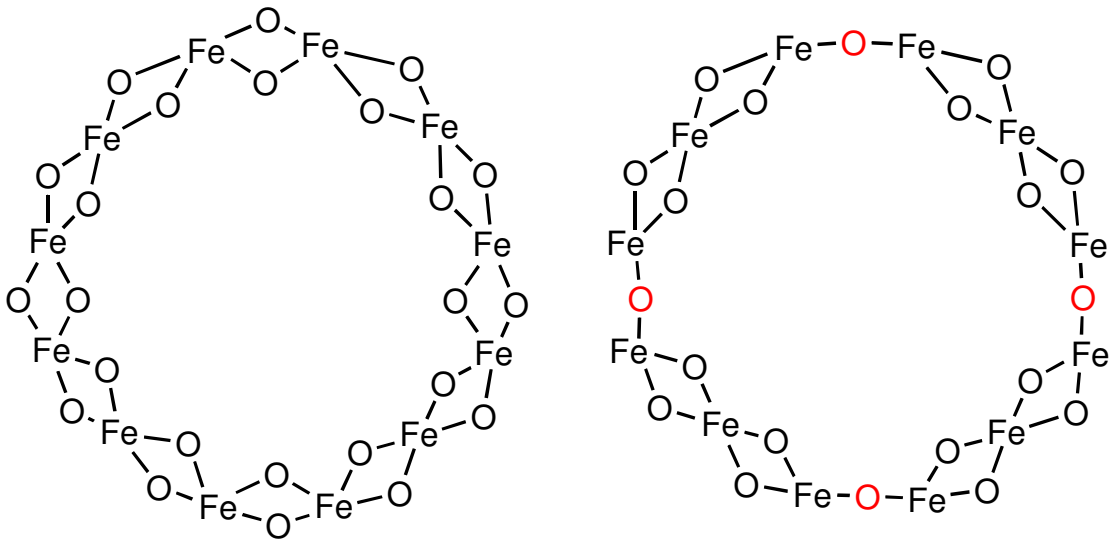

Figure 31. The cores of $[Fe_{12}(pd)_{12}(O_2CEt)_{12}]$ (a) and $[Fe_{12}O_4(pd)_8(O_2CEt)_4(tpy)_8](ClO_4)_8$ (b). Alkyl substituents are omitted.[128]

The first dodecanuclear complex with a core, which consists of a cubane unit was obtained by applying microwave–assisted synthesis (Figure 32).[129] The cubane core

unit is connected to eight iron atoms via μ_3–O^{2-}, μ_2–OH^- and η^1:η^1–μ_2–O_2CPh^- bridges.

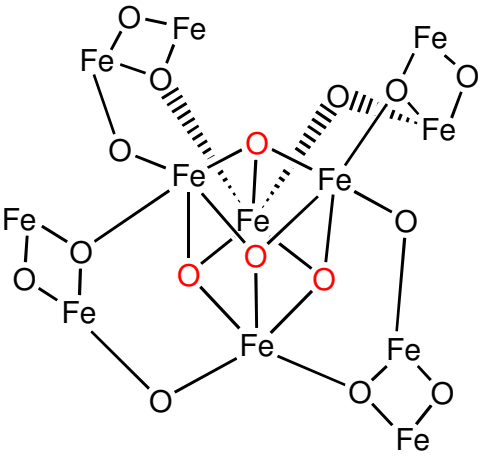

Figure 32. The core of $[Fe_{12}O_4(OH)_{12}(C_7H_5O_2)_8(C_{13}H_9N_2O_2)_4](ClO_4)_4$ with central cubane unit $\{Fe_4O_4\}^{4+}$.[129]

The reaction of trinuclear iron carboxylate $[Fe_3O(O_2CPh)_6(H_2O)_3](O_2CPh)$ with *syn*-2-**p**yridine**a**ldoxi**m**e (pamH) and NaOMe yielded the dodecanuclear complex $[Fe_{12}O_8(OMe)_2(O_2CPh)_{12}(pam)_6]$, with an unusual core topology (Figure 33).[96]

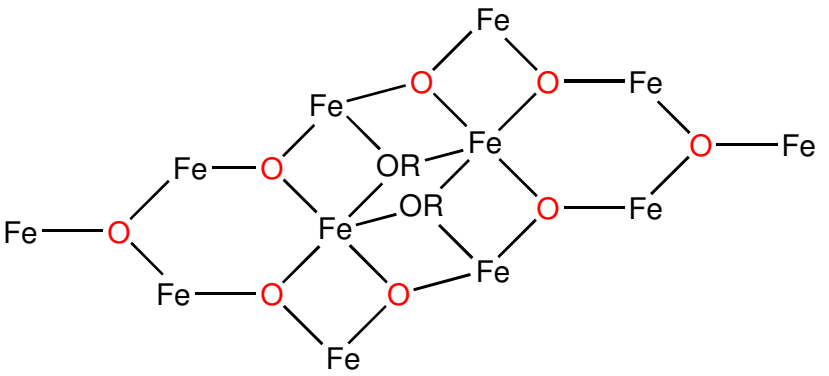

Figure 33. The core of $[Fe_{12}O_8(OMe)_2(O_2CPh)_{12}(pam)_6]$, R = Me.[96]

The central hexanuclear motif of the $\{Fe_6O_6(OR)_2\}^{4+}$ core can be described as four face–sharing partial cubanes, lacking an iron atom at one vertex, or as a hexanuclear iron ladder (see Figures 12 and 13a) with μ_3–O and μ_3–OMe bridges, above and below the ladder plane, or as four edge sharing $\{Fe_3(\mu_3\text{–}O)\}^{7+}$ units. Additionally, the central hexanuclear unit is connected via μ_3–O bridges to two $\{Fe_3(\mu_3\text{–}O)\}^{7+}$ units, resulting in a $[Fe_{12}(\mu_3\text{–}O)_8(\mu_3\text{–}OR)_2]^{18+}$ core in the form of chair.[96]

The dodecanuclear iron complexes $[Fe_{12}O_4(OH)_2(O_2CMe)_6(edte)_4(H_2O)_2](ClO_4)_4$, $[Fe_{12}O_4(OH)_8(edte)_4(H_2O)_2](ClO_4)_4$ and $[Fe_{12}O_4(OH)_8(edte)_4(H_2O)_2](NO_3)_4$ were prepared by reaction of N,N,N',N'-tetrakis(2-hydroxyethyl)ethylenediamine ($edteH_4$) with $Fe(ClO_4)_3 \cdot 6H_2O$ or $Fe(NO_3)_3 \cdot 9H_2O$ and $NaO_2CMe \cdot 3H_2O$. The complexes are composed of the same core $[Fe_{12}(\mu_4\text{–}O)_4(\mu\text{–}OH)_2(O_2CMe)_4(\mu_3\text{–}OR)_4(\mu\text{–}OR)_{12}]^{2+}$ (Figure 34). The acetate ligands are replaced with hydroxido ones in the $[Fe_{12}O_4(OH)_8(edte)_4(H_2O)_2](ClO_4)_4$ and $[Fe_{12}O_4(OH)_8(edte)_4(H_2O)_2](NO_3)_4$ cores.[110]

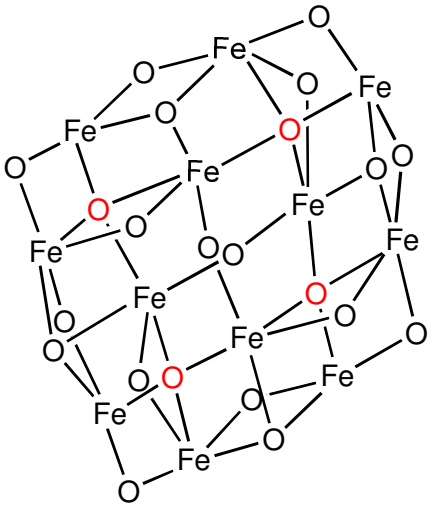

Figure 34. The central fragment of the $[Fe_{12}O_4(OH)_2(O_2CMe)_6(edte)_4(H_2O)_2](ClO_4)_4$ core. Alkyl residues are omitted for clarity.[110]

Four iron atoms of the core are seven–coordinate and eight are six–coordinate. The whole core structure can be described as two near–planar hexanuclear iron layers between three almost planar oxygen layers. Four μ_4–O bridges connect all twelve iron atoms.[110]

The dodecanuclear iron core (Figure 35) with two hexanuclear iron units bridged by two bicine ligands, has been found in the complex $[Fe_{12}O_4(bic)_4(Hbic)_4(O_2CCMe_3)_8] \cdot 5MeCN$, where bic^{3-} and $Hbic^{2-}$ are deprotonated N,N-**bis**(2-hydroxyethyl)gly**cine** (H_3bic or bicine).[108]

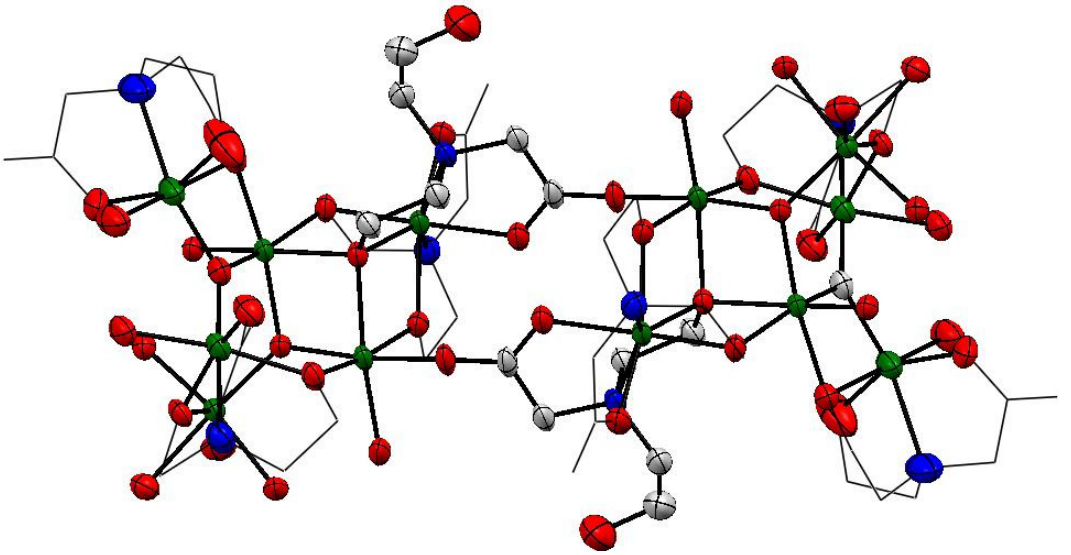

Figure 35. The core of $[Fe_{12}O_4(bic)_4(Hbic)_4(O_2CCMe_3)_8]\cdot 5MeCN$. Fe (green), O (red), C (gray), N (blue). H and C atoms from carboxylate are omitted for clarity.[108]

Rearrangement of a pentanuclear iron complex by ligand substitution yielded a dodecanuclear complex $[Fe_{12}O_4(O_2CMe)_8(thme)_2(NH_2(CH_2)_2O)_2(L')_6]$, where L' = (2-hydroxyethyl)[1-(2-hydroxyphenyl)-ethylidene]amine. The $\{Fe_{12}O_{18}\}$ core contains a central fragment $\{Fe_4O_6\}$ (Figure 36).[126]

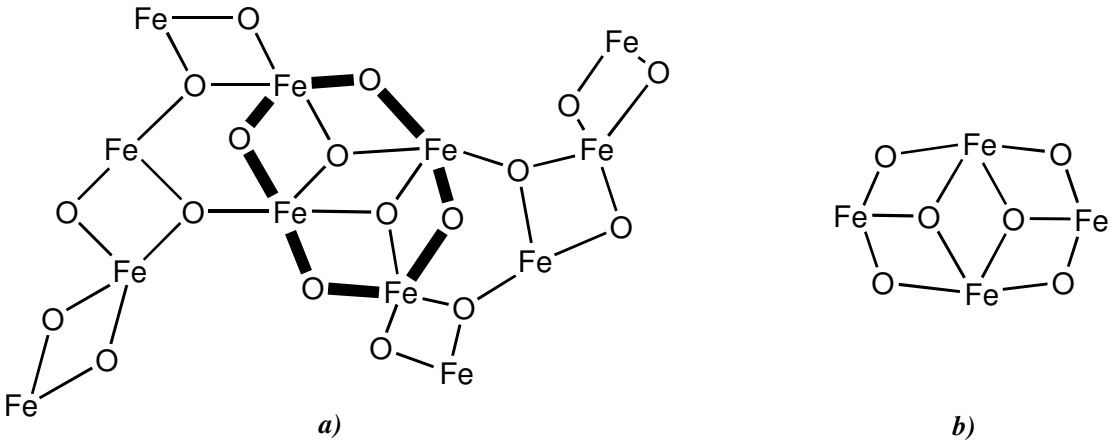

Figure 36. The core of $[Fe_{12}O_4(O_2CMe)_8(thme)_2(NH_2(CH_2)_2O)_2(L')_6]$ (a), with core central fragment $\{Fe_4O_6\}$ (b).[126]

Two structurally analogous dodecanuclear iron complexes $[Fe_{12}(\mu_2\text{–}O)_4(\mu_3\text{–}O)_4(O_2CCHPh_2)_{14}(tbpa)_6]$ and $[Fe_{12}(\mu_2\text{–}O)_4(\mu_3\text{–}O)_4(O_2CPh)_{14}(cpa)_6]$, with phosphonate ligands: **c**amphyl **p**hosphonic **a**cid ($cpaH_2 = C_{10}H_{17}PO_3H_2$) and 4-***tert*-butylphenyl **p**hosphonic **a**cid ($tbpaH_2 = 4\text{-}^tBuPhPO_3H_2$), have been recently reported.

Their cores can be described as two hexanuclear Fe overlapped ''butterflies'' or face–to–face hexanuclear Fe butterfly units sharing four phosphonates and two carboxylate ligands.[121]

A few isostructural mixed–valent dodecanuclear iron oxido complexes have been synthesized. Complexes $[Fe^{III}_4Fe^{II}_8O_2(OMe)_{18}(OAc)_6(MeOH)_4]$, $Li_2[Fe^{III}_2Fe^{II}_{10}O_2(OMe)_{14}(OAc)_{10}(MeOH)_2]$ and $[Fe^{III}_4Fe^{II}_8O_2(OMe)_{14}(O_2CCH_2Cl)_{5.3}Cl_{0.7}(OMe)_{18}(MeOH)_4]$, with an Fe/O backbone depicted in Figure 37, have been investigated as possible models for a ferritin core.[131–133] The oxidation state of iron atoms was assigned as trivalent or divalent on the basis of charge and bond length considerations.

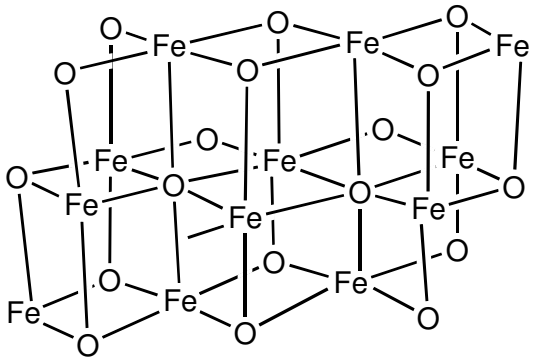

Figure 37. The Fe/O backbone of the dodecanuclear mixed–valent iron complexes.

The key role in the core structure is played by two μ_6–oxido atoms which connect ten of twelve iron atoms.

1.3.4.8 Tridecanuclear iron oxido complexes

Two similar tridecanuclear iron oxido complexes $[Fe_{13}O_6(OH)_6(H_2O)_6(Hntp)_8]^{5+}$ and $[Fe_{13}O_6(OH)_6(Hntp)_8]^{5+}$ have been synthesized as part of one aggregate $[\{Fe_{13}O_6(OH)_6(H_2O)_6(Hntp)_8\}\{Fe_{13}O_6(OH)_6(Hntp)_8\}_2]\cdot 15NO_3\cdot 13H_2O$ using **n**itrilo**t**ri-**p**ropionic acid (H_3ntp) (Figure 38).[134]

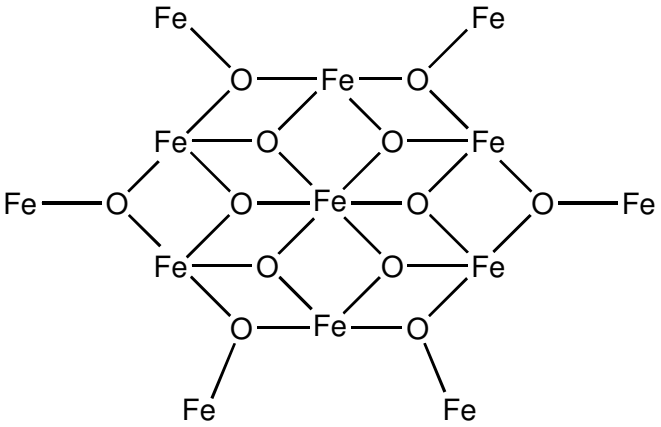

Figure 38. The core of complexes $[Fe_{13}O_6(OH)_6(H_2O)_6(Hntp)_8]^{5+}$ and $[Fe_{13}O_6(OH)_6(Hntp)_8]^{5+}$.[135]

1.3.4.9 Tetradecanuclear iron oxido complexes

The tetradecanuclear complex $[Fe_{14}(\mu_3\text{–}O)_4(O_2)_2(O_2CBu^t)_{12}(PhPO_3)_8(H_2O)_{12}](NO_3)_2$ (Figure 39) has been synthesized in the reaction of trinuclear iron *tert*-butyl-carboxylate and phenyl phosphonic acid ($PhPO_3H_2$).[112,135]

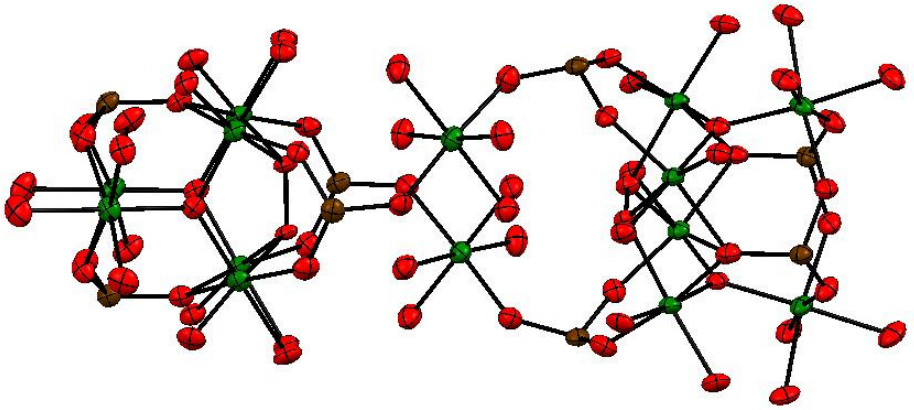

Figure 39. The structure of $[Fe_{14}(\mu_3\text{–}O)_4(O_2)_2(O_2CBu^t)_{12}(PhPO_3)_8(H_2O)_{12}](NO_3)_2$. C and H atoms are omitted for clarity.[112,135]

1.3.4.10 Hexadecanuclear iron oxido complexes

A hexadecanuclear iron complex $[Fe_{16}(EtO)_4(O_2CPh)_{16}(Hthme)_{12}](NO_3)_4$, with wheel–like core (Figure 40), has been recently prepared.[93]

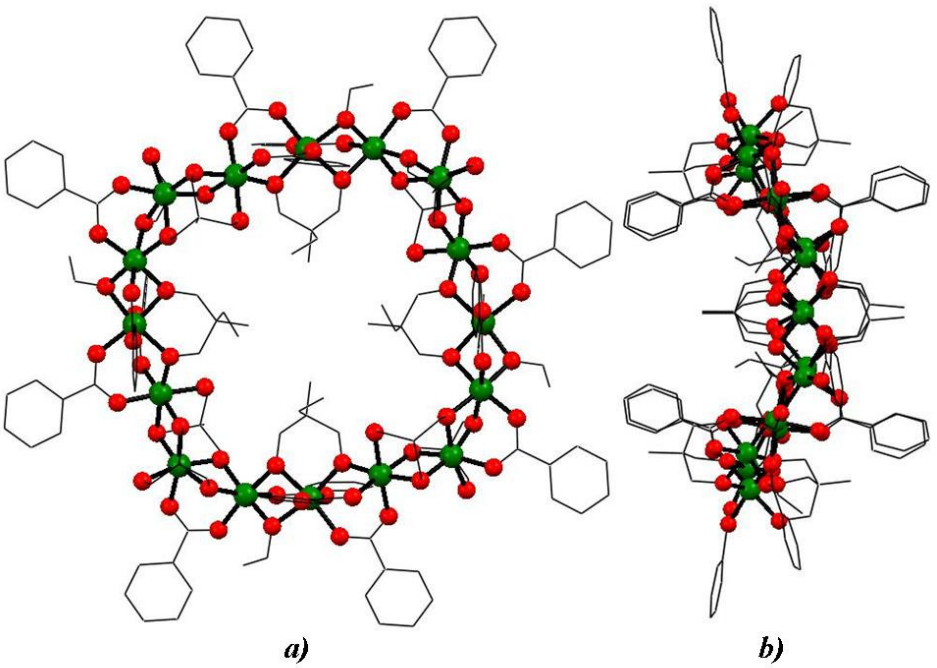

Figure 40. The structure of $[Fe_{16}(EtO)_4(O_2CPh)_{16}(Hthme)_{12}](NO_3)_4$ complex (a) and its side view (b).[93]

1.3.4.11 Heptadecanuclear iron oxido complexes

For the first time, a heptadecanuclear iron complex was crystallographically characterized as part of a cell unit, which consist of two cations: $[Fe_{17}O_4(OH)_{16}(heidi)_8(H_2O)_{12}]^{3+}$ (Figure 41) and $[Fe_{19}O_6(OH)_{14}(heidi)_{10}(H_2O)_{12}]^{+}$ (Figure 42) , four NO_3^- anions and 60 water molecules.[136] The complex was obtained by reaction of (2-**h**ydroxy**e**thyl)**i**mino**di**acetic acid (H_3heidi) with iron(III) nitrate nonahydrate in water/pyridine mixture.

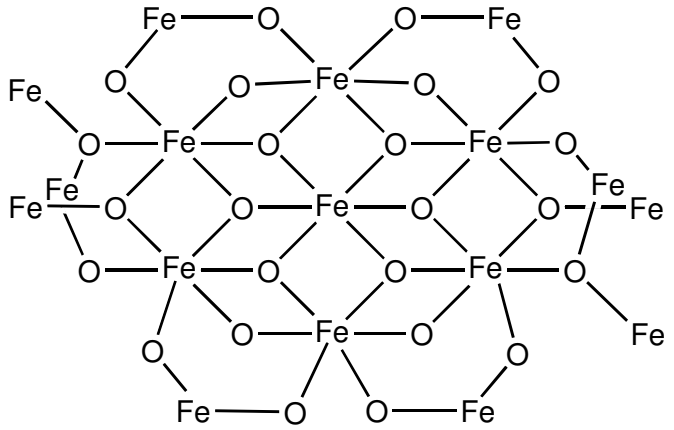

Figure 41. The core of the complex $[Fe_{17}O_4(OH)_{16}(heidi)_8(H_2O)_{12}]^{3+}$.[136]

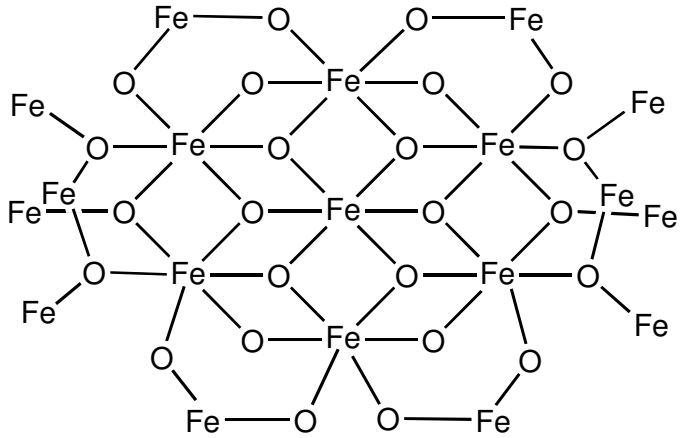

Figure 42. The core of the complex $[Fe_{19}O_6(OH)_{14}(heidi)_{10}(H_2O)_{12}]^{+}$.[136]

Earlier, a mixed–valent heptadecanuclear iron oxo complex $[Fe^{III}_{16}Fe^{II}O_{10}(OH)_{10}(O_2CPh)_{20}]$ was obtained by rearrangement of a mixed–valent trinuclear iron precursor, resulting in a low to a modest yield.[137]

1.3.4.12 Octadecanuclear iron oxido complexes

Octadecanuclear iron oxido complex $[Fe_{18}O_8(OH)_2(O_2CBu^t)_{28}(heen)_4]\cdot C_5H_{12}\cdot CH_2Cl_2$, was synthesized using N,N'-bis(2-**h**ydroxy**e**thyl)**e**thylenediami**n**e ($heenH_2$). The core of the structure contains rhombic $\{Fe_2O_2\}^{2+}$ units interconnected in the form of a ''molecular chain'' (Figure 43).[138]

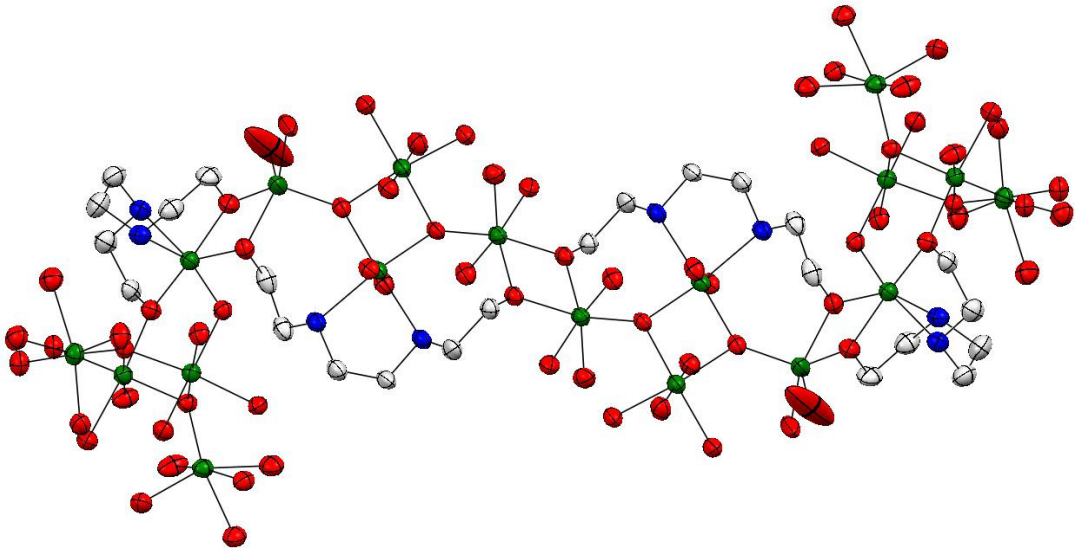

Figure 43. The structure of $[Fe_{18}O_8(OH)_2(O_2CBu^t)_{28}(heen)_4]\cdot C_5H_{12}\cdot CH_2Cl_2$. Fe (green), C (grey), O (red) and N (blue) atoms are depicted, while H atoms and *tert*-butil groups are omitted for clarity.[138]

One of the largest molecular wheels has been described for the isostructural complexes $[Fe_{18}(O_2CPh)_6(pd)_{12}(pdH)_{12}(NO_3)_6](NO_3)_6$ and $[Fe_{18}(OH)_6(OMe)(xdk)_6(O_2CMe)_{12}]$, where pdH_2 = 1,3-**p**ropane**d**iol and xdk = *m*-**x**ylene**d**iamine bis (**K**emp's triacide imide) dianion (Figure 44).[139]

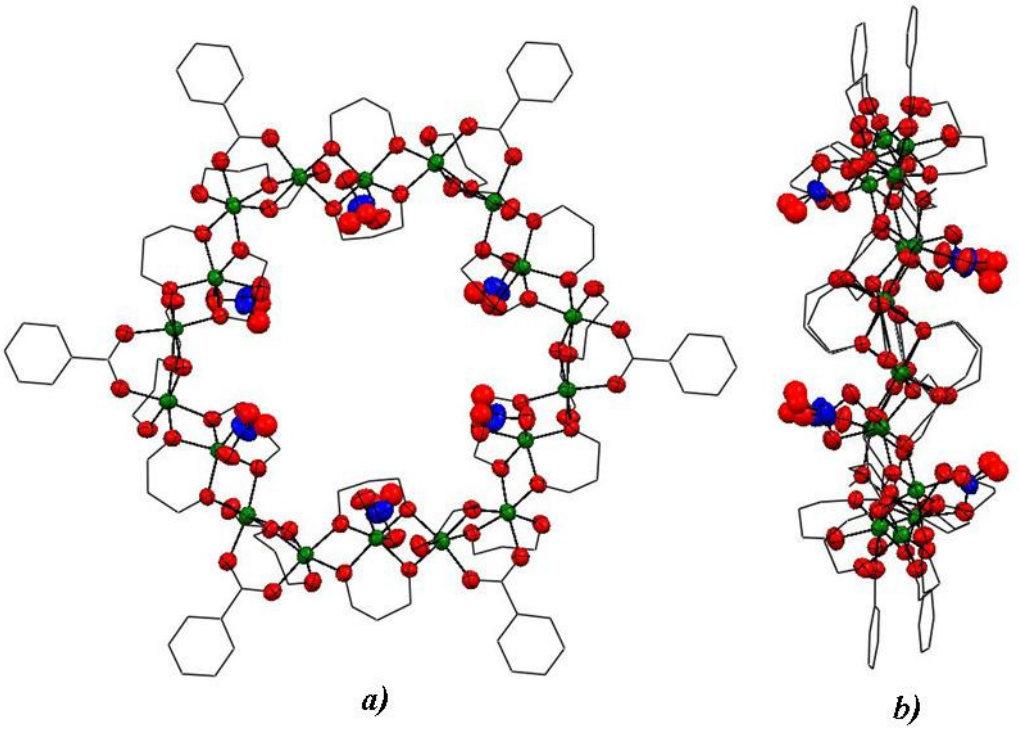

Figure 44. The structure of $[Fe_{18}(O_2CPh)_6(pd)_{12}(pdH)_{12}(NO_3)_6](NO_3)_6$ (a) and its side view (b). Fe (green), C (grey), O (red) and N (blue) atoms are depicted.[139]

1.3.4.13 Nonadecanuclear iron oxido complexes

The complexes of this nuclearity are very rare, only one has been published as part of a cell unit, which consists of two cations: $[Fe_{17}O_4(OH)_{16}(heidi)_8(H_2O)_{12}]^{3+}$ and $[Fe_{19}O_6(OH)_{14}heidi)_{10}(H_2O)_{12}]^{+}$ (Figure 42), four NO_3^- anions and 60 water molecules.[136]

1.3.5 Iron oxido complexes with very high nuclearity (Fe_{20}, Fe_{22}, Fe_{28})

A first example of icosanuclear iron oxido complex $[Fe_{20}O_{14}(tris)_2(tris\text{-}CO)_2(C_6H_{11}CO_2)_{24}]\cdot 2MeCN$, where tris = 2-[bis(2-hydroxyethyl)amino]-2-(hydroxymethyl)propane-1,3-diol and tris-CO = 4,4-bis(hydroxymethyl)-1,3-oxazolidin-2-one, has been published as a coordination polymer. The complex was obtained by solvothermal method (MeCN/dmf, 85 °C) using ligand 2-[bis(2-hydroxyethyl)amino]-2-(hydroxymethyl)propane-1,3-diol (bis-tris). The tris and tris-CO ligands were generated *in situ* by transformation of bis-tris after capture of atmospheric CO_2. The complex contains 12 six–coordinate, 6 five–coordinate and 2 four–coordinate iron(III) atoms joined by 14 μ_3–O bridges, 24 cyclohexanecarboxylates, 2 $tris^{2-}$ and 2 $tris\text{-}CO^{2-}$ ligands. The core can be described as a decanuclear iron wheel (Fe_{10}) centered by an open dicubane unit (Fe_4) and linked by two trinuclear iron oxido units (Figure 45).[140]

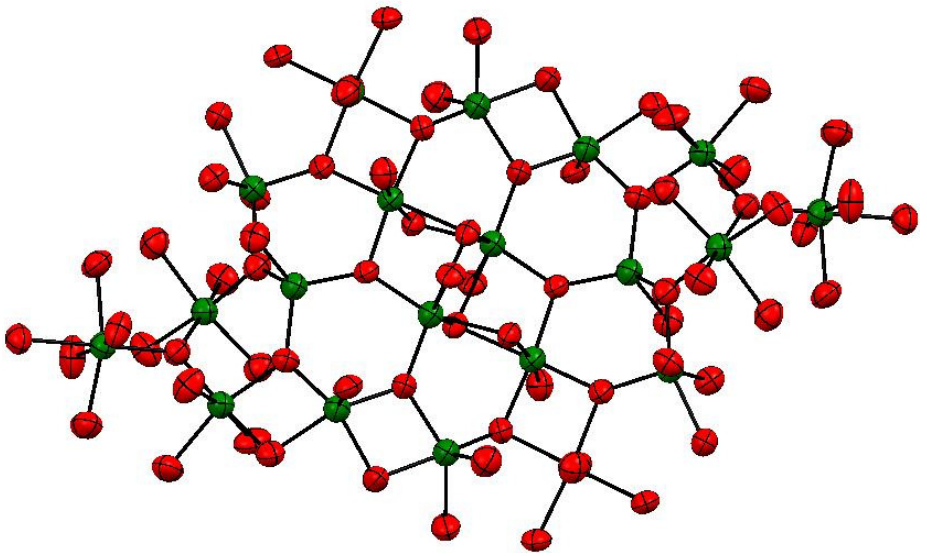

Figure 45. The core of $[Fe_{20}O_{14}(tris)_2(tris\text{-}CO)_2(C_6H_{11}CO_2)_{24}]\cdot 2MeCN$. The iron and oxygen atoms are coloured in green and red, respectively. C and H atoms are omitted for clarity.[140]

The complex $[Fe_{22}O_{14}(OH)_3(O_2CMe)_2(mda)_6](ClO_4)_2{\cdot}4H_2O{\cdot}4EtOH{\cdot}4Et_2O$ has been obtained by reaction of $FeCl_3$ with NaO_2CMe and *N*-**m**ethy**d**iethanol**a**mine ($mdaH_2$) after recrystallization from an appropriate solvent mixture. The core can be described as a hexanuclear subunit, which connects two octanuclear subunits. The hexanuclear subunit consists of a tetranuclear cubane subunit which is connected to two five–coordinate iron atoms (Figure 46).[141]

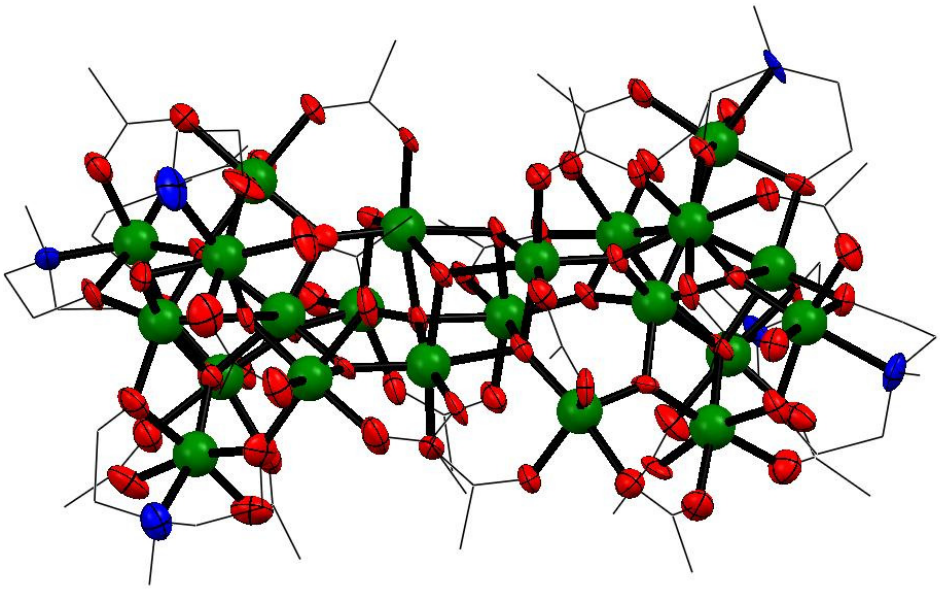

Figure 46. The structure of $Fe_{22}O_{14}(OH)_3(O_2CMe)_2(mda)_6](ClO_4)_2{\cdot}4H_2O{\cdot}4EtOH{\cdot}4Et_2O$.[141] Fe (green), O (red), N (blue) atoms are colored for clarity.[141]

The largest current enantiomeric ferric wheels $K_2Na_{18}[Fe_{28}O_8(tart)_{16}(CH_3COO)_{24}]{\cdot}29H_2O$ were prepared by reaction of iron(III) nitrate and L– or D–tartaric acid (tart) (Figure 47).[142]

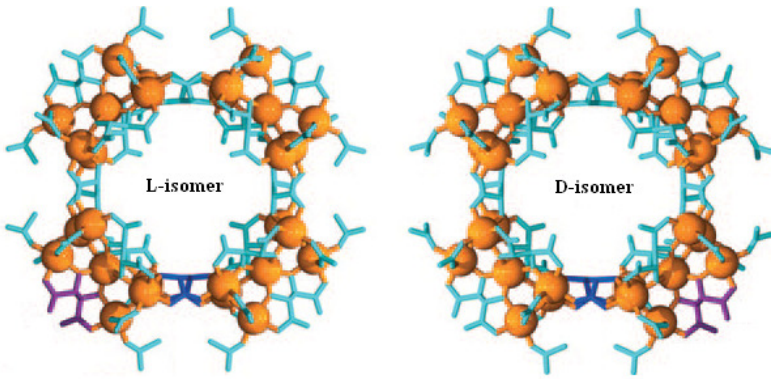

Figure 47. The structure of enantiomerically pure chiral $K_2Na_{18}[Fe_{28}O_8(tart)_{16}(CH_3COO)_{24}]{\cdot}29H_2O$.[142] Reused by permission of John Wiley & Sons, Inc.

The four heptanuclear subunits are interconnected with four tartate ligands building a $[Fe_{28}O_8(tart)_{16}(CH_3COO)_{24}]^{20-}$ anion. Heptanuclear subunits consist of one iron atom sandwiched by two trinuclear iron oxido–subunits.

1.4 Antiproliferative therapeutics – an overview

The majority of active compounds, which are used as therapeutics in medicine and pharmacy, are discovered serendipitously; one discovery induces another. It is difficult to make one clear classification of anticancer therapeutics due to their variations in chemical and structural nature and the various mechanisms of action. In this section, an insight into some approaches of anticancer therapy will be given.

One approach consists of employing an appropriate compound to act directly on the *DNA–chain* or on the *protein mechanisms (systems),* which participate in packaging, transcription regulation, replication, recombination and repair of DNA or on *enzymes* which are involved in synthesis or chain reorganization of DNA. Inhibition of these mechanisms, leads to apoptosis of the cell. A number of attempts have been undertaken to increase selectivity of the drugs effect on DNA chains. Therefore, drugs with various mechanisms of action have been developed (intercalators, cross linkers, code readers, minor and major groove inhibitors) able to interact with DNA, proteins or enzymes, and inhibit important processes during cell mitosis (Figure 48).[143]

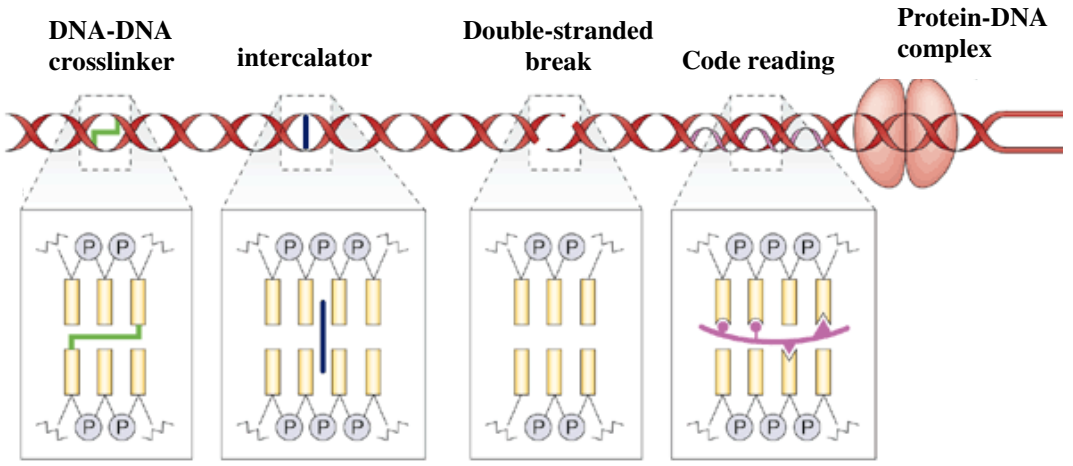

Figure 48. The DNA helix associated with proteins and the types of modifications that can occur on DNA (from left to right): crosslinks, intercalation, DNA–strand cleavage and code reading molecules.[143] Reused by permission of Nature Publishing Group.

The most active agents which are often used in clinical treatment of cancer are DNA targeting agents. On the other hand, their toxicity is high and selectivity is low. Nowadays, a trend in cancer therapeutic research is to find molecular targets in cancer cells in order to decrease toxic effects on healthy cells.[143]

By investigating soldier's symptoms after exposure to nitrogen–mustard gas (1,5-dichloro-3-thiapentane), it was found that such alkylating compounds inhibit the growth of cells with high proliferative rates (epithelial–gastrointestinal and bone–marrow cells). Selectivity of alkylating agents was based on dependence on quantitative differences in the division rates between cancer and normal cells. The era of alkylating anticancer therapeutics gave two agents *chlorambucil* and *melphalan,* which showed efficiency against chronic lymphocytic leukemia, multiple myeloma and ovarian cancer. Alkylating agents interact non–specifically with DNA, the most effective agents act as inter– or intrastrand DNA–crosslinkers (Figure 48).[143,144]

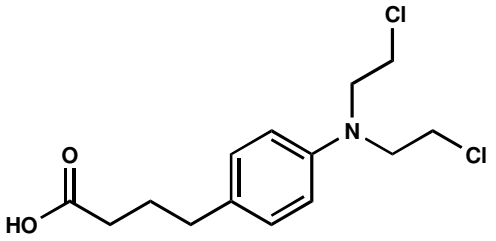

Chlorambucil

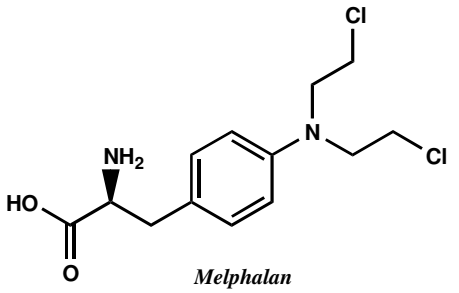

Melphalan

New generations of anticancer drugs are based on improved antibiotics. *Doxorubicin, actinomycin D* and *bleomycin* showed significant activity against cancer cells. They have been used in cancer treatment, and particularly, of testicular, breast, endometrial, cervical cancer and non–Hodgkin's lymphoma as well as soft–tissue, rhabdomyo–, Ewing's sarcomas and Wilm's tumours.[143]

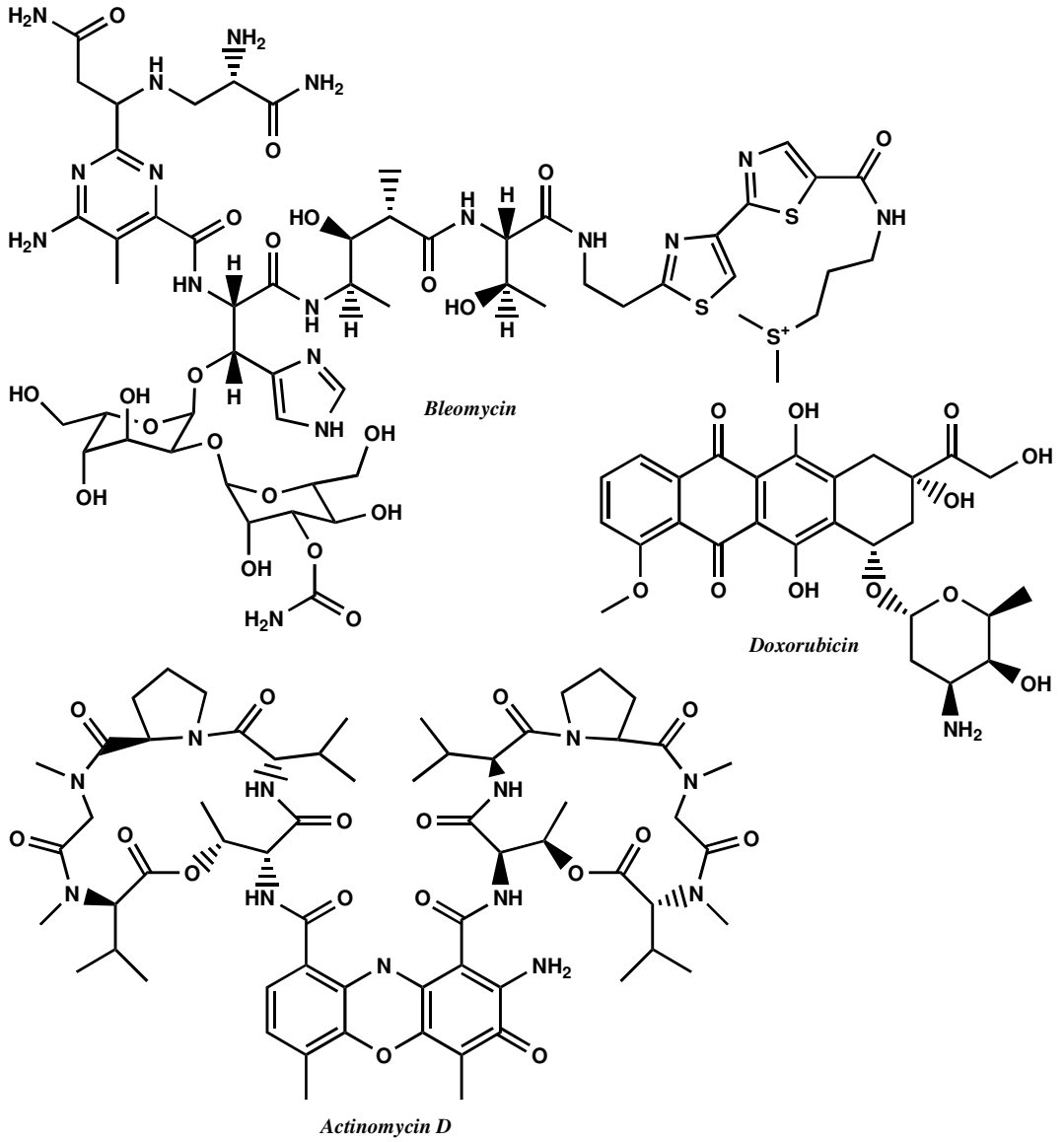

The differences in their structures are presumably responsible for the different mechanisms of action. *Bleomycin* causes double–strand DNA breaks while *doxorubicin*, as a non specific DNA–intercalating agent, induces protein–associated strand breaks by trapping topoisomerase II, covalently bound to DNA. *Actinomycin D* acts as an inhibitor in the RNA synthesis and DNA intercalator. Agents with multiple mechanisms of action are preferred in cancer treatment compared to those which have just a single mode of action.[143]

Actinomycin D awakened interest in the design of small molecules which could recognize DNA and act as code reading agents, which are able to bind to the minor or major grooves of DNA.

Netropsin and its relative *distamycin* are two peptide antibiotics which ''recognize'' and bind to the minor groove of DNA.[143]

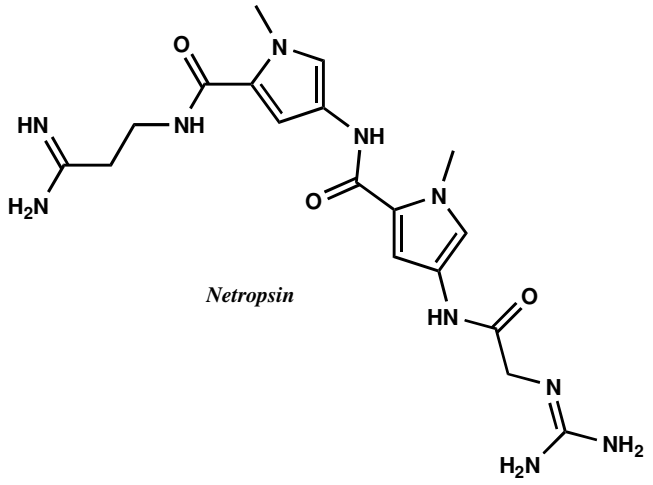

Netropsin

Oligonucleotides are able to bind to the major DNA groove and form a triple helix, targeting homopurine–homopyrimidine pair of DNA.[145]

The drugs, *topotecan*, *irinotecan* and its derivative *SN–38* (inhibitors of topoisomerase I), *mitoxantrone* (inhibition of topoisomerase II), which affect enzymes, and block their access to DNA are employed against ovarian, cervical, colon cancer.

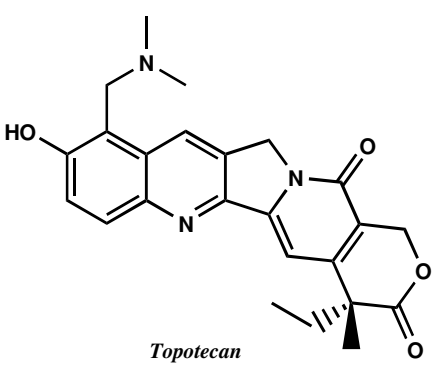

Topotecan

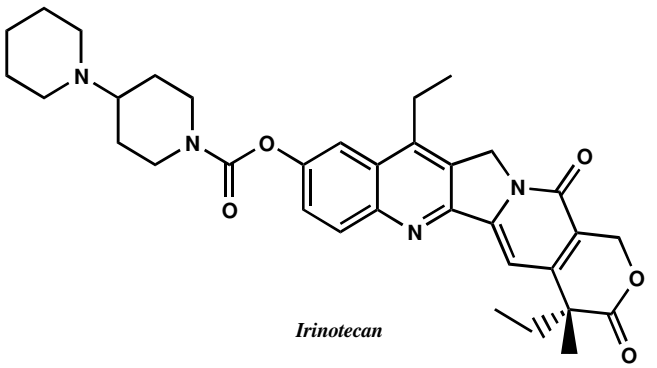

Irinotecan

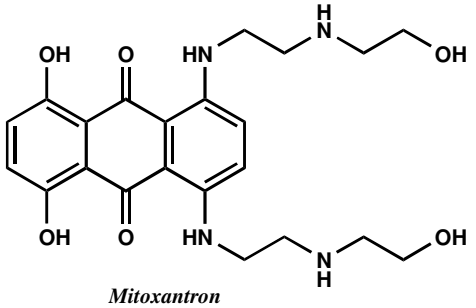

Mitoxantron

With the remarkable discovery of the cytotoxic activity of *cis*-diamminedichloridoplatinum(II) (*cisplatin*) by Barnet Rosenberg in the 1960's and the beginning of its clinical application in 1978 started a new era in the campaign against cancer. Cisplatin binds covalently to guanine in DNA leading to distortion of the strand and inhibition of the binding protein system. Cisplatin is widely used in Europe and showed good results in the treatment of testicular, ovarian and lung cancer. A clinical application of second generation of platinum drugs: *carboplatin* and *oxaliplatin* started in 1989 and 2004, respectively. They have similar mechanisms of action to alkylating agents. The formation of inter– and intra–strand crosslinks in DNA results in inhibition of DNA replication and transcription.

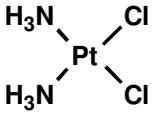

Cisplatin

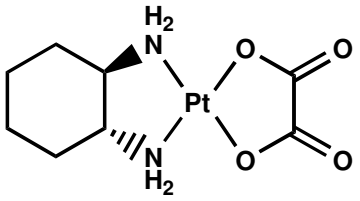

Oxaliplatin

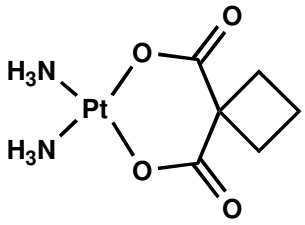

Carboplatin

A wide variety of ruthenium complexes with antineoplastic properties are known, but *NAMI–A*, *KP(418*, *1019 and 1339)* and *RAPTA–C* developed by Sawa *et al.*, Keppler *et al*., and Dyson *et al.*, respectively, seemed to be most prominent due to their remarkable *in vitro* and *in vivo* antiproliferative activity. The compounds, KP1019 and NAMI–A, are already in the phase I–II clinical trials and tend to be good candidates in the future campaign against cancer due to reduced side effects compared to platinum anticancer drugs.[146]

Simultaneously, KP1339, the precursor in the synthesis of KP1019, was selected for clinical investigation due to the possibility of application of higher doses in cancer treatment because of better water solubility. KP1339 has shown promising results in

phase I clinical investigation and its anticancer efficiency will be tested further in phase II clinical trials.[146]

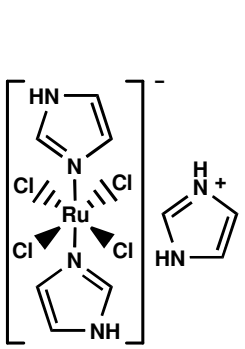

KP418

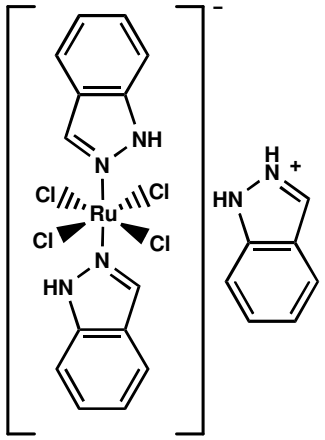

KP1019

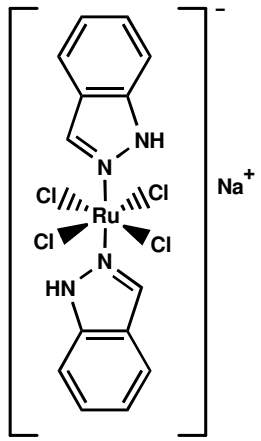

KP1339

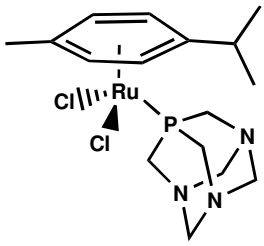

RAPTA-C

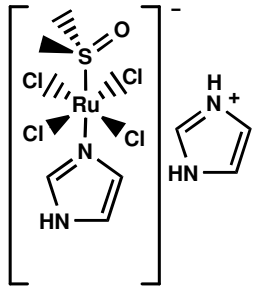

NAMI-A

KP1019 and KP1339 displayed activity against solid tumors, while NAMI–A possesses antimetastatic activity. The mechanism of action of Ru–anticancer agents is not fully understood, but one possible explanation has been given for KP1019 and KP1339. The compounds enter into the tumor cells via transferin or albumin and after activation in the cell arrest the ''mitochondrial pathway'' and inhibit superoxide dismutase (SOD) and protein GBR78, what leads to cell apoptosis.[147]

1.4.1 Thiosemicarbazones and their derivatives – Anticancer activity

Interest for the thiosemicarbazones (TSCs), as potent anticancer agents, has appeared in the 1950's, due to their capability, particularly, *p-aminobenzaldehyde-3-thiosemicarbazone*, to inhibit virus multiplication, which involves synthesis of nucleoproteins. [148] The first serious results, concerning the cytotoxic effect of thiosemicarbazones, were reported, using heterocyclic TSC, in the publications of Brockmann *et al.* (1956). [149] From a few compounds, *2-formylpyridine thiosemicarbazone* possessed the strongest activity against leukemia cells. French *et al*. (1970) and Sartorelli *et al*. (1992) developed a second generation of more effective α-N-heterocyclic thiosemicarbazones, *5-hydroxy-2-formylpyridine thiosemicarbazone (5–HP)* and *3-aminopyridine-2-carboxaldehyde thiosemicarbazone (Triapine or 3–AP)*, respectively.[150,151]

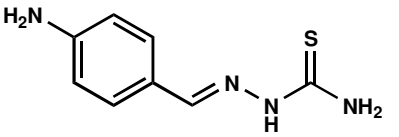

p-aminobenzaldehyde thiosemicarbazone

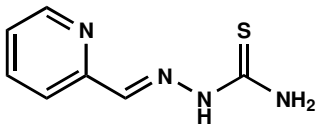

2-formylpiridine thiosemicarbazone

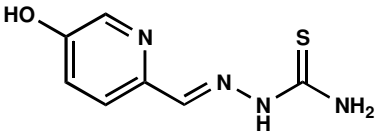

5-HP

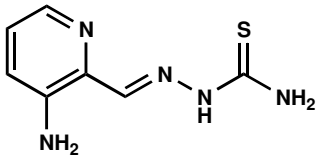

Triapine

5–HP has reached phase I in clinical trials. However, 5–HP caused gastrointestinal and hematological toxic effects. After application, in the body, half to three quarters of the administered dose were excreted within 24 h. The majority of excreted metabolites were inactive glucuronide conjugates.[152,153] These facts have prevented further clinical investigation of 5–HP.

The most promising member of this family, 3-aminopyridine-2-carboxaldehyde thiosemicarbazone (Triapine), showed remarkable activity against hematological tumors and underwent several phase I and II clinical trials, as described elsewhere.[153–155] Triapine was used alone or in combination with other drugs and treatment gave mixed results.[153,156,157] A limitation of the therapeutic potential of Triapine is caused

by its considerable side effects and poor water solubility. This is the reason for further investigation of new anticancer candidates with improved physico–chemical and biomedical properties.[158]

Generally, 2-formyl-, 2-acetyl-, 2-benzoylpyridine TSCs, and their complexes have been extensively studied, while much less attention has been given to those derived from salicyl or benzaldehyde TSCs derivatives. Attachment of bulky groups at the terminal nitrogen of TSCs, resulted in a considerable increase of cytotoxic activity.[159]

Salycilaldehyde thiosemicarbazone (STSC) showed moderate cytotoxicity, which can also be increased by attaching polar, electron–donating substituents to the salicylaldehyde and thiosemicarbazide moieties or by chelating with transition metals, leading to more potent compounds.[160,161]

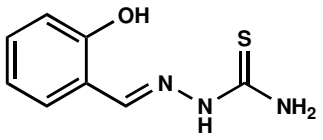

STSC

The ability of TSCs to coordinate metal ions is well known. Coordination occurs via N, N, S or O, N, S donor atoms (Scheme 4).

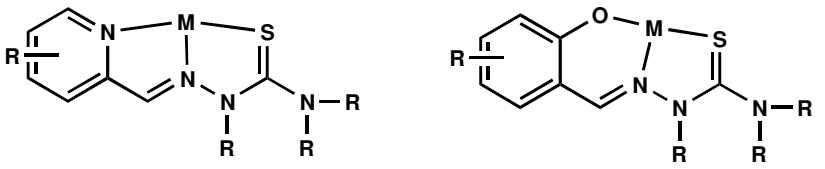

M^{+}: Re
M^{2+}: Mn, Fe, Ni, Cu, Zn, Ru, Pd, Pt, Cd, Hg, Pb
M^{3+}: Al, Fe, Co, Ru, Au, Tl, Ga, Bi, Sb
M^{4+}: Sn
M^{5+}: V
M^{6+}: U

M^{2+}: Ni, Cu, Zn, Pd, Pt
M^{3+}: Cr, Fe, Co, Rh, Ru, Ir
M^{4+}: V, Mn, Sn
M^{5+}: V
M^{6+}: Mo

Scheme 4. Coordination mode of some TSCs. R = H, CH_3, phenyl or other aliphatic and aromatic groups.[153]

TSCs are strong chelating ligands, not only for essential metals such as iron, copper or zinc, but also for other transition metals. More than 800 structurally characterized

analogs of α-pyridyl and salicylaldehyde TSCs, as well as their metal complexes have been documented.[153] Lipophilicity and chelation of TSCs are strongly linked with their biological activity.[153,161] Essential transition metals, such as iron, copper and zinc are important for cell growth. It is generally accepted, that tumor cells are more sensitive to iron deprivation than normal cells.[162] Metal complexes of TSCs, particularly, iron and copper complexes, have shown better cytotoxic effects than metal–free TSCs alone.[163–166]

Simultaneously with the synthesis of new TSCs and their metal complexes, their mode of action has been investigated. Numerous studies have been performed on the impact of TSCs and their complexes on two enzymes, ribonucleotide reductase (RR)[152,163] and topoisomerase IIα (Topo–IIα).[158,167] These were identified as possible target molecules, because the increased cytotoxicity, in major cases, can not be explained only by the differences in lipophilicity or by coordination to metal.

As have been published elsewhere, thiosemicarbazones, particularly Triapine, act as inhibitors of ribonucleotide reductase (RR).[152,163] A tumor growth is manifested by higher expression of RR, therefore, RR can be considered as a target molecule.[152] RR is an important enzyme, which generates deoxyribonucleotides, a crucial precursors, for DNA replication and repair. The substrate binding sites, polythiol moieties and tyrosyl radical–diiron center are placed in the two homodimeric subunits, R1 and R2, respectively (Figure 49).[168]

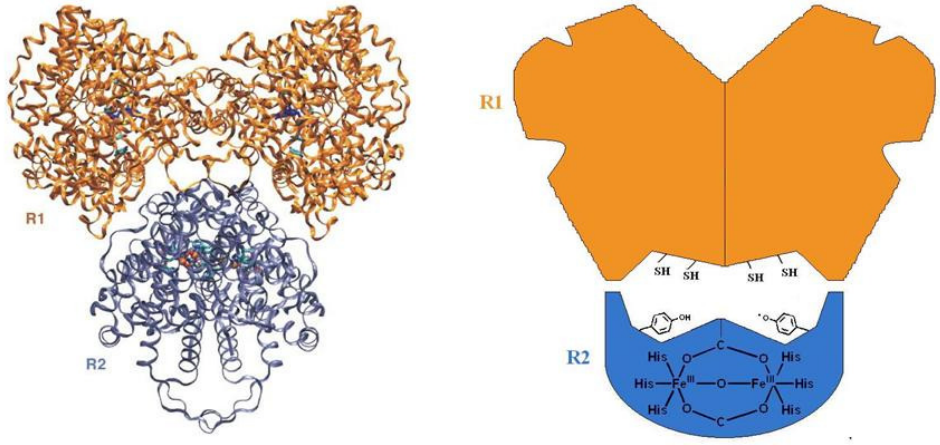

Figure 49. The molecular structure of RR (left) and graphical representation of RR (right).[168] Reused by permission of Elsevier.

The R2 unit of RR posses 80% sequence homology with the p53R2 protein, which also participates in DNA repair by supplying deoxynucleotide triphosphates in the p53–dependent manner. [169,170]

Inhibition of RR function leads to cell apoptosis, possible in a few ways: by destroying the tyrosyl radical using radical scavengers (hydroxyurea), by removing the iron center or, indirectly, by quenching the tyrosyl radical via chelating agents (desferrioxamine), and by inhibition of the substrate binding site via nucleoside and nucleotide analogues (gemcitabine, cytarabine, fludarabine).[171]

The inhibitory mechanism of RR by Triapine is based on the formation of intracellular complexes with the diiron centre of RR. Production of such complexes may cause formation of reactive oxygen species (ROS), which destroy the tyrosyl radical. Therefore, Triapine showed a 100 to 1000 fold increase of RR inhibition potency compared to hydroxyurea.[169] Recently, it has been shown that the cytotoxic activity of Triapine increases with coordination to iron. Iron complexes of Triapine exhibit a similar mode of RR inhibition by formation of ROS and destruction of the tyrosyl radical of RR.[169]

Thiosemicarbazones as iron chelators take part in iron homeostasis and block important iron pathways, producing ROS. Production of ROS was explained by Haber and Weiss after Fenton's discovery of the strong oxidative effects of Fe^{2+} and H_2O_2 on some organic substrates. Formation of ROS mediated by iron is represented in Scheme 5. [146] Other metal ion pairs: copper (Cu^{2+}/Cu^{+}), cobalt (Co^{3+}/Co^{2+}) or vanadium (V^{5+}/V^{4+}) can be involved in the production of ROS, following the same scheme.

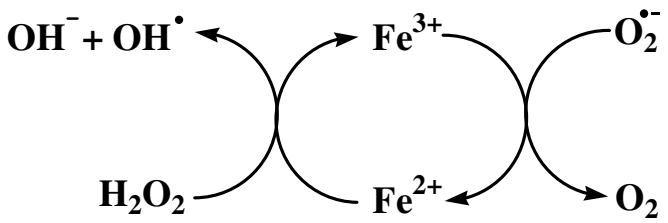

Scheme 5. Iron mediated production of ROS.[146]

As another probable target for the TSCs, Topoisomerase IIα (Topo–IIα) has also been considered. Topo–IIα is overexpressed in many forms of cancer cells and it is already a well known biomarker.[167] DNA topoisomerases are a group of two enzymes responsible for decatenation of the DNA–chain during transcription, replication or repair. They play a pivotal role in vital cellular processes. DNA topoisomerases are divided into two classes: Topoisomerase I and Topoisomerase II. Topoisomerase I is an ATP independant enzyme, which cuts one strand of DNA and attaches the 3'–end of cleaved DNA by formation of a phosphotyrosine linkage.[172] Topoisomerases of type II cut both DNA strands simultanously in order to prevent DNA tangels and supercoils. They are divided into two subtypes: Topoisomerase IIα and Toposiomerase IIβ (found in archaea and some higher plants). They possess similar strand passage mechanism and domain structure and are crucial in the ATP–dependent passage of one DNA segment through a double–stranded break, avoiding DNA chain supercoiling during replication (Figure 50).

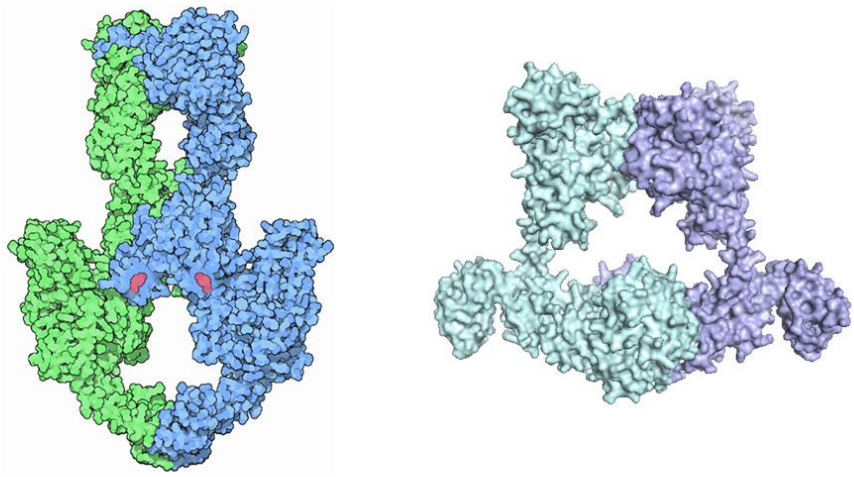

Figure 50. Topoisomerase IIα (left) and topoisomerase IIβ (right).[173,174]

Topoisomerase IIα forms double–stranded breaks with the overhanging of four–pair bases and simplifies DNA topology. Topoisomerase IIβ forms double–stranded breaks with the overhanging of two–pair bases but does not simplify DNA topology. The inhibition of these enzymes leads to cell apoptosis.[173]

Reported results showed higher efficiency of TSCs in Topo–IIα inhibition *in vitro* and *in vivo* than that of commonly used cytostatic etoposide (VP–16).[158,167]

Copper(II) complexes of α-N-heterocyclic TSC possess much higher cytotoxic potency compared to that of the corresponding ligands. One reason for the better cytotoxic efficiency of copper TSC complexes is presumably, their planarity. A square–planar complex can inhibit the enzyme binding site more strongly than the unplanar ligand.[167,175]

Two established mechanisms of Topo–IIα inhibiton are known: inhibition by agents, which bind and stabilize the DNA–Topo–IIα cleavage complex, causing double strand DNA breaks and inhibition via agents, which inactivate the catalytic ability of the enzyme. According to the mechanism of inhibition, the topoisomerase IIα inhibitors are classified in the two groups: topoisomerase II poisons and topoisomerase II catalytic inhibitors, respectively. Topoisomerase II poisons are currently used in the clinical treatment of human malignancies. Greater efficiency was observed when catalytic inhibitors act accompanied with poisons.[158,167]

The mechanism of Topo–IIα inhibition using TSCs and their metal complexes can be described, as follows: by binding to the ATP hydrolysis pocket of Topo–IIα causing impediments of hydrolysis via an ATP competition mechanism,[158] while inhibition by metal–mediated production of ROS, which cause strand breaks in DNA during Topo–IIα incubation, is less likely. However the detailed molecular mechanism remains unknown still.[167]

Recently it was shown, that some benzaldehyde TSCs arrest melanogenesis by blocking the enzyme tyrosinase (also known as phenoloxidase).[176] These compounds showed potent activity against melanogenesis in melanoma B16 cells.[176, 177] Tyrosinase is a widespread enzyme, which can be found in microorganisms, plants and animals. Tyrosinase can differ in size, primary structure and activation characteristics according to the species, from which it is isolated. Human tyrosinase is a single membrane spanning transmembrane protein, stored in melanosomes. The structure of tyrosinase comprises four subunits and an active site of the enzyme, which is built up of a dinuclear copper(II) unit.

The copper atoms, in active site, are interconnected via a N–moiety of histidine (Figure 51).

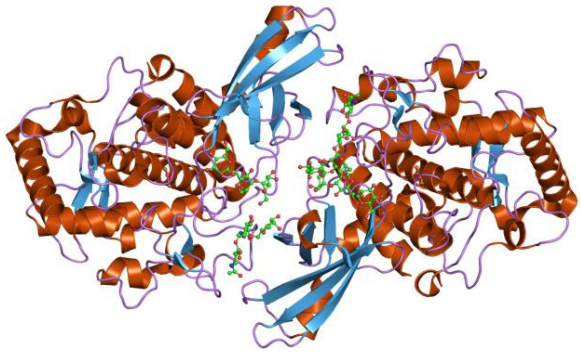

Figure 51. Structure of tyrosinase.[178]

Tyrosinase catalyzes two different reactions using molecular oxygen: the hydroxylation of monophenols to *o*-diphenols and the oxidation of *o*-diphenols to *o*-quinones.[179] The explanation of inhibiton of tyrosinase by TSC was based on formation of coordination and hydrogen bonds between tyrosinase and TSC via N and S atoms of TSC. TSCs exhibit strong affinity to copper ions, and slight changes in the dicopper centre can lead to deactivation of the enzyme.[177]

1.5 References

[1] Jones, M. N.; Bryan, N. D. *Adv. Colloid Interface Sci.*, **1998**, *78*, 1–48. Colloidal Properties of Humic Substances.

[2] *a*) Donald, L. S. *Environmental Soil Chemistry*, Academic Press Inc., San Diego, California, **1995**. *b*) Steinberg, C. E. W. *Ecology of Humic Substances in Freshwaters*, Springer-Verlag Berlin Heidelberg, Germany, **2003**.

[3] Chefetz, B.; Tarchitzky, J.; Deshmukh, A. P.; Hatcher, P. G.; Chen, Y. *Soil Sci. Soc. Am. J.*, **2002**, *66*, 129–141. Structural Characterization of Soil Organic Matter and Humic Acids in Particle–Size Fractions of an Agricultural Soil.

[4] Stevenson, F. J. *BioSci.*, **1972**, *22*, 643–650. Role and Function of Humus in Soil with Emphasis on Adsorption of Herbicides and Chelation of Micronutrients.

[5] Pompe, S. *Doctoral Thesis*: Entwicklung huminänlicher Melanoidine als Funktionalitätsmodelle für Huminsäuren und ihr Vergleich mit Fluka–Huminsäure hinsichtlich ihres Komplexbildungsverhaltens gegenüber Uran (IV), **1997**, University of Dresden (ref. therein).

[6] Thruman, E. M.; Malcolm, R. L. *Environ. Sci. Technol.*, **1981**, *15*, 463–466. Preparative Isolation of Aquatic Humic Substances.

[7] Reiter, B.; Herndl, G. J., *Limnol. Oceanogr.*, **1997**, *42*, 950–960. Role of Ultraviolet–B radiation o Photochemical and Microbial Oxygen Consumption in a Humic–rich Shallow Lake.

[8] Malcolm, R. M. *Anal.Chim. Acta*, **1990**, *234*, 19–31. The uniqueness of humic substances in each of soil, stream and marine environments.

[9] Gjessing, E. T. *Environ. Sci. Technol.*, **1970**, *4*, 437. Ultrafiltration of aquatic humus.

[10] Amir, S.; Hafidi, M.; Lemee, L.; Bailly, J.-R.; Merlina, G.; Kaemmerer, M.; Reel, J.-C.; Ambles, A. *J. Anal. Appl. Pyrolysis*, **2006**, *77*, 149–158. Structural Characterization of Fulvic Acids, Extracted from Sewage Sludge during Composting, by Thermochemolysis–Gass Chromatography–Mass Spectrometry.

[11] Chefetez, B.; Salloum, M. J.; Deshmukh, A. P. ; Hatcher, P. G. *Soil Sci. Soc. Am. J.*, **2002**, *66*, 1159–1171. Structural Components of humic Acids as Determined by Chemical Modifications and Carbon–13 NMR, Pyrolysis– and Thermolysis–Gas Chromatography/Mass Spectrometry.

[12] Losovik, P. A. *J. Anal. Chem.*, **2006**, *61*, 544–549. A Calculation Method to Estimate the Concentration and Elemental Composition of Organic Substances in Natural Waters.

[13] Piana, M. J.; Zahir, O. K. *J. Environ. Sci. Health*, **2000**, *B35*, 87–102. Investigation of Metal Ions Binding of Humic Substances using Fluorescence Emission and Synchronous–Scan Spectroscopy.

[14] Linnik, P. N. *Anal. Bioanal. Chem.*, **2003**, *376*, 405–412. Complexation as the Most Important Factor in the Fate and Transport of Heavy Metals in the Dnieper Water Bodies.

[15] Ephralm, J.; Alegret, S.; Mathuthu, A.; Blcklng, M.; Malcolm, R. L.; Marinsky, J. A. *Environ. Sci. Technol.*, **1986**, *20*, 354–366. A United Physicochemical Description of the Protonation and Metal Ion Complexation Equilibria of natural Organic Acids (Humic and Fulvic Acids). 2. Influence of polyelectrolyte Properties and Functional Group Heterogenity on the Protonation Equilibria of Fulvic Acid.

[16] Gamble, D. S. *Can. J. Chem.*, **1972**, *50*, 2680–2690. Potentiometric Titration of Fulvic Acid: Equivalence Point Calculations and Acidic Functional Groups.

[17] Miano, T. M.; Sposito, G.; Martin, J. P. *J. Amer. Soil. Sci.*, **1988**, *52*, 1016–1019. Fluorescence Spectroscopy of Humic Substances.

[18] Dos Santos, A.; Botero, W. G.; Bellin, I. C.; de Oliveira, L. C.; Rocha, J. C.; Mendonça, A. G. R.; Godinho, A. F. *J. Braz. Chem. Soc.*, **2007**, *18*, 824–830. Interaction between Humic Substances and Metallic ions: a Selectivity Study of Humic Substances and their Possible Therapeutic Application.

[19] Senesi, N.; Sposito, G.; Martin, J. P. *Sci. Total Environ.*, **1986**, *55*, 351–362. Coper(II) and Iron(III) complexation by soil humic acids: an IR and ESR study.

[20] Tipping, E.; Backes, C. A.; Hurley, M. A. *Water Res*., **1988**, *22*, 597–611. The Complexation of Protons, Aluminium and Calcium by Aquatic Humic Substances: a Model Incorporating the Binding–Site Heterogeneity and Macroionic Effect.

[21] Tipping, E.; Woof, C.; Backes C. A.; Ohnstad, M. *Water Res.*, **1988**, *22*, 321–326. Testing of a Model for Aluminium–humic Complexation.

[22] Benedetti, M. F.; Milne, C. J.; Kinniburgh, W. H. van R.; Koopal, R. K. *Environ. Sci. Technol.*, **1995**, *29*, 446–457. Metal Ion Binding to Humic Substances: Application of the Non–Ideal Competitive Adsorption Model.

[23] Rose, L. A.; Waite, D. T. *Mar. Chem.*, **2003**, *84*, 85–103. Kinetics of Iron Complexation by Dissolved Natural Organic matter in Coastal Waters.

[24] Buesseler, K. O.; Boyd, P. W. *Science*, **2003**, *300*, 67–68. Will Ocean Fertilization Work?

[25] Cooper, D. J.; Watson, A. J.; Nightingale, P. D. *Nature*, **1996**, *383*, 511–513. Large Decrease in Ocean–Surface CO_2 fugacity in Response to *in situ* Iron Fertilization.

[26] Boyle, E. A.; Edmond, J. M.; Sholkovitz, E. R. *Geochim. Cosmochim. Acta*, **1977**, *41*, 1313–1324. The Mechanism of Iron Removal in Estaurine.

[27] Wen, L. S.; Santschi, C.; Gill, G. *Mar. Chem.*, **1999**, *63*, 185–212. Estaurine Trace Metal Distributions on Galveston Bay I: Imoptance of Colloidal Forms in the Speciacion of the Dissolved Phase.

[28] Krachler, R.; Jirsa, F.; Ayromlou, S. *Biogeoscience*, **2005**, *2*, 311–315. Factor Influencing the Dissolved Iron Input by River Water to the Open Ocean.

[29] Laglera, L. M.; Battaglia, G.; van den Berg, C. M. G. *Marine Chem.*, **2011**, *127*, 134–143. Effect of Humic Substances on Iron Speciacion in Natural Waters by CLE/CSV (ref. therein).

[30] Schulten, H.-R.; Leinweber, P. *J. Anal. Appl. Pyrolysis*, **1996**, *38*, 1–53. Characterization of Humic and Soil Particles by Analytical Pyrolysis and computer modeling.

[31] Schulten, H. -R.; Plage, B. *Naturwissenschaften*, **1991**, *78*, 311–312. A Chemical Structure for Humic Substances.

[32] Schumann, G. E.; Thiele-Bruhn, S. *Geoderma*, **2011**, *166*, 1–14. Molecular Modeling of Soil Organic Matter: Squarting the Circle?

[33] Stevenson, F. J. *Humus Chemistry: Genesis Composition Reactions*, Wiley, New York, **1994**.

[34] Slawinska, D.; Polewski, K.; Rolewski, P.; Sławiński, J. *Int. Agrphysics*, **2007**, *21*, 199–208. Synthesis and Properties of Model Humic Substances Derived from Galic Acid.

[35] Sever, M. J.; Wilker, J. J. *Dalton Trans.*, **2004**, 1061–1072. Visible Absorbtion Spectra of Metal–Catecholate and Metal–Tironate Complexes.

[36] Grillo, V. A.; Hanson, G. R.; Wang, D.; Hambley, T. W.; Gahan, L. R.; Murray, K. S.; Moubaraki, B.; Hawkins, C. J. *Inorg. Chem.*, **1996**, *35*, 3568–3576. Synthesis X–ray Structural Determination, and Magnetic Susceptibility, mössbauer, and EPR Studies of $(Ph_4P)_2[Fe_2(cat)_2(H_2O)_2]$ $6H_2O$, a Catecholato–Bridged Dimer of Iron(III).

[37] Kipton, H.; Powell, J.; Taylor, M. C. *Aust. J. Chem.*, **1982**, *35*, 739–756. Interaction of Iron(II) and Iron(III) with Gallic Acid and its Homologues: a Potentiometric and Spectrophotometric Study.

[38] Lu, X.; Liu, S.; Mao, X.; Bu, X., *J. Mol. Struct.*, **2001**, *562*, 89–94. Synthesis, Crystal Structure, and EPR Spectra of *cis*-Dioxo-Molybdenum(V) with Catechol Ligand.

[39] Karpishin, T. B.; Gebhard, M. S.; Solomon, E. I.; Raymond, K. N. *J. Am. Chem. Soc.*, **1991**, *113*, 2977–2984. Spectroscopic Studies of the Electronic Structure of Iron(III) Tris(catecholates).

[40] Borges, F.; Guimaraes, C.; Lima, J. F. C.; Pinto, I.; Reis, S. *Talanta*, **2005**, *66*, 670–673. Potentiometric Studies on the Complexation of Copper(II) by Phenolic Acids as Discrete Ligand Models of Humic Substances.

[41] Erre, S. L.; Micera, G.; Piu, P.; Cariati, F.; Ciani, G. *Inorg. Chem.*, **1985**, *24*, 2297–2300. Synthesis, Spectral Properties, ans Crystal and Molecular Structure of tertakis(μ-2,6-dimethoxybenzoato)diaqua di copper(II) and of Bis(μ-2,6-dimethoxybenzoato)bis(μ-acetato)diaqua dicopper(II), a case of a dimeric copper(II) carboxylate complex with Mixed Bridges.

[42] Aletras, V.; Karliota, A.; Kamariotaki, M.; Hatzipanayioti, D.; Hadjiliadis, N. *Inorg. Chim. Acta*, **2001**, *312*, 151–162. Interaction of Ni(II) with 2,3-dihydroxybenzoic acid.

[43] Ruckebusch, C.; Duponchel, L.; Huvenne, J. P.; Caudron, A.; Boilet, L.; Cornard, J. P.; Merlin, J. C.; de Juan, A. *Anal. Chim. Acta*, **2005**, *544*, 337–344. Chemometric Strategies for the Study of the Complexation of Al(III) ions with Model Molecule of Humic Substances from UV–vis Data Sets.

[44] Kamariotaki, M.; Karaliota, A.; Stabaki, D. *Transition Met. Chem.*, **1994**, *19*, 241–247. Coordination Complexes of Iron(III) with 3-hydroxy-2(1H)-pyridinone, 2,3-dihydroxybenzoic acid and 3,4-dihydroxybenzoic acid: preparation and characterization in the solid state.

[45] Andjelkovic, M.; van Camp, J.; de Meulenaer, B.; Depaemelaere, G.; Socaciu, C.; Verloo, M.; Verhe, R. *Food Chem.*, **2006**, *98*, 23–31. Iron–Chelation Properties of Phenolic Acids Bearing Catechol and Galloyl Groups.

[46] Khokhar, S.; Apenten, R. K. O. *Food Chem.*, **2003**, *81*, 133–140. Iron Binding Characteristics of Phenolic Compounds: Some Tentative Structure-Activity Relations.

[47] Hider, R. C.; Mohd-Nor, A. R.; Silver, J.; Morrison, I. E. G.; Rees, L. V. C. *J. Chem. Soc., Dalton Trans.*, **1981**, 609–621. Model Compounds for Microbial Iron-Transport Compounds. Part 1. Solution Chemistry and Mössbauer Study of Iron(II) and Iron(III) Complexes from Phenolic and Catecholic Systems.

[48] Kazmi, A.; Quareshi, M. S.; Maqsood, Z. *Inorg. Chim. Acta.*, **1987**, *137*, 151–154. Reactivity of an Iron(III) Complex of Galic Acid.

[49] Hynes, M. J.; Coinceanainn, M. O. *J. Inorg. Biochem.*, **2001**, *85*, 131–142. The Kinetics and Mechanism of the Reaction of Iron(III) with gallic acid methyl ester and catechin.

[50] Friedman, M.; Jürgens, H. S. *J. Agric. Food Chem.*, **2000**, *48*, 2101–2110. Effect of pH on the Stability of Plant Phenolic Compounds.

[51] Litos, C.; Terzis A.; Raptopoulou, A. R.; Karaliota, A. *Polyhedron*, **2006**, *25*, 1337–1347. Polynuclear Oxomolybdenum(VI) Complexes of Dihydrobenzoic Acids: Synthesis Spectroscopic and Structure Characterization of a Tetra Nuclear Catecholato–type Coordinated 2,3-dihydroxybenzoate and Novel Tridentate Salicylato–Type Coordinated 2,5-dihydroxybemzoate Trinuclear Complex.

[52] Micera, G.; Erre, S. L.; Piu, P.; Cariati, F. ; Ciani, G.; Sironi, A. *Inorg. Chim. Acta*, **1985**, *107*, 223–227. Interaction of metal ions with humic–like models. Part VII. Mn(II), Co(II), Ni(II), Cu(II), Zn(II) and Cd(II) complexes with 2,5-dihydroxybenzoic acid.

[53] Tsin-Jao, J.; Sommer, L.; Okac, A. *Collect. Czech. Chem. Commun.*, **1962**, *27*, 1171–1190. Chelates of the o-Dihydroxybenzoic Acid with Trivalent Iron.

[54] Tsin-Jao, J.; Sommer, L.; Okac, A. *Collect. Czech. Chem. Commun.*, **1962**, *27*, 1161–1170. Chelates of Trivalent Iron with 4-Methysalicylic Acid.

[55] Weinland, R. F.; Herz, A. *Berichte d. D. Chem. Gesellschaft*, **1912**, *45*, 2662–2680. Über Ferribenzoate.

[56] Sakurai, H.; Miki, T.; Imakura, Y.; Shibuya, M.; Lee, K. H. *Molecular Pharmacol.*, **1991**, *40*, 965–973. Metal- and Photo-induced Cleavage of DNA by podophyllotoxin, etoposid, and thei related compounds.

[57] Vincent, J. B.; Olivier-Lilley, G. L.; Averill, B. A. *Chem. Rev.*, **1990**, *90*, 1447–1467. Proteins Containing Oxo-Bridged Dinuclear Iron Centers: A Bioinorganic Perspective.

[58] Armstrong, W. H.; Lippard, S. J. *Inorg. Chem.*, **1985**, *24*, 981–982. Convenient High-Yield Synthesis of $(Et_4N)_2[Fe_2OCl_6]$.

[59] Kurtz, D. M. Jr. *Chem Rev.*, **1990**, *90*, 585–606. Oxo– and Hydroxo–Bridged Diiron Complexes: a Chemical Perspective on a Biological Unit.

[60] Norman, R. E.; Yan, S.; Que, L. Jr.; Backes, G.; Ling, J.; Sanders-Loehr, J.; Zhang, J. H.; O'Conor, C. J. *J. Am. Chem. Soc.*, **1990**, *112*,1554–1562. Oxo Carboxylato iron(III) complexes with Distinct Iron Sites. Consequences of the Inequivalence and its Relevance to Dinuclear Iron Oxo Proteins.

[61] Zheng, H.; Zang, Y.; Dong, Y.; Young, V. G. Jr.; Que, L. Jr. *J. Am. Chem. Soc.*, **1999**, *121*, 2226–2235. Complexes with $Fe^{III}_2(\mu\text{-}O)(\mu\text{-}OH)$, $Fe^{III}_2(\mu\text{-}O)_2$, and $[Fe^{III}_3(\mu\text{-}O)_3]$ Cores: Structures, Spectroscopy, and Core Interconversions.

[62] Yachandra, V. K.; DeRose, V. J.; Latimer, M. J.; Mukerji, I.; Sauer, K.; Klein, M. P. *Science*, **1993**, *260*, 675–679. Where Plants Make Oxygen: A Structural Model fort he Photosynthetic Oxygen-Evolving Manganese Cluster.

[63] Gutkina, E. A.; Trukhan, V. M.; Pierpont, C. G.; Mkoyan, S.; Strelets, V. V.; Nordlander, E.; Shteinman, A. A. *Dalton Trans*., **2006**, 492–501. Tetranuclear Iron(III) Complexes of an Octadentate Pyridine-Carboxylate Ligand and Their Catalytic Activity in Alkane Oxidation by hydrogen peroxide.

[64] Weinland, R. F. *Berichte d. D. Chem. Gesellschaft*, **1908**, *41*, 3236–3245. Übersaltze einer Acetatochrombase.

[65] Weinland, R. F.; Herz A. *Berichte d. D. Chem. Gesellschaft*, **1913**, *45*, 2662–2680. Über Eisen Verbindungen der Phenole. V. Über Eisen Verbindungen der Salicylsäre.

[66] Welo, L. A. *Philos. Mag.*, **1928**, *6*, 481–509. Magnetic Studies on Salts, with Particular Reference to Those with Complex Ions.

[67] Orgel, L. E. *Nature*, **1960**, *187*, 504–505. Structure of the Trinuclear Basic Acetates.

[68] Taylor, J., *Master Thesis*: The High Temperature Synthesis of Transition Metal Oxo-Carboxylate Polynuclear Complexes, **2007**, Victroia University of Wellington, New Zeeland.

[69] Glazunova, T. Y.; Boltalin, A. I.; Troyanov, S., *Mendeleev Commun.*, **2004**, *14*, 141–143. Synthesis and Crystal Structure of Trinuclear Carboxylate Complexes $M_3(\mu_3\text{-}O)(CF_3COO)_6L_3$.

[70] White, R. P.; Wilson, L. M.; Williamson, D. J.; Moore, G. R.; Jayasooriya, U. A.; Cannon, R. D., *Spectrochim. Acta, Part A,* **1990**, *46*, 917–920. Electron Transfer in Triangular Iron Cluster: Evidence of Valence Localization in Solution.

[71] Asamaki, K.; Nakamoto, T.; Kawata, S.; Sano, H.; Katada, M.; Endo, K. *Inorg. Chim. Acta*, **1995**, *236*, 155–161. Structure and Mixed-valence States of the Trinuclear Iron (II,II,III) pivalate complex-pivalic acid adduct $[Fe_3O(O_2CCMe_3)_6(Me_3CCO_2H)_3]$ (Me= $-CH_3$).

[72] Zhong, Z. J.; Tao, J.-Q.; Li, H.; You, X.-Z.; Mak, T. C. W. *Polyhedron*, **1997**, *16*, 1719–1722. Synthesis and Crystal Structure of a Novel Oxo Centered Trinuclear Manganese Complex $[Mn_3O(C_6H_5COO)_6(py)_3]\cdot 2CH_3CN$.

[73] Cotton, F. A.; Wang, W. *Inorg. Chem.*, **1982**, *21*, 2675–2678. New Trinuclear, Oxo-Centered, Basic Carboxylate Compounds of Trasition Metals. 1. Trichromium(II,III,III) Compounds.

[74] Cotton, F. A.; Lewis, G. E.; Mott, G. N. *Inorg. Chem.*, **1982**, *21*, 3127–3130. New Trinuclear, Oxo-Centered, Basic Carboxylate Compounds of Trasition Metals. 2. Synthesis and X-ray Structure of $V_3(O)_3(THF)(C_6H_5CO_2)_6$, a Compound with Deviant Structure.

[75] Kiskin, M. A.; Fomina, I. G.; Aleksandrov, G. G.; Sidorom, A. A.; Novotortsev, V. M.; Shvedenkov Y. G.; Eremenko, I. L.; Moiseev, I. I. *Inorg. Chem. Comm.*, **2004**, *7*, 734–736. First Triangular Carboxylate Cluster with Fe(II)Fe(II)Fe(II) Metal Core.

[76] Bond, A. M.; Clark, R. J. H.; Humphrey, D. G.; Panayiotopoulos, P.; Skelton, B. W.; White, A. H. *J. Chem. Soc., Dalton Trans.*, **1998**, 1845–1852. Synthesis and Characterisation and Electrochemical Reductions of Oxo-Centered, Carboxylate-Bridged Triiron Complexes, $[Fe_3(\mu_3\text{-}O)\text{-}(O_2CR)_6L_3]$ X (R= Me, Bu^t, CH_2Cl, CCl_3, CH_2CN, or $4\text{-}NO_2C6H_4$; L=py, $3\text{-}H_2Npy$, $4\text{-}H_2Npy$, 3-NCpy, 4-NCpy or $4\text{-}CH_2CHpy$; X= ClO_4^- or NO_3^-).

[77] Losada, G.; Mendiola, A. M.; Sevilla, T. *Inorg. Chim. Acta*, **1997**, *255*, 125–133. Synthesis, Characterization and Electrochemical Properties of Trinuclear Iron(III) Complexes Containing Unsaturated Carboxylate Bridging Ligands.

[78] Boudalis, A. K.; Sanakis, Y.; Raptopoulou, C. P.; Terzis, A.; Tuchagues, J. -P.; Perlepes, S. P. *Polyhedron*, **2005**, *24*, 1540–1548. A Trinuclear Cluster Containing The $\{Fe_3(\mu_3\text{-}O)\}^{7+}$ Core: Structural, Magnetic And Spectroscopic(IR, Mössbauer, EPR) Studies.

[79] Tian, J. -L.; Gu, W.; Yan, S. -P.; Liao, D. -Z.; Jiang, Z. –H. *Z. Anorg. Allg. Chem.*, **2007**, *633*, 478–481. Synthesis, Structure and Magnetic Property of an ''Adamantane'' Type Tetranuclear iron(III) Complex.

[80] Satcher, J. H. Jr.; Olmstead, M. M.; Droege, M. W.; Parkin, S. R.; Noll, B. C.; May, L.; Balch, A. L. *Inorg. Chem.*, **1998**, *37*, 6751–6758. Novel Square Arrangements in Tetranuclear and Octanuclear Iron(III) Complexes with Asymmetric Iron Environments Created by the unsymmetric Bridging Ligand N,N,N'-tris((N-methyl)-2-benzimidazolylmethyl)-N'-methyl-1,3-diamino-2-propanol.

[81] Armstrong, W. H.; Roth, M. E.; Lippard, S. J. *J. Am. Chem. Soc.*, **1987**, *109*, 6318–6326. Tetranuclear Iron-Oxo Complexes. Synthesis, Structure, and Properties of Species Containing the Nonplanar $\{Fe_4O_2\}^{8+}$ Core and Seven Bridging Carboxylate Ligands.

[82] Yan, B.; Chen, Z. -D. *Inorg. Chem. Commun.*, **2000**, *4*, 138–141. A Novel Tetranuclear Iron Complex $[Fe_4O_2(O_2CC_2H_5)_7(bipy)_2]PF6{\cdot}2H_2O$ (bipy = 2,2'-bipyridine): Crystal Structure and Magnetic Property.

[83] Miyasato, Y.; Nogami, Y.; Ohba, M.; Sakiyama, H.; Okawa, H. *Bull. Chem. Soc. Jpn.*, **2003**, *76*, 1009–1010. Synthesis, Structure and Magnetic Property of a Tetranuclear Iron(III) Complex of ''Face-to-Face'' type.

[84] Oshio, H.; Hoshino, N.; Ito, T. *J. Am. Chem. Soc.*, **2000**, *122*, 12602–12603. Superparamagnetic Behaviour in an Alkoxo-Bridged Iron(II) Cube.

[85] Klein, D. P.; Young, V. G. Jr.; Tolman, W. B.; Que L. Jr. *Inorg. Chem.*, **2006**, *45*, 8006–8008. Mononitrisyl Iron Complexes Supported by Sterically Hindered Carboxylate Ligands.

[86] Lee, D.; Sorace, L.; Caneschi, A.; Lippard, S. J. *Inorg. Chem.*, **2001**, *40*, 6774–6781. Hydroxo-bridged Cubane Type Tetrairon(II) Clusters Supported by Sterically-Hindered Carboxylate Ligands.

[87] Li, H.; Hong, Z. J.; Chen, W.; You, X. -Z. *J. Chem. Soc., Dalton Trans.*, **1997**, 463–464. Crystal Structure and Synthesis of a Novel Tetranuclear Iron(III) Complex with a Defective double-cubane core.

[88] Stamatatos, T. C.; Boudalis, A. K.; Sanakis, Y.; Raptopolou, C. P. *Inorg. Chem.*, **2006**, *45*, 7372–7381. Reactivity and Structural and Physical Studies of Tetranuclear Iron(III) Clusters Containing the $[Fe_4(\mu_3\text{-}O)_2]^{8+}$ ''Butterfly Core'' Unit : an Fe^{III}_4 Cluster with an S=1 Ground State.

[89] Barra, A. L.; Caneschi, A.; Corina, A.; de Biani, F. F.; Gatteschi, D.; Sangregorio, C.; Sessoli, R.; Sorace, L. *J. Am. Chem. Soc.*, **1999**, *121*, 5302–5310. Single Molecule Magnet Behaviour or Tetranuclear Iron(III) Complex. The Origin of Slow Magnetic Relaxation in Iron(III) Clusters.

[90] Horn, A.; Neves, A.; Bortoluzzi, A. J.; Drago, V.; Ortiz, W. A. *Inorg. Chem. Commun.*, **2001**, *4*, 173–176. Crystal Structure and Magnetic Properties of a New Tetranuclear Iron(III) Complex with Asymmetric Iron Coordination as a Model for polynuclear Iron Proteins.

[91] Murch, B. P.; Boyle, P. D.; Que, L. Jr. *J. Am. Chem. Soc.*, **1985**, *107*, 6728–6729. Structures of binuclear and Tetranuclear Iron(III) Complexes as Models for Ferritin Core Formation.

[92] Ako, A. M.; Mereacre, V.; Lan, Y.; Wernsdorfer, W.; Clerac, R.; Anson, C. E.; Powell, A. K. *Inorg. Chem.*, **2010**, *49*, 1–3. An Undecanuclear Fe^{III} Single-Molecule Magnet.

[93] Jones, L. F.; Low, D. M.; Helliwell, M.; Raftery, J.; Collison, D.; Aromi, G.; Cano, J.; Mallah, T.; Wernsdorfer, W.; Brecin, E. K.; McInnes, E. J. L. *Polyhedron*, **2006**, *25*, 325–333. Fe(III) Clusters with Tripodal Alcohol Ligands.

[94] Gorun, M. S.; Lippard, S. J. *Nature*, **1986**, *319*, 666–668. A new synthetic approach to the ferritin core uncovers the soluble iron(III) oxo–hydroxo aggregate $[Fe_{11}O_6(OH)_6(O_2CPh)_{15}]$.

[95] Trettenhan, G.; Nagl, M.; Neuwirth, N.; Arion, V. B.; Walter, J.; Pöchlauer, P.; Schmid, W. *Angew. Chem. Int. Ed.*, **2006**, *45*, 2794–2798. A Hexanuclear Iron(III) Carboxylate with an $[Fe_6(\mu_3\text{-}O)_3(\mu_2\text{-}OH)]^{11+}$ Core as an Efficient Catalyst for Cycloalkane Oxidation.

[96] Murugesu, M.; Abboud, K. A.; Christou, G. *Polyhedron*, **2004**, *23*, 2779–2788. New Hexanuclear and Dodecanuclear Fe(III) Clusters with Carboxylate and Alkoxide-Based Ligands from Cluster Aggregation Reactions.

[97] Gorun, S. M.; Papaefthymiou, G. C.; Frankel, R. B.; Lippard, S. J. *J. Am. Chem. Soc.*, **1987**, *109*, 3337–3348. Synthesis, Structure, and Properties of an Undecanucleariron(III) Oxo-Hydroxo Aggregate: An Approach to the Polyiron Core in Ferritin.

[98] Smith, A. A.; Coxall, R. A.; Harrison, A.; Helliwell, M.; Parsons, S.; Winpenny, R. E. P. *Polyhedron*, **2004**, *23*, 1557–1565. High-temperature synthesis of Polynuclear Iron Oxo-Hydroxo Complexes.

[99] Laye, R. H.; McInnes, E. J. L. *Eur. J. Inorg. Chem.*, **2004**, 2811–2818. Solvothermal Synthesis of Paramagnetic Molecular Clusters.

[100] Canada-Vilalta, C.; O'Brien, T. A.; Pink, M.; Davidson, E. R.; Christou, G. *Inorg. Chem.*, **2003**, *42*, 7819–7829. Methanolysis and Phenolysis Routes to Fe_6, Fe_8, and Fe_{10} Complexes and Their magnetic Properties: A New Type of Fe_8 Ferric Wheel.

[101] Sanudo, E. C.; Font-Bardia, M.; Solans, X.; Laye, R. H. *New J. Chem.*, **2011**, *35*, 842–848. Hexanuclear Fe(III) Complexes and their Thermal Decomposition into an Undecanuclear Species.

[102] Tong, J.-P.; Shao, F.; Huang, R. -B.; Zheng, L. -S. *Inorg. Chem.*, **2011**, *50*, 2067–2069. Microwave-Assisted Synthesis of a Ferrimagnetic Dodecanuclear Iron(III) Complex with a $Fe_4(OH)_4$ Cubane Core.

[103] Winpenny, R. E. P. *J. Chem. Soc., Dalton Trans.*, **2002**, 1–10. Serendipitious Assembly of Polynuclear Cage Compounds.

[104] Micklitz, W.; Lippard. S. J. *Inorg. Chem.*, **1988**, *27*, 3069–3075. A Novel Hexairon(III)Aggregate Prepared from a bsic Iron(III) Benzoate. Possible building blocks in Ferritin Core Formation.

[105] Celenligil-Cetin, R.; Staples, R.; Stavropoulos, P. *Inorg. Chem.*, **2000**, *39*, 5838–5848. Synthesis, Characterization, and Reactivity of Ferrous and Ferric Oxo/Peroxo Pivalate Complexes in Relation to Gif-Type Oxygenation of Substrates.

[106] Ammala, P. S; Batten, S. R.; Cashion, J. D.; Kepert, C. M; Moubaraki, B.; Murray, K. S.; Spicca, L.; West, B. O. *Inorg. Chim. Acta.*, **2002**, *331*, 90–97. Synthesis, Molecular Structure and Magnetic Properties of Fe_6.

[107] Seddon, E. J.; Yoo, J.; Folting, K.; Huffman, J. C.; Hendrickson, D. N. *J. Chem. Soc., Dalton Trans.*, **2000**, 3640–3648. Dinuclear and Hexanuclear Iron(III) Carboxylate Clusters with a Bis(bipyridine) Ligand: Supramolecular Aggregation of $[Fe_2O_2]$ Units to Give $[Fe_6O_6]$ Ladder Structure.

[108] Graham, K.; Darwish, A.; Ferguson, A.; Parsons, S.; Murrie, M., *Polyhedron*, **2009**, *28*, 1830–1833. Synthesis and Characterisation of Fe_6 and Fe_{12} Clusters Using Bicine.

[109] Grant, C. M.; Knapp, M. J.; Huffman, J. C.; Hendrickson, D. N.; Christou, G. *Chem. Commun.*, **1998**, 1753–1754. A New Structural Type in Iron Carboxylate Cluster Chemistry Via Use of Bis-bipyridine Ligands: $[Fe_6O_4Cl_4(O_2CPh)_4L_2][FeCl_4]_2$.

[110] Bagai, R.; Daniels, M. R.; Abboud, K. A.; Christou, G. *Inorg. Chem.*, **2008**, *47*, 3318–3327. Unusual Structural Types in Polynuclear Iron Chemistry from the Use of N,N,N',N'-tetrakis(2-hydroxyethyl)ethylenediamine (edeteH_4): Fe_5, Fe_6 and Fe_{12} Clusters.

[111] Yao, H. -C.; Li, Y. -Z.; Zheng, L. -M.; Xin, X. -Q. *Inorg. Chim. Acta*, **2005**, *358*, 2523–2529. Syntheses, Structures and Magnetic Properties of Tetra- and Heptanuclear Iron(III) Clusters Incorporating Phosphonate Ligands.

[112] Khanra, S.; Konar, S.; Clearfield, A.; Helliwell, M.; McInnes, E. J. L.; Tolis, E.; Tuna, F.; Winpenny, R. E. P. *Inorg. Chem.*, **2009**, *48*, 5338–5349. Synthesis, Structural and Magnetochemical Studies of Iron Phosphonate Cages based on $\{Fe_3O\}^{7+}$ Core.

[113] Jones, L. F.; Jensen, P. ; Moubaraki, B.; Berry, K. J.; Boas, J. F.; Pilbrow, J. R.; Murray, K. S. *J. Mater. Chem.*, **2006**, *16*, 2690–2697. Heptanuclear Iron(III) Triethanolamine Clusters Exhibiting ''Millennium Dome''-like Topologies and Octanuclear Analogue with Ground Spin States of S=5/2 and 0, respectively.

[114] Ako, A. M.; Waldmann, O.; Mereacre, V.; Klower, F.; Hewitt, I. J.; Anson, C. E.; Güdel, H. U.; Powell, A. K. *Inorg. Chem.*, **2007**, *46*, 756–766. Odd-numbered FeIII Complexes: Synthesis, Molecular Structure, Reactivity, and Magnetic Properties.

[115] Bagai, R.; Datta, S.; Betancur-Rodriguez, A.; Abboud, K. A.; Hill, S.; Christou, G. *Inorg. Chem.*, **2007**, *46*, 4535–4547. Diversity of a New Structural Types in Polynuclear Iron Chemistry with a Tridentate N,N,O Ligand.

[116] Baca, S. G.; Botezat, O.; Filippova, I.; Speldrich, M.; Jeanneau, E.; Kögerler, P. *Z. Anorg. Allg. Chem.*, **2011**, *637*, 821–823. A Heptanuclear Iron(III) Oxo-Carboxylate Cluster.

[117] Masello A.; Sanakis Y.; Boudalis A. K.; Abboud K. A.; Christou G., *Inorg. Chem.*, **2011**, *50*, 5646–5654. Iron(III) Cluster with Ferrocene-1,1'-dicarboxylic Acid (fdcH_2) : An Fe7 Cluster with Oxidized fdc^- Ligand.

[118] Murugesu, M.; Abboud, K. A.; Christou, G. *Dalton Trans.*, **2003**, 4552–4556. Preparation of New Fe6 and Fe8 Clusters of Iron(III) with Tripodal Ligands.

[119] Gass, I. A., Milios, C. J.; Whittaker, G. A.; Fabiani, F. P. A.; Parsons, S.; Murrie, M.; Perlepes, S. P.; Brecin, E. K. *Inorg. Chem.*, **2006**, *45*, 5281–5283. A Cube in tetrahedron: Microwave-Assisted Synthesis of an Octametallic Fe^{III} Cluster.

[120] Konar, S.; Bhuvanesh, N.; Clearfield, A. *J. Am. Chem. Soc.*, **2006**, *128*, 9604–9605. Oxo-, Hydroxo-, and Peroxo-Bridges Fe(III) Phosphonate Cages.

[121] Konar, S.; Clearfield, A. *Inorg. Chem.*, **2008**, *47*, 5573–5579. Synthesis and Characterization of High Nuclearity Iron(III) Phosphonate Molecular Clusters.

[122] Taft, K. L.; Delfs, C. D.; Papaefthymiou, G. C.; Foner, S.; Gatteschi, D.; Lippard, S. J. *J. Am. Chem. Soc.*, **1994**, *116*, 823–832. $[Fe(OMe)_2(O_2CCH_2Cl)]_{10}$, A Molecular Ferric Wheel.

[123] Stamatatos, T. C.; Christou, A. G.; Mukherjee, S.; Poole, K. M.; Lampropoulos, C.; Abboud, K. A.; O'Brien, T. A.; Christou, G. *Inorg. Chem.*, **2008**, *47*, 9021–9034. High-Yield Syntheses and Reactivity Studies of Fe_{10} ''Ferric Wheels'': Structural, Magnetic, and Computational Characterization of a Star-Shaped Fe_8 Complex.

[124] Ferguson, A.; McGregor, J.; Parkin, A.; Murrie, M. *Dalton Trans.*, **2008**, 731–733. Linking Iron(III) Carboxylates inot High-Nuclearity Complexes by using Bis-tris.

[125] Jones, L. F.; Brecin, E. K.; Collison, D.; Helliwell, M.; Mallah, T.; Piligkos, S.; Rajaraman, G.; Wernsdorfer, W. *Inorg. Chem.*, **2003**, *42*, 6601–6603. A Novel Undecametallic iron(III) Cluster with an S = 11/2 Spin Ground State.

[126] Boskovic, C.; Gudel, H. U.; Labat, G.; Neels, A.; Wernsdorfer, W. *Inorg. Chem.*, **2005**, *44*, 3181–3189. High-Nuclearity Mixed-Chelate Ferric Complexes from a New Family of Polynuclear Precursors.

[127] Ruiz, E.; Cano, J.; Alvarez, S. *Polyhedron*, **2005**, *24*, 2364–2367. An Fe_{11} Complex Showing Single-Molecule Magnet Behavior: Theoretical Study using Density Functional Methods and Monte Carlo Simulations.

[128] Stamatos, T. C.; Christou, A. G.; Jones, C. M.; O'Callaghan, B. J.; Abboud, K. A.; O'Brien, T A.; Christou, G. *J. Am. Chem. Soc.*, **2007**, *129*, 9840–9841. ''Squaring the Circle'': Molecular Squares and Rectangles from Chelate-Induced Structural Transformations of Known Fe_{10} and New Fe_{12} Ferric Wheels.

[129] Tong, J. -P.; Shao, F.; Tao, J.; Huang, R. -B.; Zheng, L. -S. *Inorg. Chem.*, **2011**, *50*, 2067–2069. microwave-Assisted Synthesis of Ferrimagnetic Dodecanuclear Iron(III) Complex with a $Fe_4(OH)_4$ Cubane Core.

[130] Raptopoulou, C. P.; Tangoulis, V.; Devlin, E. *Angew. Chem. Int. Ed.*, **2002**, *41*, 2386–2389. [{$Fe(OMe)_2[O_2CC(OH)Ph_2]12$}] : Synthesis and Characterization of a New Member in the Family of Molecular Ferric Wheels with the Carboxylatobis(alkoxo) Bridiging Unit.

[131] Taft, K. J.; Papaefthymiou, G. C.; Stephen, L. J. *Inorg. Chem.*, **1994**, *33*, 1510–1520. Synthesis, Structure, and Electric Properties of a Mixed-Valent Dodecanuclear Oxo Complex, a Model for the Biomineralization o Ferritin.

[132] Taft, K. J.; Papaefthymiou, G. C.; Stephen, L. J. *Science*, **1993**, *259*, 1302–1305. A Mixed-Iron Polyiron Complexes that Models Biomineralizatio of the Ferritin Core.

[133] Caneschi, A.; Cornia, A.; Lippard, S. J.; Papaefthymiou, G. C.; Sessoli, R. *Inorg. Chim. Acta*, **1996**, *243*, 295–304. Magnetic Properties of Dodecanuclear Mixed Valence Iron Clusters.

[134] Murugesu, M.; Clerac, R.; Wernsdorfer, W.; Anson, C. E.; Powell, A. K. *Angew. Chem. Int. Ed.*, **2005**, *44*, 6678–6682. Hierarchical Assembly of {Fe_{13}} Oxygen-bridged Clusters into a Close-Packed Superstructure.

[135] Tolis, E. I.; Helliwell, M.; Langley, S.; Raftery, J.; Winpenny, R. E. P. *Angew. Chem. Int. Ed.*, **2003**, *42*, 3804–3808. Synthesis and Characterization of Iron (III) Phosphonate Cage Complexes.

[136] Powell, A. K.; Heath, S. L.; Gatteschi, D.; Pardi, L.; Sessoli, R.; Spina, G.; Del Gialo, F.; Pieralli, F. *J. Am. Chem. Soc.*, **1995**, *117*, 2491–2502. Synthesis, structure, and magnetic Properties of Fe_2, Fe_{17}, and Fe_{19} Oxo-Bridged Iron Clusters: Stabilization of High Ground State Spins by Cluster Aggregates.

[137] Micklitz, W.; McKnee, V.; Rardin, L. R.; Pence, L. E.; Papaefthymiou, G. C.; Bott, S. G.; Lippard, S. J. *J. Am Chem. Soc.*, **1994**, *116*, 8061–8069. Polyiron Oxo Chemistry at the Molecular/Solid-State Boundary: Synthesis, Structure, and Magnetic and Mössbauer Properties of [$Fe_{16}MO_{10}(OH)_{10}(O_2CPh)_{20}$] Complexes, M = Mn, Fe, or Co.

[138] Bagai, R.; Abboud, K. A.; Christou, G. *Chem. Commun.*, **2007**, 3359–3361. A discrete Fe_{18} 'Molecular Chain'.

[139] King, P.; Stamatatos, T. C.; Abboud, K. A.; Christou, G. *Angew. Chem. Int. Ed. Engl.*, **2006**, *45*, 7379–7383. Reversible Size Modification of Iron and Gallium Molecular Wheels: A Ga_{10} ''Gallic Wheel'' and Large Ga_{18} and Fe_{18} Wheels.

[140] Zeng, Y. -F; Hu, X.; Xue, L.; Liu, X. -J.; Hu, T. -L.; Bu, X. -H. *Inorg. Chem.*, **2012**, *51*, 9571–9573. Fe_{20} Cluster Units Based Coordination Polymer from in Situ Ligand Conversion and Trapping of Intermediate.

[141] Foguet-Albiol, D.; Abboud, K. A.; Christou, G. *Chem. Commun.*, **2005**, 4282–4284. High-nuclearity Homometalic Iron and Nickel Clusters: Fe_{22} and Ni_{24} Complexes Form the Use of *N*-methylethanolamine.

[142] Zhang, Z. -M.; Li, Y. -G.; Yao, S.; Wang, E. -B.; Wang, Y. -H.; Clerac, R. *Angew. Chem. Int. Ed.*, **2009**, *48*, 1581–1584. Enantiomerically Pure Chiral {Fe_{28}} Wheels.

[143] Hurley, L. H. *Nature Rev.*, **2002**, *2*, 188–200. DNA and Its Associated Processes as Targets for Cancer Therapy.

[144] Francisco, A. P.; Perry, M. d. J.; Moreira, R.; Mendes, E. *Anticancer therapeutics*, Missailidis S., Ed.; Wiley-Blackwell: Chichester, **2008**.

[145] Thoung, N. T.; Helene, C. *Angew. Chem. Int. Ed. Engl.*, **1993**, *32*, 666–690. Sequence-Specific Recognition and Modification of Double-Helical DNA by Oligonucleotides.

[146] Jungwirth, U.; Kowol, C. R.; Keppler, B. K.; Hartinger, C. G.; Berger, W.; Heffeter, P. *Antioxid. Redox Signaling*, **2011**, *15*, 1085–1127. Anticancer Activity of Metal Complexes: Involvement of Redox Processes.

[147] http://medienportal.univie.ac.at/presse/aktuelle-pressemeldungen/detailansicht/artikel/neuer-wirkstoff-im-kampf-gegen-krebs/.

[148] Hamre, D.; Bernstein, J.; Donovick, R. *Proc. Soc. Exper. Biol. & Med.*, **1950**, *73*, 275–278. Activity of *p*-Aminobenzaldehyde, 3-Thiosemicarbazone on Vacinia Virus in the Chick Embryo and in the Mouse.

[149] Brockman, W. R.; Thomson, R. J.; Bell, M. J.; Skipper, H. *Cancer Res.*, **1956**, *16*, 167–170. Observations on the Antileukemic Activity of Pyridine-2-carboxaldehyde Thiosemicarbazone and Thiocarbohydrazone.

[150] Blanz, E. J.; French, F. A.; DoAmaral, J. R.; French, D. A. *J. Med. Chem.*, **1970**, *13*, 1124–1130. Carcinostatic Activity of Thiosemicarbazones of Formyl Heteroaromatic Compounds. VII.. 2-Formylpyridine Derivatives Bearing Additional Ring Substituents.

[151] Liu, M. -C.; Lin, T. -S.; Sartorelli, A. C. *J. Med. Chem.*, **1992**, *35*, 3672–3677. Synthesis and Antitumor Activity of Amino Derivatives of Pyridine-2-carboxaldehyde Thiosemicarbazone.

[152] Kowol, C. R.; Trondl, R.; Heffeter, P.; Arion, V. B.; Jakupec, M. A.; Roller, A.; Galanski, M.; Berger, W.; Keppler, B. K. *J. Med. Chem.*, **2009**, *52*, 5032–5043. Impact of Metal Coordination on Cytotoxicity of 3-Aminopyridine-2-carboxaldehyde Thiosemicarbazone (Triapine) and Novel Insights into Terminal Dimethylation (ref. therein).

[153] Yu, Y.; Kalinowski, D. S.; Kovacevic, Z.; Siafakas, A. R.; Jansson, P. J.; Stefani, C.; Lovejoy, D. B.; Sharpe, P. C.; Bernhardt, P. V.; Richardson, D. R. *J. Med. Chem.*, **2009**, *52*, 5271–5294. Thiosemicarbazones from Old to New: Iron Chelators That Are More Than Just Ribonucleotide Reductase Inhibitors.

[154] Ma, B.; Goh, B. C.; Tan, E. H.; Lam, K. C.; Soo, R.; Leong, S. S.; Wang, L. Z.; Mo, F.; Chan, A. T. C.; Zee, B.; Mok, T. *Invest. New Drugs*, **2008**, *26*, 169–173. A Multicancer phase II Trial of 3-Aminopyridine-2-carboxaldehyde Thiosemicarbazone (3-AP, Triapine) and Gencitabine in Advanced Non-Small-Cell Lung Cancer with Pharmacokinetic Evaluation Using Peripheral Blood Mononuclear Cells.

[155] Karp, J. E.; Giles, F. J.; Gojo, I.; Morris, L.; Greer, J.; Johnson, B.; Thein, M.; Sznol, M.; Low, J. *Leuk. Res.*, **2008**, *32*, 71–77. A Phase I Study of the Novel Ribonucleotide Reductase Inhibitor 3-Aminopyridine-2-carboxaldehyde Thiosemicarbazone (3-AP, Triapine) in Combination with the Nucleoside Analog Fludarabine for Patients with Refractory Acute Leukemias and Aggressive Myeloproliferative Disorders.

[156] Mackenzie, M. J.; Saltman, D.; Hirte, H.; Low, J.; Johnson, B.; Pond, G.; Moore, M. J. *Invest. New Drugs*, **2007**, *25*, 553–558. A Phase II Study of 3-Aminopyridine-2-carboxaldehyde

Thiosemicarbazone (3-AP) and Gemcitabine in Advanced Pancreatic Carcinoma. A Trial of the Princess Margaret Hospital Phase II Consortium.

[157] Chao, J.; Synold, T. W.; Morgan, R. J. Jr.; Kunos, C.; Longmate, J.; Lenz, J. -J.; Lim, D.; Shibata, S.; Chung, V.; Stoller, R. G.; Belani, C. P.; Gandara, D. R.; McNamara, M.; Gitlitz, B. J.; Lau, D. H.; Ramalingam, S. S.; Davies, A.; Espinoza-Delgado, I.; Newman, E. M.; Yen, Y. *Cancer Chemother. Pharmacol.*, **2012**, *69*, 835–843. A Phase I and Pharmacokinetic Study of Oral 3-Aminopyridine-2-carboxaldehyde Thiosemicarbazone (3-AP, NSC#663249) in the Treatment of Advanced-stage Solid Cancers: A California Cancer Cosortium Study.

[158] Huang, H.; Chen, Q.; Ku, X.; Meng, L.; Lin, L.; Wang, X.; Zhu, C.; Wang, Y.; Chen, Z.; Li, M.; Jiang, H.; Chen, K.; Ding, J.; Liu, H. *J. Med. Chem.*, **2010**, *53*, 3048–3064. A Series of α-Heterocyclic Carboxaldehyde Thiosemicarbazones Inhibit Topoisomerase IIα Catalytic Activity.

[159] Joseph, M.; Suni, V.; Kurup, M. R. P.; Nethaji, M.; Kishore, A.; Bhat, S. G. *Polyhedron*, **2004**, *23*, 3069–3080. Structural, Spectral and Antimicrobial Studies of Copper(II) Complexes of Benzoylpyridine *N*(4)-Cyclohexyl Thiosemicarbazone.

[160] Dilovic, I.; Rubcic, M.; Vrdoljak, V.; Pavelic, S. K.; Kralj, M.; Piantanida, I.; Cindric, M. *Bioorg. Med. Chem.*, **2008**, *16*, 5189–5198. Novel Thiosemicarbazone Derivatives as Potential Antitumor Agents: Synthesis, Physicochemical and Structural Properties, DNA Interactions and Antiproliferative Activity.

[161] Lovejoy, D. B.; Richardson, D. R. *Blood*, **2002**, *100*, 666–676. Novel ''hybrid'' iron Chelators Derived from Aroylhydrazones and Thiosemicarbazones Demonstrate Selective Antiproliferative Activity against Tumor Cells.

[162] Yuan, J.; Lovejoy, D. B.; Richardson, D. R. *Blood*, **2004**, *104*, 1450–1458. Novel di-2-pyridyl-Derived Iron Chelators with Marked and SelectiveAntitumor Activity: *in vitro* and *in vivo* Assessment.

[163] Shao, J.; Zhou, B.; Di Bilio, A. J.; Zhu, L.; Wang, T.; Qi, C.; Shih, J.; Yen, Y. *Mol. Cancer Ther.*, **2006**, *5*, 586–592. A Ferrous-Tripine Complex Mediates Formation of Reactive Oxygen Species That Inactivate Human Ribonucleotide Reductase.

[164] Chaston, T. B.; Lovejoy, D. B.; Watts, R. N.; Richardson, D. R. *Clin. Cancer Res.*, **2003**, *9*, 402–414. Examination of the Antiproliferative Activity of Iron Chelators: Multiple Cellular Targets and the Different Mechanism of Action of Triapine Compared with Desferrioxamine and Potent Pyridoxal Isonicotinoyl Hydrazone Analogue 311.

[165] Antholine, W.; Knight, J.; Whelan, H.; Petering, D. H. *Mol. Pharmacol.*, **1977**, *13*, 89–98. Studies of The Reaction of 2-formylpydridine Thiosemicarbazone and Its Iron and Copper Complexes With Biological Systems.

[166] Saryan, L. A.; Mailer, K.; Krishnamurti, C.; Antholine, W.; Petering, D. H. *Biochem. Pharmacol.*, **1981**, *30*, 1595–1604. Interactions of 2-formylpydridine Thiosemicarbazonato Copper (II) With Ehrlich Ascites Tumor Cells.

[167] Zeglis, B. M.; Divilov, V.; Lewis, J. S. *J. Med. Chem.*, **2011**, *54*, 2391–2398. Role of Metalation in the Topoisomerase IIα Inhibition and Antiproliferative Activity of a Series of α-Heterocyclic-N^4-Substitued Thiosemicarbazones and Their Cu(II) Complexes.

[168] Lendzian, F. *Biochim. Biophys. Acta*, **2005**, *1707*, 67–90. Structure and Interactions of Amino Acid Radicals in Class I Ribonucleotide Reductase Studied by ENDOR and High-field EPR Spectroscopy.

[169] Shao, J.; Zhou, B.; Di, Bilio, A. J.; Zhu, L.; Wang, T.; Qi, C.; Shih, J.; Yen, Y. *Mol. Cancer. Ther.*, **2006**, *5*, 586–592. A Ferrous-triapine Complex Mediatets Formation of Reactive Oxygen Species That Inactivate Human Ribonucleotide Reductase.

[170] Lozano, G.; Elledge, S. J. *Nature*, **2000**, *404*, 42–49. p53 Sends Nucleotides to Repair DNA.

[171] Kowol, C. R.; Berger, R.; Eichinger, R.; Roller, A.; Jakupec, M. A.; Schmidt, P. P.; Arion, V. B.; Keppler, B. K. *J. Med. Chem.*, **2007**, *50*, 1254–1265. Galium(III) and Iron(III) Complexes of N-heterocyclic Thiosemicarbazones: Synthesis, Characterization, Cytotoxicity, and Interaction with Ribonucleotide Reductase.

[172] Roy, A.; Das, B. B.; Ganguly, A.; Bose, Dasgupta, S.; Khalkho, N. V. M.; Pal, C.; Dey, S.; Giri, V. S.; Jaisankar, P.; Dey, S.; Majumder, H. K. *Biochem J.*, **2008**, *409*, 611–622. An Isight into the Mechanism of Inhibition of Unusual bi-subunit Topoisomerase I from Leismania Donovani by 3,3'-di-indolymethane, an Novel Topoisomerase I Poison with a Strong Binding Activity.

[173] http://en.wikipedia.org/wiki/Type_II_topoisomerase.

[174] http://helicase.pbworks.com/w/page/17605643/Justin-Neese.

[175] Jansson, P. J.; Sharpe, P. C.; Bernhardt, P. V.; Richardson, D. R. *J. Med. Chem.*, **2010**, *53*, 5759–5769. Novel Thiosemicarbazones of the ApT and Dpt Series and their Copper Complexes: Identification of Pronounced Redox Activity and Characterization of Their Antitumor Activity.

[176] Lee, K. -C.; Thanigaimalai, P.; Sharma, V. K.; Kim, M. -S.; Roh, E.; Hwang, B. -Y.; Kim, Y.; Jung, S. -H. *Bioorg. Med. Chem. Lett.*, **2010**, *20*, 6794–6796. Structural Characteristics of Thiosemicarbazones as Inhibitors of Melanogenesis.

[177] Chen, L. -H.; Hu, Y. -H.; Song, W.; Song, K. -K.; Liu, X.; Jia, Y. -L.; Zhuang, J. -X.; Chen, Q. -X. *J. Agric. Food Chem.*, **2012**, *60*, 1542–1547. Synthesis and Antityrosinase Mechanism of Benzaldehyde Thiosemicarbazones: Novel Tyrosinase Inhibitors.

[178] http://en.wikipedia.org/wiki/Tyrosinase.

[179] Sanchez-Ferrer, A.; Rodriguez-Lopez, J. N.; Garcia-Canovas, F.; Garcia-Carmona, F., *Biochim. Biophys. Acta*, **1995**, *1247*, 1–11. Tyrosinase: A Comprenchensive Review of its Mechanism.

2 Aim of the thesis

The goal of this PhD thesis was the synthesis, characterization and complexation behaviour of benzoic acid derivatives and proline–thiosemicarbazone conjugates, as a models of humic acids and possible application of the compounds prepared in catalysis and in the development of metal–based anticancer drug candidates.

3 Results

This cumulative PhD thesis is constituted of the following articles, published in Inorganic Chemistry (American Chemical Society) and Dalton Transactions (Royal Chemical Society):

L– and D–Proline Thiosemicarbazone Conjugates: Coordination Behaviour in Solution and the Effect of Copper(II) Coordination on Their Antiproliferative Activity

Miljan N. M. Milunovic, Éva A. Enyedy, Nóra V. Nagy, Tamás Kiss, Robert Trondl, Michael A. Jakupec, Bernhard K. Keppler, Regina Krachler, Ghenadie Novitchi, Vladimir B. Arion

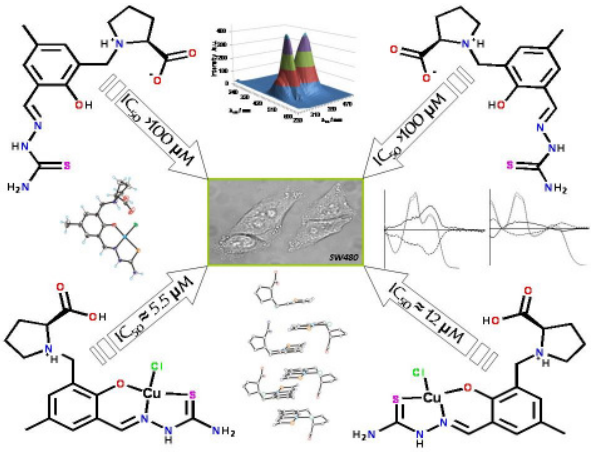

Inorg. Chem. **2012**, *51*, 9309–9321

Hexanuclear and Undecanuclear Iron(III) Carboxylates as Catalyst Precursors for Cyclohexane Oxidation

Miljan N. M. Milunovic, Luísa M. D. R. S. Martins, Elisabete C. B. Alegria, Armando J. L. Pombeiro, Regina Krachler, Günter Trettenhahn, Constantin Turta, Sergiu Shova, Vladimir B. Arion

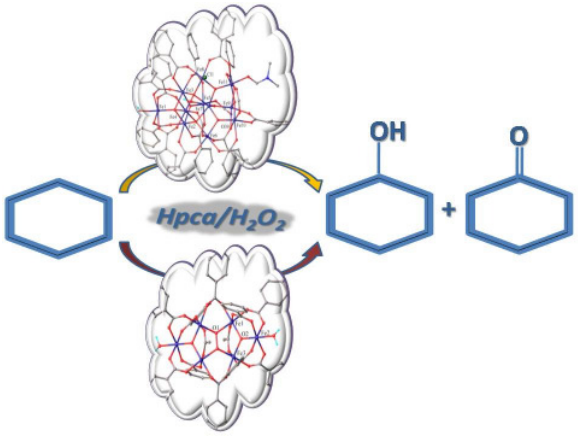

Dalton Trans. **2013**, *42*, 14388–14401

3.1 L– and D–Proline thiosemicarbazone conjugates: coordination behaviour in solution and the effect of copper(II) coordination on their antiproliferative activity

Miljan N. M. Milunovic, Éva A. Enyedy, Nóra V. Nagy, Tamás Kiss, Robert Trondl, Michael A. Jakupec, Bernhard K. Keppler, Regina Krachler, Ghenadie Novitchi, Vladimir B. Arion

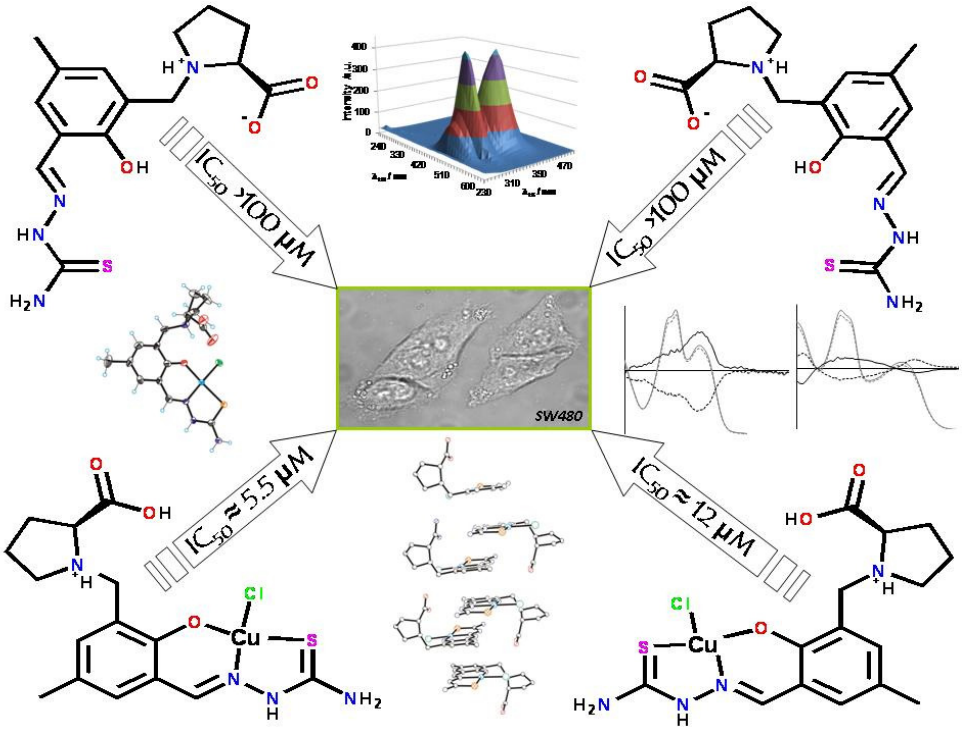

Inorg. Chem. **2012**, *51*, 9309–9321

Contribution to the paper: Synthesis and characterization of L– and D–Proline Thiosemicarbazone conjugates and their copper(II) complexes. Investigation of the coordination behaviour of L–Proline thiosemicarbazone conjugate in solution toward transition metals Fe(III), Fe(II), Cu(II), Zn(II) by UV–vis spectrophotometry, spectrofluorimetry, circular dichroism and ^{1}H NMR spectroscopy, as well as determination of the distribution coefficient (D). Interactive participation in writing introduction, discussion of the results, conclusions and proof-readings of the manuscript as well as design of the graphical abstract.

Inorganic Chemistry

Article

pubs.acs.org/IC

L- and D-Proline Thiosemicarbazone Conjugates: Coordination Behavior in Solution and the Effect of Copper(II) Coordination on Their Antiproliferative Activity

Miljan N. M. Milunovic,[†] Éva A. Enyedy,*[,‡] Nóra V. Nagy,[§] Tamás Kiss,[‡,⊥] Robert Trondl,[†] Michael A. Jakupec,[†] Bernhard K. Keppler,[†] Regina Krachler,[†] Ghenadie Novitchi,[¶] and Vladimir B. Arion*[,†]

[†]Institute of Inorganic Chemistry, University of Vienna, Währinger Strasse 42, A-1090 Vienna, Austria

[‡]Department of Inorganic and Analytical Chemistry, University of Szeged, Dóm tér 7, H-6720 Szeged, Hungary

[§]Institute of Molecular Pharmacology, Research Centre for Natural Sciences, Hungarian Academy of Sciences, Pusztaszeri út 59−67, H-1025 Budapest, Hungary

[⊥]Bioinorganic Chemistry Research Group of the Hungarian Academy of Sciences, University of Szeged, Dóm tér 7, H-6720 Szeged, Hungary

[¶]Laboratoire National des Champs Magnétiques Intenses, CNRS UPR-3228, 25 rue des Martyrs, 38042 Grenoble Cedex 9, France

Supporting Information

ABSTRACT: Two enantiomerically pure thiosemicarbazone−proline conjugates with enhanced aqueous solubility, namely, 2-hydroxy-3-methyl-(*S*)-pyrrolidine-2-carboxylate-5-methylbenzaldehyde thiosemicarbazone [L-Pro-STSC or (*S*)-H_2L] and 2-hydroxy-3-methyl-(*R*)-pyrrolidine-2-carboxylate-5-methylbenzaldehyde thiosemicarbazone [D-Pro-STSC or (*R*)-H_2L] have been synthesized and characterized by elemental analysis, spectroscopic methods (UV−vis and ^{1}H and ^{13}C NMR), and electrospray ionization mass spectrometry. The metal complexation behavior of L-Pro-STSC, stoichiometry, and thermodynamic stability of iron(II), iron(III), copper(II), and zinc(II) complexes in 30% (w/w) dimethyl sulfoxide/H_2O solvent mixture have been studied by pH-potentiometric, UV−vis-spectrophotometric, circular dichroism, electron paramagnetic resonance, ^{1}H NMR spectroscopic, and spectrofluorimetric measurements. By the reaction of $CuCl_2 \cdot 2H_2O$ with (*S*)-H_2L and (*R*)-H_2L, respectively, the complexes [Cu[(*S*)-H_2L]Cl]Cl and [Cu[(*R*)-H_2L]Cl]Cl have been prepared and comprehensively characterized. An X-ray diffraction study of [Cu[(*R*)-H_2L]Cl]Cl showed the formation of a square-planar copper(II) complex, which builds up stacks with interplanar separation of 3.3 Å. The antiproliferative activity of two chiral ligands and their corresponding copper(II) complexes has been tested in two human cancer cell lines, namely, SW480 (colon carcinoma) and CH1 (ovarian carcinoma). The thiosemicarbazone−proline conjugates L- and D-Pro-STSC show only moderate cytotoxic potency with IC_{50} values of 62 and 75 μM, respectively, in CH1 cells and >100 μM in SW480 cells. However, the corresponding copper(II) complexes are 13 and 5 times more potent in CH1 cells, based on a comparison of IC_{50} values, and in SW480 cells the increase in the antiproliferative activity is even higher. In both tested cell lines, L-Pro-STSC as well as its copper(II) complex show slightly stronger antiproliferative activity than the compounds with a D-Pro moiety, yielding IC_{50} values of 4.6 and 5.5 μM for [Cu(L-Pro-STSC)Cl]Cl in CH1 and SW480 cells, respectively.

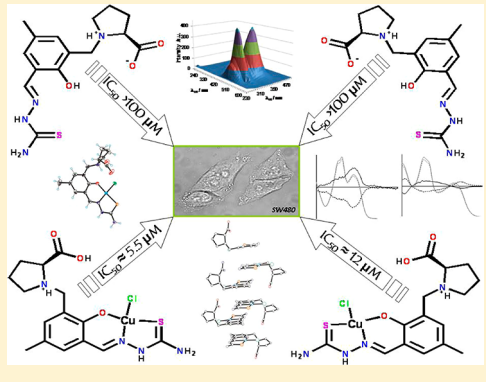

INTRODUCTION

Thiosemicarbazones (TSCs) are strong chelating ligands for transition metals with a broad spectrum of biological activity.[1,2] α(N)-Heterocyclic TSCs are known as potential antitumor drugs.[3,4] Triapine (3-aminopyridine-2-carboxaldehyde thiosemicarbazone) is the most prominent example of this family of compounds and has been extensively studied as a single agent and in combinations with established drugs in phase I and II clinical trials with mixed results.[5−8] Triapine and other related TSCs, as well as their metal complexes, are known as strong inhibitors of ribonucleotide reductase (RNR), an important enzyme promoting the production of deoxyribonucleotides required for DNA synthesis and cell proliferation,[9−14] while some copper(II) thiosemicarbazonates inhibit topoisomerase IIα, an enzyme responsible for regulation of the DNA topology,[15−17] or induce oxidative stress.[18] The formation of an iron(II) complex with Triapine, its reaction with molecular oxygen, and the subsequent formation of reactive oxygen species, which destroy the tyrosyl radical of RNR, are

Received: May 10, 2012
Published: August 13, 2012

considered the main steps in their mode of action.[19,20] A potential specific binding pocket for Triapine on the surface of the mouse R2 RNR protein has been proposed quite recently.[21] The ability of TSCs to act as chelators of transition-metal ions is well documented in the literature by isolation and characterization of the resulting complexes in the solid state[22] and by solution equilibrium studies, which provide valuable information about the chemical species present in aqueous solution at physiological pH and their thermodynamic stability.[23] Studies in solution are of utmost importance for an understanding of the mechanism of action of biologically active compounds and the design of even stronger chelators. However, such investigations are very often hampered by the low aqueous solubility of TSCs.

2-Hydroxybenzaldehyde (or salicylaldehyde) TSC (STSC) was also reported to form complexes with transition metals.[24] However, this organic compound shows only a moderate cytotoxic activity in tumor cells,[25,26] in comparison with α(N)-heterocyclic TSCs exhibiting IC_{50} values in the low-micromolar or even high-nanomolar range,[27,22f] and the reasons for this dramatic drop in activity are still unknown. The antiproliferative activity of STSC can be enhanced to some extent by attachment of polar, electron-donating substituents, e.g., dimethylamino and/or methoxy group(s) to the 2-hydroxybenzaldehyde moiety,[26] or by coordination to metal ions.[25]

Copper(II) chloride forms a square-planar complex with 2-hydroxy-3-methoxybenzaldehyde TSC (HL) of 1:1 stoichiometry, namely, $[Cu(L)Cl]\cdot H_2O$.[28] The methoxy group and the cocrystallized water molecule are involved in the formation of one-dimensional planar chains via intermolecular hydrogen-bonding interactions. By the reaction of copper(II) sulfate with salicylaldehyde-β-D-glycoside TSC followed by recrystallization of the precipitate from dimethyl sulfoxide (DMSO), the complex $[Cu(L^1)(H_2O)]_2SO_4\cdot 2DMSO\cdot 6H_2O$, where HL^1 = 2-hydroxybenzaldehyde TSC, was isolated and characterized.[25] The crystal structure consists of centrosymmetric dinuclear cations stabilized by $\pi-\pi^*$ interaction between four-coordinate square-planar monocations. The X-ray diffraction structures of both copper(II) complexes imply that both species are potential DNA intercalators. Moreover, it has been reported recently that square-planar coordination geometry of some copper(II) TSCs is likely the biologically active configuration in Topo-IIα inhibition via an ATP binding-site-based mechanism.[16,17]

Reports on the thermodynamic stability of the metal complexes of STSC and its derivatives are scarce in the literature[29] because of their generally low aqueous solubility hampering solution equilibrium studies. Quite recently, some of us studied in detail the stoichiometry and thermodynamic stability of iron(II), iron(III), copper(II), zinc(II), and gallium(III) complexes with STSC in a H_2O/DMSO mixture by pH-potentiometric, UV–vis-spectrophotometric, electron paramagnetic resonance (EPR), ^{1}H NMR spectroscopic, and spectrofluorimetric measurements and compared these data with those for α(N)-heterocyclic TSCs.[23b,c,29] Herein we report on the synthesis and spectroscopic characterization of two enantiomerically pure Pro-STSC conjugates with enhanced aqueous solubility, namely, 2-hydroxy-3-methyl-(*S*)-pyrrolidine-2-carboxylate-5-methylbenzaldehyde thiosemicarbazone [L-Pro-STSC or (*S*)-H_2L] and 2-hydroxy-3-methyl-(*R*)-pyrrolidine-2-carboxylate-5-methylbenzaldehyde thiosemicarbazone [D-Pro-STSC or (*R*)-H_2L] (Scheme 1). The metal complexation behavior of L-Pro-STSC, stoichiometry, and thermodynamic stability of iron(II) and iron(III), copper(II), and zinc(II) complexes in a 30% (w/w) DMSO/H_2O solvent mixture have been studied by pH-potentiometric, UV–vis-spectrophotometric, EPR, ^{1}H NMR, circular dichroism (CD) spectroscopic, and spectrofluorimetric measurements. In addition, the isolation and characterization of square-planar copper(II) complexes with enantiomerically pure Pro-STSC conjugates in the solid state are reported. The effect of copper(II) coordination, as well as the chirality of the Pro moiety on the antiproliferative activity of conjugates in two human cancer cell lines, has been studied as well.

Scheme 1. Synthesis of Chiral Thiosemicarbazone–Proline Derivatives (*S*)-H_2L and (*R*)-H_2L[a]

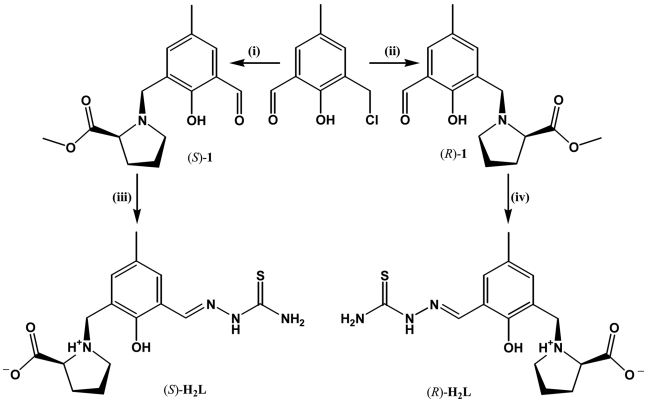

[a]Reagents and conditions: (i) methyl (*S*)-pyrrolidine-2-carboxylate hydrochloride, triethylamine, 1.5:1 THF/CH_2Cl_2, room temperature, purification by column chromatography [(*S*)-**1**, 51%]; (ii) methyl (*R*)-pyrrolidine-2-carboxylate hydrochloride, triethylamine, 1.5:1 THF/CH_2Cl_2, room temperature, purification by column chromatography [(*R*)-**1**, 39%]; (iii) thiosemicarbazide, 1:1 EtOH/H_2O, 70–75 °C, 75 h, [(*S*)-H_2L, 41%]; (iv) thiosemicarbazide, 1:1 EtOH/H_2O, 70–75 °C, 12 h, [(*R*)-H_2L, 18%].

RESULTS AND DISCUSSION

Synthesis and Characterization of Chiral TSCs. The chiral thiosemicarbazone–proline conjugates have been prepared in three steps, as shown in Scheme 1. First, 3-(chloromethyl)-2-hydroxy-5-methylbenzaldehyde[30] was allowed to react with L- or D-proline methyl ester hydrochloride in the presence of triethylamine with the formation of compounds (*S*)- and (*R*)-**1**, respectively. Condensation reactions of these latter compounds with thiosemicarbazide followed by hydrolysis of the methyl ester groups afforded the corresponding TSCs coupled via a methylene group to Pro moiety [(*S*)-H_2L and (*R*)-H_2L]. The formation of the desired species has been confirmed by ^{1}H and ^{13}C NMR measurements, as well as by electrospray ionization mass spectrometry (ESI-MS). The number of ^{1}H and ^{13}C resonances in NMR spectra is in accordance with the proposed structure of C_1 point symmetry. The mass spectra recorded in positive-ion mode showed peaks at m/z 359 and 337 due to $[M + Na]^+$ and $[M + H]^+$ ions, respectively. The pH-metric titrations (vide infra) suggest that L-Pro-STSC is tribasic in the studied pH range and adopts a zwitterionic structure, as shown in Scheme 2.

Aqueous solutions of L- and D-Pro-STSC ligands at neutral pH are indeed optically active and show Cotton effects for both enantiomers (see Figure S1A in the Supporting Information, SI). As expected, they are roughly mirror images over the 240–

dx.doi.org/10.1021/ic300967j | Inorg. Chem. 2012, 51, 9309–9321

Scheme 2. Deprotonation Steps of H_3L^+ (Relevant for Both Pro-STSC Enantiomers)[a]

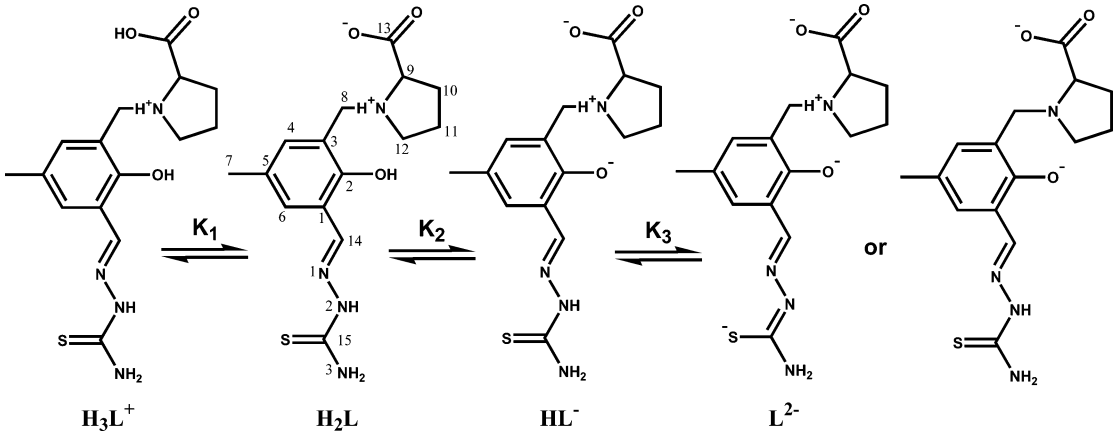

[a]Atom labeling was introduced for assignment of the proton resonances.

400 nm region of the circular dichroism (CD) spectra, while their UV–vis spectra are identical.

Synthesis and Characterization of [Cu[(*S*)-H_2L]Cl]Cl and [Cu[(*R*)-H_2L]Cl]Cl. By the reaction of a methanolic solution of $CuCl_2·2H_2O$ with (*S*)-H_2L and (*R*)-H_2L, the complexes [Cu[(*S*)-H_2L]Cl]Cl and [Cu[(*R*)-H_2L]Cl]Cl have been isolated in 55 and 84% yield, respectively. The positive-ion ESI mass spectra showed the presence of a strong peak at *m*/*z* 398 attributed to $[Cu^{II}(HL)]^+$. In the negative-ion mass spectra, ions with *m*/*z* 396 and 432 due to $[Cu^{II}(LH)]^-$ and $[Cu^{II}LCl]^-$, respectively, were observed. The protonation form of the Pro-STSC ligand adopted in the prepared copper(II) complexes has been unequivocally established by the X-ray diffraction study of [Cu^{II}[(*R*)-H_2L]Cl]Cl. Note that for the charge-neutral-coordinated ligand in this complex we use for consistency the same abbreviation H_2L, although the charge distribution differs from that shown in Scheme 2.

The CD spectra of both copper(II) complexes of L-Pro-STSC and D-Pro-STSC recorded at pH 7.4 in the UV range in a pure aqueous solution are shown in Figure S1B in the SI.

X-ray Crystallography. X-ray diffraction quality crystals were obtained by the slow diffusion of diethyl ether into a methanolic solution of [Cu[(*R*)-H_2L]Cl]Cl. The result of an X-ray diffraction study of [Cu[(*R*)-H_2L]Cl]Cl is shown in Figure 1. The complex crystallizes in the noncentrosymmetric monoclinic space group $P2_1$ with two crystallographically independent ionic complexes in the asymmetric unit. The copper(II) ion has a square-planar coordination geometry. The multidentate ligand (H_2L) uses only, in part, its donor capacity and acts in the complex as a tridentate one, binding to Cu^{2+} via phenolate oxygen O1a, imine nitrogen N1a, and thione atom S1a. The bond length C8a–S1a of 1.698(6) is equal within 3σ with that in [Cu(L)Cl]·H_2O,[28] where HL = 2-hydroxy-3-methoxybenzaldehyde thiosemicarbazone. The fourth position in the coordination polyhedron is occupied by a chlorido ligand. In addition, the Pro-STSC ligand is protonated at proline nitrogen atom N4a. Protonation is corroborated by a difference Fourier map and by the presence of intramolecular bifurcated hydrogen-bonding interactions N4a–H···O1a [N4a···O1a 2.695(5) Å; N4a–H···O1a 131.1°] and N4a–H···O2a [N4a···O2a 2.696(5) Å; N4a–H···O2a 113.8°]. The nitrogen atom N2a acts as a proton donor in hydrogen-bonding interaction N2a–H···Cl2 [N2a···Cl2 3.072(5) Å; N2a–H···Cl2 147.9°], while O3a in hydrogen-bonding interaction O3a–H···$Cl1a^i$ [O3a···$Cl1a^i$ 3.038(4) Å; O3a–H···$Cl1a^i$ 171.1°], where i denotes a symmetry-related Cl1a atom generated via symmetry code $x - 1, y, z$. Other hydrogen-bonding interactions are shown in the unit cell plot in Figure S2 in the SI. The two crystallographically independent complex cations form stacks in the crystal via π–π* interactions with interplanar separation of about 3.3 Å, as shown in Figure S3 in the SI. This implies that copper(II) complexes can be considered as potential DNA intercalators, similarly to other square-planar metal complexes with chemically related ligands.[31]

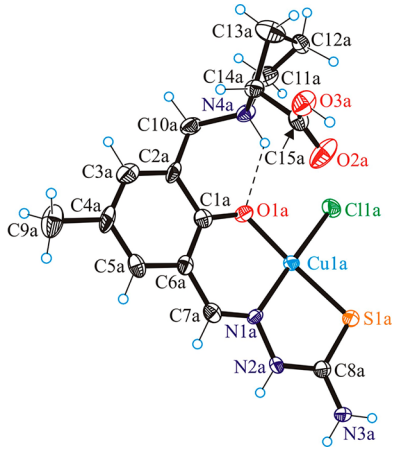

Figure 1. ORTEP view of one of the crystallographically independent cations [Cu[(*R*)-H_2L]Cl]$^+$ with thermal displacement ellipsoids drawn at the 50% probability level. Selected bond distances (Å) and bond angles (deg): Cu1a–Cl1a 2.2669(16), Cu1a–S1a 2.2256(15), Cu1a–O1a 1.887(3), Cu1a–N1a 1.956(4), C1a–O1a 1.321(7), C1a–C6a 1.404(8), C6a–C7a 1.422(7), C7a–N1a 1.291(7), N1a–N2a 1.392(6), N2a–C8a 1.336(7), C8a–S1a 1.706(6), C8a–N3a 1.311(6), C15a–O2a 1.193(6), C15a–O3a 1.330(5); O1a–Cu1a–N1a 92.17(17), N1a–Cu1a–S1a 87.26(13), S1a–Cu1a–Cl1a 90.44(6), O1a–Cu1a–Cl1a 90.49(12).

SOLUTION CHEMISTRY

Proton-Dissociation Processes and Lipophilicity. Proton-dissociation processes of (*S*)-H_2L (Scheme 2) were followed by pH potentiometry, UV–vis spectrophotometry, and spectrofluorimetry as well as ^{1}H NMR titrations. Measurements were performed in a 30% (w/w) DMSO/H_2O

dx.doi.org/10.1021/ic300967j | Inorg. Chem. 2012, 51, 9309–9321

solvent mixture. Consecutive titrations showed that no ligand decomposition occurred in the pH range studied under an argon atmosphere. Three proton-dissociation constants could be determined by different methods (Table 1), and constants obtained are in reasonably good agreement. pK_1 can presumably be attributed to deprotonation of the carboxylic group in (*S*)-H_3L^+, while pK_2 belongs presumably to the phenolic OH. pK_3 can be related to the proton dissociation of the N^2–H group of the thiosemicarbazide moiety or proton dissociation of the tertiary Pro nitrogen. On the basis of the methods used, we cannot distinguish these most probably overlapping deprotonation processes. It is worth noting that the magnitudes of the pK_1 and pK_3 values, low and high, respectively, hamper their accurate determination by pH-metry because these deprotonation steps take place in the pH ranges where the pH measurements become uncertain.

Table 1. Proton-Dissociation Constants (pK_a) of the Ligand L-Pro-STSC Determined by Various Methods,[a] λ_{max} and Molar Absorptivity (M^{-1} cm^{-1}) Values for Ligand Species H_2L, HL^-, and L^{2-} Determined by UV–Vis-Spectrophotometric Titrations, and Calculated Chemical Shifts (ppm) for H_3L^+, H_2L, and HL^- Obtained by ^1H NMR Titrations [T = 298 K, I = 0.10 M (KCl) in 30% (w/w) DMSO/H_2O]

	pH-metry	UV–vis	^1H NMR[b]
pK_1	2.17(8)		2.36(5)
pK_2	7.90(3)	7.79(8)	7.85(2)
pK_3	11.88(12)	11.66(10)	
		λ_{max}, nm (ε, M^{-1} cm^{-1})	
H_2L		308 (19250), 336 (15820)	
HL^-		302 (16490), 388 (11640)	
L^{2-}		308 (14700), 362 (12200)	

	$C^{14}H$	C^4H	C^6H	C^7H_3	C^8H_2		C^9H
δ,[b] ppm	(s)	(s)	(s)	(s)	(d)	(d)	(m)
H_3L^+	8.243	7.400	7.320	2.294	3.644	4.195	3.311
H_2L	8.239	7.392	7.319	2.292	3.601	3.975	3.231
HL^-	8.420	7.609	7.043	2.184	3.294	3.743	2.916

[a]The numbers in parentheses are standard uncertainties of the quoted pK_a values. [b]Determined in 30% (w/w) DMSO-d_6/H_2O.

The pH-dependent physicochemical properties of the L-Pro-STSC ligand such as fluorescence emission, absorbance, and chemical shifts were monitored by different spectroscopic methods with a different level of sensitivity to the certain proton-dissociation processes. The UV–vis spectra are almost unchanged in the pH range where deprotonation of the carboxylic group occurs (Figure 2); thus, pK_1 could not be determined by this method with acceptable accuracy. Deprotonation of the phenolic OH is accompanied by a considerable shift of the λ_{max} value from 336 to 388 nm, and the colorless solution of the ligand turns into yellow. Two well-separated isosbestic points are seen at 355 and 373 nm due to the deprotonation equilibria $H_2L \rightleftharpoons HL^- + H^+$ and $HL^- \rightleftharpoons L^{2-} + H^+$, respectively. Therefore, pK_2 and pK_3 values and the spectra of the individual ligand species H_2L, HL^-, and L^{2-} (Table 1 and Figure S4 in the SI) were calculated on the basis of deconvolution of the UV–vis spectra.

L-Pro-STSC possesses intrinsic fluorescence because of its extended conjugated electronic system (see Figure 3 and its inset for the three-dimensional fluorescence spectrum), which is a valuable property for, e.g., monitoring of the cellular uptake or intracellular distribution of the ligand or its metal complexes by fluorescence microscopy. The fluorescence emission of L-Pro-STSC in its zwitterionic H_3L^+ or H_2L forms is negligible at any excitation wavelength; however, proton dissociation at the phenolic OH results in a significant increase of the intensity, which is diminished by the third deprotonation step above pH 10.5 (Figure 3).

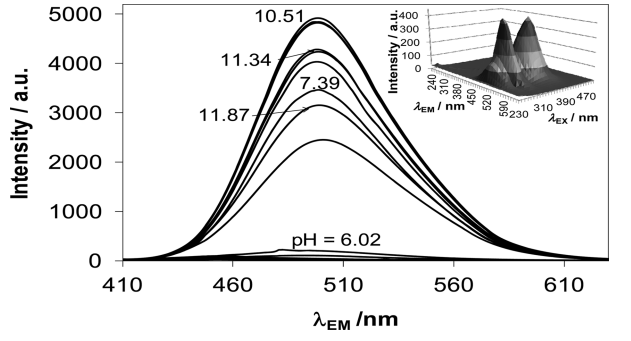

Figure 3. Fluorescence emission spectra of L-Pro-STSC at different pH values [c_{ligand} = 5.0 × 10^{-6} M; λ_{EX} = 393 nm; T = 298 K, I = 0.10 M (KCl) in 30% (w/w) DMSO/H_2O; slits = 5 nm/5 nm]. The inset shows the three-dimensional fluorescence spectrum at pH 10.0 (slits = 2.5 nm/2.5 nm).

The pH-dependent ^1H NMR spectra of the ligand (Figure S5 in the SI) revealed that the protons C^9H and C^8H_2 are most sensitive to deprotonation of the COOH group. Therefore, pK_1 was calculated based on the changes of the chemical shifts (δ) of these protons (Figure 4). The second proton dissociation step is accompanied by significant electronic shielding effects,

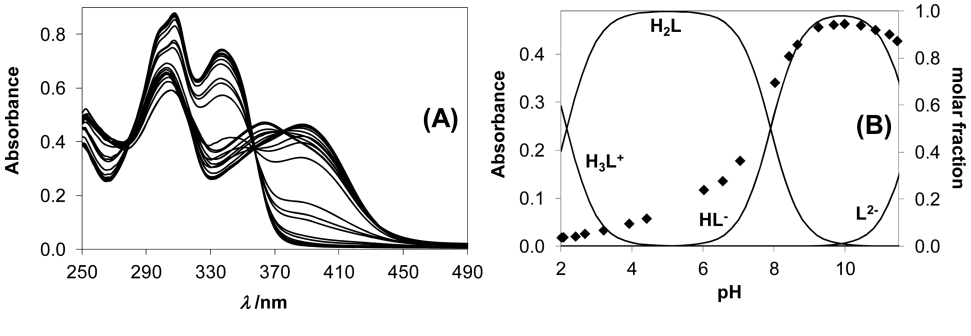

Figure 2. UV–vis spectra of L-Pro-STSC at different pH values (A). Concentration distribution curves for ligand species with the pH dependence of the absorbance values at 384 nm (◆) (B) [c_{ligand} = 4.0 × 10^{-5} M; T = 298 K, I = 0.10 M (KCl) in 30% (w/w) DMSO/H_2O].

dx.doi.org/10.1021/ic300967j | Inorg. Chem. 2012, 51, 9309–9321

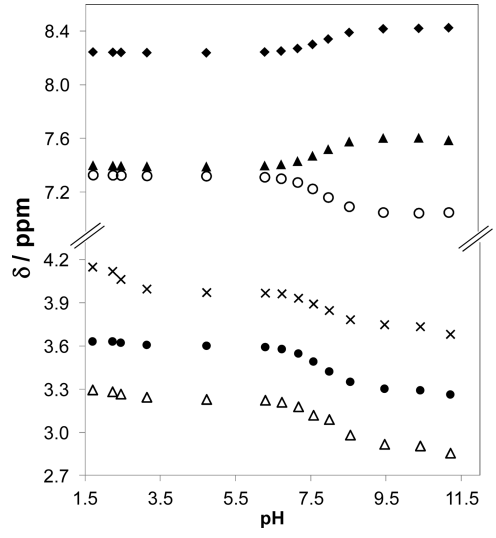

Figure 4. pH dependence of the chemical shifts (δ) of the various protons of the ligand L-Pro-STSC: $C^{14}H$ (♦); $C^{4}H$ (▲); $C^{6}H$ (○); $C^{8}H_2$ (●, ×); $C^{9}H$ (△) [T = 298 K; I = 0.10 M (KCl) in 30% (w/w) DMSO-d_6/H_2O]. For the assignment of particular proton resonances, see Scheme 2 and Figure S5 in the SI.

namely, upfield shifts of the $C^{6}H$, $C^{8}H_2$, and $C^{9}H$ protons, while the $C^{14}H$ and $C^{4}H$ resonances were downfield-shifted upon increasing pH (see Figure S5 in the SI). Further changes were observed at pH > 11 due to the third deprotonation step, but data were not appropriate for calculation of the pK_3 value. We should note here that $C^{8}H_2$ protons are displayed in ^{1}H NMR spectra as two doublets because of the nonequivalent orientation in space of the two protons.

The phenolic OH of the ligand L-Pro-STSC is considerably more acidic compared to that of reference STSC (pK = 8.89[29]). This is presumably due to the formation of a hydrogen bond between the phenolate group and the protonated nitrogen atom of the Pro moiety, which can stabilize the conjugate base and, hence, decrease the pK.

Distribution coefficients (D) of L- and D-Pro-STSC were determined at pH 7.4 via the partitioning between n-octanol and water (Figure S6 in the SI). The Pro-STSC conjugates show more hydrophilic character (log $D_{7.4}$ = −0.56 ± 0.01 for the L enantiomer and −0.60 ± 0.01 for the D enantiomer) compared to the reference STSC (log $D_{7.4}$ = +1.74)[29] or Triapine (log $D_{7.4}$ = +0.85).[29] At physiological pH, the Pro-STSC ligand is mainly present in the neutral form (75% H_2L; 25% HL^-) and the carboxylic group is fully deprotonated. This relatively low log D value is manifested in enhanced aqueous solubility compared to other chemically related TSCs. The lipophilicity of both complexes was determined via n-octanol/water partitioning (Figure S7 in the SI) at physiological pH. As expected, similar log $D_{7.4}$ = +0.25 ± 0.01 and +0.24 ± 0.01 values were obtained for the copper(II) complexes with L and D enantiomers, respectively, showing a more lipophilic character compared to the metal-free ligands. (It should be noted that the distribution coefficients were calculated strictly on the basis of the aqueous phase spectra and the log $D_{7.4}$ values are equal to their partition coefficients (P) as the neutral [CuL] species predominate at this pH.)

Complexation Reactions of Copper(II), Zinc(II), Iron(II), and Iron(III) with L-Pro-STSC. The complex formation processes of the ligand L-Pro-STSC with Cu^{2+}, Zn^{2+}, Fe^{2+}, and Fe^{3+} were studied primarily by pH potentiometry in a 30% (w/w) DMSO/H_2O solvent mixture. The complex formation with Fe^{3+} and Cu^{2+} starts at low pH (pH ∼ 2) in the millimolar concentration range, while that with Zn^{2+} and Fe^{2+} only starts at pH > 4 (see Figure 5 for Fe^{2+}). The formation of some

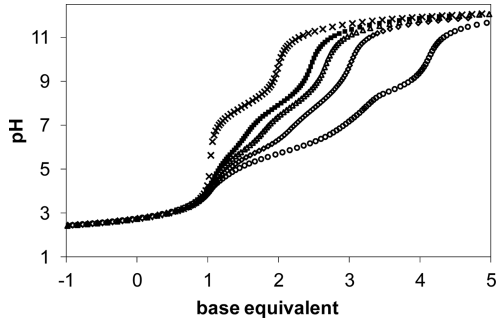

Figure 5. Representative pH-potentiometric titration curves for ligand (×) and for the Fe^{2+}–L-Pro-STSC system at 1:1.2 (○), 1:2.3 (◇), 1:3.3 (△), and 1:4.5 (■) metal-to-ligand ratios [c_{ligand} = 2 × 10^{-3} M, 30% (w/w) DMSO/H_2O), T = 298 K, I = 0.10 M (KCl)].

mixed hydroxido species occurred at basic pH mainly at a 1:1.2 metal-to-ligand ratio, as concluded from the base consumption exceeding the number of dissociable protons in the ligand. The stoichiometries of the metal complexes and the cumulative stability constants furnishing the best fits to the experimental data are listed in Table 2. The stability constant of the species $[Fe^{III}LH]^{2+}$ was determined by spectrophotometry on individual samples following the changes of the metal-to-ligand charge-transfer (CT) and ligand bands in the region of 300–470 nm between pH 1 and 2. Then the determined value was kept constant during the pH-metric data evaluation.

The data reveal the formation of merely monoligand complexes of Cu^{2+} and Zn^{2+}, while Fe^{2+} and Fe^{3+} ions, in addition, form bis-ligand complexes. A direct comparison of the overall stability constants undoubtedly shows the significantly higher stability of the Fe^{3+} and Cu^{2+} complexes over that of the Zn^{2+} and Fe^{2+} species. pM values have been computed to provide a basis for a comparison of the relative chelating ability of L-Pro-STSC at physiological pH (Table 2). (pM stands for the negative logarithm of the equilibrium concentrations of the free metal ion under certain conditions. pM* was also calculated for Fe^{3+}, which involves the various hydroxido species $[Fe^{III}{}_pH_r]$ because they belong to the unbound fraction, in addition to the free Fe^{3+} ion.)

According to these pM (pM*) values, the ligand effectiveness is varied in the following order at pH 7.4: Fe^{2+} ∼ Zn^{2+} < Fe^{3+} < Cu^{2+}. It is worth noting that L-Pro-STSC shows the formation of similar types of complexes and quite similar pM values with those of its reference model ligand, STSC. However, a slightly higher efficacy of L-Pro-STSC is seen in the case of Fe^{3+} and Zn^{2+}.[29] These findings suggest that both ligands coordinate to the metal centers in a similar fashion and the L-Pro moiety does not alter significantly the composition and stability of the metal complexes but improves their aqueous solubility. In order to elucidate the most probable coordination modes of L-Pro-STSC in metal complexes and to confirm the speciation obtained by the pH potentiometry, UV–vis, EPR, CD, and ^{1}H NMR spectroscopies were applied.

Weak bands in the visible wavelength range belong mainly to the d–d transitions of the Cu^{2+}–L-Pro-STSC complexes ($\varepsilon_{580\ nm}$ ∼ 100–180 M^{-1} cm^{-1}), which are partly overlapped

dx.doi.org/10.1021/ic300967j | Inorg. Chem. 2012, 51, 9309–9321

Table 2. Stability Constants ($\log \beta[M_pL_qH_r]$) for the Cu^{2+}, Zn^{2+}, Fe^{2+}, and Fe^{3+} Complexes of L-Pro-STSC with Some Stepwise Constants and p*M* Values [*T* = 298 K, *I* = 0.10 M (KCl) in 30% (w/w) DMSO/H_2O][a]

	Cu^{2+}	Zn^{2+}	Fe^{2+}	Fe^{3+}
$\log \beta([MLH])$	21.58(3)	18.12(3)	18.14(4)	22.39(4)[b]
$\log \beta([ML])$	17.54(3)	12.40(3)	12.24(6)	19.48(3)
$\log \beta([MLH_{-1}])$	6.97(4)	2.51(3)		
$\log \beta([ML_2H])$			28.86(5)	38.24(3)
$\log \beta([ML_2])$			21.07(6)	33.32(4)
$\log \beta([ML_2H_{-1}])$			10.99(7)	22.13(8)
fitting parameter, mL	5.15×10^{-3}	5.52×10^{-3}	8.64×10^{-3}	3.01×10^{-3}
$\log K([ML_2])$[e]			8.83	13.84
p*M*[c]	13.4	8.3	8.2	18.9[d]

[a]The numbers in parentheses are standard uncertainties for the stability constants of the complexes. Charges of the complexes are omitted for simplicity (H_2L is charge-neutral). [b]Determined by UV–vis-spectrophotometric measurements at pH 1–2. [c]p*M* (=−log [M]) values at pH 7.4; $c_M = 1 \times 10^{-6}$ M; M:L = 1:10. [d]p*M** = $-\log(S[M_pH_r]) = 10.9$ at pH 7.4; $c_M = 1 \times 10^{-6}$ M; M:L = 1:10. [e]The $K[ML_2]$ stepwise constant is related to the equilibrium ML + L ⇌ ML_2. The definition of the other overall stability constants is given in the SI.

with the S–Cu^{2+} ligand-to-metal CT bands and represent characteristic pH-dependent changes (Figure 6A). The λ_{max} value of this band is decreased significantly parallel to the formation of species [CuL] from $[CuLH]^+$. The formation of $[CuLH_{-1}]^-$ is accompanied by a smaller decrease of λ_{max} along with an increment in the ligand field and a change of the coordination mode of the ligand in complexes (Figure 6B). Because the ligand is optically active due to the presence of chirality at the proline moiety, CD spectra in the wavelength range 460–650 nm were recorded (Figure 6C). The location of the maxima and minima of the peaks shows a pH dependence, and parallel changes with the transformation processes of the complexes are seen; e.g., the negative peak is shifted from 650 via 615 to 562 nm as species [CuL] and $[CuLH_{-1}]^-$ are formed.

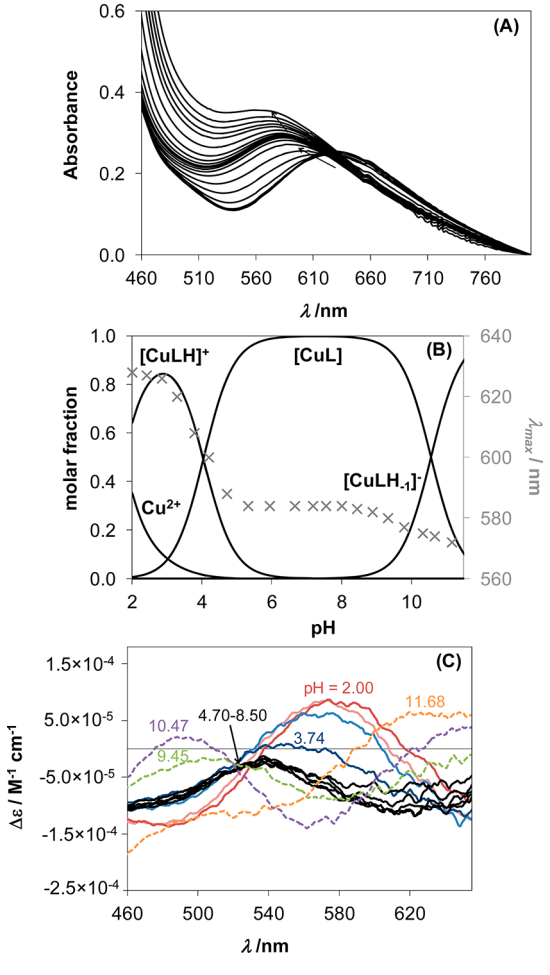

Figure 6. UV–vis spectra of the Cu^{2+}–L-Pro-STSC system recorded at different pH values (A) with the corresponding concentration distribution curves calculated with the stability constants obtained by pH-metry depicted together with the λ_{max} values plotted against the pH (B) and the pH-dependent CD spectra of the system (C) [$c_M = 2.0 \times 10^{-3}$ M, M:L = 1:1, *T* = 298 K, *I* = 0.10 M (KCl) in 30% (w/w) DMSO/H_2O].

EPR spectra of Cu^{2+}–L-Pro-STSC species in 30% (w/w) DMSO/H_2O recorded at various pH values at room temperature (Figure 7) and at 77 K (Figure S8 in the SI) confirm the speciation obtained by the pH potentiometry and reveal the coordination modes of the ligand in each Cu^{2+} complex. A two-dimensional simulation of the solution EPR spectra resulted in the individual isotropic EPR parameters of the different Cu^{2+}–L-Pro-STSC species (Table 3). The fitted experimental and individual spectra are depicted in Figure 7. The isotropic values

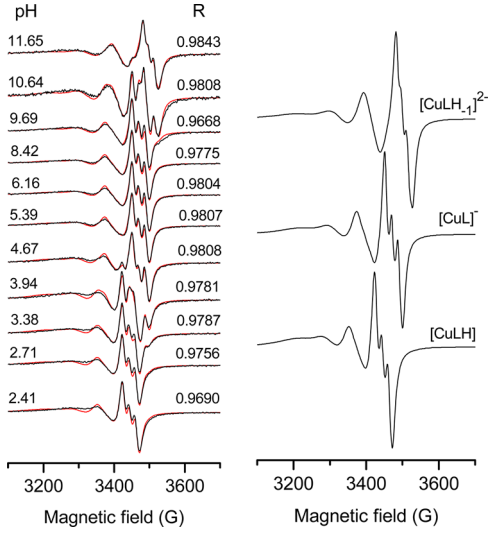

Figure 7. Experimental (black) and simulated (red) EPR spectra for the Cu^{2+}–L-Pro-STSC system (left) and calculated component spectra for complexes [CuLH], $[CuL]^-$, and $[CuLH_{-1}]^{2-}$ (right) [c_{ligand} = 2 mM, M:L = 1:1, *T* = 298 K, *I* = 0.10 M (KCl) in 30% (w/w) DMSO/H_2O].

dx.doi.org/10.1021/ic300967j | Inorg. Chem. 2012, 51, 9309–9321

Table 3. Isotropic EPR Parameters of the Components Obtained for the Cu^{2+}–L-Pro-STSC System from the Two-Dimensional Simulation of EPR Spectra[a,b]

	g_0	A_0, G	a_0^N, G	a, G	b, G	g, G
Cu^{2+} [c]	2.1970	34.3		51.9	−2.2	0.7
$[CuLH]^+$	2.1061(1)	66.1(1)	17.3(1)	35.5(1)	−21.8(1)	3.9(1)
[CuL]	2.0946(1)	76.7(1)	17.5(1)	32.9(1)	−23.0(1)	5.3(1)
$[CuLH_{-1}]^-$	2.0872(2)	84.1(2)	14.9(2)	36.2(1)	−26.5(1)	6.5(1)

[a]The numbers in parentheses are standard uncertainties. [b]Anisotropic EPR parameters for [CuLH]: g_x = 2.0509(1); g_y = 2.0326(1); g_z = 2.2236(1); A_x = 25.4(2) G; A_y = 23.7(2) G; A_z = 170.0(1) G; a_x^N = 6.1 G; a_y^N = 17.1 G; a_z^N = 6.0 G; $g_{0,calc}$ = 2.1024; $A_{0,calc}$ = 75.85 G. Anisotropic EPR parameters for $[CuL]^-$: g_x = 2.0497(1); g_y = 2.0251(1); g_z = 2.2038(1); A_x = 16.3(2) G; A_y = 25.7(2) G; A_z = 176.5(1) G; a_x^N = 15.3 G; a_y^N = 19.5 G; a_z^N = 6.0 G; $g_{0,calc}$ = 2.0929; $A_{0,calc}$ = 75.56 G. [c]Fixed values obtained from separate measurements of Cu^{2+} without ligand.

calculated by averaging the anisotropic values ($g_{0,calc}$ and $A_{0,calc}$; Table 3) are in good agreement with the corresponding values measured in solution, indicating that the coordination modes adopted by the ligand in solution are preserved upon freezing. The nitrogen hyperfine splitting, caused by the equatorial coordination of one nitrogen atom, is well-resolved in all component spectra. Deconvolution of the EPR spectra clearly shows that the species $[CuLH]^+$ predominates in solutions already at pH ∼2.5−3, and with increasing pH, the species [CuL] is formed in a wide pH range (pH 6−9), and then above pH 10, the species $[CuLH_{-1}]^-$ predominates. No dinuclear or bis-ligand complexes were found under these conditions. On the basis of the low g_0 and high A_0 isotropic values, the tridentate coordination of L-Pro-STSC and nearly square-planar coordination geometry is suggested for all of the complexes. In $[CuLH]^+$, coordination of the ligand via phenolate O^-, N^1, and the thione S, while the hydrazinic N^2H moiety is still protonated, is the most likely. (The carboxylic group is supposed to be deprotonated in all species in the partly aqueous solution.) Deprotonation of the hydrazinic N^2H group of the complex results in lower g_0 and higher A_0 parameters; thus, the (O^-, N^1, S^-) binding mode is feasible in the species [CuL]. A further decrease in g_0 and an increase in A_0 values support deprotonation of the water molecule coordinating in the fourth position of the square-planar complex $[CuLH_{-1}]^-$. Thus, this species is regarded as a mixed hydroxido complex, $[CuL(OH)]^-$. On the basis of EPR data, the same coordination modes are realized in the corresponding complexes of L-Pro-STSC and STSC,[29] and the carboxylate group of L-Pro-STSC is not involved in metal coordination. However, the line widths in the component spectra of L-Pro-STSC and STSC[29] differ significantly (Figure 7). The broader lines observed for the copper(II) complexes of L-Pro-STSC are due to the non-coordinating carboxylate group of the ligand, which leads to a slightly hindered rotation of these complexes in solution. As a consequence, the orientation-dependent EPR parameters are not completely averaged out, and the fourth copper line detected in the lower field becomes very broad. Therefore, the simulated spectra, using the equation $\sigma_{M_I} = \alpha + \beta M_I + \gamma M_I^2$ for the line-width description, showed a systematic deviation from the measured spectra at around 3350 G (Figure 7).

The tridentate (O^-, N^1, S) coordination mode of Pro-STSC was confirmed by the X-ray diffraction structure of [Cu((*R*)-H_2L)Cl]Cl (Figure 1). It should also be noted (based on the stability constants) that the species [CuL] is highly stable even at micromolar concentrations and practically does not dissociate at physiological pH.

In the Zn^{2+}–L-Pro-STSC system, analogous complexes with 1:1 metal-to-ligand ratios were detected, although with considerably lower stability compared to copper(II) species. The speciation model obtained for the zinc(II) complexes was supported by ^1H NMR titrations (Figure 8). In the first

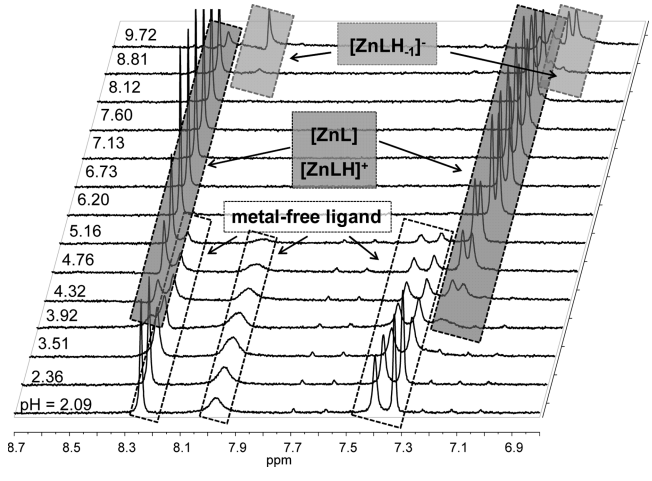

Figure 8. pH-dependent ^1H NMR spectra of Zn^{2+}–L-Pro-STSC [c_{ligand} = 2.0 × 10^{-3} M, M:L = 1:1, 30% (w/w) DMSO-d_6/H_2O].

instance, a slow ligand-exchange process was found with respect to the NMR time scale because the chemical shifts of the protons of the metal-free and bound ligands can be seen separately. At pH < 4, only the peaks of the metal-free ligand are present. A new set of signals can be found additionally with increasing pH, which most probably belongs to the minor protonated complex $[ZnLH]^+$. These signals with a slightly shifted position become predominant between pH 6.5 and 9, where the species [ZnL] is formed. There was no free ligand detected at a 1:1 metal-to-ligand ratio at pH > 6.5. Another species, the mixed hydroxido $[ZnLH_{-1}]^-$ (= $[ZnL(OH)]^-$) starts to be formed at pH > 8.5, and its proton resonances are well-separated from those of [ZnL] because of the relatively slow ligand-exchange equilibrium between them (Figure S9 in the SI). Distribution of the ligand between the bound and unbound fractions at a 1:1 metal-to-ligand ratio was calculated on the basis of the integrated area of the signals of the various ligand protons, and the result is in good agreement with the concentration distribution curves calculated with the stability constants (Figure 9).

Because of the ability of Fe^{2+} and Fe^{3+} ions to form octahedral complexes, bis-ligand iron species could be detected as well (Table 2). In the protonated iron complexes, a coordination mode (O^-, N^1, S) is supposed when the noncoordinating hydrazinic N^2 atom is protonated, and in the $[ML_2]$ types of species, the ligand binds via a (O^-, N^1, S^-) donor set based on the X-ray diffraction structures of complexes of analogous TSCs.[32−35] Species $[ML_2H_{-1}]$ formed

dx.doi.org/10.1021/ic300967j | Inorg. Chem. 2012, 51, 9309−9321

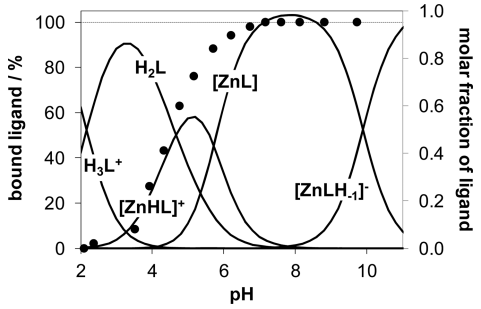

Figure 9. Concentration distribution curves for the Zn^{2+}–L-Pro-STSC system (solid lines) calculated on the basis of the stability constants together with the molar fraction of the bound ligand (●) estimated from the integrated area of the signals of the $C^{14}H$, $C^{4}H$, $C^{6}H$, $C^{7}H_3$, and $C^{8}H_2$ protons [c_{ligand} = 2.0 × 10^{-3} M, M:L = 1:1, 30% (w/w) DMSO-d_6/H_2O].

at basic pH are most probably mixed hydroxido species in which a coordinated donor group is displaced by an OH^-. UV–vis-spectrophotometric titrations of the Fe^{2+}–L-Pro-STSC system under strictly anaerobic conditions show that the formation of the monoligand iron(II) species resulted in a shoulder between 430 and 480 nm, whereas the formation of the green bis-ligand complexes was accompanied by the development of a wide absorption band with a maximum at ca. 600 nm (not shown here). The absorbance values at 520 nm are increased mainly because of the formation of the bis-ligand complexes (Figure 10). These iron(II) species have intense

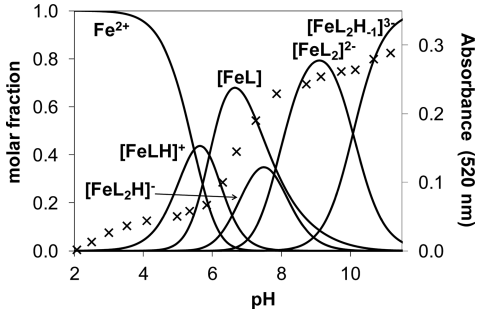

Figure 10. Concentration distribution curves for the Fe^{2+}–L-Pro-STSC system (solid lines) calculated on the basis of the stability constants together with the molar fraction of the absorbance values plotted against pH at 520 nm (×) [c_{ligand} = 2.0 × 10^{-4} M, M:L = 1:2, T = 298 K, I = 0.10 M (KCl) in 30% (w/w) DMSO/H_2O].

color, although their molar absorptivities are considerably lower compared to those of the α(N)-pyridyl TSC complexes.[23b,c] In the case of the iron(III) complexes, the CT bands are found to be strongly overlapped with the ligand bands (Figure S10 in the SI) and the pH-dependent UV–vis spectra indicate the predominant formation of the $[Fe^{III}L_2]^-$ complex (λ_{max} = 380 nm; $\varepsilon_{380\ nm}$ = 18600 M^{-1} cm^{-1}) between pH 6.8 and 9.8 even in a diluted solution (c = 2 × 10^{-5} M), as is expected on the basis of pH-metry (Figure S10 in the SI). As a consequence of the high stability of the Fe^{3+}–L-Pro-STSC complexes, the bis-ligand species is able to preserve its original integrity almost completely with dilution up to the micromolar concentration range at physiological pH, while the iron(II) complexes with much lower stability can dissociate to the monoligand species with decreasing analytical concentrations (Figure 11). When the stability of the Fe–L-Pro-STSC complexes is compared to

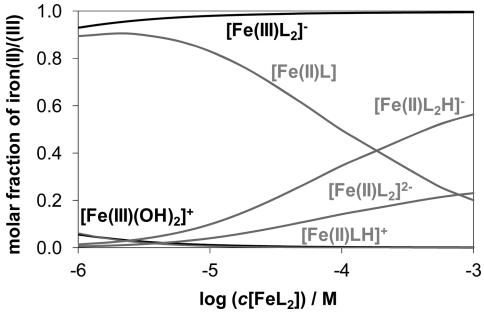

Figure 11. Representative concentration distribution diagram for the Fe^{2+}–L-Pro-STSC (gray lines) and Fe^{3+}–L-Pro-STSC (black lines) bis-ligand complexes at various total concentrations at pH 7.4 [T = 298 K, M:L = 1:2, I = 0.10 M (KCl) in 30% (w/w) DMSO/H_2O].

that of the α(N)-pyridyl TSCs, it can be noted that substitution of the pyridyl moiety by the phenolic one results in an increased binding ability for Fe^{3+} and a diminished binding ability for Fe^{2+} at pH 7.4, as was found for the STSC complexes previously.[29]

Because the ligand L-Pro-STSC is strongly fluorescent at physiological pH (see above), the effect of the metal-ion binding on the emission was also investigated. The metal coordination can quench the intensity but at different extents depending on the metal ions (Figure S11 in the SI). Fe^{3+} and Cu^{2+} quench almost completely the emission. The fluorescence is still observed in the presence of Zn^{2+} and Fe^{2+} and might be satisfactory for monitoring the cellular distribution of these complexes by fluorescence microscopy.

Cytotoxicity in Cancer Cell Lines. The capacity of inhibiting cancer cell growth in vitro of compounds L- and D-Pro-STSC and their corresponding copper(II) complexes was determined in human CH1 (ovarian carcinoma) and SW480 (colon carcinoma) cells by means of the colorimetric MTT assay. IC_{50} values are displayed in Table 4. Remarkably,

Table 4. Cytotoxicity of L- and D-Pro-STSC and Their Copper(II) Complexes Compared to Copper(II) Chloride in Two Human Cancer Cell Lines

	IC_{50},[a] μM					
	SW480			CH1		
L-Pro-STSC	>100			62	±	3
[Cu(L-Pro-STSC)Cl]Cl	5.5	±	0.4	4.6	±	0.6
D-Pro-STSC	>100			75	±	8
[Cu(D-Pro-STSC)Cl]Cl	12	±	1	14	±	2
$CuCl_2$·$2H_2O$[b]	>160			43	±	3

[a]50% inhibitory concentrations in SW480 and CH1 cells after exposure for 96 h in the MTT assay. Values are the mean ± standard deviation obtained from at least three independent experiments. [b]Taken from ref 36.

complexation with copper(II) results in a marked increase of the antiproliferative activity in both cell lines, with IC_{50} values being substantially lower than those of the ligand as well as those of a simple copper(II) salt ($CuCl_2$), indicating that the cytotoxicity of the complexes cannot be explained by their potential dissociation products. The ESI-MS spectra of [Cu(L-Pro-STSC)Cl]Cl in minimum essential medium (containing a variety of biological chelating ligands, e.g., amino acids) measured over 22 h indicate that the complex is resistant to transchelation (Figure S12 in the SI). The IC_{50} values of [Cu(L-

dx.doi.org/10.1021/ic300967j | Inorg. Chem. 2012, 51, 9309–9321

Pro-STSC)Cl]Cl in CH1 and SW480 cells are 4.6 and 5.5 μM, respectively, whereas [Cu(D-Pro-STSC)Cl]Cl shows IC_{50} values of 14 and 12 μM, respectively. In contrast, L- and D-Pro-STSC showed a moderate cytotoxic potency with IC_{50} values of 62 and 75 μM in CH1 cells, respectively. In SW480 cells, no IC_{50} value could be determined within the chosen range of concentrations up to 100 μM. When IC_{50} values of L- and D-Pro-STSC are compared with those of their copper(II) complexes in CH1 cells, complexation with copper(II), hence, results in 13- and 5-fold increases in cytotoxicity. In both tested cell lines, the ligand as well as the complex with an L-proline moiety led to slightly improved antiproliferative activity over the compounds with a D-proline moiety. Assuming that the presence of the proline moiety results in an interference with the cellular amino acid metabolism, this might reflect an influence of the stereoselectivity of certain components of this metabolism, which normally deals only with the L isomers.

Final Remarks. The stability and stoichiometry of Cu^{2+}, Zn^{2+}, Fe^{2+}, and Fe^{3+} complexes of L-Pro-STSC were determined by pH potentiometry, and the speciation was confirmed. The most feasible coordination modes were proposed based on various spectroscopic methods (EPR, ^{1}H NMR, CD, and UV−vis). The formation of monoligand complexes for Cu^{2+} and Zn^{2+} was found, while Fe^{2+} and Fe^{3+} ions form, in addition to monoligand complexes, bis-ligand species. In the protonated complexes, the tridentate coordination mode via the (O^-, N^1, S) set with a protonated noncoordinating hydrazinic N^2 atom is the most probable. The (O^-, N^1, S^-) coordination mode is realized in [ML] and [ML_2] complexes, while the formation of mixed hydroxido species is found at basic pH values. Complexes $[Fe^{III}L_2]^-$ and [CuL] possess so high stability that their dissociation at physiological pH hardly takes place at the micromolar, the biologically more relevant, concentration range. However, the extent of complex dissociation in the case of the lower stability Zn^{2+} and Fe^{2+} species is significant. The complexes formed with L-Pro-STSC exhibit fairly similar behavior compared to STSC, the reference model compound, regarding the type, stability, and coordination mode, although the formation of somewhat higher stability Fe^{3+} complexes is found with L-Pro-STSC. The effect of the side-chain proline moiety is mainly manifested in the increase of the water solubility of the ligand and its metal complexes.

Whereas the thiosemicarbazone−proline conjugates L- and D-Pro-STSC show only a moderate cytotoxic potency in cancer cells, the corresponding copper(II) complexes display a tremendously increased potency. L-Pro-STSC as well as its copper(II) complex shows slightly higher antiproliferative activity than the compounds with a D-Pro moiety. Studies on the impact of the copper(II) coordination of proline−thiosemicarbazones on the topoisomerase IIα inhibition and the antiproliferative activity in cancer cells expressing different levels of topoisomerase IIα are underway because the increased potency of copper(II) complexes cannot be explained by the difference in the lipophilicity alone.

EXPERIMENTAL SECTION

Chemicals. 2-Hydroxy-5-methylbenzaldehyde, thiosemicarbazide, and triethylamine were purchased from Acros Organics, whereas methyl (*S*)-pyrrolidine-2-carboxylate hydrochloride was from VWR and methyl (*R*)-pyrrolidine-2-carboxylate hydrochloride from Alfa Aesar. 3-(Chloromethyl)-2-hydroxy-5-methylbenzaldehyde was synthesized according to the slightly modified published procedure.[30] Prolonged reaction time (2 h) resulted in a 15% increase of the yield. $CuCl_2$, $ZnCl_2$, and $FeCl_3$ (puriss, Reanal) were dissolved in known amounts of HCl in order to get the Cu^{2+}, Zn^{2+}, and Fe^{3+} stock solutions, respectively. Their concentrations were determined by complexometry via ethylenediaminetetraacetic acid complexes. The Fe^{2+} stock solution was obtained from fine iron powder (puriss, Reanal) dissolved in a known amount of a HCl solution under a purified, strictly oxygen-free argon atmosphere, then filtered, stored, and used under anaerobic conditions. A KSCN (Sigma-Aldrich) solution was used to check the absence of Fe^{3+} traces in the Fe^{2+} stock solution. The concentration of the Fe^{2+} solution was determined by permanganometric titrations under acidic conditions. Accurate strong acid contents of the metal stock solutions were determined by pH-potentiometric titrations.

Synthesis of Ligands. *(S)-1*. To a solution of 3-(chloromethyl)-2-hydroxy-5-methylbenzaldehyde (1.34 g, 7.25 mmol) in THF (50 mL) was added under stirring a solution of methyl (*S*)-pyrrolidine-2-carboxylate hydrochloride (1.49 g, 9.00 mmol) in CH_2Cl_2 (50 mL). Afterward, triethylamine (2.52 mL, 18.00 mmol) in THF (25 mL) was added and stirring continued at room temperature overnight. The next day the reaction mixture was diluted with THF (300 mL) and the precipitate of triethylammonium chloride was filtered off. The solution was freed from solvent under reduced pressure, and the residue was purified by column chromatography using as the eluent 3:7 ethyl acetate/hexane. The product was dried in vacuo. Yield: 1.02 g, 51%. Anal. Calcd for $C_{15}H_{19}NO_4$ (M_r 277.32 g mol^{-1}): C, 64.97; H, 6.91; N, 5.05. Found: C, 64.85; H, 6.67; N, 4.98. ^{1}H NMR (DMSO-d_6): δ 10.29 (s, 1H, HC═O), 7.38 (s, 1H, Ar), 7.26 (s, 1H, Ar), 4.08 (d, 1H, J = 13.98 Hz, CH_2), 3.68 (s, 3H, −OCH_3), 3.6 (d, 1H, J = 13.98 Hz, CH_2), 3.48−3.43 (m, 1H, Pro), 2.92−2.86 (m, 1H, Pro), 2.42−2.36 (m, 1H, Pro), 2.24 (s, 3H, CH_3), 2.22−2.16 (m, 1H, Pro), 1.91−1.70 (m, 3H, Pro). ^{13}C{^{1}H} NMR (DMSO-d_6): δ 191.49, 174.45, 158.86, 136.73, 128.17, 127.65, 125.50, 122.40, 65.03, 55.27, 53.02, 52.41, 29.52, 23.57, 20.32. ESI-MS in MeOH (negative): m/z 276 ([M − H]$^-$).

(R)-1. To a solution of 3-(chloromethyl)-2-hydroxy-5-methylbenzaldehyde (1.95 g, 10.6 mmol) in THF (50 mL) was added under stirring a solution of methyl (*R*)-pyrrolidine-2-carboxylate hydrochloride (2.51 g, 15.1 mmol) in CH_2Cl_2 (50 mL). Afterward, triethylamine (4.5 mL, 30.0 mmol) in THF (14 mL) was added and stirring continued at room temperature overnight. The next day the reaction mixture was diluted with THF (300 mL) and the precipitate of triethylammonium chloride was filtered off. The solution was freed from solvent, and the residue was purified by column chromatography by using as the eluent 3:7 ethyl acetate/hexane. The product was dried in vacuo. Yield: 1.14 g, 39%. Anal. Calcd for $C_{15}H_{19}NO_4$ (M_r 277.32 g mol^{-1}): C, 64.97; H, 6.91; N, 5.05. Found: C, 64.85; H, 6.67; N, 4.98. ^{1}H NMR (DMSO-d_6): δ 10.29 (s, 1H, HC═O), 7.38 (s, 1H, Ar), 7.26 (s, 1H, Ar), 4.08 (d, 1H, J = 13.90 Hz, CH_2), 3.68 (s, 3H, -OCH_3), 3.60 (d, 1H, J = 13.90 Hz, CH_2), 3.48−3.43 (m, 1H, Pro), 2.92−2.86 (m, 1H, Pro), 2.42−2.36 (m, 1H, Pro), 2.24 (s, 3H, CH_3), 2.22−2.16 (m, 1H, Pro), 1.91−1.70 (m, 3H, Pro). ^{13}C{^{1}H} NMR (DMSO-d_6): δ 191.45, 174.43, 158.86, 136.70, 128.15, 127.61, 125.48, 122.39, 65.01, 55.28, 53.00, 52.39, 29.51, 23.56, 20.30. ESI-MS in MeOH (negative): m/z 276 ([M − H]$^-$). ESI-MS in MeOH (positive): m/z 278 ([M + H]$^+$).

2-Hydroxy-3-methyl-(S)-pyrrolidine-2-carboxylate-5-methylbenzaldehyde Thiosemicarbazone (L-Pro-STSC). To a warm solution of the (*S*)-**1** (1.14 g, 4.10 mmol) in ethanol (30 mL) was added a solution of thiosemicarbazide (0.46 g, 5.00 mmol) in hot water (30 mL). The reaction mixture was heated at 70−75 °C with continuous stirring for 75 h. After cooling to room temperature, chloroform (100 mL) was added. The aqueous phase was separated and allowed to stand at 5 °C overnight. The white precipitate was filtered off, washed with water, ethanol, and chloroform, and dried in vacuo. Yield: 0.56 g, 41%. Anal. Calcd for $C_{15}H_{20}N_4O_3S{\cdot}1.5H_2O$ (M_r 363.4 g mol^{-1}): C, 49.57; H, 6.38; N, 15.42; S, 8.82. Found: C, 49.62; H, 6.37; N, 15.51; S, 9.07. ^{1}H NMR (DMSO-d_6): δ 11.41 (s, 1H, N^2H), 8.39 (s, 1H, HC^{14}═N^2), 8.11 (s, 1H, N^3H_2), 7.91 (s, 1H, N^3H_2), 7.75 (s, 1H, C^4H), 6.95 (s, 1H, C^6H), 4.14 (d, 1H (J = 13.52 Hz), C^8H), 3.49 (d,

dx.doi.org/10.1021/ic300967j | Inorg. Chem. 2012, 51, 9309−9321

1H (J = 13.52 Hz), C^8H), 3.39−3.37 (m, 1H, C^9H), 2.93−2.84 (m, 1H, $C^{12}H$), 2.45−2.36 (m, 1H, $C^{12}H$), 2.27−2.23 (m, 1H, $C^{10}H$), 2.21 (s, 3H, C^7H_3), 1.91−1.78 (m, 2H, $C^{10}H$, $C^{11}H$), 1.77−1.66 (m, 1H, $C^{11}H$). $^{13}C\{^1H\}$ NMR (DMSO-d_6): δ 178.11, 174.94, 154.60, 139.61, 131.83, 127.79, 126.11, 123.46, 120.61, 65.59, 56.39, 53.04, 29.46, 23.46, 20.5. ESI-MS in MeOH (positive): m/z 359 ($[H_2L + Na]^+$), 337 ($[H_2L + H]^+$).

2-Hydroxy-3-methyl-(R)-pyrrolidine-2-carboxylate-5-methylbenzaldehyde Thiosemicarbazone (D-Pro-STSC). To a warm solution of (*R*)-**1** (2.05 g; 7.40 mmol) in ethanol (30 mL) was added a solution of thiosemicarbazide (0.78 g, 8.50 mmol) in hot water (30 mL). The reaction mixture was heated at 70−75 °C with continuous stirring for 12 h. After cooling to room temperature, chloroform (100 mL) was added. The aqueous phase was separated and allowed to stand at 5 °C overnight. The white precipitate was filtered off, washed with water, ethanol, and chloroform, and dried in vacuo. Yield: 0.45 g, 18%. Anal. Calcd for $C_{15}H_{20}N_4O_3S{\cdot}H_2O$ (M_r 354.43 g mol^{-1}): C, 50.83; H, 6.26; N, 15.81; S, 9.05. Found: C, 51.05; H, 6.21; N, 15.84; S, 9.20. ^1H NMR (DMSO-d_6): δ 11.41 (s, 1H, NH), 8.39 (s, 1H, HC=N), 8.11 (s, 1H, NH_2), 7.91 (s, 1H, NH_2), 7.75 (s, 1H, Ar), 6.95 (s, 1H, Ar), 4.14 (d, 1H (J = 13.52 Hz), CH_2), 3.50 (d, 1H (J = 13.52 Hz), CH_2), 3.39−3.37 (m, 1H, Pro, overlapped water peak), 2.93−2.84 (m, 1H, Pro), 2.45−2.36 (m, 1H, Pro), 2.27−2.23 (m, 4H, Pro, CH_3), 1.91−1.78 (m, 2H, Pro), 1.77−1.66 (m, 1H, Pro). $^{13}C\{^1H\}$ NMR (DMSO-d_6): δ 178.12, 174.92, 154.60, 139.63, 131.84, 127.8, 126.14, 123.44, 120.61, 65.59, 56.37, 53.04, 29.46, 23.45, 20.5. ESI-MS in MeOH (positive): m/z 359 ($[H_2L + Na]^+$), 337 ($[H_2L + H]^+$).

Synthesis of Copper(II) Complexes. *[Cu[(S)-H$_2$L]Cl]Cl.* To a solution of L-Pro-STSC (0.04 g, 0.12 mmol) in methanol (50 mL) was added a solution of $CuCl_2{\cdot}2H_2O$ (0.04 g, 0.26 mmol) in methanol (3 mL), and the reaction mixture was refluxed for 1 h. After cooling to room temperature, the solution was evaporated under reduced pressure to about 5 mL. The green crystalline product was obtained by the slow vapor diffusion of diethyl ether into a concentrated methanolic solution. The product was washed with 5:1 diethyl ether/methanol (5 mL) and dried in vacuo overnight. Yield: 0.03 g; 55.4%. Anal. Calcd for $C_{15}H_{20}Cl_2CuN_4O_3S{\cdot}0.4CH_3OH$ (M_r 483.68 g mol^{-1}): C, 38.24; H, 4.5; N, 11.58; S, 6.63. Found: C, 38.05; H, 4.45; N, 11.23; S, 6.48. ESI-MS in MeOH (positive): m/z 398 ($[Cu^{II}(HL)]^+$). ESI-MS in MeOH (negative): m/z 396 ($[Cu^{II}(LH)]^-$), 432 ($[Cu^{II}(L)Cl]^-$).

[Cu[(R)-H$_2$L]Cl]Cl. To a solution of D-Pro-STSC (0.04 g, 0.12 mmol) in methanol (50 mL) was added a solution of $CuCl_2{\cdot}2H_2O$ (0.04 g, 0.26 mmol) in methanol (3 mL), and the reaction mixture was refluxed for 1 h. After cooling to room temperature, the solution was evaporated under reduced pressure to about 5 mL. The green crystalline product was obtained by the slow vapor diffusion of diethyl ether into a concentrated methanolic solution. The product was washed with 5:1 diethyl ether/methanol (5 mL) and dried in vacuo overnight. Yield: 0.05 g, 83.9%. Anal. Calcd for $C_{15}H_{20}Cl_2CuN_4O_3S{\cdot}0.3CH_3OH$ (M_r 480.47 g mol^{-1}): C, 38.25; H, 4.45; N, 11.66; S, 6.67. Found: C, 37.95; H, 4.35; N, 11.28; S, 6.58. ESI-MS in MeOH (positive): m/z 398 ($[Cu^{II}(HL)]^+$). ESI-MS in MeOH (negative): m/z 396 ($[Cu^{II}(LH)]^-$), 432 ($[Cu^{II}(L)Cl]^-$).

pH-Potentiometric Measurements. The purity and aqueous phase stability of the ligand L-Pro-STSC was verified, and the exact concentrations of the stock solutions prepared were determined by the Gran method.[37]

The pH-metric measurements for determination of the protonation constants of the ligand and the overall stability constants of the metal complexes were carried out at 298.0 ± 0.1 K in 30:70 (w/w) DMSO/H_2O as the solvent and at an ionic strength of 0.10 M (KCl, Sigma-Aldrich) in order to keep the activity coefficients constant. (In previous studies on STSC and α(N)-pyridyl TSCs, a 30% (w/w) DMSO/H_2O solvent mixture was used.[23b,c,29] In order to obtain comparable data, the same conditions were applied, although the presence of only 20% (w/w) DMSO was found to be sufficient for dissolution of L-Pro-STSC at the concentration levels necessary for pH-potentiometric titrations, i.e., ≥ 1−2 mM.) The titrations were performed with a carbonate-free KOH solution of known concentration (0.10 M). Both the base and HCl were Sigma-Aldrich products, and their concentrations were determined by pH-potentiometric titrations. An Orion 710A pH-meter equipped with a Metrohm combined electrode (type 6.0234.100) and a Metrohm 665 Dosimat buret were used for the pH-metric measurements. The electrode system was calibrated to the pH = log $[H^+]$ scale in the DMSO/H_2O solvent mixture by means of blank titrations (strong acid vs strong base; HCl vs KOH), similarly to the method suggested by Irving et al.[38] in pure aqueous solutions. The average water ionization constant, pK_w, is 14.52 ± 0.05 with 30:70 (w/w) DMSO/H_2O as the solvent at 298 K, which corresponds well to the literature data.[23b,c,39] The reproducibility of the titration points included in the calculations was within 0.005 pH. The pH-metric titrations were performed in the pH range 2.0−12.5. The initial volume of the samples was 10.0 mL. The ligand concentration was in the range (2−3) × 10^{-3} M, and metal-ion-to-ligand ratios of 1:1−1:4 were used. The accepted fitting of the titration curves was always less than 0.01 mL. Samples were deoxygenated by bubbling purified argon through them for ca. 10 min prior to the measurements. In the case of Fe^{2+} samples, argon overpressure was used when Fe^{2+} was added to the samples in tightly closed vessels, which were prior completely deoxygenated by bubbling a stream of purified argon through them for ca. 20 min. Argon was also passed over the solutions during the titrations.

The protonation constants of the ligands were determined with the computer program *SUPERQUAD*.[40] *PSEQUAD*[41] was utilized to establish the stoichiometry of the complexes and to calculate the stability constants [log $\beta(M_pL_qH_r)$] from the literature data for iron(III) hydroxido complexes.[42] $\beta(M_pL_qH_r)$ is defined for the general equilibrium $pM + qL + rH \rightleftharpoons M_pL_qH_r$ as $\beta(M_pL_qH_r) = [M_pL_qH_r]/[M]^p[L]^q[H]^r$, where M denotes the metal ion and L the completely deprotonated ligand (see the SI for details). The calculations were always made from the experimental titration data measured in the absence of any precipitate in solution.

UV−Vis-Spectrophotometric, Spectrofluorimetric, CD, and ^{1}H NMR Measurements. A Hewlett-Packard 8452A diode-array spectrophotometer was used to record the UV−vis spectra in the interval 260−820 nm. The path length was 1 cm. Protonation and stability constants and the individual spectra of the species were calculated by the computer program *PSEQUAD*.[41] The spectrophotometric titrations were performed on samples of L-Pro-STSC alone or with Cu^{2+}, Fe^{3+}, or Fe^{2+} ions; the concentration of the ligand was 4 × 10^{-5} M (for the ligand and Fe^{3+}-containing samples), 2 × 10^{-4} M (for Fe^{2+}-containing samples), or 2 × 10^{-3} M (for Cu^{2+}-containing samples), and the metal-to-ligand ratios were 0:1, 1:1, and 1:2 over the pH range between 2 and 12 at an ionic strength of 0.10 M (KCl) in 30% (w/w) DMSO/H_2O at 298.0 ± 0.1 K. For Fe^{2+} samples, spectra were recorded under strictly anaerobic conditions. Measurements for the Fe^{3+}−L-Pro-STSC system at metal-to-ligand ratio 1:1 were also carried out by preparing individual samples in which 0.1 M KCl was partially or completely replaced by HCl and pH values, varying in the range ca. 1.0−1.8, were calculated from the HCl content. For calculation of the stability constants of the protonated monoligand Fe^{3+}−L-Pro-STSC complex, mainly CT bands (which are strongly overlapped with the ligand bands) were used (λ = 300−470 nm).

The pH-dependent fluorescence measurements were carried out on a Hitachi-4500 spectrofluorimeter with excitation at 393 nm. The emission spectra were recorded using 5 nm/5 nm slit widths in a 1 cm quartz cell in the pH range between 2 and 12 in 30% (w/w) DMSO/H_2O at 298.0 ± 0.1 K. Samples contained 5 × 10^{-6} M L-Pro-STSC ligand alone or with 5 × 10^{-6} M Cu^{2+} or Zn^{2+} ions or 2.5 × 10^{-6} M Fe^{2+} at 0.1 M (KCl) ionic strength. Three-dimensional spectra were recorded at 230−500 nm excitation and at 240−600 nm emission wavelengths for the 5 × 10^{-6} M ligand containing samples at pH 5.1, 7.6, and 10.0 using 2.5 nm/2.5 nm slit widths.

^{1}H NMR studies were carried out on a Bruker Ultrashield 500 Plus instrument. L-Pro-STSC was dissolved in a 30% (w/w) DMSO-d_6/H_2O mixture in a concentration of 2 × 10^{-3} M, and the Zn^{2+}-to-ligand ratios were 0:1 and 1:1. The direct pH-meter readings were corrected according to the method of Irving et al.[38]

CD spectra were recorded on a Jasco J-815 spectrometer in an optical cell of 1.0 cm path length. The analytical concentration of D- or

dx.doi.org/10.1021/ic300967j | Inorg. Chem. 2012, 51, 9309−9321

L-Pro-STSC ligands or the Cu^{2+}-D- or L-Pro-STSC complexes was 6.5 × 10^{-5} M at pH 7.4 in a pure aqueous solution, and spectra were recorded in the wavelength interval from 215 to 500 nm. A 2.0 × 10^{-3} M ligand concentration was used for the Cu^{2+}–L-Pro-STSC system at 1:1 metal-to-ligand ratio in a 30% (w/w) DMSO/H_2O mixture; the pH was varied between 2 and 12, and spectra were analyzed in the range of 460–700 nm. CD data are given as the differences in molar absorptivities between left and right circularly polarized light, based on the concentration of the ligand ($\Delta\varepsilon = \Delta A/l/c_{\text{ligand or complex}}$).

Determination of the Distribution Coefficient (D). The *D* values of L- and D-Pro-STSC and their copper(II) complexes were determined by the traditional shake flask method in an *n*-octanol/buffered aqueous solution at pH 7.4 [4-(2-hydroxyethyl)-1-piperazineethanesulfonic acid] at 298.0 ± 0.2 K as described previously.[29] Two parallel experiments were performed for each sample. The ligands were dissolved at 4 × 10^{-5} M and the complexes at 6.4 × 10^{-5} M in the *n*-octanol presaturated aqueous solution of the buffer (0.01 M) at a constant ionic strength (0.10 M KCl). The aqueous solutions and *n*-octanol with a 1:1 phase ratio were gently mixed with 360° vertical rotation for 3 h to avoid emulsion formation, and the mixtures were centrifuged at 5000 rpm for 3 min by a temperature-controlled centrifuge (Sanyo) at 298 K. After separation, UV–vis spectra of the ligands or complexes in the aqueous phase were compared to those of the original aqueous solutions, and $D_{7.4}$ value was calculated as the mean of [absorbance (original solution)/absorbance (aqueous phase after separation) − 1] obtained at the region of λ_{max} ± 10 nm values.

EPR Measurements and Deconvolution of the Spectra. All continuous-wave (CW)-EPR spectra were recorded with a Bruker EleXsys E500 spectrometer (microwave frequency 9.81 GHz, microwave power 10 mW, modulation amplitude 5 G, and modulation frequency 100 kHz). During titration, the isotropic EPR spectra were recorded at room temperature in a circulating system. A total of 11 and 10 EPR spectra were recorded for samples with 1:1 and 1:2 Cu^{2+}-to-ligand ratios, respectively, at 2.0 × 10^{-3} M L-Pro-STSC concentration between pH 2.4 and 12 in 30% (w/w) DMSO/H_2O at I = 0.10 M (KCl). A KOH solution was added to the stock solution to change the pH, which was measured with a Radiometer PHM240 pH/ion meter equipped with a Metrohm 6.0234.100 glass electrode. A Heidolph Pumpdrive 5101 peristaltic pump was used to circulate the solution from the titration pot through a capillary tube into the cavity of the instrument. The titrations were carried out under an argon atmosphere. At various pH values, samples of 0.10 mL were taken and frozen in liquid nitrogen, and the CW-EPR spectra were recorded under the same instrumental conditions as the room-temperature spectra described above.

The series of room-temperature CW-EPR spectra were simulated simultaneously by the "two-dimensional" method using the 2D_EPR program.[43] Each component curve was described by the isotropic EPR parameters g_0 and A_0^{Cu} copper hyperfine and A_0^{N} nitrogen hyperfine couplings and the relaxation parameters α, β, and γ, which define the line widths in the equation $s_{M_I} = \alpha + \beta M_I + \gamma M_I^2$, where M_I denotes the magnetic quantum number of the copper nucleus. The concentrations of the complexes were varied by fitting their formation constants $\beta(M_pL_qH_r)$ defined by the general equilibrium found in the pH-potentiometric studies section.

For each spectrum, the noise-corrected regression parameter (R_j for the *j*th spectrum) is derived from the average square deviation (SQD) between the experimental and calculated intensities. For the series of spectra, the fit is characterized by the overall regression coefficient *R*, calculated from the overall average SQD. The details of the statistical analysis were published previously.[44]

The anisotropic spectra were analyzed individually with the EPR program,[44] which gives the anisotropic EPR parameters (g_x, g_y, g_z, A_x^{Cu}, A_y^{Cu}, A_z^{Cu}, A_x^{N}, A_y^{N}, and A_z^{N}) and the orientation-dependent line-width parameters. Because a natural $CuCl_2$ was used for the measurements, the spectra were calculated as the sum of the spectra of ^{63}Cu and ^{65}Cu weighted by their natural abundances. The quality of fit was characterized by the noise-corrected regression parameter R_j as above. The copper and nitrogen coupling constants and the relaxation parameters were obtained in field units (gauss = 10^{-4} T).

Crystallographic Structure Determination. X-ray diffraction measurement was performed on a Bruker X8 APEXII CCD diffractometer. A single crystal of [Cu[(*R*)-H_2L]Cl]Cl was positioned at 40 mm from the detector, and 1138 frames were measured, each for 60 s over a 1° scan width. The data were processed using *SAINT* software.[45] Crystal data, data collection parameters, and structure refinement details are given in Table 5. The structure was solved by direct methods and refined by full-matrix least-squares techniques. Non-hydrogen atoms were refined with anisotropic displacement parameters. Hydrogen atoms were inserted in calculated positions and refined with a riding model. The five-membered proline ring in both crystallographically independent complex cations (A and B) of [Cu[(*R*)-H_2L]Cl]Cl was found to be disordered over two positions with sof 0.50:0.50. In addition, one oxygen atom of the –COOH group in complex cation B is also disordered over two positions, each with 50% occupancy. The disorder was resolved with restraints on the displacement parameters and on bond distances using the DELU and SADI instructions of *SHELX-97*, respectively. The following software programs and computer were used: structure solution, *SHELXS-97*; refinement, *SHELXL-97*;[46] molecular diagrams, *ORTEP-3*;[47] computer, Intel CoreDuo.

Table 5. Crystal Data and Details of Data Collection for [Cu[(*R*)-H_2L]Cl]Cl

compound	[Cu[(*R*)-H_2L]Cl]Cl
empirical formula	$C_{15}H_{20}Cl_2CuN_4O_3S$
fw	470.85
space group	$P2_1$
a, Å	7.3130(3)
b, Å	21.8734(8)
c, Å	11.7535(5)
β, deg	99.423(2)
V, Å^3	1854.72(13)
Z	4
λ, Å	0.71073
ρ_{calcd}, g cm^{-3}	1.686
cryst size, mm^3	0.16 × 0.05 × 0.03
T, K	120(2)
μ, mm^{-1}	1.602
R1[a]	0.0356
wR2[b]	0.0795
GOF[c]	1.014

[a] $R1 = \sum||F_o| - |F_c||/\sum|F_o|$. [b] $wR2 = \{\sum[w(F_o^2 - F_c^2)^2]/\sum[w(F_o^2)^2]\}^{1/2}$. [c] $GOF = \{\sum[w(F_o^2 - F_c^2)^2]/(n-p)\}^{1/2}$, where *n* is the number of reflections and *p* is the total number of parameters refined.

Cell Lines and Culture Conditions. Human CH1 (ovarian carcinoma) and SW480 (colon carcinoma) cells were kindly provided by Lloyd R. Kelland (CRC Centre for Cancer Therapeutics, Institute of Cancer Research, Sutton, U.K.) and Brigitte Marian (Institute of Cancer Research, Department of Medicine I, Medical University of Vienna, Vienna, Austria), respectively. Cells were grown in 75 cm^2 culture flasks (CytoOne/Starlabs, Germany) as adherent monolayer cultures in Minimum Essential Medium (MEM) supplemented with 10% heat-inactivated fetal bovine serum, 1 mM sodium pyruvate, 4 mM L-glutamine, and 1% nonessential amino acids (from 100× ready-to-use stock; all purchased from Sigma-Aldrich, Vienna, Austria). Cultures were maintained at 37 °C in a humidified atmosphere containing 5% CO_2.

Cytotoxicity Tests in Cancer Cell Lines. Antiproliferative effects were determined by means of a colorimetric microculture assay [MTT assay, MTT = 3-(4,5-dimethyl-2-thiazolyl)-2,5-diphenyl-2*H*-tetrazolium bromide]. Cells were harvested from culture flasks by

dx.doi.org/10.1021/ic300967j | Inorg. Chem. 2012, 51, 9309–9321

trypsinization and seeded in 100 μL aliquots into 96-well microculture plates (CytoOne/Starlabs, Germany) in densities of 2×10^3 cells/well (SW480) and 1×10^3 cells/well (CH1), in order to ensure exponential growth of untreated controls throughout the experiment. After a 24 h preincubation, dilutions of the test compounds in a 100 μL well^{-1} complete culture medium were added. Because of low aqueous solubility, the test compounds were dissolved in DMSO first and then serially diluted in a complete culture medium such that the effective DMSO content did not exceed 0.5%. After exposure for 96 h, all media were replaced by a 100 μL well^{-1} RPMI 1640 medium (supplemented with 10% heat-inactivated fetal bovine serum and 2 mM L-glutamine) plus a 20 μL well^{-1} MTT solution in phosphate-buffered saline (5 mg mL^{-1}). After incubation for 4 h, the medium/MTT mixtures were removed, and the formazan crystals formed by viable cells were dissolved in 150 μL of DMSO per well. Optical densities at 550 nm were measured with a microplate reader (Biotek ELx808), using a reference wavelength of 690 nm to correct for unspecific absorption. The quantity of viable cells was expressed in terms of the T/C values by a comparison to untreated control microcultures, and 50% inhibitory concentrations (IC_{50}) were calculated from concentration−effect curves by interpolation. Evaluation is based on means from at least three independent experiments, each comprising three microcultures per concentration level.

■ ASSOCIATED CONTENT

Ⓢ Supporting Information

CD and UV−vis spectra of L-Pro-STSC and D-Pro-STSC (Figure S1), unit cell and hydrogen-bonding interactions for [Cu[(*R*)-Pro-STSC]Cl]Cl (Figure S2), stack formation in the crystal structure of [Cu[(*R*)-Pro-STSC]Cl]Cl (Figure S3), calculated UV−vis spectra of the individual species of L-Pro-STSC (Figure S4), pH-dependent ^{1}H NMR spectra of L-Pro-STSC (Figure S5), log $D_{7.4}$ determination for L-Pro-STSC by UV−vis spectroscopy (Figure S6), log $D_{7.4}$ determination for [Cu(L-Pro-STSC)Cl]Cl by UV−vis spectroscopy (Figure S7), experimental and simulated EPR spectra of the Cu^{2+}− L-Pro-STSC system (Figure S8), ^{1}H NMR spectra of L-Pro-STSC at pH 9.8 and the Zn^{2+}−L-Pro-STSC system at pH 8.1 and 9.7 (Figure S9), pH-dependent UV−vis spectra of the Fe^{3+}−L-Pro-STSC system and the corresponding concentration distribution curves (Figure S10), fluorescence intensity of emission at 498 nm for L-Pro-STSC and 1:1 mixtures of Zn^{2+}, Fe^{2+}, and Cu^{2+} with L-Pro-STSC (Figure S11), ESI mass spectra of [Cu(L-Pro-STSC)Cl]Cl in MEM (Figure S12), definition of the stability constants of the metal complexes, and crystallographic data for [Cu[(*R*)-Pro-STSC]Cl]Cl in CIF format. This material is available free of charge via the Internet at http://pubs.acs.org.

■ AUTHOR INFORMATION

Corresponding Author

*E-mail: enyedy@chem.u-szeged.hu (É.A.E.), vladimir.arion@univie.ac.at (V.B.A.).

Notes

The authors declare no competing financial interest.

■ ACKNOWLEDGMENTS

This work has been supported by the Austrian Science Fund (Project P19629-N19), Hungarian Research Foundation (OTKA K77833 and K72781), and the Hungarian−Austrian Action Foundation (TÁMOP-4.2.1/B-09/1/KONV-2010-0005). É.A.E. gratefully acknowledges the financial support of Bolyai J. research fellowships. We thank Alexander Roller for collection of the X-ray data.

■ REFERENCES

(1) (a) West, D. X.; Padhye, S. B.; Sonawane, P. B. *Struct. Bonding (Berlin)* **1991**, *76*, 1−50. (b) Casas, J. S.; Garcia-Tasende, M. S.; Sordo, J. *Coord. Chem. Rev.* **2000**, *209*, 197−261.
(2) (a) Knox, J. J.; Hotte, S. J.; Kollmannsberger, C.; Winquist, E.; Fisher, B.; Eisenhauer, E. A. *Invest. New Drugs* **2007**, *25*, 471−477. (b) Stringer, T.; Chellan, P.; Therrien, B.; Shunmoogam-Gounden, N.; Hendricks, D. T.; Smith, G. S. *Polyhedron* **2009**, *28*, 2839−2846. (c) Stringer, T.; Hendricks, D. T.; Guzgay, H.; Smith, G. S. *Polyhedron* **2012**, *31*, 486−493.
(3) Easmon, J.; Heinisch, G.; Holzer, W.; Rosenwirth, B. *J. Med. Chem.* **1992**, *35*, 3288−3296.
(4) Klayman, D. L.; Bartosevich, J. F.; Griffin, T. S.; Mason, C. J.; Scovill, J. P. *J. Med. Chem.* **1979**, *22*, 855−862.
(5) Ma, B.; Goh, B. C.; Tan, E. H.; Lam, K. C.; Soo, R.; Leong, S. S.; Wang, L. Z.; Mo, F.; Chan, A. T. C.; Zee, B.; Mok, T. *Invest. New Drugs* **2008**, *26*, 169−173.
(6) Karp, J. E.; Giles, F. J.; Gojo, I.; Morris, L.; Greer, J.; Johnson, B.; Thein, M.; Sznol, M.; Low, J. *Leuk. Res.* **2008**, *32*, 71−77.
(7) Mackenzie, M. J.; Saltman, D.; Hirte, H.; Low, J.; Johnson, C.; Pond, G.; Moore, M. J. *Invest. New Drugs* **2007**, *25*, 553−558.
(8) Chao, J.; Synold, T. W.; Morgan, R. J., Jr.; Kunos, C.; Longmate, J.; Lenz, J.-J.; Lim, D.; Shibata, S.; Chung, V.; Stoller, R. G.; Belani, C. P.; Gandara, D. R.; McNamara, M.; Gitlitz, B. J.; Lau, D. H.; Ramalingam, S. S.; Davies, A.; Espinoza-Delgado, I.; Newman, E. M.; Yen, Y. *Cancer. Chemother. Pharmacol.* **2012**, *69*, 835−843.
(9) Yu, Y.; Wong, J.; Lovejoy, D. B.; Kalinowski, D. S.; Richardson, D. R. *Clin. Cancer Res.* **2006**, *12*, 6876−6883.
(10) Moore, E. M.; Zedeck, M. S.; Agrawal, K. C.; Sartorelli, A. C. *Biochemistry* **1970**, *9*, 4492−4498.
(11) Kolberg, M.; Strand, K. R.; Graff, P.; Andersson, K. K. *Biochim. Biophys. Acta* **2004**, *1699*, 1−34.
(12) French, F. A.; Blanz, E. J., Jr. *J. Med. Chem.* **1974**, *17*, 172−181.
(13) Moore, E.; Sartorelli, A. C. *Pharmacol. Ther.* **1984**, *24*, 439−447.
(14) Finch, R. A.; Liu, M.; Cory, A. H.; Cory, J. G.; Sartorelli, A. C. *Adv. Enzyme Regul.* **1999**, *39*, 3−12.
(15) (a) Easmon, J.; Puerstinger, G.; Heinisch, G.; Roth, T. *J. Med. Chem.* **2001**, *44*, 2164−2171. (b) Miller, M. C.; Stineman, N. C.; Vance, R. J.; West, D. X.; Hall, H. I. *Anticancer Res.* **1998**, *18*, 4131−4139.
(16) Huang, H.; Chen, W.; Ku, X.; Meng, L.; Lin, L.; Wang, X.; Zhu, C.; Wang, Y.; Chen, Z.; Li, M.; Jiang, H.; Chen, K.; Ding, J.; Liu, H. *J. Med. Chem.* **2010**, *53*, 3048−3064.
(17) Zeglis, B. M.; Divilov, V.; Lewis, J. S. *J. Med. Chem.* **2011**, *54*, 2391−2398.
(18) Kowol, C. R.; Heffeter, P.; Miklos, W.; Gille, L.; Trondl, R.; Cappellacci, L.; Berger, W.; Keppler, B. K. *J. Biol. Inorg. Chem.* **2012**, *17*, 409−423.
(19) Shao, J.; Zhou, B.; Di Bilio, A. J.; Zhu, L.; Wang, T.; Qi, C.; Shih, J.; Yen, Y. *Mol. Cancer Ther.* **2006**, *5*, 586−592.
(20) Chaston, T. B.; Lovejoy, D. B.; Watts, R. N.; Richardson, D. R. *Clin. Cancer Res.* **2003**, *9*, 402−414.
(21) Popović-Bijelić, A.; Kowol, C. R.; Lind, M. E. S.; Luo, J.; Enyedy, E. A.; Arion, V. B.; Gräslund, A. *J. Inorg. Biochem.* **2011**, *105*, 1422−1431.
(22) (a) Richardson, D. R.; Sharpe, P. C.; Lovejoy, D. B.; Senaratne, D.; Kalinowski, D. S.; Islam, M.; Bernhardt, P. V. *J. Med. Chem.* **2006**, *49*, 6510−6521. (b) Opletalova, V.; Kalinowski, D. S.; Vejsova, M.; Kunes, J.; Pour, M.; Jampilek, J.; Buchta, V.; Richardson, D. R. *Chem. Res. Toxicol.* **2008**, *21*, 1878−1889. (c) Jansson, P. J.; Sharpe, P. C.; Bernhardt, P. V.; Richardson, D. R. *J. Med. Chem.* **2010**, *53*, 5759−5769. (d) Kalinowski, D. S.; Yu, Y.; Sharpe, P. C.; Bernhardt, P. V.; Richardson, D. R. *J. Med. Chem.* **2007**, *50*, 3716−3729. (e) Richardson, D. R.; Kalinowski, D. S.; Richardson, V.; Sharpe, P. C.; Lovejoy, D. B.; Islam, M.; Bernhardt, P. J. *J. Med. Chem.* **2009**, *52*, 1459−1470. (f) Kowol, C. R.; Berger, R.; Eichinger, R.; Roller, A.; Jakupec, M. A.; Schmidt, P. P.; Arion, V. B.; Keppler, B. K. *J. Med. Chem.* **2007**, *50*, 1254−1265.

(23) (a) Knight, J. M.; Whelan, H.; Petering, D. H. *J. Inorg. Biochem.* **1979**, *11*, 327−338. (b) Enyedy, E. A.; Nagy, N. V.; Zsigó, E.; Kowol, C. R.; Arion, V. B.; Keppler, B. K.; Kiss, T. *Eur. J. Inorg. Chem.* **2010**, 1717−1728. (c) Enyedy, E. A.; Primik, M. F.; Kowol, C. R.; Arion, V. B.; Kiss, T.; Keppler, B. K. *Dalton Trans.* **2011**, *40*, 5895−5905.
(24) (a) Ryabova, N. A.; Ponomarev, V. I.; Zelentsov, V. V.; Atovmyan, L. O. *Kristallografiya* **1981**, *26*, 101−108. (b) Ryabova, N. A.; Ponomarev, V. I.; Zelentsov, V. V.; Atovmyan, L. O. *Kristallografiya* **1982**, *27*, 81−91. (c) Schulte, G.; Luo, X.-L.; Crabtree, R. H.; Zimmer, M. *Angew. Chem., Int. Ed. Engl.* **1991**, *30*, 193−194. (d) Argay, G.; Kalman, A.; Leovac, V. M.; Cesljevic, V. I.; Ribar, B. *J. Coord. Chem.* **1996**, *37*, 165−171. (e) Soriano-Garcia, M.; Valdes-Martinez, J.; Toscano, R. A.; Gomez-Lara, J. *Acta Crystallogr.* **1985**, *C41*, 500−502.
(25) Belicchi Ferrari, M.; Capacchi, S.; Pelosi, G.; Reffo, G.; Tarasconi, P.; Albertini, R.; Pinelli, S.; Lunghi, P. *Inorg. Chim. Acta* **1999**, *286*, 134−141.
(26) Đilović, I.; Rubčić, M.; Vrdoljak, V.; Kraljević Pavelić, S.; Kralj, M.; Piantanida, I.; Cindrić, M. *Bioorg. Med. Chem.* **2008**, *16*, 5189−5198.
(27) (a) Kowol, C. R.; Eichinger, R.; Jakupec, M. A.; Galanski, M.; Arion, V. B.; Keppler, B. K. *J. Inorg. Biochem.* **2007**, *101*, 1946−1957. (b) Arion, V. B.; Jakupec, M. A.; Galanski, M.; Unfried, P.; Keppler, B. K. *J. Inorg. Biochem.* **2002**, *91*, 298−305.
(28) Sen, S.; Shit, S.; Mitra, S.; Batten, S. R. *Struct. Chem.* **2008**, *19*, 137−142.
(29) Enyedy, E. A.; Zsigo, E.; Nagy, N. V.; Kowol, C. R.; Roller, A.; Keppler, B. K.; Kiss, T. *Eur. J. Inorg. Chem.* DOI: 10.1002/ejic.201200360.
(30) (a) Wang, Q.; Wilson, C.; Blake, J. A.; Collinson, R. S.; Tasker, A. P.; Schröder, M. *Tetrahedron Lett.* **2006**, *47*, 8983−8987. (b) Huisman, M.; Koval, I. A.; Gamez, P.; Reedijk, J. *Inorg. Chim. Acta* **2006**, *359*, 1786−1794.
(31) (a) Lee, W. Y.; Lee, P. P. F.; Yan, Y. K.; Lau, M. *Metallomics* **2010**, *2*, 694−705. (b) Lee, W. Y.; Yan, Y. K.; Lee, P. P. F.; Tan, S. J.; Lim, K. H. *Metallomics* **2012**, *4*, 188−196.
(32) Wu, W. S.; Feng, Y.-L. *Z. Kristallogr.* **2003**, *218*, 529−530.
(33) Ryabova, N. A.; Ponomarev, V. I.; Atovmyan, L. O.; Zelentsov, V. V.; Shipilov, V. I. *Coord. Chem.* **1978**, *37*, 119−129.
(34) Ryabova, N. A.; Ponomarev, V. I.; Zelentsov, V. V.; Atovmyan, L. O. *Kristallografiya* **1982**, *27*, 279−287.
(35) Floquet, S.; Guillou, N.; Negrier, P.; Riviere, E.; Boillot, M. L. *New J. Chem.* **2006**, *30*, 1621−1627.
(36) Primik, M. F.; Mühlgassner, G.; Jakupec, M. A.; Zava, O.; Dyson, P. J.; Arion, V. B.; Keppler, B. K *Inorg. Chem.* **2010**, *49*, 302−311.
(37) Gran, G. *Acta Chem. Scand.* **1950**, *4*, 559−577.
(38) Irving, H. M.; Miles, M. G.; Pettit, L. D. *Anal. Chim. Acta* **1967**, *38*, 475−488.
(39) *SCQuery, The IUPAC Stability Constants Database, Academic Software*, version 5.5; Royal Society of Chemistry: London, 1993−2005.
(40) Sabatini, A.; Vacca, A.; Gans, P. *Talanta* **1974**, *21*, 53−77.
(41) Zékány, L.; Nagypál, I. In *Computational Methods for the Determination of Stability Constants*; Leggett, D. L., Ed.; Plenum Press: New York, 1985; pp 291−353.
(42) Baes, C. F.; Mesmer, R. E. *The Hydrolysis of Cations*; Wiley: New York, 1976.
(43) Rockenbauer, A.; Szabó-Plánka, T.; Arkowi, Zs.; Korecz, L. *J. Am. Chem. Soc.* **2001**, *123*, 7646−7654.
(44) Rockenbauer, A.; Korecz, L. *Appl. Magn. Reson.* **1996**, *10*, 29−43.
(45) *SAINT-Plus*, version 7.06a, and *APEX2*; Bruker-Nonius AXS Inc.: Madison, WI, 2004.
(46) Sheldrick, G. M. *Acta Crystallogr.* **2008**, *A46*, 112−122.
(47) Burnett, M. N.; Johnson, G. K. *ORTEPIII, Report ORNL-5138*; Oak Ridge National Laboratory: Oak Ridge, TN, 1996.

SUPPORTING INFORMATION

L- and *D*-proline thiosemicarbazone conjugates: coordination behavior in solution, and the effect of copper(II) coordination on their antiproliferative activity

Miljan N. M. Milunovic,[a] Éva A. Enyedy,*[b] Nóra V. Nagy,[c] Tamás Kiss,[b,d] Robert Trondl,[a] Michael A. Jakupec,[a] Bernhard K. Keppler,[a] Regina Krachler,[a] Ghenadie Novitchi,[e] Vladimir B. Arion[a,]*

[a]*Institute of Inorganic Chemistry, University of Vienna, Währinger Strasse, 42, A-1090 Vienna, Austria*
E-mail: vladimir.arion@univie.ac.at; Fax: +43-1-4277-52680
[b]*Department of Inorganic and Analytical Chemistry, University of Szeged, Dóm tér 7. H-6720 Szeged, Hungary*
E-mail: enyedy@chem.u-szeged.hu; Fax: +36 62 420505
[c]*Institute of Molecular Pharmacology, Research Centre for Natural Sciences, Hungarian Academy of Sciences, Pusztaszeri út 59-67, H-1025 Budapest, Hungary*
[d]*Bioinorganic Chemistry Research Group of the Hungarian Academy of Sciences, University of Szeged, Dóm tér 7. H-6720 Szeged, Hungary*
[e]*Laboratoire National des Champs Magnétiques Intenses, CNRS UPR-3228, 25 rue des Martyrs, 38042 Grenoble cedex 9, France*

CONTENT

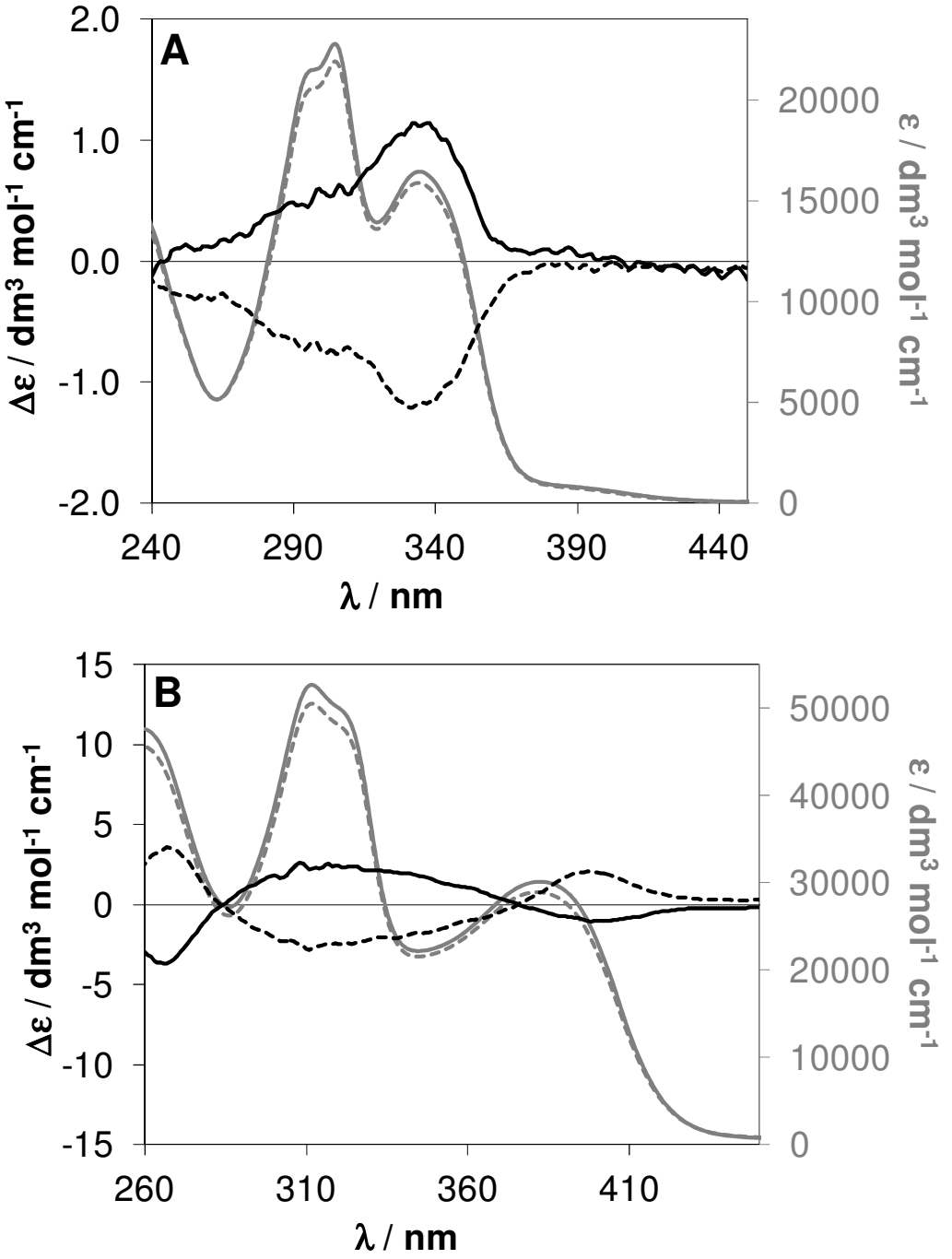

Figure S1. Circular dichroism (black lines) and UV−vis (grey lines) spectra of the ligands (A) and of the Cu^{2+} complexes (B) recorded at pH 7.4 in aqueous solution. Solid lines stand for the *L*- and dashed lines for the *D*-enantiomers {$c_{L \text{ or complex}} = 6.5 \times 10^{-5}$ M; (T = 298 K, I = 0.10 M (KCl) in H_2O}.

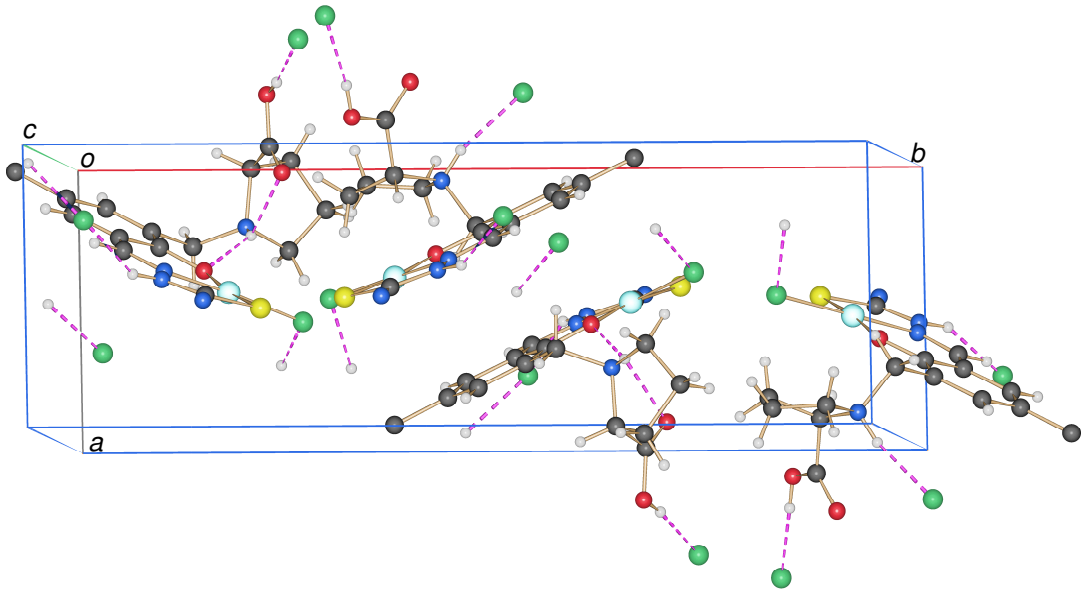

Figure S2. Unit cell and hydrogen bonding interactions in [Cu(*R*-H_2L)Cl]Cl.

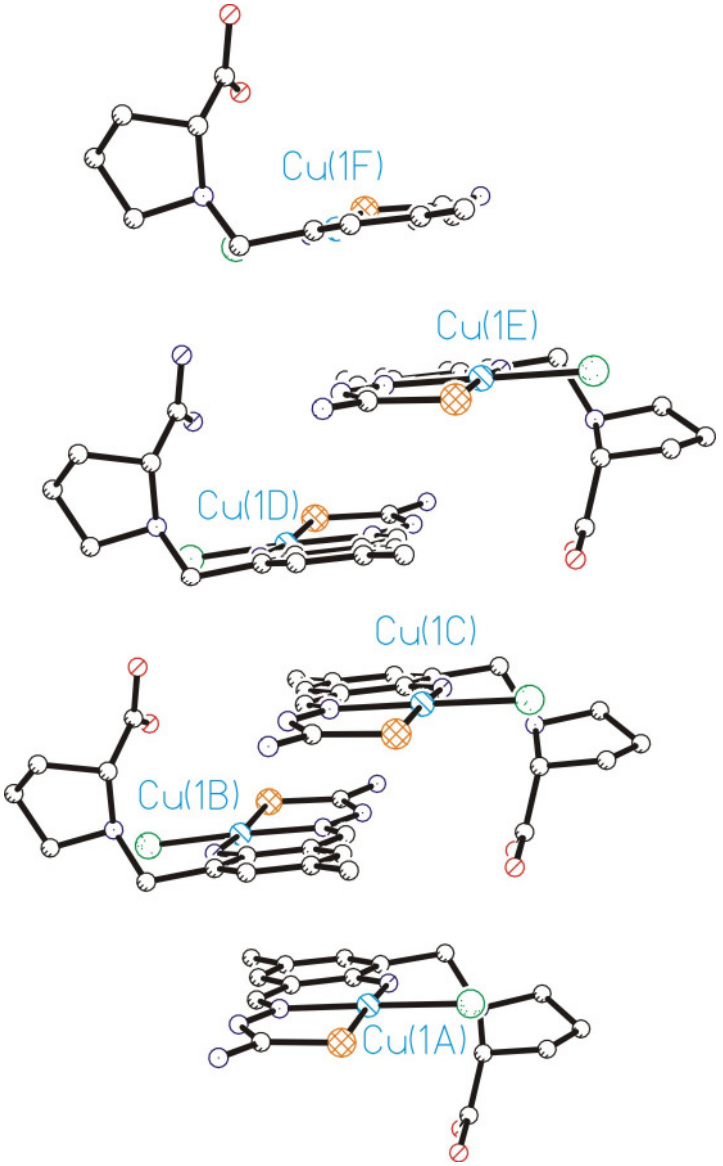

Figure S3. Stack formation in the crystal structure of [Cu(*R*-H_2L)Cl]Cl.

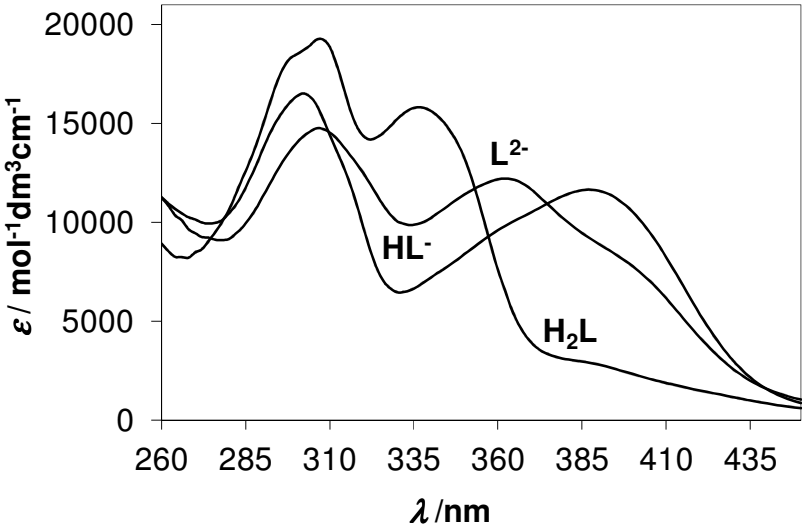

Figure S4. Calculated UV–vis spectra of the individual species of *L*-Pro-STSC {T = 298 K, I = 0.10 M (KCl) in 30% (w/w) DMSO/H_2O}.

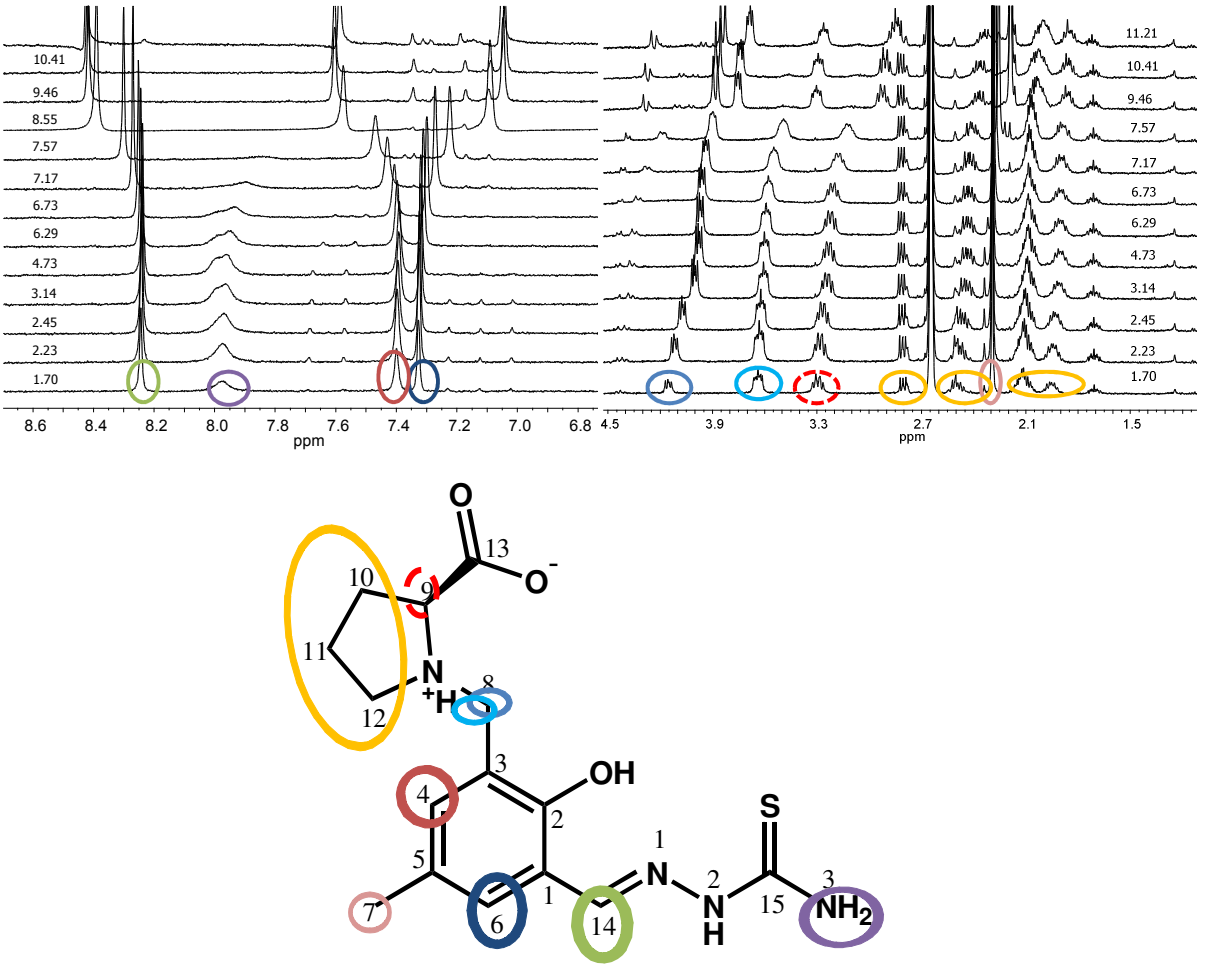

Figure S5. pH-dependent ^{1}H NMR spectra of *L*-Pro-STSC with the proton assignments {$c_{ligand} = 2.0 \times 10^{-3}$ M in 30% (w/w) d_6-DMSO/H_2O}.

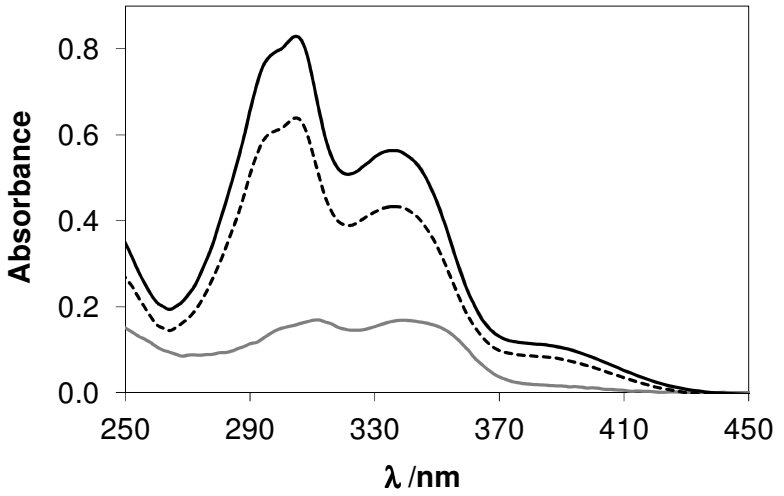

Figure S6. UV–vis spectra of *L*-Pro-STSC containing samples of the original solution (black solid line), in the aqueous phase (black dashed line) and in the *n*-octanol phase (grey solid line) following the separation for the log$D_{7.4}$ determination {$c_{\text{ligand}} = 4.0 \times 10^{-5}$ M, pH = 7.40 (HEPES), I = 0.10 M (KCl) in aqueous phase}.

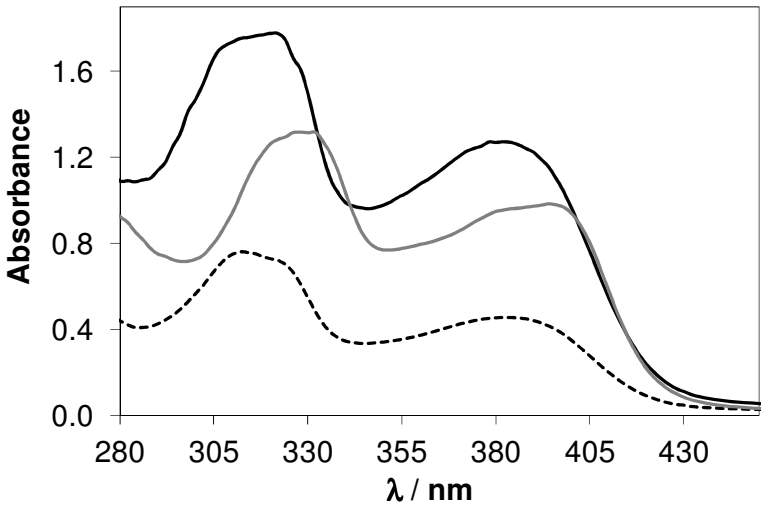

Figure S7. UV–vis spectra of [Cu(*L*-Pro-STSC)Cl]Cl: original solution (black solid line), the aqueous phase (black dashed line) and the *n*-octanol phase (grey solid line) following the separation for the log$D_{7.4}$ determination {$c_{\text{complex}} = 6.4 \times 10^{-5}$ M, pH = 7.40 (HEPES), I = 0.10 M (KCl) in aqueous phase}.

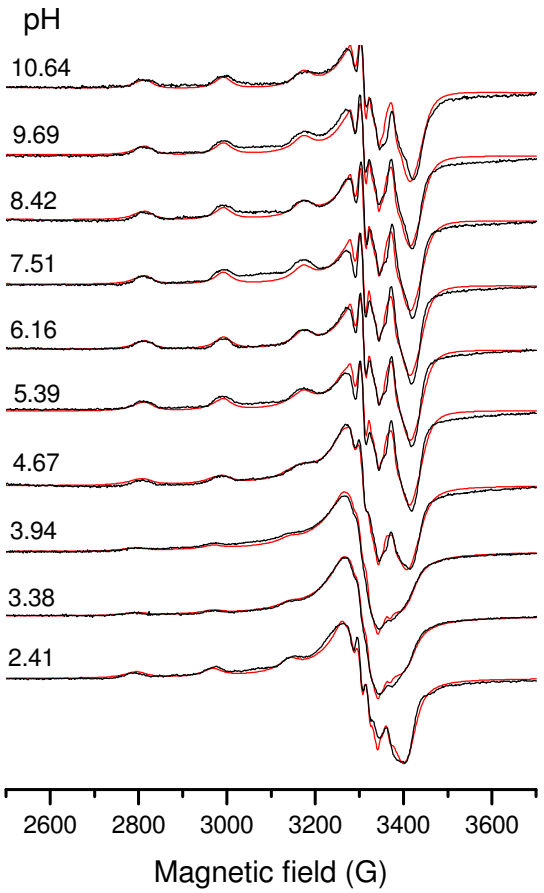

Figure S8. Experimental (black) and simulated (red) EPR spectra of the Cu^{2+} – *L*-Pro-STSC system {$c_{ligand} = 2\times10^{-3}$ M; M : L = 1:1; T = 77 K, I = 0.10 M (KCl) in 30% (w/w) DMSO/H_2O}.

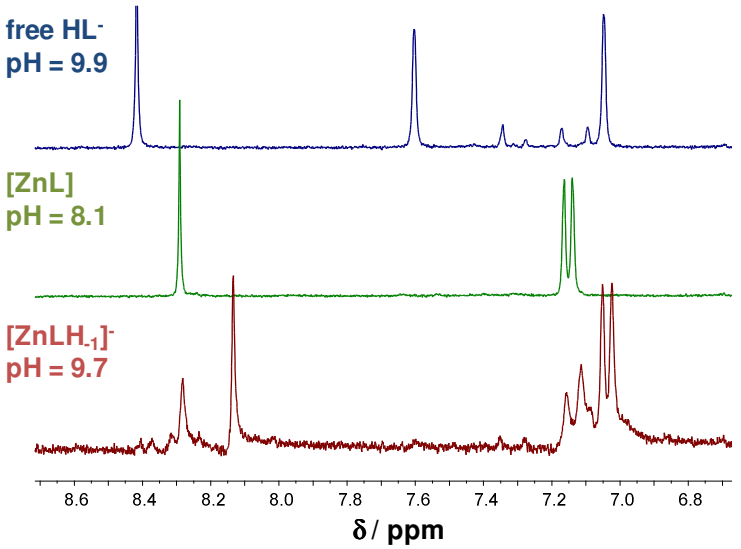

Figure S9. ^{1}H NMR spectra of *L*-Pro-STSC at pH 9.9; for the Zn^{2+} – *L*-Pro-STSC system at pH 8.1 and 9.7 {$c_{ligand} = 2.0 \times 10^{-3}$ M; M:L = 1:1; 30% (w/w) d_6-DMSO/H_2O}.

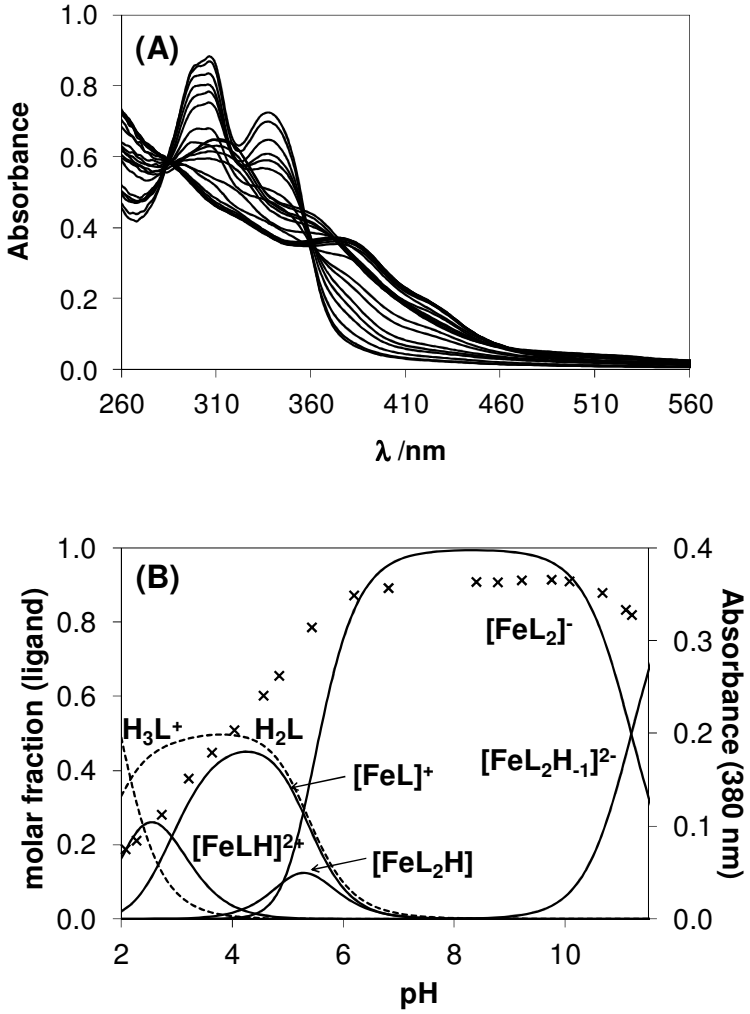

Figure S10. UV–vis spectra of the Fe^{3+} – *L*-Pro-STSC system at different pH values (A) and the corresponding concentration distribution curves depicted together with the absorbance values plotted against pH at 380 nm {$c_L = 4.0 \times 10^{-5}$ M; M:L = 1:2; T = 298 K, I = 0.10 M (KCl) in 30% (w/w) DMSO/H_2O}.

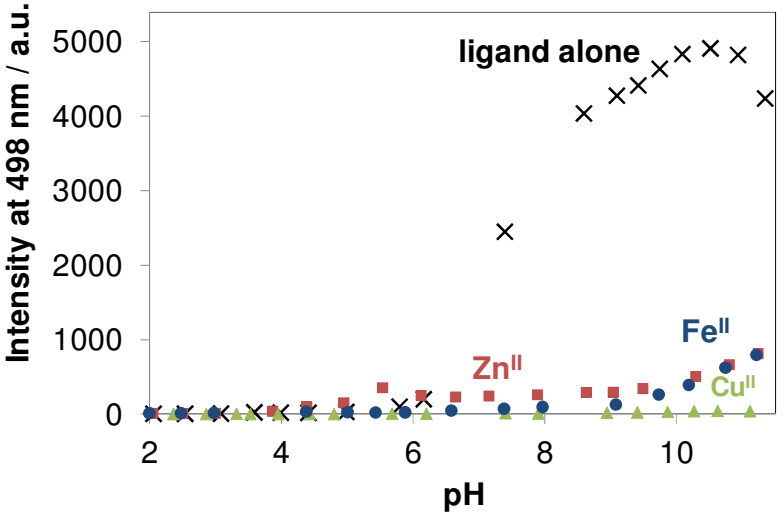

Figure S11. Fluorescence intensity of emission at 498 nm for the *L*-Pro-STSC (×), mixtures of Zn^{2+}, Fe^{2+} and Cu^{2+} with *L*-Pro-STSC at M:L = 1:1 (1:2 in the case of Fe^{2+}) ratio {λ_{EX} = 393 nm; c_{ligand} = 5 ×10^{-6} M; T = 298 K, I = 0.10 M (KCl); 5-5 nm slits; 30% (w/w) DMSO/H_2O)}.

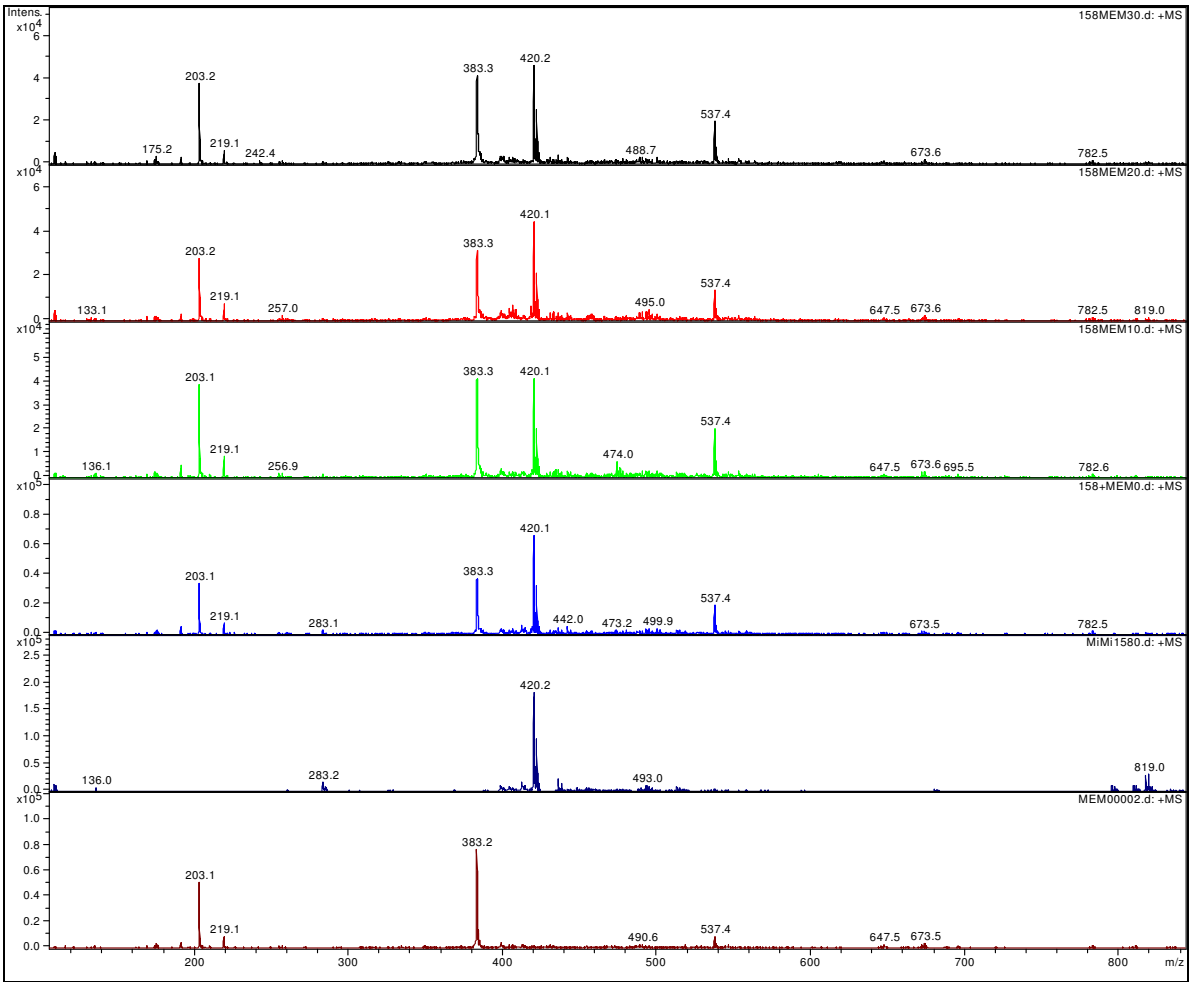

Figure S12. ESI-MS spectra of MEM (red), [Cu(*L*-Pro-STSC)Cl]Cl in water (dark blue), in MEM (dark red) after 0 h (blue), 1 h (green), 6h (red) and 22 h (black). The peak with *m/z* 420 is due to $[Cu^{II}L + Na]^+$.

Definition of the stability constants of the metal complexes collected in Table 2.

General formula:

M = metal ion; L= deprotonated form of the ligand; H = H^+

Charges are omitted for simplicity.

constant:	equilibrium:
$\beta(M_pL_qH_r) = [M_pL_qH_r]/[M]^p[L]^q[H]^r$	$pM + qL + rH \rightleftharpoons M_pL_qH_r$
$\beta(\mathbf{MLH}) = [MLH]/[M][L][H]$	$M + L + H \rightleftharpoons MLH$
$\beta(\mathbf{ML}) = [ML]/[M][L]$	$M + L \rightleftharpoons ML$
$\beta(\mathbf{MLH_{-1}}) = [MLH_{-1}]/[M][L][H]^{-1}$	$M + L - H \rightleftharpoons MLH_{-1}$
(*-H = deprotonation of a coordinated water molecule)*	
$\beta(\mathbf{ML_2H}) = [ML_2H]/[M][L]^2[H]$	$M + 2\,L + H \rightleftharpoons ML_2H$
$\beta(\mathbf{ML_2}) = [ML_2]/[M][L]^2$	$M + 2\,L \rightleftharpoons ML_2$
$\beta(\mathbf{ML_2H_{-1}}) = [ML_2H_{-1}]/[M][L]^2[H]^{-1}$	$M + 2\,L - H \rightleftharpoons ML_2H_{-1}$
(-H = deprotonation of a coordinated water molecule or coordination of OH^-)	

3.2 Hexanuclear and undecanuclear iron(III) carboxylates as catalyst precursors for cyclohexane oxidation

Miljan N. M. Milunovic, Luísa M. D. R. S. Martins, Elisabete C. B. Alegria, Armando J. L. Pombeiro, Regina Krachler, Günter Trettenhahn, Constantin Turta, Sergiu Shova, Vladimir B. Arion

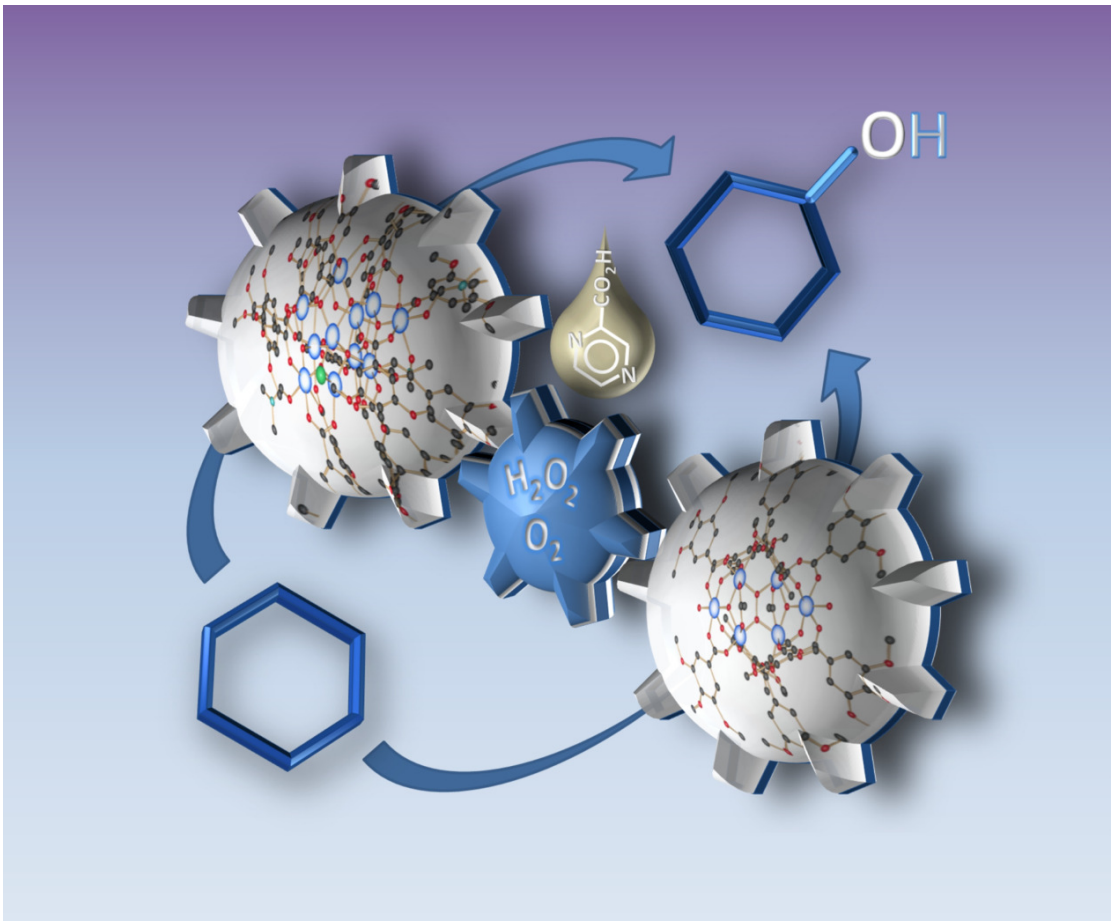

Dalton Trans. **2013**, *42*, 14388–14401

Contribution to the paper: Synthesis and characterization of hexanuclear and undecanuclear iron(III) carboxylates, UV–vis kinetic measurements, interactive participation in writing the introduction, discussion of the results, conclusions and proof-readings of the manuscript as well as design of the graphical abstract and the artwork for front journal cover.

Dalton Transactions

An international journal of inorganic chemistry

www.rsc.org/dalton

Volume 42 | Number 40 | 28 October 2013 | Pages 14333–14640

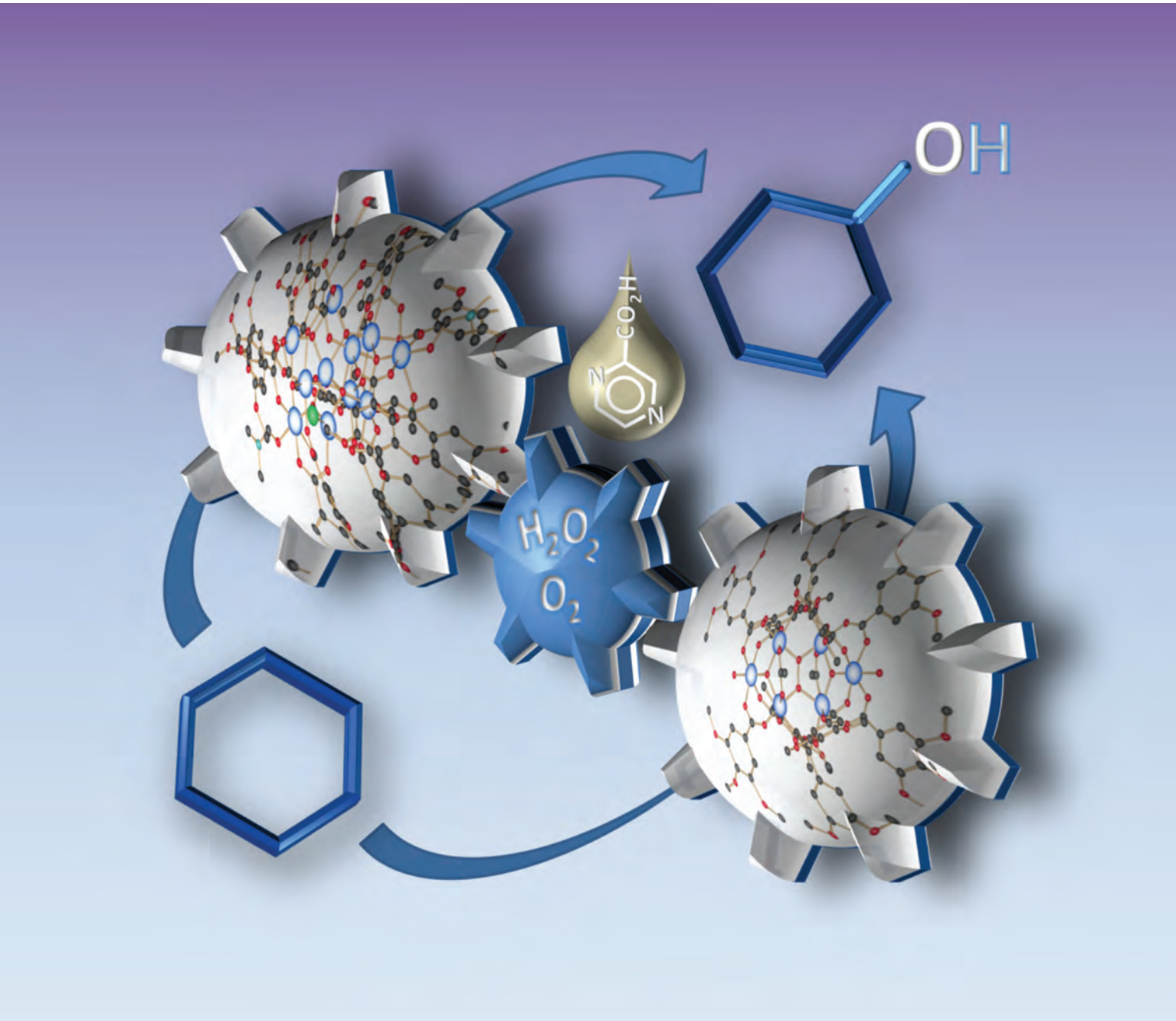

ISSN 1477-9226

RSC Publishing

COVER ARTICLE

Pombeiro, Arion *et al.*

Hexanuclear and undecanuclear iron(III) carboxylates as catalyst precursors for cyclohexane oxidation

1477-9226(2013)42:40;1-K

Dalton Transactions

RSC Publishing

PAPER

View Article Online
View Journal | View Issue

Cite this: *Dalton Trans.*, 2013, **42**, 14388

Hexanuclear and undecanuclear iron(III) carboxylates as catalyst precursors for cyclohexane oxidation†

Miljan N. M. Milunovic,[a] Luísa M. D. R. S. Martins,[b,c] Elisabete C. B. A. Alegria,[b,c] Armando J. L. Pombeiro,*[c] Regina Krachler,[a] Günter Trettenhahn,[d] Constantin Turta,[e] Sergiu Shova[f] and Vladimir B. Arion*[a]

Received 12th April 2013,
Accepted 27th June 2013

DOI: 10.1039/c3dt50966d

www.rsc.org/dalton

Two multinuclear complexes $[Fe_6(\mu_3\text{-}O)_2(\mu_4\text{-}O_2)L_{10}(OAc)_2(H_2O)_2]\cdot 2.625Et_2O\cdot 2.375H_2O$ (**1**) and $[Fe^{III}_{11}Cl(\mu_4\text{-}O)_3(\mu_3\text{-}O)_5L_{16}(dmf)_{2.5}(H_2O)_{0.5}]\cdot Et_2O\cdot 1.25dmf\cdot 3.8H_2O$ (**2**), where HL = 3,4,5-trimethoxybenzoic acid and dmf = dimethylformamide, have been prepared from trinuclear iron(III) carboxylates *via* their structural rearrangement in dimethylformamide or diethyl ether–dimethylformamide 9 : 1, respectively, and slow vapor diffusion of diethyl ether into the reaction mixture. Both compounds have been characterized by X-ray diffraction, optical, Mössbauer spectroscopy, and magnetic measurements. Complex **1** possesses a hexanuclear ferric peroxido–dioxido $\{Fe_6(O_2)(O)_2\}^{12+}$ core unit, which adopts a recliner conformation, while complex **2** contains an unprecedented $\{Fe_{11}O_8Cl\}^{16+}$ core, in which 9 ferric ions are six-coordinate and the remaining two are five-coordinate. Another structural feature of note of the undecanuclear core is the presence of a deformed cubane entity $\{Fe_4(\mu_3\text{-}O)(\mu_4\text{-}O)_3\}^{4+}$. Both complexes act as catalyst precursors for the oxidation of cyclohexane to cyclohexanol and cyclohexanone with aqueous H_2O_2, in the presence of pyrazinecarboxylic acid. Remarkable TONs and TOFs (the latter mainly for **1**) with concomitant quite good yields have been achieved under mild conditions. Moreover, **1** exhibits remarkably high activity in an exceptionally short reaction time (45 min), being unprecedented for any metal catalyzed alkane oxidation by H_2O_2. The catalytic reactions proceed *via* Fenton type chemistry.

Introduction

Low nuclearity iron complexes with structural motifs $\{Fe_2O\}^{4+}$, $\{Fe_3O\}^{7+}$ and $\{Fe_4O_2\}^{8+}$ are suitable starting materials for the synthesis of higher nuclearity complexes[1–3] due to their relatively easy chemical rearrangement in solution.[4] The dominant structural unit in polynuclear iron complexes is $\{Fe_3O\}^{7+}$, although iron clusters with an $\{Fe_4O_4\}^{4+}$ cubane entity or with a defected double-cubane core have also been reported.[5] Hexanuclear iron(III) clusters, and, in particular, those containing a central peroxido group bridging four ferric ions in a μ_4–η^2:η^2 fashion, have been prepared by using basic iron(III) carboxylates containing the $\{Fe_3O\}^{7+}$ unit as starting materials.[4b,c,6] The range of this type of polynuclear cage has been extended by using displacement reactions of initially used carboxylates by other carboxylate or phosphonate ligands.[4c,7,8] A hexanuclear iron(III) complex with three μ_4–η^2:η^2 peroxido ligands bridging two Fe_3O triangles resulted from a similar reaction of basic iron(III) acetate with H_2O_2 in the presence of $NaOCH_3$ as a base.[4b] The family of undecanuclear iron complexes is also small. In the past 25 years just a few compounds have been synthesized.[4e,f,9–11] Some of them possess SMM features[4f,9] due to their capacity to retain magnetization after removal of a magnetic field. Others were investigated as model compounds for ferritin,[4e] a physiologically important iron storage protein in mammals. However, their catalytic ability remains little explored. Hydrocarbons, particularly alkanes, are interesting compounds as the main constituents of natural oil and gas and their C–H bonds can be converted to C–OH or C=O functional groups leading to the formation of more valuable products for a fine chemical synthesis. This requires the use of transition metals as catalysts. Nature uses iron to oxidize C–H bonds by dioxygen activation mechanisms, in

[a]*University of Vienna, Institute of Inorganic Chemistry, Währinger Strasse 42, A-1090 Vienna, Austria. E-mail: vladimir.arion@univie.ac.at*
[b]*Área Departamental de Engenharia Química, ISEL, R. Conselheiro Emídio Navarro, 1959-007 Lisboa, Portugal*
[c]*Centro de Química Estrutural, Complexo I, Instituto Superior Técnico, Technical University of Lisbon, Av. Rovisco Pais, 1049-001 Lisboa, Portugal. E-mail: pombeiro@ist.utl.pt*
[d]*University of Vienna, Institute of Physical Chemistry, Währinger Strasse 42, A-1090 Vienna, Austria*
[e]*Institute of Chemistry of the Academy of Sciences of Moldova, Academiei str. 3, MD-2028, Chisinau, Moldova*
[f]*Petru Poni' Institute of Macromolecular Chemistry, Aleea Gr. Ghica Voda 41A, 700487 Iasi, Romania*
†Electronic supplementary information (ESI) available. CCDC 889029 and 933668. For ESI and crystallographic data in CIF or other electronic format see DOI: 10.1039/c3dt50966d

which high-valent oxido-iron species act as actual oxidizing agents.[12,13] Therefore, the synthesis of metal-based systems with similar catalytic ability is a challenge in catalytic chemistry.[4a,14–16] Variable architecture of their cores and structural similarity with active centers of biologically important enzymes such as methane monooxygenase (MMOx),[17] toluene monooxygenase (TMOx),[18] Δ-9-desaturase (Δ-9-D),[19] and ribonucleotide reductase (RNR)[20] make them well suited for assaying the catalytic activity in organic reactions.[4a,c,21] We have a general interest in the metal catalyzed, mild oxidative functionalization of alkanes and alcohols.[4a,22–40] The use of polynuclear iron(III) carboxylates in alkane oxidation has been recently reported by us,[4a] and peroxido species formation has been hypothesized on reaction of the hexanuclear iron(III) complex with hydrogen peroxide. This prompted us to attempt the synthesis of other polynuclear iron carboxylates, isolation of peroxido species and elucidation of their role in catalytic alkane oxidation.

Herein, we report on the synthesis, X-ray diffraction structure, spectroscopic characterization, magnetism and catalytic activity of two multinuclear iron(III) carboxylates, namely a hexanuclear μ_4–η^2:η^2-peroxido complex $[Fe_6(\mu_3\text{-}O)_2(\mu_4\text{-}O_2)L_{10}(OAc)_2(H_2O)_2]\cdot 2.625Et_2O\cdot 2.375H_2O$ (**1**) and an undecanuclear complex $[Fe^{III}{}_{11}Cl(\mu_4\text{-}O)_3(\mu_3\text{-}O)_5L_{16}(dmf)_{2.5}(H_2O)_{0.5}]\cdot Et_2O\cdot 1.25dmf\cdot 3.8H_2O$ (**2**) with a new core topology, where HL = 3,4,5-trimethoxybenzoic acid. The compounds were tested as catalyst precursors for cyclohexane oxidation to cyclohexanol and cyclohexanone, the mainstream starting materials in the production of adipic acid, nylon-6,6′, and polyamide-6.[41]

Experimental section

Materials and physical measurements

Pyrazinecarboxylic acid (Hpca), trifluoroacetic acid, *n*-butyric acid and 3,4,5-trimethoxybenzoic acid were purchased from Sigma Aldrich, nitric acid (65%) and potassium peroxodisulfate from Fluka, $FeCl_3\cdot 6H_2O$ from Riedel-de-Haën and $Fe(NO_3)_3\cdot 9H_2O$, $FeSO_4\cdot 7H_2O$ and $Fe(CF_3SO_3)_3$ from Acros Organics. Acetonitrile (Riedel-de-Haën), cyclohexane (Aldrich), cyclopentane (Aldrich), cyclohexanol (Aldrich), cyclohexanone (Aldrich), cycloheptanone (Aldrich), *n*-pentane (Aldrich), *n*-heptane (Aldrich), hydrogen peroxide (30% and 50% in water) (Fluka), diethyl ether (Riedel-de-Haën), triphenylphosphine, diphenylamine (Fluka), bromotrichloromethane (Fluka), nitromethane (Aldrich), ethane (AlphaGaz), carbon monoxide (Air Products) and dinitrogen (Air Liquid Portugal) were used as received from the suppliers. The solvents were dried over appropriate drying agents and degassed using standard methods. Elemental analysis was carried out by the Microanalytical Service of the Institute of Physical Chemistry of the University of Vienna. UV-vis spectra were recorded on an Agilent 8453 UV-vis spectrophotometer. The MIR spectra were measured on a Bruker Vertex 70 FT-IR spectrometer (4000–400 cm^{-1}) by using an ATR unit. The Mössbauer spectra were acquired using a conventional spectrometer in the constant-acceleration mode (MS4, Edina, USA) equipped with a ^{57}Co source (3.7 GBq) in a rhodium matrix. Isomer shifts are quoted relative to α-Fe at room temperature. The spectra of the samples measured at 300 and 80 K were fitted using the NORMOS Mössbauer Fitting Program. The sample measured at 4.2 and 2.7 K was inserted inside an Oxford Instruments Mössbauer-Spectromag 4000 Cryostat, which has a split-pair superconducting magnet system for applied fields up to 5 T, with the field of the sample oriented perpendicular to the gamma-ray direction. Magnetic data were obtained with a Quantum Design MPMS SQUID susceptometer. Magnetic susceptibility measurements were performed in the 2–300 K temperature range under a 0.1 T applied magnetic field, and diamagnetic corrections were applied by using Pascal's constants.[42] Isothermal magnetization measurements were performed up to 6 T at 2 K. Gas chromatographic (GC) measurements were carried out using a FISONS Instruments GC 8000 series gas chromatograph with a FID detector and a capillary column (DB-WAX, column length: 30 m; internal diameter: 0.32 mm) and the Jasco-Borwin v.1.50 software. The temperature of injection was 240 °C. The initial temperature was maintained at 100 °C (for peroxidative oxidation of cyclohexane, alkane carboxylation and hydrocarboxylation or 80 °C for *n*-heptane oxidation to corresponding alcohols and ketones) for 1 min, then raised to 180 °C (10 °C min^{-1}) and held at this temperature for 1 min. Helium was used as the carrier gas. GC-MS analyses were performed using a Perkin Elmer Clarus 600C instrument (He as the carrier gas), equipped with a 30 m × 0.22 mm × 25 μm, BPX5 (SGE) capillary column.

Preparation of complexes

$[Fe_3OL_6(H_2O)_3]NO_3\cdot HL$. 3,4,5-Trimethoxybenzoic acid (HL) (3.00 g, 14.14 mmol) was neutralized with a solution of sodium hydrogen carbonate (1.19 g, 14.14 mmol) in water (20 mL) under stirring at 50–60 °C until effervescence of CO_2 was completed. To the filtered solution of the sodium salt of 3,4,5-trimethoxybenzoic acid at room temperature was added dropwise a solution of iron(III) nitrate nonahydrate (2.85 g, 7.07 mmol) in water (25 mL). The reaction mixture was stirred for 15 min and allowed to stand at room temperature. The orange precipitate was filtered off, dissolved in $CHCl_3$ (200 mL), and solution filtered. After removing the solvent, the red solid was dried *in vacuo* overnight. Yield 2.78 g, 66.5%. Found: C, 47.61; H, 4.86; N, 0.43. Calc. for $C_{70}H_{84}Fe_3NO_{42}$ (M_r 1778.9 g mol^{-1}): C, 47.26; H, 4.76; N 0.79. ESI-MS in MeOH (positive): *m*/*z* 1450 ($[Fe_3OL_6]^+$). ESI-MS in MeOH (negative): *m*/*z* 1183.5 ($[Fe_2OL_5]^-$).

$[Fe_6(\mu_3\text{-}O)_2(\mu_4\text{-}O_2)L_{10}(OAc)_2(H_2O)_2]\cdot 2.625Et_2O\cdot 2.375H_2O$ (1). To a solution of $[Fe_3OL_6(H_2O)_3]NO_3\cdot HL$ (0.8 g, 0.45 mmol) in methyl ethyl ketone (9 mL), a 30% solution of H_2O_2 (0.2 mL) was added and the reaction mixture was stirred at room temperature for 1 h. The slow diffusion of Et_2O into the reaction mixture produced dark-red X-ray diffraction quality crystals in *ca.* 10 days, which were filtered off and dried *in vacuo*.

A sample for X-ray diffraction study was left in contact with the mother liquor to prevent the loss of solvent. Yield: 0.45 g, 75.0%. Found: C, 46.00; H, 4.43. Calc. for $C_{104}H_{124}Fe_6O_{62}$ (M_r 2701.1 g mol^{-1}): C, 46.24; H, 4.63. λ_{max}(MeCN)/nm 265 (ε/dm^3 mol^{-1} cm^{-1} 130 000), 343 (24 000). ν/cm^{-1}: 3470, 2942, 2837, 1589, 1544, 1450, 1436, 1389, 1318, 1225, 1182, 1122, 1002, 958, 882, 783, 758, 728.

$[Fe_3OL_6(H_2O)_3]Cl\cdot HL$. 3,4,5-Trimethoxybenzoic acid (HL) (4.00 g, 18.85 mmol) was neutralized with a solution of sodium hydrogen carbonate (1.58 g, 18.85 mmol) in water (55 mL) under stirring at 60 °C until effervescence of CO_2 was completed. To the filtered solution of the sodium salt of 3,4,5-trimethoxybenzoic acid was added dropwise a solution of iron(III) chloride hexahydrate (2.54 g, 9.43 mmol) in water (39 mL). The reaction mixture was stirred at 60 °C for 4 h. The orange precipitate was filtered off, dried *in vacuo* overnight and stored in a desiccator over $CaCl_2$. Yield 3.65 g, 75.7%. Found: C, 47.81; H, 4.84; Cl, 2.03. Calc. for $C_{70}H_{84}ClFe_3O_{39}$ (M_r 1752.4 g mol^{-1}): C, 47.98; H, 4.83; Cl, 2.02. ESI-MS in MeOH (positive): m/z 1450 ($[Fe_3OL_6]^+$).

$[Fe^{III}_{11}Cl(\mu_4\text{-}O)_3(\mu_3\text{-}O)_5L_{16}(dmf)_{2.5}(H_2O)_{0.5}]\cdot Et_2O\cdot 1.25dmf\cdot 3.8H_2O$ (2). A solution of $[Fe_3OL_6(H_2O)_3]Cl\cdot HL$ (0.56 g, 0.36 mmol) in dmf–Et_2O = 1 : 9 (50 mL) was stirred at room temperature for 1 h. Slow diffusion of Et_2O into the reaction mixture produced X-ray diffraction quality dark-red crystals of **2** in two months. Yield: 0.05 g, 11.0%. The sample for elemental analysis was dried *in vacuo* for 6 h. Anal. Found: C, 45.53; H, 4.21; N, 0.33; Cl, 1.16. Calc. for $C_{166.75}H_{197.75}ClFe_{11}N_{2.25}O_{93.25}$ (M_r 4375.3 g mol^{-1}): C, 45.77; H, 4.56; N, 0.72; Cl, 0.81. λ_{max}(MeCN)/nm 265 (ε/dm^3 mol^{-1} cm^{-1} 264 000), 350 sh (54 400). ν/cm^{-1}: 3510, 3074, 2939, 2836, 1645, 1546, 1385, 1223, 1186, 1120, 998, 776, 760.

X-ray crystallography

X-ray diffraction measurements were performed on a Bruker X8 APEXII CCD diffractometer. Single crystals of **1** and **2** were positioned at 40 mm from the detector, and 2491 and 6982 frames were measured, each for 30 and 20 s over 1° scan width. The data were processed using *SAINT* software.[43] Crystal data, data collection parameters, and structure refinement details are given in Table S1.† The structures were solved by direct methods and refined by full-matrix least-squares techniques. The disorder in some carboxylate ligands in **1** was resolved with restraints on the displacement parameters and on bond distances using mainly the EADP and SADI instructions of SHELX-97, respectively. The following software programs and computer were used: structure solution SHELXS-97, refinement SHELXL-97,[44] molecular diagrams ORTEP-3,[45] computer, Intel CoreDuo. CCDC 933668 and CCDC 889029 contain the supplementary crystallographic data for this paper.

Typical procedures for the catalytic oxidation of alkanes and product analysis

The peroxidative oxidation reactions were carried out in Schlenk tubes and under a dinitrogen or air atmosphere as follows: 0.05–26 μmol of the catalyst precursor (**1** or **2**) and 8.6–130 μmol of pyrazinecarboxylic acid (Hpca) (*i.e.* a (**1** or **2**) : Hpca molar ratio of 1 : 5 to 1 : 150) were dissolved in MeCN (3.00 mL) with vigorous stirring, whereafter 10.00 mmol of 30% H_2O_2 (1.02 mL) and 5.00 mmol of cyclohexane (0.54 mL) were added and the reaction solution was stirred for 6 h, at room temperature (r.t.) and normal pressure. In the experiments with radical traps, $CBrCl_3$ (5.00 mmol) or $NHPh_2$ (5.00 mmol) was added to the reaction mixture. The product analysis was performed as follows: 90 μL of cycloheptanone (internal standard), 10.00 mL of diethyl ether (to extract the substrate and the organic products from the reaction mixture) and an excess of triphenylphosphine (in order to reduce the formed cyclohexyl hydroperoxide to the corresponding alcohol, and hydrogen peroxide to water, following a method developed by Shul'pin)[46] were added. The obtained mixture was stirred for 10 min and then a sample (1 μL) was taken from the organic phase and analyzed by gas chromatography (GC) using the internal standard method. Blank tests indicate that no oxidation takes place in the absence of the iron complex or the oxidant.

For *n*-heptane oxidation, 1.3 μmol of **1** or **2**, a catalyst precursor : Hpca molar ratio of 1 : 50, a 50% aqueous solution of H_2O_2 (0.2 mL) and *n*-heptane (100.0 μL) were vigorously stirred, in MeCN (up to 2.50 mL), whereafter the reaction solution was stirred for 3 h, at 50 °C and normal pressure. The product analysis by GC was performed directly on the reaction mixture.

Hydrocarboxylation and carboxylation reactions of alkanes were carried out in a stainless steel autoclave with a capacity of 13.00 mL. Typical conditions are as follows: 0.002 mmol of **1** or **2**, 2 mmol of potassium peroxodisulfate $K_2S_2O_8$ (1000 : 1 molar ratio of $K_2S_2O_8$ to catalyst precursor), MeCN (2.50 mL), H_2O (2.50 mL) (total solvent volume 5.00 mL) for hydrocarboxylation or TFA (5.00 mL) for carboxylation, the substrate (1.00 mmol of liquid alkanes and 10 atm (2.66 mmol) of C_2H_6) and a Teflon-coated magnetic stirring bar were placed in the autoclave. Then, the autoclave was closed and flushed with CO (three times for removing the air) and finally pressurized with 20 atm (5.33 mmol) of CO (due to the high toxicity of CO, all the manipulations should be performed with due care!). The autoclave was introduced into an oil bath and heated at 60 °C for 4 h, for hydrocarboxylation, or at 80 °C for 20 h, for carboxylation, with magnetic stirring of the reaction solution. After the reaction was complete, the autoclave was cooled with an ice bath to room temperature, degassed, opened and the contents transferred to a flask. Diethyl ether was added to extract the organic products. The mixture was vigorously stirred and filtered off, and 90 μL of cycloheptanone (GC internal standard) were added to the filtered ether solution, whereafter aliquots (1 μL) of the solution were analyzed by GC using the internal standard method. Blank tests indicated that the hydrocarboxylations also proceed in the metal-free systems.[47–49] The formation of dicarboxylic acids was not observed.

Results and discussion

Crystal structure of 1

The result of the X-ray diffraction study of **1** is shown in Fig. 1. The hexanuclear complex has C_i point symmetry. The structure consists of two $[Fe_3(\mu_3\text{-}O)(H_2O)(\mu_2\text{-}O_2CR)_4(\mu_2\text{-}OAc)]^{2+}$ units bridged by two carboxylate ligands $(\mu_2\text{-}O_2CR)^-$ and a $\mu_4,\eta^2\text{:}\eta^2$-peroxido ion (Fig. 1). The atoms Fe1 and Fe3 are spanned by an acetate ligand adopting a $\mu_2\text{–}\eta^1\text{:}\eta^1$ binding mode. The coordination number of the distal atom Fe2 is completed to six by coordination of water molecules.

As in $[Fe_6(O_2)(O)_2(O_2CCMe_3)_{12}(HO_2CCMe_3)_2]$, the core unit $[Fe_6(O_2)(O)_2]^{12+}$ in **1** adopts a recliner conformation as shown in Fig. 2.[4c] This contrasts with the 'butterfly'-like conformation discovered in other related complexes.[4c] The dihedral angle between the mean plane through Fe1, Fe2 and Fe3 and that through Fe1, Fe3 and $Fe1^i$, $Fe3^i$ in **1** is at 137.6°. Atoms marked with i were generated by symmetry transformation $-x$, $-y + 1$, $-z + 2$. The peroxido oxygen atoms O1 and $O1^i$ come out from the mean plane through Fe1, Fe3, $Fe1^i$ and $Fe_3{}^i$ by 0.16 and −0.16 Å, respectively. Thus the weakly pyramidally distorted geometry of peroxido oxygen atoms can be mentioned here. The sum of bond angles around O1 is 355.7°. This value, which indicates the extent of planarity of peroxido oxygen atoms, is at 357.4 and 359.2° in $[Fe_6(O_2)(O)_2(O_2CPh)_{12}(H_2O)_2]$.[6] Strong pyramidality of peroxido oxygen atoms was observed in $[Fe_6(O_2)_3(O)_2(OAc)_9]^-$,[4b] where the sum of bond angles around peroxido oxygen atoms is 322.0° and 331.8°.

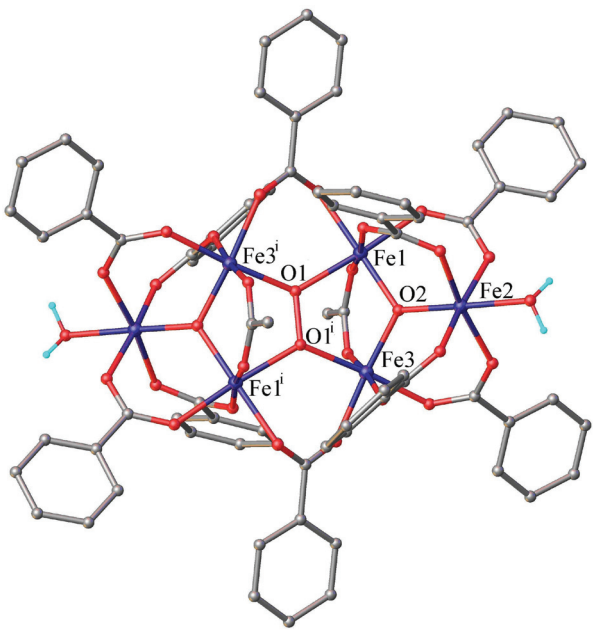

Fig. 1 The molecular structure of **1**. Hydrogen atoms, trimethoxy and some trimethoxyphenyl groups were omitted for clarity. Selected bond distances (Å) and bond angles (°): Fe1–O1 2.047(3), Fe1–O2 1.889(3), Fe2–O2 1.895(3), Fe3–O2 1.895(3), O1–$O1^i$ 1.471(5), Fe1–O1–$Fe3^i$ 127.75(14), Fe1–O2–Fe2 122.39(15), Fe1–O2–Fe3 114.55(15), Fe2–O2–Fe3 122.83(15). Atoms marked with i were generated by symmetry transformation $-x$, $-y + 1$, $-z + 2$.

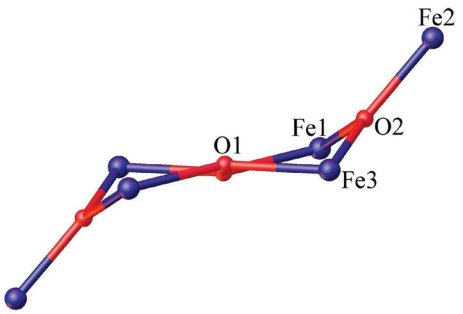

Fig. 2 Recliner conformation of the $\{Fe_6(O_2)(O)_2\}^{12+}$ core in **1**.

Crystal structure of 2

Likewise, complex **2** crystallizes in the triclinic centrosymmetric space group $P\bar{1}$. The result of an X-ray diffraction study is shown in Fig. 3. The structure of **2** consists of an $\{Fe^{III}{}_{11}O_8\}^{17+}$ core, which possesses C_1 point symmetry, with three $\mu_4\text{-}O^{2-}$ and five $\mu_3\text{-}O^{2-}$ bridges. Of the 11 ferric ions, 9 are six-coordinate while the remaining 2 (Fe7 and Fe8) are five-coordinate. Peripheral coordination is provided by 15 bridging carboxylate groups adopting a $\mu_2\text{–}\eta^1\text{:}\eta^1$ binding mode and one $\mu_2\text{–}\eta^1\text{:}\eta^2$-carboxylate (O39 acts as a bridging atom between Fe9 and Fe10), one chlorido ligand and three dmf–H_2O molecules.

One interesting feature of the core structure in **2** is the presence of a distorted cubane $\{Fe_4O_4\}^{4+}$ unit, in which the iron atoms Fe2, Fe3, Fe4, Fe7 and oxygen atoms O1, O2, O3, O4 are involved (Fig. 4 and 5). The distortion is manifested by the lack of bonding interaction between Fe7 and O2 (Fe7–O2 2.925 Å compared to Fe2–O7 at 1.955 Å). Of the four oxygen atoms building the distorted cubane unit, three (O1, O3 and O4) are $\mu_4\text{-}O^{2-}$ and O2 acts as a $\mu_3\text{-}O^{2-}$ ligand. The atom Fe7 plays an important role in the core structure sharing its

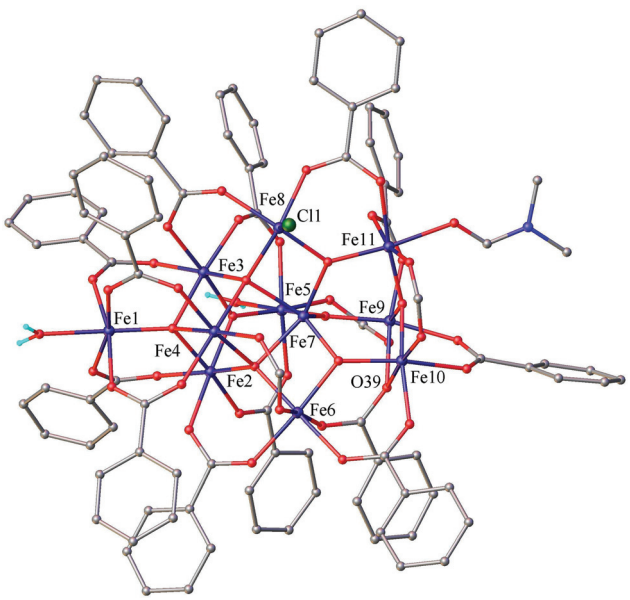

Fig. 3 The molecular structure of **2**. Hydrogen atoms, trimethoxy and some trimethoxyphenyl groups were omitted for clarity.

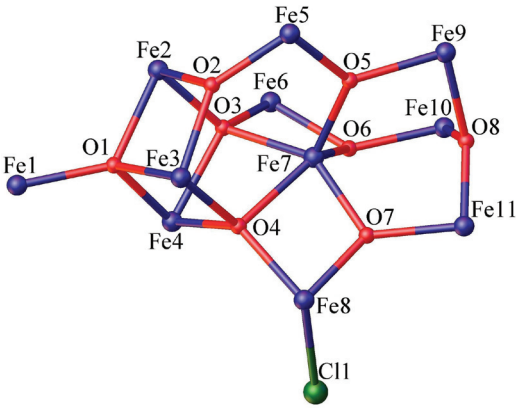

Fig. 4 The core unit $\{Fe_{11}O_8Cl\}^{16+}$ of **2**. Selected bond distances (Å) and bond angles (°): Fe1–O1 1.917(4), Fe2–O1 2.089(4), Fe3–O1 2.074(4), Fe4–O1 2.033(4), Fe2–O2 1.955(4), Fe3–O2 1.946(4), Fe5–O2 1.892(4), Fe2–O3 1.968(4), Fe4–O3 2.077(4), Fe6–O3 1.959(4), Fe7–O3 2.095(4), Fe3–O4 1.997(4), Fe4–O4 2.001(4), Fe7–O4 2.115(4), Fe8–O4 1.990(4), Fe5–O5 1.939(4), Fe7–O5 1.904(4), Fe9–O5 1.948(4), Fe6–O6 1.965(4), Fe7–O6 1.923(4), Fe10–O6 1.894(4), Fe7–O7 1.931(4), Fe8–O7 1.874(4), Fe11–O7 1.897(4), Fe9–O8 1.929(4), Fe10–O8 1.939(4), Fe11–O8 1.895(4), Fe8–Cl1 2.2411(17), O1–Fe2–O2 83.53(15), O1–Fe2–O3 83.40(15), O1–Fe3–O2 84.13(15), O1–Fe4–O3 82.13(15), O1–Fe4–O4 83.79(15), O2–Fe3–O4 95.45(16), Fe4–O4–Fe7, Fe2–O3–Fe7 116.23(19), Fe4–O3–Fe7 96.16(16).

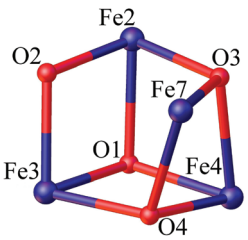

Fig. 5 Distorted cubane unit $\{Fe_4(\mu_3\text{-}O)(\mu_4\text{-}O)_3\}^{4+}$ of **2**.

position with three μ_3-oxido centered iron(III) triangles (Fig. 4). The dihedral angles formed between the plane through Fe7, Fe5, Fe9 with those through Fe7, Fe8, Fe11 and Fe7, Fe6, Fe10 are of 68.4 and 72.7°, respectively. Note that the coordination environment of the five-coordinate atom Fe7 consists of two μ_4-O^{2-} and three μ_3-O^{2-} ligands exclusively, while that of Fe8 consists of μ_4-O^{2-} (O4), μ_3-O^{2-} (O7), and two μ-carboxylate ligands in the basal plane of the square-planar pyramid and apical chloride. The terminal iron ions Fe9, Fe10 and Fe11 are joined together by the μ_3-oxido bridging ligand O8. The Fe1 atom is connected to O1 of the cubane entity. The other four octahedral sites are occupied by 4 carboxylate oxygens (of four different 3,4,5-trimethoxybenzoate ligands), while the sixth position by dmf and H_2O with equal probability.

Syntheses

Complex **1** was obtained by oxidation of $[Fe_3OL_6(H_2O)_3]$-NO_3·HL, where HL = 3,4,5-trimethoxybenzoic acid, with H_2O_2 in methyl ethyl ketone and crystallized within two weeks by slow diffusion of diethyl ether into the reaction mixture at room temperature. On this occasion methyl ethyl ketone served not only as a solvent, but also as a source of acetic acid. Complex **2** was prepared by dissolution of basic iron(III) carboxylate $[Fe_3OL_6(H_2O)_3]Cl$·HL (HL = 3,4,5-trimethoxybenzoic acid) in a mixture of dmf–Et_2O 1 : 9 and crystallized within two months by slow diffusion of Et_2O into the reaction mixture at room temperature.

Mössbauer spectroscopy and magnetic susceptibility measurements

The Mössbauer spectra of **1** show a symmetric quadrupole doublet with an isomer shift δ = 0.54 mm s^{-1} and a splitting ΔE_Q = 0.75 mm s^{-1}, and δ = 0.43 mm s^{-1} and ΔE_Q = 0.75 mm s^{-1}, at 80 and 300 K, respectively (Fig. 6 and Fig. S1†), indicating a high-spin ferric compound.[4a]

The Mössbauer spectrum of **2**–^{57}Fe (compound **2** prepared from ^{57}Fe) at 80 K displays a quadrupole doublet (Fig. 7) with an isomer shift δ = 0.57 mm s^{-1} and a splitting ΔE_Q = 0.88 mm s^{-1} very close to those reported for a hexanuclear ferric carboxylate with a $[Fe_6(\mu_3\text{-}O)_3(\mu_2\text{-}OH)]^{11+}$ core (δ = 0.53 mm s^{-1},

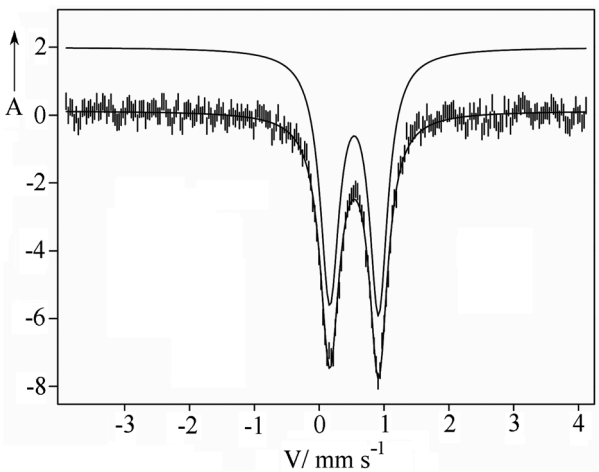

Fig. 6 Mössbauer spectrum of **1** at 80 K (δ = 0.54 mm s^{-1}, ΔE_Q = 0.75 mm s^{-1}).

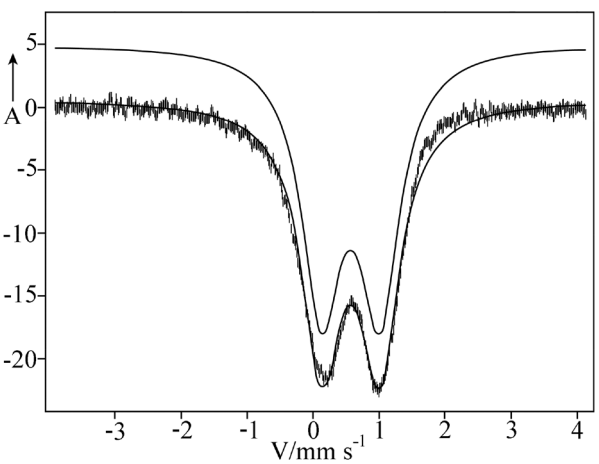

Fig. 7 Mössbauer spectrum of **2**–^{57}Fe at 80 K (δ = 0.57 mm s^{-1}, ΔE_Q = 0.88 mm s^{-1}).

ΔE_Q = 0.96 mm s^{-1}).[4a] The parameters of **2** are also close to those of **1**.

The temperature dependence of the magnetic susceptibility of **2** is shown in Fig. S2.† The room temperature $\chi_M T$ value is 11.68 cm^3 K mol^{-1}, which is much less than the value 48.13 cm^3 K mol^{-1} expected for 11 uncoupled S = 5/2 centers with g = 2. As the temperature is decreased, $\chi_M T$ decreases steadily to a value of 0.55 cm^3 K mol^{-1} at 2.0 K, indicating strong antiferromagnetic interactions between the Fe^{III} ions. This is suggestive of an S = 1/2 ground state with a partially populated low lying S = 3/2 excited state as $\chi_M T$ is calculated to be 0.375 and 1.875 cm^3 K mol^{-1} for S = 1/2 and S = 3/2 systems with g = 2.0. We have not attempted to simulate the magnetic susceptibility data, as a large number of different exchange parameters would be required, taking into account the high nuclearity and low symmetry of **2**.

Catalytic oxidation of alkanes

Complexes **1** and **2** act as catalyst precursors for the peroxidative oxidation of cyclohexane with aqueous H_2O_2, in the presence of pyrazinecarboxylic acid.

Peroxidative oxidation of cyclohexane

The system **1** (or **2**)–pyrazinecarboxylic acid (Hpca)–H_2O_2 exhibits remarkable catalytic activity toward the oxidation of cyclohexane to cyclohexanol (OL) and cyclohexanone (ONE), *via* cyclohexyl hydroperoxide (CyOOH, primary product), according to Scheme 1 (without a defined stoichiometry) and Table 1. The formation of CyOOH is proved by using the method proposed by Shul'pin.[46] In fact, addition of PPh_3 prior to the GC analysis of the products results in a marked increase of the amount of cyclohexanol (due to reduction of CyOOH by PPh_3) and a corresponding decrease of cyclohexanone, as observed in other catalytic systems.[23d,25,34,46,49–51]

Overall turnover numbers (TON, moles of product per mol of catalyst precursor) and yields up to *ca.* 2.2 × 10^3 (**1**) or 3.5 × 10^3 (**2**) and 22% (**1**) or 20% (**2**) (relative to the alkane), respectively, have been achieved at room temperature (r.t.), after 45 min (**1**) or 6 h (**2**) reaction time (Fig. 8). In fact, **1** is, to our knowledge, the first metal catalyst precursor able to provide such combined high yield and TON values in a remarkably reduced reaction time (corresponding to a TOF value of *ca.* 3.0 × 10^3 h^{-1}) and under the mild reaction conditions used.

The achieved TONs (and TOFs) are remarkably high, much above those reported[4a,34,39a,b,52] for iron or other metal complex catalysts in spite of the mild conditions, in aqueous acetonitrile at a low temperature with a green oxidant, in the presence of a weak acid. The yields are also higher than those observed for [Fe^{III}(gma)(PBu_3)] (gmaH$_2$ = glyoxal-bis(2-mercaptoanil); up to 8%)[39b] or [Fe{$HOCH_2C(pz)_3$}$_2$][Fe_2OCl_6]($Cl)_2$·$4H_2O$ (pz = pyrazolyl; up to 14%),[25,34b,52] comparable with those exhibited by Li[$FeCl_2${$SO_3C(pz)_3$}] (up to 24%),[34a] by the Co(III)–Fe(III) Schiff base complex [$Co_4Fe_2OSae_8$]·4dmf·H_2O (H_2Sae = salicylidene-2-ethanolamine) (up to 26%)[53] and by the hexanuclear iron(III) *p*-nitrobenzoate complex [Fe_6O_3(OH)-(*p*-$NO_2C_6H_4COO)_{11}$($dmf)_4$] (20%) which displays a much lower TON (100).[4a] They are lower than those for Fe(III)–Cr(III) hydroxides[39a] (up to 45%) but the latter system requires the use of a strong acid (HNO_3) and leads to a much lower TON value of 30. The combination of such a high yield and TON (and TOF), reached in a short reaction time and under mild conditions, is very rare and indicates exceptional activity of the catalytic system based on complex **1**. For example, the above heterometallic Co_4Fe_2 Schiff base complex reaches concomitantly high TON (3.6 × 10^3) and yield (26%) values only after 5 h reaction time (TOF = 7.2 × 10^2 h^{-1}), in the presence of HNO_3 (a much stronger acid than Hpca in our case).[53] Moreover, the oxidation of cyclohexane with hydrogen peroxide in the presence of decamethylosmocene, $(Me_5C_5)_2Os$, and pyridine, also an exceptionally active system,[50] needs 24 h to exhibit higher TON values (up to *ca.* 5.1 × 10^4) although the TOF values are lower (up to *ca.* 2.1 × 10^3 h^{-1}) and the yields remain low (up to *ca.* 6%).

A high selectivity toward the formation of cyclohexanol and cyclohexanone is exhibited by our systems, since no traces of by-products were detected by GC analysis of the final reaction mixtures.

For oxidation in the presence of **2**, in general, cyclohexanol is the main product after treatment of the final reaction mixture with triphenylphosphine, and *ca.* 92% selectivity (Table 1, entry 34) can thus be reached toward alcohol formation, expected to occur mainly *via* cyclohexyl hydroperoxide (ROOH). However, the yield of cyclohexanone increases upon prolonged reaction times (Table 1, entry 52). For **1**, the trend is not so clear, but cyclohexanone is the main product in most of the performed experiments.

The presence of Hpca (pyrazinecarboxylic acid) is essential for these reactions, since without it only traces of products are formed (Table 1, entries 1 and 26, Fig. 9). The addition of Hpca (up to an Hpca : catalyst precursor molar ratio of 25 : 1 (**1**) or 50 : 1 (**2**)) leads to a remarkable yield growth for both alcohol and ketone (Fig. 9). A high promoting effect of that heteroaromatic acid on the peroxidative oxidation of alkanes catalyzed by homogeneous iron species[39b,54] on the oxyfunctionalization of cyclohexane with dioxygen catalyzed by scorpionate vanadium complexes,[55] as well as by pyrazole–rhenium complexes supported on modified silica gel,[38] has been previously recognized. The role of Hpca, *via* coordination of pca^- to iron, upon displacement of labile ligands in **1** or **2** (namely H_2O and dmf), conceivably consists in assisting proton-transfer from ligated H_2O_2 to an oxido- or a hydroxido-ligand, thus promoting the formation of hydroperoxyl ($HOO^{\cdot}$) and hydroxyl ($HO^{\cdot}$) radicals, as was proposed[46,54,56] for vanadium catalyst–Hpca–H_2O_2 systems and supported by theoretical calculations.[54c,57] However, an excessive amount of Hpca leads to a

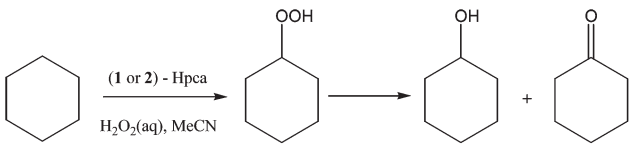

Scheme 1 Peroxidative oxidation of cyclohexane.

Table 1 Peroxidative oxidation of cyclohexane with H_2O_2 (selected data)[a]

Entry	Catalyst	n(Hpca)/n(precat.)	$n(H_2O_2)/n$(precat.) × 10^{-3}	Reaction time (h)	Yield[b] (%)			TON[c]
					OL	ONE	Total[d]	
1	**1**	—	20	0.75	0.1	0	0.1	1
2	**1**	5	20	0.75	3.7	0.1	3.8	380
3	**1**	15	20	0.75	3.9	6.6	10.5	1.05×10^3
4	**1**	25	20	0.75	9.7	12.4	22.1	2.21×10^3
5	**1**	35	20	0.75	5.1	7.8	12.9	1.29×10^3
6	**1**	50	20	0.75	2.8	6.6	9.4	940
7	**1**	100	20	0.75	1.9	6.5	8.4	840
8	**1**	150	20	0.75	0.9	5.2	6.1	610
9[e]	**1**	25	20	0.75	8.8	9.5	18.3	183
10[f]	**1**	25	20	0.75	5.3	5.9	11.2	112
11[g]	**1**	25	20	0.75	2.3	3.4	5.7	570
12	**1**	25	20	0.25	2.4	7.3	9.7	970
13	**1**	25	20	0.5	5.5	9.0	14.5	1.45×10^3
14	**1**	25	20	1	8.4	8.2	16.6	1.66×10^3
15	**1**	25	20	3	7.9	6.0	13.9	1.39×10^3
16	**1**	25	20	6	6.4	5.6	12.0	1.20×10^3
17	**1**	25	20	12	6.2	5.4	11.6	1.16×10^3
18	**1**	25	20	24	6.0	5.1	11.1	1.16×10^3
19	**1**	25	20	30	6.1	4.1	10.2	1.02×10^3
20	**1**	25	1	0.75	5.0	1.8	6.8	680
21	**1**	25	4	0.75	3.8	10.6	14.4	1.44×10^3
22	**1**	25	40	0.75	7.5	11.1	18.6	1.86×10^3
23[h]	**1**	25	20	0.75	1.7	0	1.7	170
24[i]	**1**	25	20	0.75	0.9	0.1	1.0	100
25[j]	**1**	25	20	0.75	6.5	10.0	16.5	1.65×10^3
26	**2**	—	40	6	0.4	0	0.4	81
27	**2**	5	40	6	3.7	0.9	4.6	80
28[k]	2	5	40	6	1.2	0	1.2	289
29	**2**	25	40	6	7.5	1.5	9.0	1.65×10^3
30	**2**	35	40	6	6.3	3.4	9.7	2.24×10^3
31[k]	**2**	35	40	6	0.2	0	0.2	42
32	**2**	50	40	6	12.4	4.7	17.1	3.42×10^3
33	**2**	100	40	6	11.4	4.0	15.4	2.73×10^3
34	**2**	150	40	6	14.7	1.2	15.9	1.59×10^3
35	**2**	5	20	6	4.2	1.0	5.2	520
36	**2**	25	20	6	9.7	3.5	13.2	1.32×10^3
37	**2**	35	20	6	10.3	7.2	17.5	1.75×10^3
38	**2**	100	20	6	12.2	5.9	18.0	1.80×10^3
39	**2**	150	20	6	12.7	4.8	17.5	1.75×10^3
40	**2**	50	1	6	2.6	1.1	3.7	36
41	**2**	50	2	6	5.7	3.7	9.4	90
42	**2**	50	20	6	13.4	6.0	19.8	1.98×10^3
43[l]	**2**	50	20	6	5.6	0.6	6.2	623
44[m]	**2**	50	20	6	2.5	1.2	3.7	335
45	**2**	50	4	0.25	2.2	2.0	4.2	81
46	**2**	50	4	0.5	3.9	2.6	6.5	129
47	**2**	50	4	0.75	3.6	3.4	7.0	137
48	**2**	50	4	1	5.3	4.7	10.0	193
49	**2**	50	4	3	8.0	6.3	14.3	255
50	**2**	50	4	6	11.3	8.5	19.8	380
51	**2**	50	4	10	10.4	9.0	19.4	376
52	**2**	50	4	24	6.8	7.5	14.3	276
53[h]	**2**	50	20	6	0.2	1.0	1.2	118
54[i]	**2**	50	20	6	0.9	0.1	1.0	102
55[j]	**2**	50	20	6	13.2	6.3	19.6	1.96×10^3

[a] Reaction conditions (unless stated otherwise): acetonitrile (3.0 mL), cyclohexane (5.0 mmol), r.t., under dinitrogen; (0.25–10) μmol of **1** or (0.25–10) μmol of **2**, (**1** or **2**) : Hpca (molar ratio 1 : 5 to 1 : 150), H_2O_2 (1000 : 1 to 40 000 : 1 molar ratio of oxidant to catalyst precursor). Percentage of yield, TON determined by GC analysis (upon treatment with PPh_3). [b] Molar yield (%) based on substrate, *i.e.* moles of products (cyclohexanol (Ol) and cyclohexanone (One)) per 100 mol of cyclohexane. [c] Turnover number (moles of product per mol of catalyst precursor). [d] Moles of cyclohexanol + cyclohexanone per 100 moles of cyclohexane. [e] 2nd run of catalyst resulting from **1** used in entry 4 (same reaction conditions). [f] 3rd run of catalyst resulting from **1** used in entry 4 (same reaction conditions). [g] 4th run of catalyst resulting from **1** used in entry 4 (same reaction conditions). [h] Reaction in the presence of $CBrCl_3$ (5 mmol). [i] Reaction in the presence of Ph_2NH (5 mmol). [j] Reaction performed in the presence of O_2. [k] Reaction in the presence of nitric acid instead of Hpca (same amount). [l] 2nd run of catalyst resulting from **2** used in entry 41 (same reaction conditions). [m] 3rd run of catalyst resulting from **2** used in entry 41 (same reaction conditions).

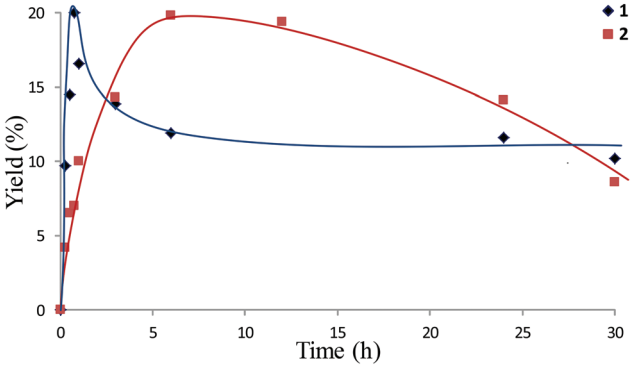

Fig. 8 Dependence of the overall yield (mol%, based on substrate) of the products on the reaction time. Reaction conditions: MeCN (3.0 mL), cyclohexane (5.0 mmol), 0.5 μmol of **1** or 2.5 μmol of **2**, $n(H_2O_2)/n$(catalyst precursor) (2×10^4), n(Hpca)/n(**1**) (25.0), n(Hpca)/n(**2**) (50.0), r.t.

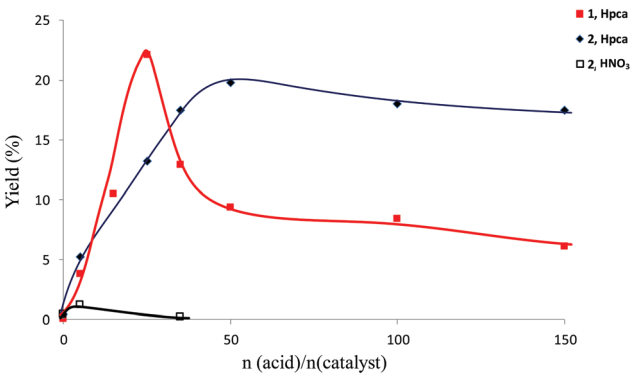

Fig. 9 Effects of the Hpca amount (molar ratios relative to **1** (■) or **2** (◆)) and of the HNO_3 amount (molar ratio relatively to **2** (□)) on the overall yield (mol%, based on substrate) of the products of cyclohexane oxidation. Reaction conditions: $n(H_2O_2)/n$(catalyst precursor) (2×10^4), 0.5 μmol of **1** or **2**, MeCN (3.0 mL), cyclohexane (5.0 mmol), n(Hpca)/n(**1** or **2**) (150–0), $n(HNO_3)/n$(**2**) (35–0), 45 min (**1**) or 6 h (**2**), r.t.

decrease in the overall yield of cyclohexanol and cyclohexanone (Fig. 9, Fig. S3 and S4†), conceivably due to the competition with H_2O_2 for the active metal center, eventually leading to inactive Fe(pca)$_2$ type species.[54d]

The activity of **2** is also promoted by addition of a mineral acid such as HNO_3 (Table 1, entries 28 and 31; Fig. 9), as recognized by us for other metal catalysts,[23d,25,31–34,36,39a,b,51,52,58,59] but to a much lower (almost insignificant) extent, even showing an inhibiting role for an $n(HNO_3)/n$(catalyst precursor) ratio of 35 (Fig. 9).

The effect of the peroxide-to-catalyst precursor molar ratio was investigated and is depicted in Fig. 10 (Fig. S5 and S6†). The increase of the peroxide amount up to an $n(H_2O_2)/n$(catalyst precursor) molar ratio of 2×10^4 leads to the maximum product yield of 22% (**1**) or 20% (**2**). Further increase of the $n(H_2O_2)/n$(catalyst precursor) molar ratio results in a slight yield drop, eventually due to overoxidation reactions at higher H_2O_2 amounts. In fact, some products of overoxidation such as 1,4-cyclohexanedione and 1,2-epoxycyclohexane were detected by

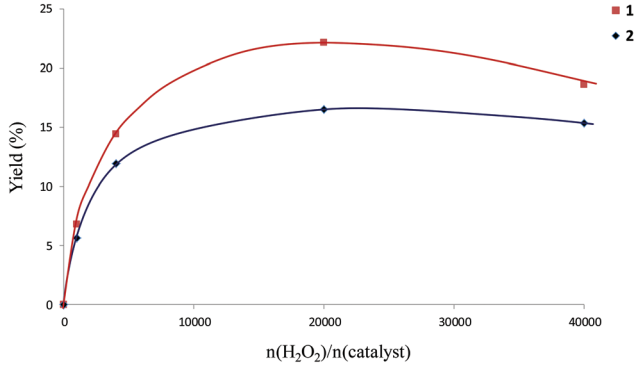

Fig. 10 Dependence of the overall yield (mol%, based on substrate) of the products on the amount of oxidant (H_2O_2, molar ratio relative to **1** (■) or **2** (◆)) in the oxidation of cyclohexane. Reaction conditions: $n(H_2O_2)/n$(catalyst precursor) ($0–4 \times 10^4$), MeCN (3.0 mL), cyclohexane (5.0 mmol), 0.25–10 μmol of **1** or **2**, n(Hpca)/n(**1**) (25.0), n(Hpca)/n(**2**) (50.0), 45 min (**1**) or 6 h (**2**), r.t.

GC-MS for the conditions of entries 4 and 42, for **1** and **2**, in Table 1.

The oxidation of cyclohexane proceeds even if a very small relative amount of **1** (or **2**) is used leading to rather high TONs (Table 1, *e.g.*, entry 32 for **2**). The effect of the catalyst precursor amount on the overall yield is illustrated in Fig. 11, the latter increasing with the former up to *ca.* 22% (**1**) or 20% (**2**) for an n(catalyst precursor)/n(cyclohexane) molar ratio of *ca.* 1×10^{-4} and 3×10^{-4}, respectively. Higher catalyst amounts result in a yield drop, possibly due to overoxidation (Fig. S7 and S8†).

Under the same reaction conditions, $FeSO_4 \cdot 7H_2O$, $Fe(CF_3SO_3)_3$ and $[Fe_3OL_6(H_2O)_3]NO_3 \cdot HL$ (HL = 3,4,5-trimethoxybenzoic acid) demonstrated markedly lower catalytic activity in terms either of yields of products or TOFs (see Fig. S9†).

Experiments in the presence of O_2 were also performed (Table 1, entries 25 and 55). For **1**, the obtained overall yield and TON values for 0.75 h in air (Table 1, entry 25) are quite similar to the ones obtained for 1 h under dinitrogen (Table 1, entry 14), suggesting only a slightly promoting effect of the air

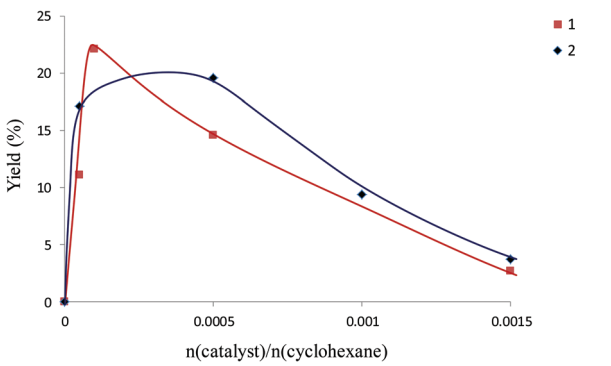

Fig. 11 Dependence of the overall yield (mol%, based on substrate) of the products on the amount of catalysts **1** (■) or **2** (◆) in the oxidation of cyclohexane. Reaction conditions: $n(H_2O_2)/n$(catalyst precursor) (2×10^4), MeCN (3.0 mL), cyclohexane (5.0 mmol), 0.25–10 μmol of **1** or **2**, n(Hpca)/n(**1**) (25.0), n(Hpca)/n(**2**) (50.0), 45 min (**1**) or 6 h (**2**), r.t.

atmosphere. In accord with more oxidant availability, the ratio cyclohexanone–cyclohexanol increased. For **2**, the obtained results (Table 1, entry 55) are also not significantly different from the ones performed under dinitrogen. Moreover, experiments using O_2 as the sole oxidant were performed for both catalyst precursors **1** and **2**, but no oxidation product could be detected. This is consistent with the proposed mechanism (see below) which requires the presence of H_2O_2 as the source of the hydroxyl radical.

On completion of each stage, the products were analyzed and the assumed catalyst (which precipitates upon addition of ether) was isolated by filtration. The subsequent cycles were initiated upon addition of new standard portions of all the other reagents; in a second, third and fourth run, the observed activity was 83%, 61% and 51% (for catalyst resulting from **1**, Table 1, entries 9, 10 and 11, respectively) or 32% and 17% (for catalyst resulting from **2**, Table 1, entries 43 and 44, respectively) of the initial one, with maintenance of the selectivity. This recycling possibility was not reported[34,39a,b,52,53] for other catalytic iron systems for the peroxidative oxidation of cyclohexane.

In order to examine the general type of mechanism involved in the studied oxidation, we also performed it in the presence of radical traps. The peroxidative oxidation of cyclohexane is believed to proceed mainly *via* a radical mechanism which involves both carbon- and oxygen-centered radicals, in view of the inhibition effect observed when it is carried out in the presence of either a carbon-radical trap such as $CBrCl_3$ (Table 1, entry 23 (**1**) or entry 53 (**2**)) or an oxygen-radical trap such as Ph_2NH[60] (Table 1, entry 24 (**1**) or entry 54 (**2**)). In the experiments performed in the presence of $CBrCl_3$, the formation of CyBr was detected (13.4 and 14.2% relative to CyH, respectively for **1** and **2**) by GC analysis.

Metal-catalyzed (and Hpca-assisted) decomposition of H_2O_2 can lead to the oxygen-centered radicals $HOO^{\bullet}$ and $HO^{\bullet}$, upon oxidation of H_2O_2 by Fe^{III} and reduction by Fe^{II}, respectively, as suggested for some Fe[39a,b,52–54,61] and V[30,34,46,52,56,62] catalysts. Water is believed to promote H^+-shift steps toward the formation of $HO^{\bullet}$ from H_2O_2.[56a,63] The cyclohexyl radical $Cy^{\bullet}$ is then formed upon H-abstraction from cyclohexane CyH by $HO^{\bullet}$ (Scheme 2, reaction 1). Reaction of $Cy^{\bullet}$ with dioxygen leads to $CyOO^{\bullet}$, and CyOOH can then be formed upon H-abstraction from H_2O_2 by $CyOO^{\bullet}$ (Scheme 2, reactions 2 and 3) or upon reduction of the latter to $CyOO^-$ by Fe^{II} followed by protonation. Metal-assisted decomposition of CyOOH to $CyO^{\bullet}$ and $CyOO^{\bullet}$ (reactions 4 and 5) would then afford the cyclohexanol (CyOH) and cyclohexanone ($Cy_{-H}{=}O$) products (reactions 6 and 7).[64] For the metal (iron) assisted steps, a change of the metal oxidation state (+2/+3) often occurs[13d,16g,65] and the iron centers of our catalyst precursors appear to be particularly favorable.

$$HO^{\bullet} + CyH \longrightarrow H_2O + Cy^{\bullet} \quad (1)$$

$$Cy^{\bullet} + O_2 \longrightarrow CyOO^{\bullet} \quad (2)$$

$$CyOO^{\bullet} + H_2O_2 \longrightarrow CyOOH + HOO^{\bullet} \quad (3)$$

$$CyOOH + [Fe^{II}] \longrightarrow CyO^{\bullet} + [Fe^{III}] + HO^- \quad (4)$$

$$CyOOH + [Fe^{III}] \longrightarrow CyOO^{\bullet} + [Fe^{II}] \quad (5)$$

$$CyO^{\bullet} + CyH \longrightarrow CyOH + Cy^{\bullet} \quad (6)$$

$$2CyOO^{\bullet} \longrightarrow CyOH + Cy_{-H}{=}O + O_2 \quad (7)$$

Scheme 2 Mechanistic consideration of catalytic oxidation of cyclohexane.

Peroxidative oxidation of *n*-heptane

Compound **2** is also active for the peroxidative oxidation of linear alkanes, such as *n*-heptane, to the corresponding alcohols and ketones. In fact, after 3 h stirring at 50 °C, *n*-heptane, in the presence of **2**, H_2O_2 (50% aqueous solution)–MeCN and Hpca (1 : 50), yields heptanol and heptanone, with a selectivity of 1 : 9 : 10 : 10 for C(1) : C(2) : C(3) : C(4) (relative normalized reactivities of H atoms at carbon atoms C(1), C(2), C(3) and C(4)). These selectivity parameters are comparable to those achieved by using the systems $[Cu(H_3L^1)(NCS)]$/*t*-BuOOH (H_4L^1 = *N*,*N*,*N*′,*N*′-tetrakis(2-hydroxyethyl)ethylenediamine) (1 : 10 : 8 : 11),[66] $FeSO_4$–H_2O_2 (1 : 5 : 5 : 4.5)[54b] or $[Fe_2(HPTB)(\mu\text{-}OH)(NO_3)_2](NO_3)_2$–Hpca–$H_2O_2$ [HPTB = *N*,*N*,*N*′,*N*′-tetrakis(2-benzimidazolylmethyl)-2-hydroxo-1,3-diaminopropane] (1 : 6 : 6 : 5),[54a] which are believed to operate *via* the $HO^{\bullet}$ radical.

Hydrocarboxylation and carboxylation of alkanes to carboxylic acids

Following the recent system for the mild hydrocarboxylation of C_n alkanes into C_{n+1} carboxylic acids developed by some of us,[47–49,67] we tested the catalytic behavior of **1** using C_2, C_5 linear and C_5, C_6 cyclic alkanes by reacting the alkane (substrate) with carbon monoxide, water and potassium peroxodisulfate, at 60 °C, for 4 h and in a neutral H_2O–MeCN medium. In contrast to most of the known methods for the synthesis of carboxylic acids,[68] including the carboxylation of alkanes with TFA,[69,70] the carboxylation of alkanes with CO and H_2O proceeds even in the absence of metal-catalyst (metal-free).[47] However, the presence of both H_2O and MeCN is crucial since the carboxylation does not proceed in either only water or only acetonitrile, or in the absence of both.

Under typical conditions, the hydrocarboxylations in the presence of complex **2** show maximum overall yields (based on alkane) of the corresponding carboxylic acid of *ca.* 7.6, 8.2, 16.4 or 9.5% for the conversion of cyclopentane, cyclohexane, *n*-pentane or ethane, respectively. However, in these studies, **2** did not exhibit a promoting effect, since metal-free transformations yield[47] 8.2, 12.3, 17.6 or 9.9% for the conversions of the corresponding alkanes.

Compound **2** also shows low catalytic activity (TON = 5, yield = 3.2%), although with high selectivity, for the oxidation of ethane to acetic acid (only product), in a single-pot process, under mild conditions, in the presence of potassium peroxodisulfate and trifluoroacetic acid (TFA).

Stoichiometric oxidation reactions of *cis*-stilbene and adamantane with peroxido complexes $[Fe_6(O_2)(O)_2(O_2CCMe_3)_{12}(HO_2CCMe_3)_2]$ and $[Fe_6(O_2)(O)_2(O_2CCMe_3)_{12}(py)_2]\cdot 0.5Me_2CO$ in benzene or py/HO_2CCMe_3 have been studied.[4c] The reactions performed at 70 and 66 °C, respectively, produced benzaldehyde, *trans*-stilbene oxide, and oxoproducts of adamantane, namely 1-ol and 2-one, as well as 2-(1-Ad)py and 2-(2-Ad)py in low yields. In the case of adamantane, the *tert*/*sec* selectivity achieved (~8) was different from that resulting from catalytic Gif-type oxygenation of adamantane by $[Fe_3O(O_2CCMe_3)_6(py)_3]/O_2$/Zn or H_2O_2 (~3–5), suggesting that the peroxido species do not directly participate as active oxidants in those catalytic reactions.

UV-vis and Mössbauer spectroscopy kinetic studies involving complex 2

Although the structure of the catalyst remains elusive, optical and Mössbauer spectra provide compelling evidence for the transformation of **2** into a new Fe(III) high spin compound with a more symmetric ligand environment of Mössbauer ions.

Kinetic studies of the systems **2**–H_2O_2 (1 : 2000) at 0, 15, 30, and 45 °C, **2**–Hpca (1 : 50) at 45 °C, and **2**–Hpca–H_2O_2 (1 : 50 : 40 000) at 15 °C by UV-vis spectroscopy indicate the formation of new species. The solution of **2** in MeCN–dmf was stable over at least 3 h (Fig. S10†). Dimethylformamide was added to prevent dissociation of coordinated dmf to iron in **2**.

The solution of **2** in MeCN–dmf (10 : 1) was used as a blank, and changes in the spectral bands with minima at about 394 nm and maxima at nearly 490 nm (Fig. 12), immediately after addition of 30% H_2O_2 aqueous solution, indicate that **2** reacts with H_2O_2, presumably with formation of peroxido species. The rate constant of this reaction was examined by an Arrhenius plot (Fig. S11†), which gave an activation energy value of E_A = 76.17 kJ mol^{-1} and a frequency factor $A = 2.03 \times 10^{11}$ s^{-1}. These parameters can be compared with those calculated for the reaction of $[Fe_6O_3(OH)(p\text{-}NO_2C_6H_4COO)_{11}(dmf)_4]$ with H_2O_2 (E_A = 48 kJ mol^{-1}, $A = 1.9 \times 10^7$ s^{-1}).[4a]

Similarly, it has been shown that **2** reacts also with Hpca. A new band with a maximum between 400 and 500 nm developing in time immediately after addition of a solution of Hpca to the solution of **2** in MeCN–dmf is seen in Fig. 13.

The changes in the UV-vis spectra of the solution of **2** in MeCN–dmf 10 : 1 used as a blank after simultaneous addition of H_2O_2 and Hpca in the first 15 s also indicate formation of new species (minimum between 350 and 400 nm in Fig. 14). After 1 h, precipitation of an orange product was observed.

To establish the role of **2** in catalytic oxidation reactions, **2**–^{57}Fe was synthesized and the mixture of **2**–^{57}Fe, Hpca and H_2O_2 in molar ratio 1 : 50 : 40 000 in MeCN was monitored by Mössbauer spectroscopy. The Mössbauer spectrum of the solution prepared and frozen immediately showed one quadrupole doublet with an isomer shift δ = 0.49 mm s^{-1} and a splitting ΔE_Q = 0.62 mm s^{-1} (Fig. S12†). Comparison of these parameters with those of **2**–^{57}Fe (δ = 0.57 mm s^{-1} and ΔE_Q = 0.88 mm s^{-1}) indicates that the initial complex reacts very quickly with H_2O_2 and/or Hpca in agreement with UV-vis

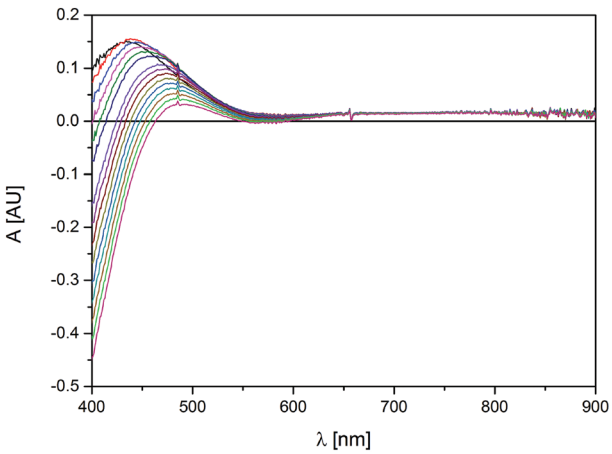

Fig. 13 UV-vis spectra of the **2**–Hpca system ($c_2 = 1.25 \times 10^{-4}$ M; **2** : Hpca = 1 : 50; T = 45 °C; t = 1–70 s; in MeCN–dmf = 10 : 1).

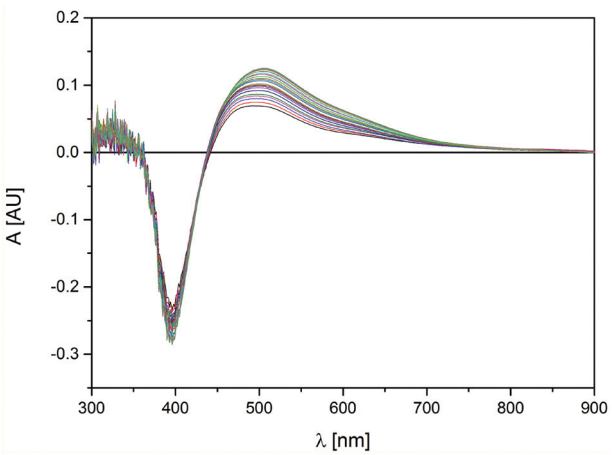

Fig. 12 UV-vis spectra of the **2**–H_2O_2 system ($c_2 = 1.25 \times 10^{-4}$ M; **2** : H_2O_2 = 1 : 2000; T = 45 °C, t = 0.5–25.5 s; in MeCN–dmf = 10 : 1).

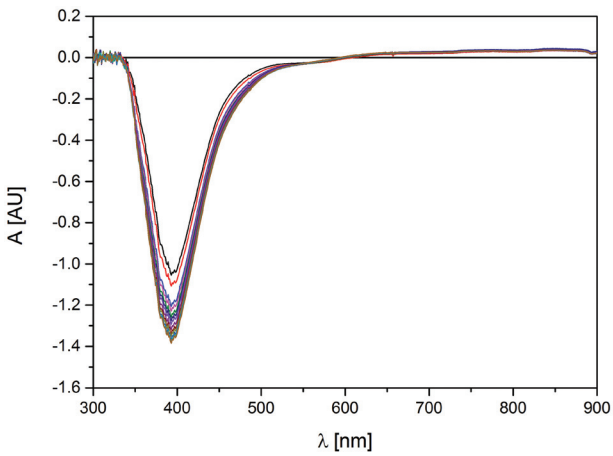

Fig. 14 UV-vis spectra of the **2**–H_2O_2–Hpca system ($c_2 = 1.25 \times 10^{-4}$ M; **2** : H_2O_2 : Hpca = 1 : 40 000 : 50; T = 15 °C, t = 1–15 s; in MeCN–dmf = 10 : 1).

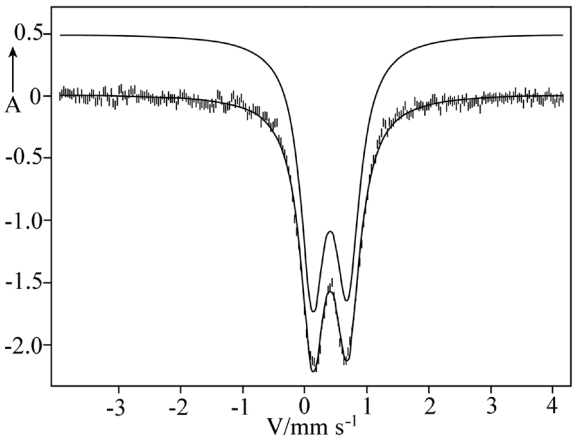

Fig. 15 Mössbauer spectrum of the **2**–$^{57}Fe/H_2O_2$/Hpca system at 80 K after 1 h.

measurements, leading to a more symmetrical ligand environment of the Mössbauer ions. The asymmetry of the doublet obtained for the mixture frozen after 30 min (Fig. S13†) indicates continuous transformation of the initial complex. The iron ions remain in the same high spin state, but the spectrum is approximated by one doublet with a low value of quadrupole splitting at 0.42 mm s^{-1} and another nearly 3 times larger, ΔE_Q = 1.10 mm s^{-1}. The solution which was stirred at room temperature for 1 h and then frozen gave a Mössbauer spectrum as one doublet with isomer shift δ = 0.45 mm s^{-1} and ΔE_Q = 0.52 mm s^{-1}. These parameters are comparable with those of the Mössbauer spectrum of the solid finally isolated from the solution after 1 h reaction time shown in Fig. 15 with δ = 0.40 mm s^{-1} and ΔE_Q = 0.56 mm s^{-1}.

The Mössbauer spectrum at 4.2 K also represents a doublet (Fig. 16). Even at this very low temperature the rapid motion of the iron electronic moments causes the quenching of the magnetic hyperfine structures. The observed values for δ and ΔE_Q (see the caption of Fig. 16) are in good agreement with those obtained at higher temperatures. The line width is relatively large, which is due to the lowering of fast electronic relaxation processes. At 2.7 K the spectrum is dominated by intermediate relaxation processes. It is significantly broadened, with wings that extend from about −6 to +6 mm s^{-1}. The spectra at 2.7 K and applied magnetic fields of 3 and 5 T represent broad sextets with very large line widths. This feature looks typical of a broad distribution of hyperfine fields and indicates the presence of a distribution of spin–spin relaxation frequencies, which is caused by superposition of spectra arising from chemically nonequivalent iron sites.

Although attempts to perform the same reaction at larger scale to further characterize the emerging catalyst failed, the Mössbauer data clearly indicate that **2** underwent transformations in the studied oxidation reactions. Moreover, the compound resulting from **2** is different from **1**, which was initially regarded by us as a possible reaction product of **2** with H_2O_2 under the conditions explored in catalytic oxidation reactions.

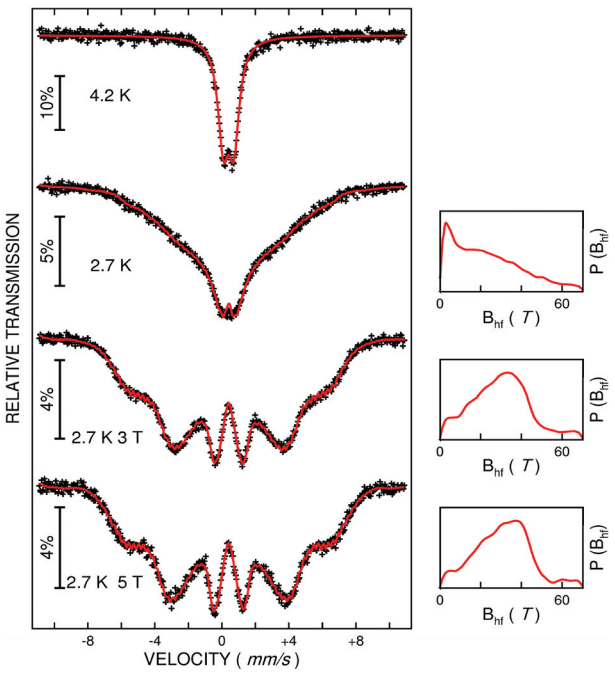

Fig. 16 Zero-field and magnetic field Mössbauer spectra of the solid isolated from the **2**–$^{57}Fe/H_2O_2$/Hpca system after 1 h reaction time at 4.2 and 2.7 K. The probability distribution of the magnetic hyperfine field is shown on the right side (δ = 0.48 mm s^{-1} and ΔE_Q = 0.58 mm s^{-1}).

Conclusions

The family of hexanuclear iron complexes containing a central peroxido group bridging four ferric ions in an almost planar μ_4–η^2:η^2 fashion and that of undecanuclear iron(III) carboxylates have been further extended by preparation of $[Fe_6(O)_2(O_2)L_{10}(OAc)_2(H_2O)_2]$ with two different carboxylate ligands, 3,4,5-trimethoxybenzoate and acetate (the latter is presumably formed *in situ* by oxidation of methyl ethyl ketone used as a solvent), and $[Fe_{11}Cl(\mu_4\text{-}O)_3(\mu_3\text{-}O)_5L_{16}(solvent)_3]$ with an unprecedented topology of the $[Fe^{III}{}_{11}ClO_8]^{16+}$ core consisting of nine six-coordinate and two five-coordinate ferric ions. The present study shows that **1** and **2** can act as efficient catalyst precursors for the partial oxygenation of alkanes to alkyl peroxides, alcohols and ketones. Remarkable TONs and TOFs (the latter mainly for **1**) with concomitant quite good yields have been achieved under mild conditions, for the peroxidative oxidation of cyclohexane, in the presence of pyrazinecarboxylic acid as a promoter. Moreover, **1** exhibits remarkably high activity in an exceptionally short reaction time (45 min), being unprecedented for any metal catalyzed alkane oxidations by H_2O_2. The low catalytic activity of systems containing simple iron(III) salts, μ_3-oxido iron(III) carboxylates, as well as inactivity of the $Fe(pca)_2$ complex indicate that most probably the species acting as real catalysts are iron(III) carboxylates with higher nuclearity. Mössbauer spectroscopy and UV-vis data provide evidence that original complex **2** reacts with pyrazinecarboxylic acid–H_2O_2 with formation of a new high spin iron(III) species with a more symmetric ligand environment of

Mössbauer ions. We hypothesize that replacement of monodentate (H_2O, dmf) ligands or even in part 3,4,5-trimethoxybenzoate may take place. Formation of peroxido species in this case cannot be ruled out as well.

Acknowledgements

This work was supported by the Austrian Science Fund (Project P19629-N19), the Fundação para a Ciência e a Tecnologia (FCT), Portugal, and projects PTDC/QUI-QUI/102150/2008, PTDC/EQU-EQU/122025/2010 and PEst-OE/QUI/UI0100/2011 and by the European Regional Development Fund, Sectoral Operational Programme 'Increase of Economic Competitiveness', Priority Axis 2 (SOP IEC-A2-O2.1.2-2009-2, ID 570, COD SMIS-CSNR: 12473, Contract 129/2010-POLISILMET). We thank Alexander Roller for collection of the X-ray data.

References

1 (*a*) W. H. Armstrong and S. J. Lippard, *Inorg. Chem.*, 1985, **24**, 981–982; (*b*) D. M. Kurtz, *Chem. Rev.*, 1990, **90**, 585–606; (*c*) T. Ookubo, H. Sugimoto, T. Nagayama, H. Masuda, T. Sato, K. Tanaka, Y. Maeda, H. Okawa, Y. Hayashi, A. Uehara and M. Suzuki, *J. Am. Chem. Soc.*, 1996, **118**, 701–702.

2 (*a*) A. K. Boudalis, Y. Sanakis, C. P. Raptopoulou, A. Terzis, J.-P. Tuchagues and S. P. Perlepes, *Polyhedron*, 2005, **24**, 1540–1548; (*b*) C. E. Anson, J. P. Bourke, R. D. Cannon, U. A. Jayasooriya, M. Molinier and A. K. Powell, *Inorg. Chem.*, 1997, **36**, 1265–1267.

3 (*a*) W. H. Armstrong, M. E. Roth and S. J. Lippard, *J. Am. Chem. Soc.*, 1987, **109**, 6318–6326; (*b*) T. C. Stamatatos, A. K. Boudalis, Y. Sanakis and C. P. Raptopoulou, *Inorg. Chem.*, 2006, **45**, 7372–7381; (*c*) J.-L. Tian, W. Gu, S.-P. Yan, D.-Z. Liao and Z.-H. Jiang, *Z. Anorg. Allg. Chem.*, 2007, **633**, 478–481; (*d*) A. Horn, A. Neves, A. J. Bortoluzzi, V. Drago and W. A. Ortiz, *Inorg. Chem. Commun.*, 2001, **4**, 173–176.

4 (*a*) G. Trettenhahn, M. Nagl, N. Neuwirth, V. B. Arion, W. Jary, P. Poechlauer and W. Schmid, *Angew. Chem., Int. Ed.*, 2006, **45**, 2794–2798; (*b*) I. Shweky, L. E. Pence, G. C. Papaefthymiou, R. Sessoli, J. W. Yun, A. Bino and S. J. Lippard, *J. Am. Chem. Soc.*, 1997, **119**, 1037–1042; (*c*) R. Celenligil-Cetin, R. J. Staples and P. Stavropoulos, *Inorg. Chem.*, 2000, **39**, 5838–5846; (*d*) E. J. Seddon, J. C. Huffman and G. Christou, *Dalton*, 2000, 4446–4452; (*e*) S. M. Gorun and S. J. Lippard, *Nature*, 1986, **319**, 666–668; (*f*) L. F. Jones, E. K. Brechin, D. Collison, M. Helliwell, T. Mallah, S. Piligkos, G. Rajaraman and W. Wernsdorfer, *Inorg. Chem.*, 2003, **42**, 6601–6603; (*g*) C. Canada-Vilalta, T. A. O'Brien, M. Pink, E. R. Davidson and G. Christou, *Inorg. Chem.*, 2003, **42**, 7819–7829.

5 (*a*) I. A. Gass, C. J. Milios, A. G. Whittaker, F. P. A. Fabiani, S. Parsons, M. Murrie, S. P. Perlepes and E. K. Brechin, *Inorg. Chem.*, 2006, **45**, 5281–5283; (*b*) J.-P. Tong, F. Shao, J. Tao, R.-B. Huang and L.-S. Zheng, *Inorg. Chem.*, 2011, **50**, 2067–2069; (*c*) P. Baran, R. Boca, I. Chakraborty, J. Giapintzakis, R. Herchel, Q. Huang, J. E. McGrady, R. G. Raptis, Y. Sanakis and A. Simopoulos, *Inorg. Chem.*, 2008, **47**, 645–655; (*d*) H. Li, Z. J. Zhong, W. Chen and X.-Z. You, *J. Chem. Soc., Dalton Trans.*, 1997, 463–464.

6 W. Micklitz, S. G. Bott, J. G. Bentsen and S. J. Lippard, *J. Am. Chem. Soc.*, 1989, **111**, 372–374.

7 E. I. Tolis, M. Helliwell, S. Langley, J. Raftery and R. E. P. Winpenny, *Angew. Chem., Int. Ed.*, 2003, **42**, 3804–3808.

8 S. Khanra, S. Konar, A. Clearfield, M. Helliwell, E. J. L. McInnes, E. Tolis, F. Tuna and R. E. P. Winpenny, *Inorg. Chem.*, 2009, **48**, 5338–5349.

9 A. M. Ako, V. Mereacre, Y. Lan, W. Wernsdorfer, R. Clerac, C. E. Anson and A. K. Powell, *Inorg. Chem.*, 2010, **49**, 1–3.

10 C. Boskovic, H. U. Guedel, G. Labat, A. Neels, W. Wernsdorfer, B. Moubaraki and K. S. Murray, *Inorg. Chem.*, 2005, **44**, 3181–3189.

11 E. C. Sanudo, M. Font-Bardia, X. Solans and R. H. Laye, *New J. Chem.*, 2011, **35**, 842–848.

12 P. C. A. Bruijnincx, K. G. van Koten and R. J. M. K. Gebbink, *Chem. Soc. Rev.*, 2008, **37**, 2716–2744.

13 (*a*) M. Sono, M. P. Roach, E. D. Coulter and J. H. Dawson, *Chem. Rev.*, 1996, **96**, 2841–2887; (*b*) B. J. Wallar and J. D. Lipscomb, *Chem. Rev.*, 1996, **96**, 2625–2657; (*c*) E. I. Solomon, T. C. Brunold, M. I. Davis, J. N. Kemsley, S.-K. Lee, N. Lehnert, F. Neese, A. J. Skulan, Y.-S. Yang and J. Zhou, *Chem. Rev.*, 2000, **100**, 235–349; (*d*) M. Costas, M. P. Mehn, M. P. Jensen and L. Que, *Chem. Rev.*, 2004, **104**, 939–986.

14 M. C. Esmelindro, E. G. Oestreicher, H. Marquez-Alvarez, C. Dariva, S. M. S. Egues, C. Fernandes, A. J. Bortoluzzi, V. Drago and O. A. C. Antunes, *J. Inorg. Biochem.*, 2005, **99**, 2054–2061.

15 A. E. Shilov and G. B. Shul'pin, *Chem. Rev.*, 1997, **97**, 2879–2932.

16 (*a*) Y. He and C. R. Goldsmith, *Chem. Commun.*, 2012, **48**, 10532–10534; (*b*) K. Chen and L. Que, *J. Am. Chem. Soc.*, 2001, **123**, 6327–6337; (*c*) R. A. Leising, B. A. Brennan, L. Que, B. G. Fox and E. Münck, *J. Am. Chem. Soc.*, 1991, **113**, 3988–3990; (*d*) T. Okuno, S. Ito, S. Ohba and Y. Nishida, *J. Chem. Soc., Dalton Trans.*, 1997, 3547–3551; (*e*) Y. Mekmouche, C. Duboc-Toia, S. Menage, C. Lambeaux and M. Fontecave, *J. Mol. Catal. A: Chem.*, 2000, **156**, 85–89; (*f*) X. Wang, S. Wang, L. Li, E. B. Sundberg and G. P. Gacho, *Inorg. Chem.*, 2003, **42**, 7799–7808; (*g*) J. England, G. J. P. Britovsek, N. Rabadia and A. J. P. White, *Inorg. Chem.*, 2007, **46**, 3752–3767; (*h*) J. England, C. R. Davies, M. Banaru, A. J. P. White and G. J. P. Britovsek, *Adv. Synth. Catal.*, 2008, **350**, 883–897.

17 D. A. Whittington and S. J. Lippard, *J. Am. Chem. Soc.*, 2001, **123**, 827–838.

18 M. H. Sazinsky, J. Bard, D. Di and S. J. Lippard, *J. Biol. Chem.*, 2004, **279**, 30600–30610.

19 Y. Lindqvist, W. Huang, G. Schneider and J. Shanklin, *EMBO J.*, 1996, **15**, 4081–4092.

20 H. Eklund, U. Uhlin, M. Farnegardh, D. T. Logan and P. Nordlund, *Prog. Biophys. Mol. Biol.*, 2001, **77**, 177–268.
21 (*a*) P.-G. Lassahn, V. Lozan, G. A. Timco, P. Christian, C. Janiak and R. E. P. Winpenny, *J. Catal.*, 2004, **222**, 260–267; (*b*) B. Singh, J. R. Long, F. F. de Biani, D. Gatteschi and P. Stavropoulos, *J. Am. Chem. Soc.*, 1997, **119**, 7030–7047.
22 (*a*) P. J. Figiel, M. N. Kopylovich, J. Lasri, M. F. C. Guedes da Silva, J. J. R. Frausto da Silva and A. J. L. Pombeiro, *Chem. Commun.*, 2010, **46**, 2766–2768; (*b*) P. J. Figiel, A. Sibaouih, J. U. Ahmad, M. Nieger, M. T. Raeisaenen, M. Leskelae and T. Repo, *Adv. Synth. Catal.*, 2009, **351**, 2625–2632; (*c*) P. J. Figiel, M. Leskela and T. Repo, *Adv. Synth. Catal.*, 2007, **349**, 1173–1179.
23 (*a*) K. T. Mahmudov, M. N. Kopylovich, M. F. C. Guedes da Silva, P. J. Figiel, Y. Y. Karabach and A. J. L. Pombeiro, *J. Mol. Catal. A: Chem.*, 2010, **318**, 44–50; (*b*) M. N. Kopylovich, K. T. Mahmudov, M. Haukka, P. J. Figiel, A. Mizar, J. A. L. da Silva and A. J. L. Pombeiro, *Eur. J. Inorg. Chem.*, 2011, 4175–4181; (*c*) A. M. Kirillov, M. N. Kopylovich, M. V. Kirillova, M. Haukka, M. F. C. Guedes da Silva and A. J. L. Pombeiro, *Angew. Chem., Int. Ed.*, 2005, **44**, 4345–4349; (*d*) M. N. Kopylovich, A. C. C. Nunes, K. T. Mahmudov, M. Haukka, T. C. O. MacLeod, L. M. D. R. S. Martins, M. L. Kuznetsov and A. J. L. Pombeiro, *Dalton Trans.*, 2011, **40**, 2822–2836.
24 A. M. Kirillov, M. N. Kopylovich, M. V. Kirillova, E. Y. Karabach, M. Haukka, M. F. C. Guedes da Silva and A. J. L. Pombeiro, *Adv. Synth. Catal.*, 2006, **348**, 159–174.
25 R. R. Fernandes, J. Lasri, M. F. C. Guedes da Silva, J. A. L. da Silva, J. J. R. Frausto da Silva and A. J. L. Pombeiro, *J. Mol. Catal. A: Chem.*, 2011, **351**, 100–111.
26 C. Di Nicola, Y. Y. Karabach, A. M. Kirillov, M. Monari, L. Pandolfo, C. Pettinari and A. J. L. Pombeiro, *Inorg. Chem.*, 2007, **46**, 221–230.
27 Y. Y. Karabach, A. M. Kirillov, M. Haukka, M. N. Kopylovich and A. J. L. Pombeiro, *J. Inorg. Biochem.*, 2008, **102**, 1190–1194.
28 M. V. Kirillova, A. M. Kirillov, M. F. C. Guedes da Silva and A. J. L. Pombeiro, *Eur. J. Inorg. Chem.*, 2008, 3423–3427.
29 K. R. Gruenwald, A. M. Kirillov, M. Haukka, J. Sanchiz and A. J. L. Pombeiro, *Dalton Trans.*, 2009, 2109–2120.
30 L. S. Shul'pina, M. V. Kirillova, A. J. L. Pombeiro and G. B. Shul'pin, *Tetrahedron*, 2009, **65**, 2424–2429.
31 S. Contaldi, C. Di Nicola, F. Garau, Y. Y. Karabach, L. M. D. R. S. Martins, M. Monari, L. Pandolfo, C. Pettinari and A. J. L. Pombeiro, *Dalton Trans.*, 2009, 4928–4941.
32 C. Di Nicola, F. Garau, Y. Y. Karabach, L. M. D. R. S. Martins, M. Monari, L. Pandolfo, C. Pettinari and A. J. L. Pombeiro, *Eur. J. Inorg. Chem.*, 2009, 666–676.
33 D. S. Nesterov, V. N. Kokozay, V. V. Dyakonenko, O. V. Shishkin, J. Jezierska, A. Ozarowski, A. M. Kirillov, M. N. Kopylovich and A. J. L. Pombeiro, *Chem. Commun.*, 2006, 4605–4607.
34 (*a*) T. F. S. Silva, E. C. B. A. Alegria, L. M. D. R. S. Martins and A. J. L. Pombeiro, *Adv. Synth. Catal.*, 2008, **350**, 706–716; (*b*) T. F. S. Silva, M. F. C. Guedes da Silva, G. S. Mishra, L. M. D. R. S. Martins and A. J. L. Pombeiro, *J. Organomet. Chem.*, 2011, **696**, 1310–1318.
35 G. S. Mishra, J. J. R. Frausto da Silva and A. J. L. Pombeiro, *J. Mol. Catal. A: Chem.*, 2007, **265**, 59–69.
36 E. C. B. Alegria, M. V. Kirillova, L. M. D. R. S. Martins and A. J. L. Pombeiro, *Appl. Catal., A*, 2007, **317**, 43–52.
37 (*a*) A. M. Kirillov, M. Haukka, M. F. C. Guedes da Silva and A. J. L. Pombeiro, *Eur. J. Inorg. Chem.*, 2005, 2071–2080; (*b*) G. B. Shul'pin, M. V. Kirillova, T. Sooknoi and A. J. L. Pombeiro, *Catal. Lett.*, 2008, **123**, 135–141.
38 G. S. Mishra, E. C. B. Alegria, L. M. D. R. S. Martins, J. J. R. Frausto da Silva and A. J. L. Pombeiro, *J. Mol. Catal. A: Chem.*, 2008, **285**, 92–100.
39 (*a*) M. N. Kopylovich, A. M. Kirillov, A. K. Baev and A. J. L. Pombeiro, *J. Mol. Catal. A: Chem.*, 2003, **206**, 163–178; (*b*) R. R. Fernandes, M. V. Kirillova, J. A. L. da Silva, J. J. R. Frausto da Silva and A. J. L. Pombeiro, *Appl. Catal., A*, 2009, **353**, 107–112.
40 N. V. Gerbeleu, S. S. Palanciuc, Yu. A. Simonov, A. A. Dvorkin, P. N. Bourosh, M. T. Reetz, V. B. Arion and K. Toellner, *Polyhedron*, 1995, **14**, 521–527.
41 H. Ulrich, *Raw Materials for Industrial Polymers*, Hanser Publ., 1988.
42 P. Pascal, *Ann. Chim. Phys.*, 1910, **19**, 5–70.
43 *SAINT-Plus, version 7.06a, and APEX2*, Bruker-Nonus AXS Inc., Madison, WI, 2004.
44 G. M. Sheldrick, *Acta Crystallogr., Sect. A: Found. Crystallogr.*, 2008, **A64**, 112–122.
45 M. N. Burnett and J. K. Johnson, ORTEPIII, Report ORNL-5138, Oak Ridge National Laboratory, Oak Ridge, TN, 1996.
46 (*a*) G. B. Shul'pin, *J. Mol. Catal. A: Chem.*, 2002, **189**, 39–66; (*b*) G. B. Shul'pin, *C. R. Chim.*, 2003, **6**, 163–178; (*c*) G. B. Shul'pin, Y. N. Kozlov, L. S. Shul'pina, A. R. Kudinov and D. Mandelli, *Inorg. Chem.*, 2009, **48**, 10480–10482; (*d*) G. B. Shul'pin, Y. N. Kozlov, L. S. Shul'pina and P. V. Petrovskiy, *Appl. Organomet. Chem.*, 2010, **24**, 464–472.
47 M. V. Kirillova, A. M. Kirillov, M. L. Kuznetsov, J. A. L. da Silva, J. J. R. Frausto da Silva and A. J. L. Pombeiro, *Chem. Commun.*, 2009, 2353–2355.
48 M. V. Kirillova, A. M. Kirillov and A. J. L. Pombeiro, *Appl. Catal., A*, 2011, **401**, 106–113.
49 (*a*) M. V. Kirillova, A. M. Kirillov and A. J. L. Pombeiro, *Adv. Synth. Catal.*, 2009, **351**, 2936–2948; (*b*) M. V. Kirillova, A. M. Kirillov and A. J. L. Pombeiro, *Chem.–Eur. J.*, 2010, **16**, 9485–9493.
50 G. B. Shul'pin, M. V. Kirillova, Y. N. Kozlov, L. S. Shul'pina, A. R. Kudinov and A. J. L. Pombeiro, *J. Catal.*, 2011, **277**, 164–172.
51 (*a*) T. F. S. Silva, K. V. Luzyanin, M. V. Kirillova, M. F. C. Guedes da Silva, L. M. D. R. S. Martins and A. J. L. Pombeiro, *Adv. Synth. Catal.*, 2010, **352**, 171–187; (*b*) T. F. S. Silva, G. S. Mishra, M. F. C. Guedes da Silva, R. Wanke, L. M. D. R. S. Martins and A. J. L. Pombeiro, *Dalton Trans.*, 2009, 9207–9215.

52 R. R. Fernandes, J. Lasri, A. M. Kirillov, M. F. C. Guedes da Silva, J. A. L. da Silva, J. J. R. Frausto da Silva and A. J. L. Pombeiro, *Eur. J. Inorg. Chem.*, 2011, 3781–3790.

53 D. S. Nesterov, E. N. Chygorin, V. N. Kokozay, V. V. Bon, R. Boca, Y. N. Kozlov, L. S. Shul'pina, J. Jezierska, A. Ozarowski, A. J. L. Pombeiro and G. B. Shul'pin, *Inorg. Chem.*, 2012, **51**, 9110–9122.

54 (*a*) G. V. Nizova, B. Krebs, G. Suss-Fink, S. Schindler, L. Westerheide, C. Gonzalez and G. B. Shul'pin, *Tetrahedron*, 2002, **58**, 9231–9237; (*b*) G. B. Shul'pin, G. V. Nizova, Y. N. Kozlov, L. G. Cuervo and G. Suess-Fink, *Adv. Synth. Catal.*, 2004, **346**, 317–332; (*c*) R. Z. Khaliullin, A. T. Bell and M. Head-Gordon, *J. Phys. Chem. B*, 2005, **109**, 17984–17992; (*d*) G. B. Shul'pin, M. V. Kirillova, L. S. Shul'pina, A. J. L. Pombeiro, E. E. Karslyan and Y. N. Kozlov, *Catal. Commun.*, 2013, **31**, 32–36; (*e*) A. M. Kirillov and G. B. Shul'pin, *Coord. Chem. Rev.*, 2013, **257**, 732–754; (*f*) G. B. Shul'pin, C. C. Golfeto, G. Suess-Fink, L. S. Shul'pina and D. Mandelli, *Tetrahedron Lett.*, 2005, **46**, 4563–4567.

55 G. S. Mishra, T. F. S. Silva, L. M. D. R. S. Martins and A. J. L. Pombeiro, *Pure Appl. Chem.*, 2009, **81**, 1217–1227.

56 (*a*) G. B. Shul'pin, D. Attanasio and L. Suber, *J. Catal.*, 1993, **142**, 147–152; (*b*) Y. N. Kozlov, V. B. Romakh, A. Kitaygorodskiy, P. Buglyo, G. Suess-Fink and G. B. Shul'pin, *J. Phys. Chem. A*, 2007, **111**, 7736–7752; (*c*) M. V. Kirillova, M. L. Kuznetsov, V. B. Romakh, L. S. Shul'pina, J. J. R. Frausto da Silva, A. J. L. Pombeiro and G. B. Shul'pin, *J. Catal.*, 2009, **267**, 140–157.

57 M. V. Kirillova, M. L. Kuznetsov, Y. N. Kozlov, L. S. Shul'pina, A. Kitaygorodskiy, A. J. L. Pombeiro and G. B. Shul'pin, *ACS Catal.*, 2011, **1**, 1511–1520.

58 M. N. Kopylovich, T. C. O. MacLeod, M. Haukka, G. I. Amanullayeva, K. T. Mahmudov and A. J. L. Pombeiro, *J. Inorg. Biochem.*, 2012, **115**, 72–77.

59 A. M. Kirillov, M. N. Kopylovich, M. V. Kirillova, M. Haukka, M. F. C. Guedes da Silva and A. J. L. Pombeiro, *Angew. Chem., Int. Ed.*, 2005, **44**, 4345–4349.

60 (*a*) L. M. Slaughter, J. P. Collman, T. A. Eberspacher and J. I. Brauman, *Inorg. Chem.*, 2004, **43**, 5198–5204; (*b*) J. A. Howard, in *Free Radicals*, ed. J. K. Kochi, Wiley-Interscience, 1973, vol. 2, p. 3; (*c*) R. E. Huie and C. L. Clifton, *Int. J. Chem. Kinet.*, 1989, **21**, 611–619.

61 (*a*) R. R. Fernandes, J. Lasri, M. F. C. Guedes da Silva, J. A. L. da Silva, J. J. R. Frausto da Silva and A. J. L. Pombeiro, *Appl. Catal., A*, 2011, **402**, 110–120; (*b*) S. Tanase, P. Marques-Gallego, W. R. Browne, R. Hage, E. Bouwman, B. L. Feringa and J. Reedijk, *Dalton Trans.*, 2008, 2026–2033; (*c*) S. Tanase, C. Foltz, R. de Gelder, R. Hage, E. Bouwman and J. Reedijk, *J. Mol. Catal. A: Chem.*, 2005, **225**, 161–167.

62 G. B. Shul'pin, Y. N. Kozlov, G. V. Nizova, G. Suss-Fink, S. Stanislas, A. Kitaygorodskiy and V. S. Kulikova, *J. Chem. Soc., Perkin Trans. 2*, 2001, 1351–1371.

63 M. L. Kuznetsov and A. J. L. Pombeiro, *Inorg. Chem.*, 2009, **48**, 307–318.

64 G. B. Shul'pin and G. Suss-Fink, *J. Chem. Soc., Perkin Trans. 2*, 1995, 1459–1463.

65 (*a*) M. Costas, K. Chen and L. Que, *Coord. Chem. Rev.*, 2000, **200–202**, 517–544; (*b*) A. Company, L. Gomez, M. Gueell, X. Ribas, J. M. Luis, L. Que and M. Costas, *J. Am. Chem. Soc.*, 2007, **129**, 15766–15767.

66 A. M. Kirillov, M. V. Kirillova, L. S. Shul'pina, P. J. Figiel, K. R. Gruenwald, M. F. C. Guedes da Silva, M. Haukka, A. J. L. Pombeiro and G. B. Shul'pin, *J. Mol. Catal. A: Chem.*, 2011, **350**, 26–34.

67 (*a*) A. M. Kirillov, Y. Y. Karabach, M. V. Kirillova, M. Haukka and A. J. L. Pombeiro, *Dalton Trans.*, 2011, **40**, 6378–6381; (*b*) A. M. Kirillov, J. A. S. Coelho, M. V. Kirillova, M. F. C. Guedes da Silva, D. S. Nesterov, K. R. Gruenwald, M. Haukka and A. J. L. Pombeiro, *Inorg. Chem.*, 2010, **49**, 6390–6392.

68 *Ulmann's Encyclopedia of Industrial Chemistry*, ed. B. Elvers, Wiley-VCH, Weinheim, 6th edn, 2002.

69 (*a*) C. Jia, T. Kitamura and Y. Fujiwara, *Acc. Chem. Res.*, 2001, **34**, 633–639; (*b*) Y. Fujiwara, K. Takaki and Y. Taniguchi, *Synlett*, 1996, 591–599.

70 (*a*) M. V. Kirillova, M. L. Kuznetsov, P. M. Reis, J. A. L. da Silva, J. J. R. Frausto da Silva and A. J. L. Pombeiro, *J. Am. Chem. Soc.*, 2007, **129**, 10531–10545; (*b*) M. V. Kirillova, A. M. Kirillov, P. M. Reis, J. A. L. da Silva, J. J. R. Frausto da Silva and A. J. L. Pombeiro, *J. Catal.*, 2007, **248**, 130–136.

Electronic Supplementary Information

Hexanuclear and Undecanuclear Iron(III) Carboxylates as Catalyst Precursors for Cyclohexane Oxidation

Miljan N. M. Milunovic,[a] Luísa M. D. R. S. Martins,[b,c] Elisabete C. B. A. Alegria,[b,c] Armando J. L. Pombeiro,*[c] Regina Krachler,[a] Günter Trettenhahn,[d] Constantin Turta,[e] Sergiu Shova,[f] Vladimir B. Arion*[a]

[a]*University of Vienna, Institute of Inorganic Chemistry, Währinger Strasse 42, A-1090 Vienna, Austria*

E-mail: vladimir.arion@univie.ac.at; Fax: +43-1-4277-52680

[b]*Área Departamental de Engenharia Química, ISEL, R. Conselheiro Emídio Navarro, 1959-007 Lisboa, Portugal*

[c]*Centro de Química Estrutural, Complexo I, Instituto Superior Técnico, Technical University of Lisbon, Av. Rovisco Pais, 1049-001 Lisboa, Portugal*

E-mail: pombeiro@ist.utl.pt; Fax: (+351)218464455

[d]*University of Vienna, Institute of Physical Chemistry, Währinger Strasse 42, A-1090 Vienna, Áustria*

[e]*Institute of Chemistry of the Academy of Sciences of Moldova, Academiei str. 3, MD-2028, Chisinau, Moldova.*

[f]*"Petru Poni" Institute of Macromolecular Chemistry, Aleea Gr. Ghica Voda 41A, 700487 Iasi, Romania*

CONTENT

Table S1 Crystal data and details of data collection for **1** and **2**.

Compound	**1**	**2**
Empirical formula	$C_{114.5}H_{150.5}Fe_6O_{65}$	$C_{175.25}H_{220.85}ClFe_{11}N_{3.75}O_{97.05}$
Fw	2901.95	4582.51
Space group	*P*–1	*P*–1
a [Å]	15.3674(7)	19.4468(13)
b [Å]	16.1325(7)	23.6865(16)
c [Å]	16.2835(7)	25.9226(17)
α[°]	73.631(2)	78.197(4)
β[°]	80.246(3)	87.186(4)
γ[°]	65.635(2)	71.921(4)
V [Å^3]	3521.8(3)	11109.8(13)
Z	1	2
λ [Å]	0.71073	0.71073
ρ_{calcd} [g cm^{-3}]	1.368	1.370
crystal size [mm^3]	$0.50 \times 0.50 \times 0.17$	$0.40 \times 0.35 \times 0.35$
T [K]	100(2)	100(2)
μ [mm^{-1}]	0.695	0.800
R_1[a]	0.0798	0.0824
wR_2[b]	0.2795	0.272
GOF[c]	1.046	1.067

[a] $R_1 = \Sigma||F_o| - |F_c||/\Sigma|F_o|$. [b] $wR_2 = \{\Sigma[w(F_o^2 - F_c^2)^2]/\Sigma[w(F_o^2)^2]\}^{1/2}$. [c] GOF = $\{\Sigma[w(F_o^2 - F_c^2)^2]/(n - p)\}^{1/2}$, where *n* is the number of reflections and *p* is the total number of parameters refined.

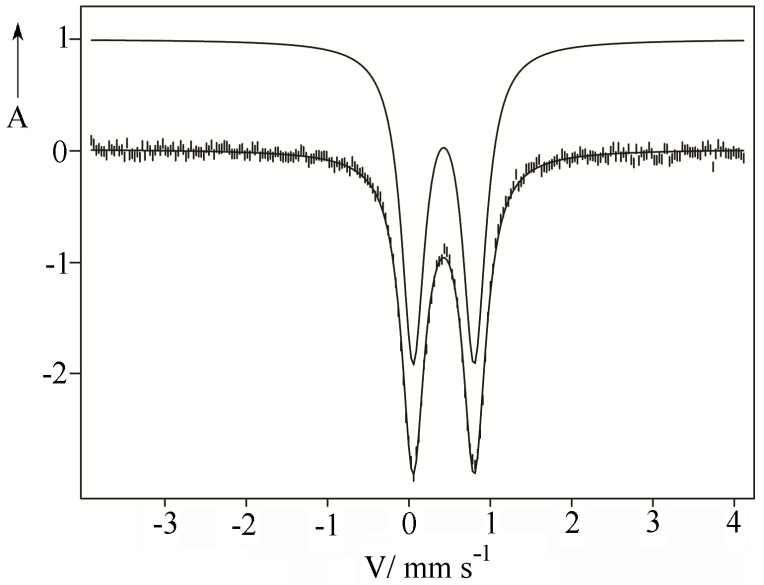

Fig. S1 Mössbauer spectrum of **1** at 300 K (δ = 0.43 mm s^{-1}, ΔE_Q = 0.75 mm s^{-1}).

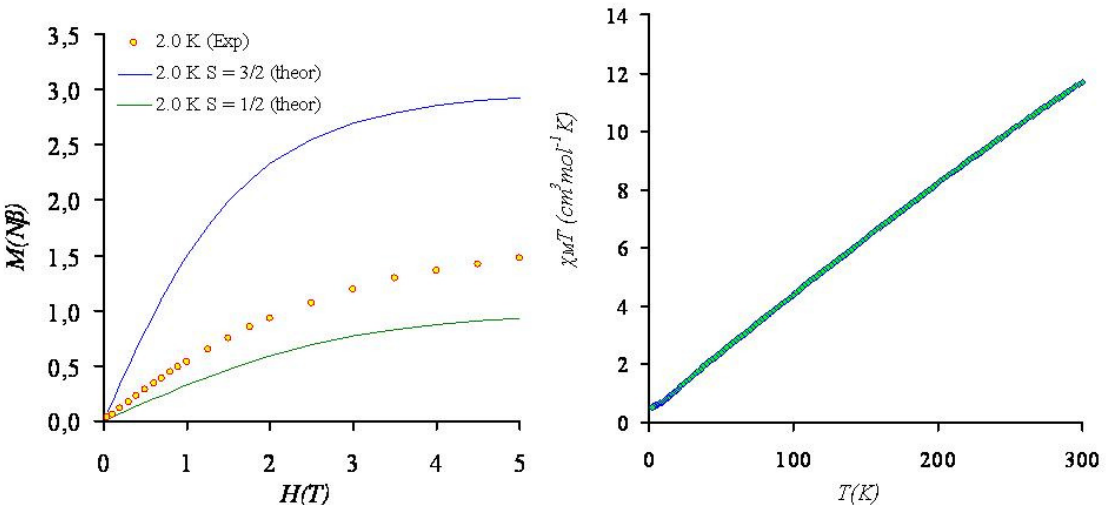

Fig. S2 Magnetization data for **2** at 2 K (left). Solid lines represent simulated according Brillouin function for S=1/2 (green line) and S=3/2 (blue line). Magnetic susceptibility (right) in a temperature range of 2 – 300 K under a field of 0.1 T.

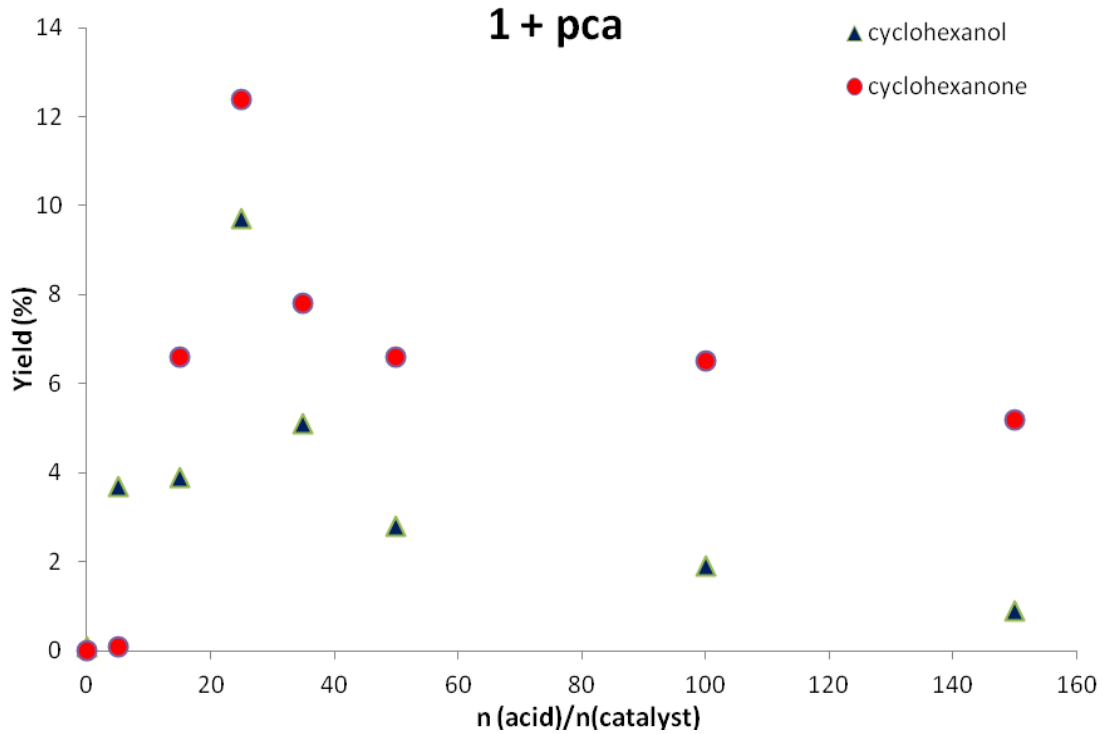

Fig. S3 Effects of the Hpca amount (molar ratios relatively to **1**) on the cyclohexanol (▲) or cyclohexanone (●) yield (mol%, based on substrate). Reaction conditions: $n(H_2O_2)/n(\mathbf{1})$ (2×10^4), MeCN (3.0 mL), cyclohexane (5.0 mmol), Hpca (0 – 150 mmol), 45 min, r.t.

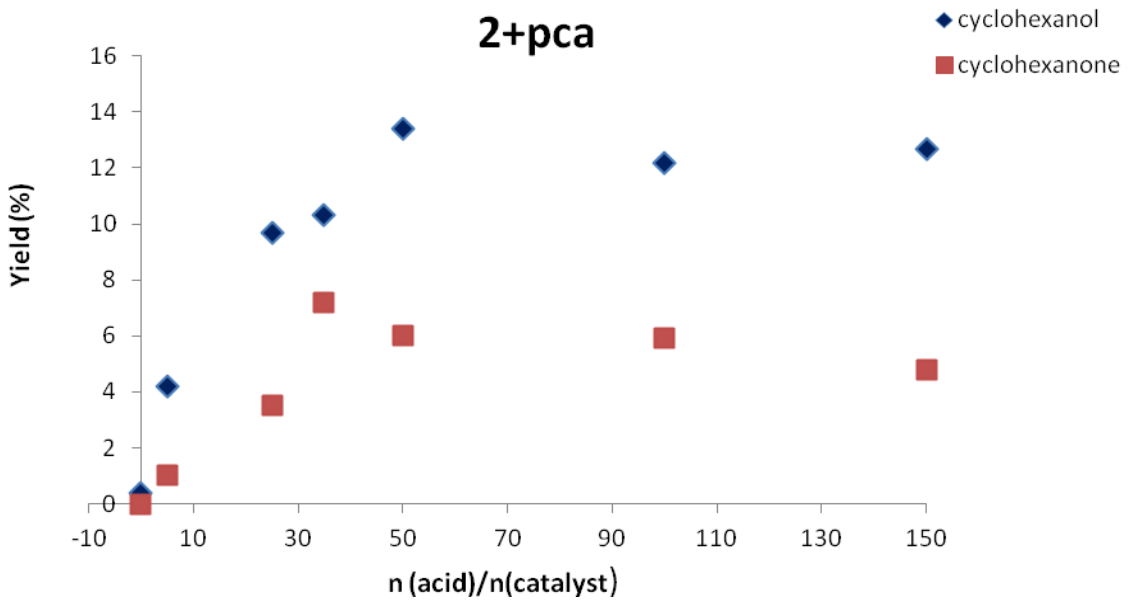

Fig. S4 Effects of the Hpca amount (molar ratios relatively to **2**) on the cyclohexanol (◆) or cyclohexanone (■) yield (mol%, based on substrate). Reaction conditions: $n(H_2O_2)/n(\mathbf{2})$ (2×10^4), MeCN (3.0 mL), cyclohexane (5.0 mmol), Hpca (0 – 150 mmol), 6 h, r.t.

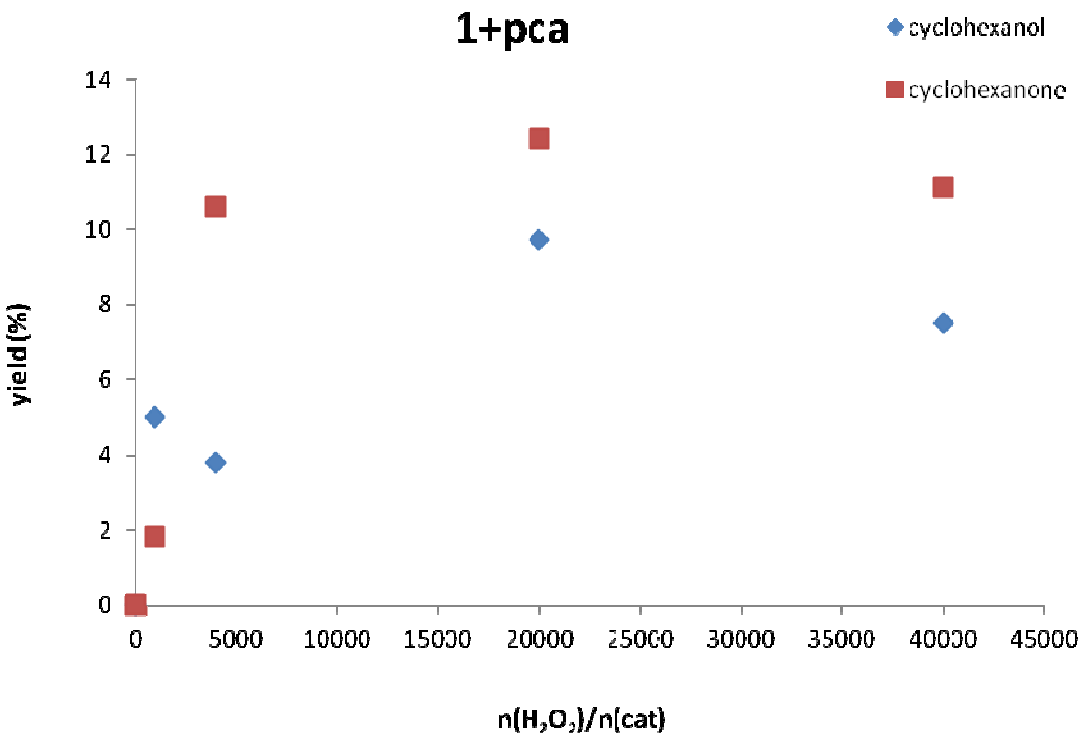

Fig. S5 Dependence of the cyclohexanol (◆) or cyclohexanone (■) yield (mol%, based on substrate) on the amount of oxidant (H_2O_2, molar ratio relatively to **1**) in the oxidation of cyclohexane. Reaction conditions: $n(H_2O_2)/n(\mathbf{1})$ (0 – 4 × 10^4), MeCN (3.0 mL), cyclohexane (5.0 mmol), n(Hpca)/n(**1**) (25.0), 45 min., r.t.

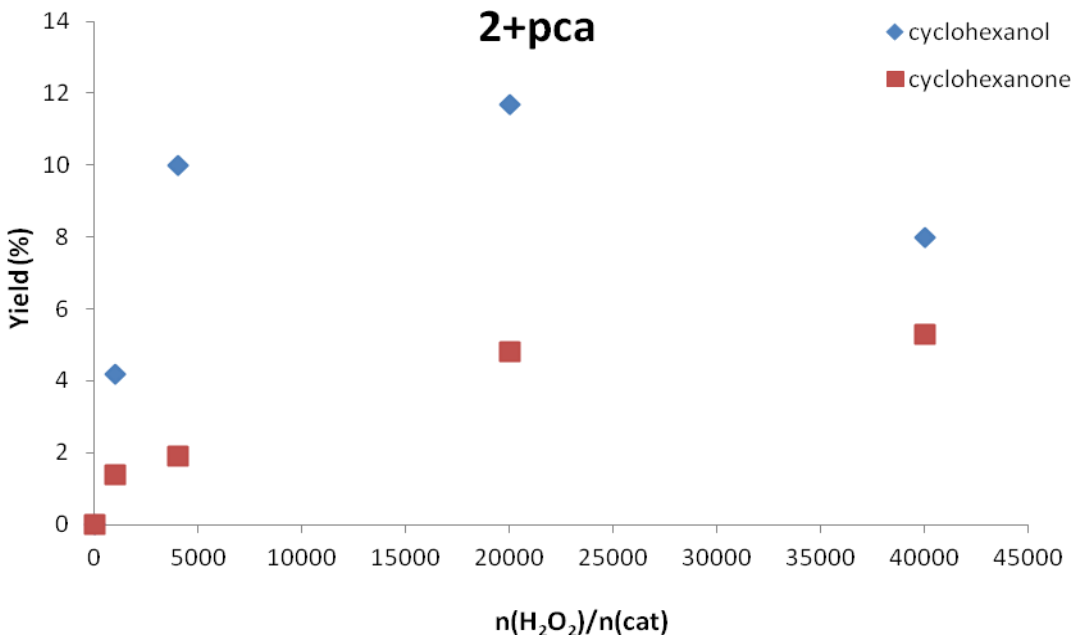

Fig. S6 Dependence of the cyclohexanol (◆) or cyclohexanone (■) yield (mol%, based on substrate) on the amount of oxidant (H_2O_2, molar ratio relatively to **2**) in the oxidation of cyclohexane. Reaction conditions: $n(H_2O_2)/n(\mathbf{2})$ (0 – 4 × 10^4), MeCN (3.0 mL), cyclohexane (5.0 mmol), n(Hpca)/n(**2**) (50.0), 6 h, r.t.

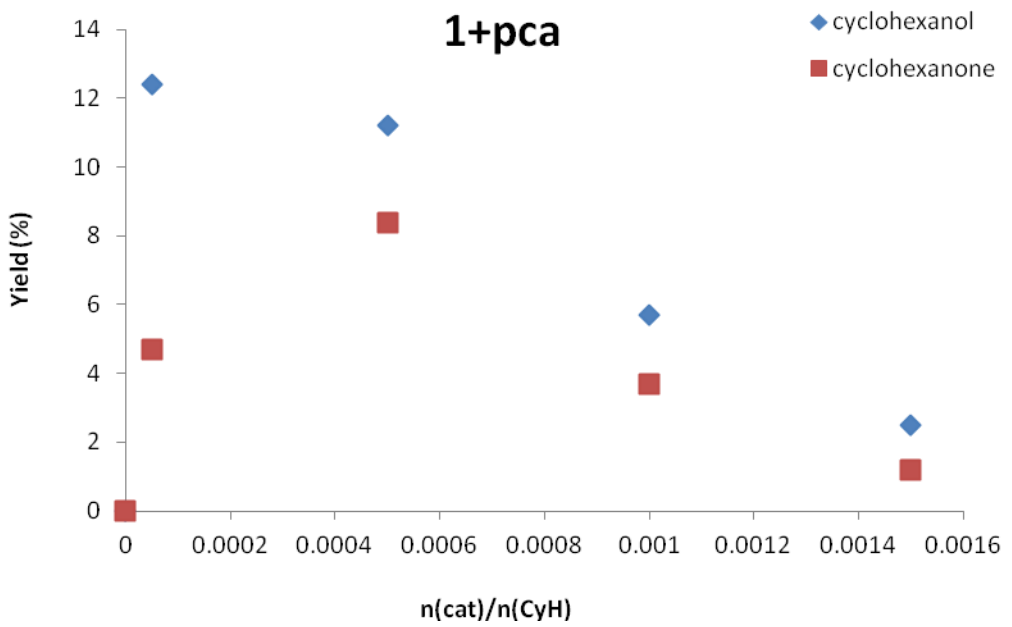

Fig. S7 Dependence of the cyclohexanol (◆) or cyclohexanone (■) yield (mol%, based on substrate) on the amount of catalyst **1** in the oxidation of cyclohexane. Reaction conditions: $n(H_2O_2)/n(\mathbf{1})$ (2×10^4), MeCN (3.0 mL), cyclohexane (5.0 mmol), *n*(Hpca)/*n*(**1**) (25.0), 45 min., r.t.

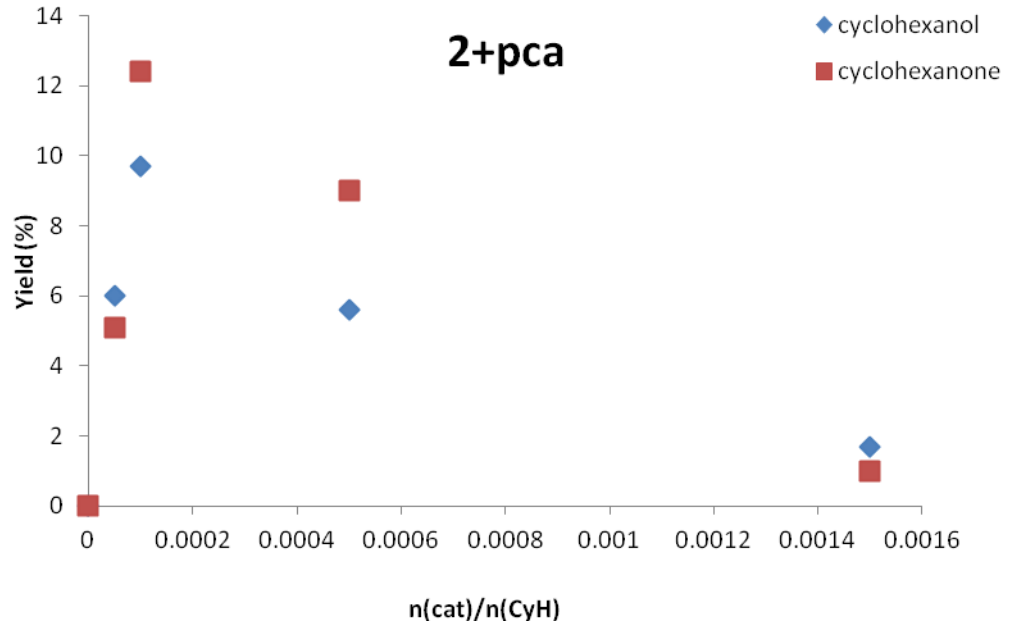

Fig. S8 Dependence of the cyclohexanol (◆) or cyclohexanone (■) yield (mol%, based on substrate) on the amount of catalyst **2** in the oxidation of cyclohexane. Reaction conditions: $n(H_2O_2)/n(\mathbf{2})$ (2×10^4), MeCN (3.0 mL), cyclohexane (5.0 mmol), *n*(Hpca)/*n*(**2**) (50.0), 6 h, r.t.

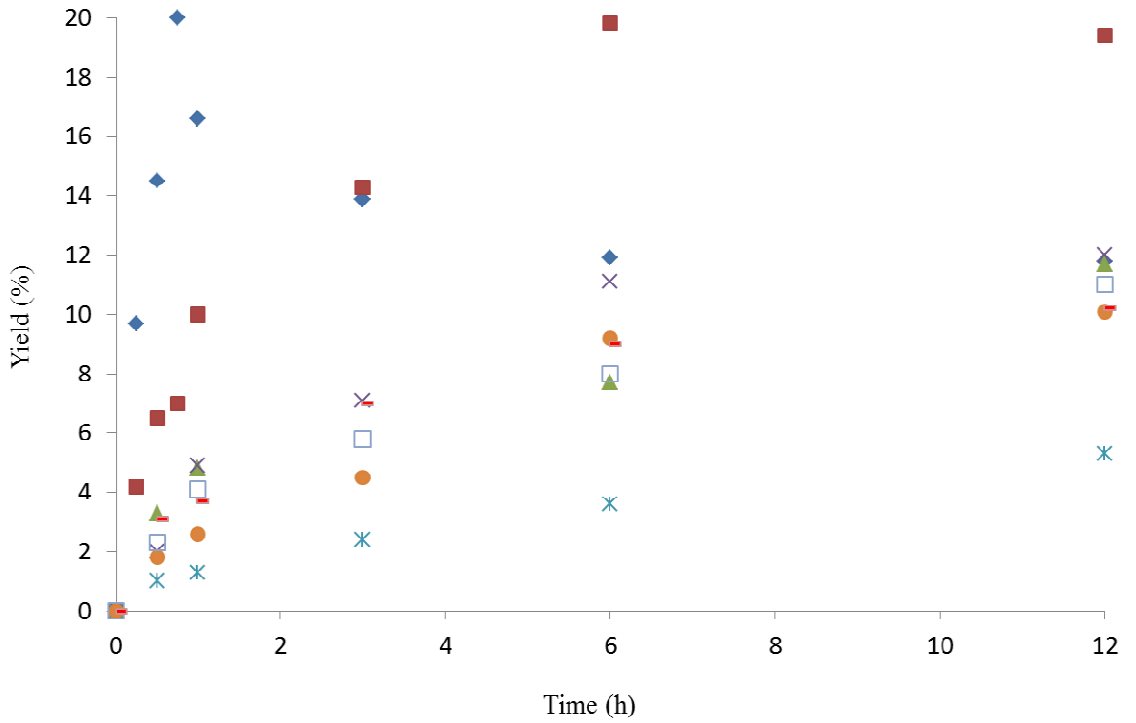

Fig. S9 Dependence of the overall yield (mol%, based on substrate) of the products on the reaction time in the presence of different iron species: **1**, **2**, $FeSO_4 \cdot 7H_2O$, $Fe(CF_3SO_3)_3$ or $[Fe_3OL_6(H_2O_3)_3]NO_3 \cdot HL$ (HL = 3,4,5-trimethoxybenzoic acid). Reaction conditions: MeCN (3.0 mL), cyclohexane (5.0 mmol), 0.5 μmol of catalyst percursor, $n(H_2O_2)/n$(catalyst precursor) (2×10^4), n(Hpca)/n(**1**) (25.0, ◆), n(Hpca)/n(**2**) (50.0, ■), n(Hpca)/$n(FeSO_4 \cdot 7H_2O)$ (25.0, ▲ or 50.0, X), n(Hpca)/$n(Fe(CF_3SO_3)_3)$ (25.0, ✳ or 50.0, ●), n(Hpca)/$n([Fe_3OL_6(H_2O_3)_3]NO_3 \cdot HL)$ (25.0, □ or 50.0, -), r.t.

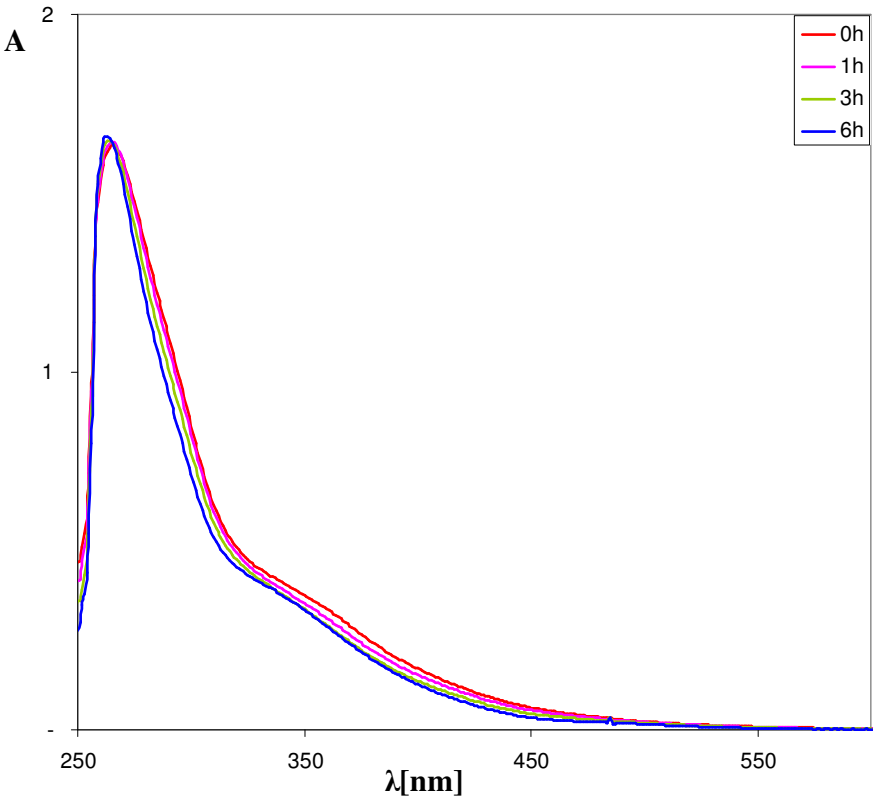

Fig. S10 UV–vis spectra of **2** in MeCN/dmf = 10:1 for 0, 1, 3 and 6 h.

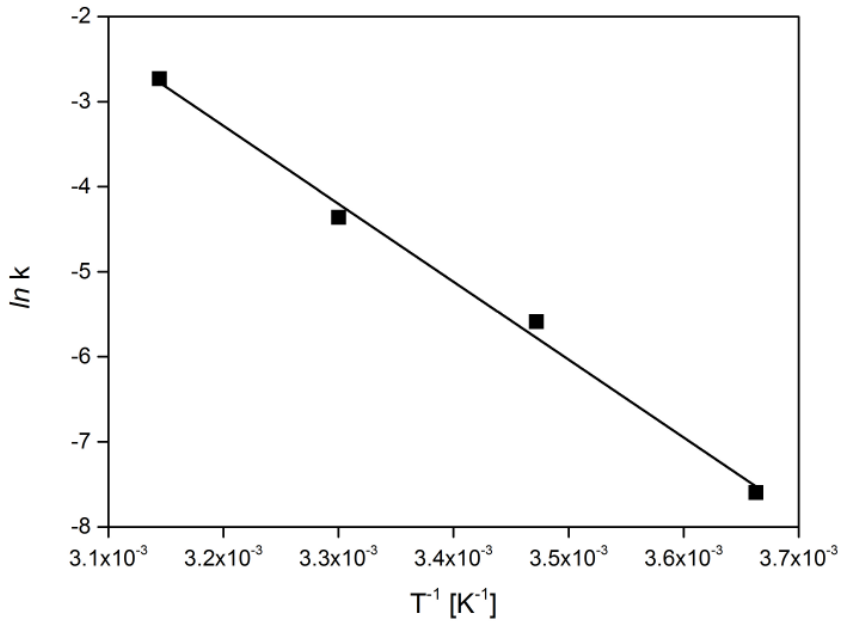

Fig. S11 Arrhenius plot for the **2**–H_2O_2 system. {$c_{\mathbf{2}}$ = 1.25 × 10^{-4} M; **2**:H_2O_2 = 1:2000; in MeCN/dmf = 10:1; *k (rate constant)* at 0, 15, 30, 45 °C}

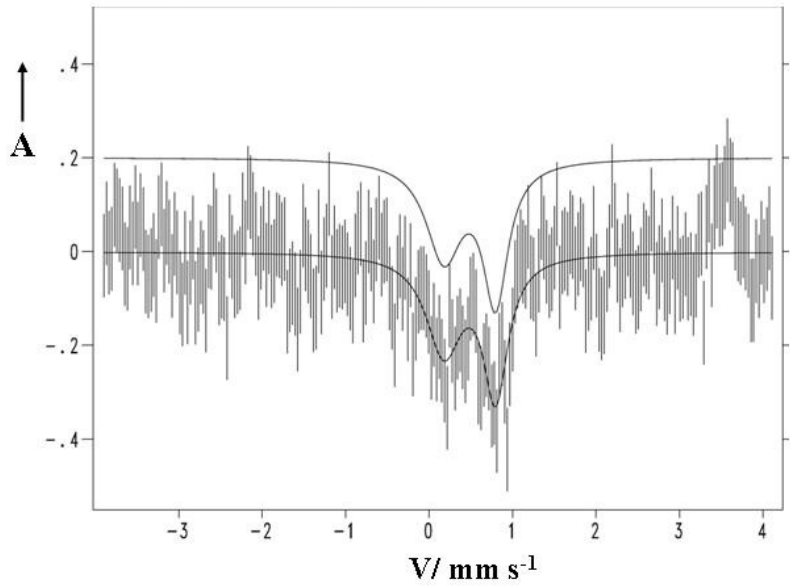

Fig. S12 Mössbauer spectrum of **2**-$^{57}Fe/H_2O_2$/Hpca system in MeCN measured immediately after its preparation at 80 K (δ = 0.49 mm s^{-1}, ΔE_Q = 0.62 mm s^{-1}, Γ_{left} = 0.52 mm s^{-1}, Γ_{right} = 0.36 mm s^{-1}).

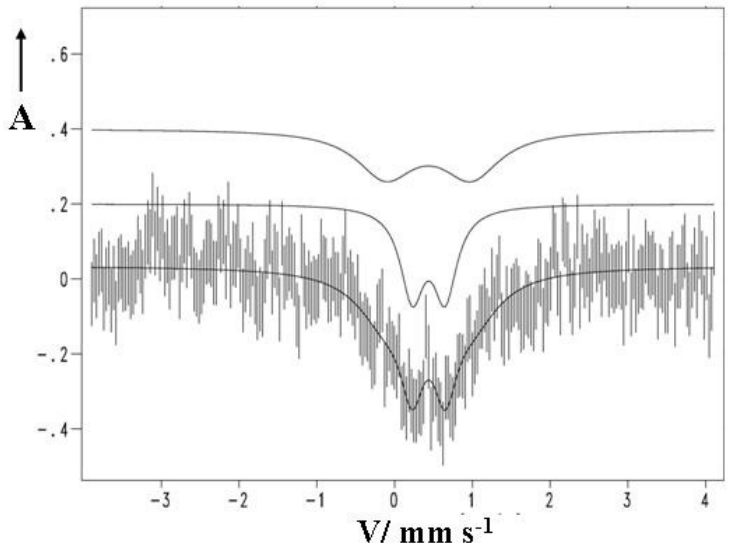

Fig. S13 Mössbauer spectrum of **2**-$^{57}Fe/H_2O_2$/Hpca system in MeCN at 80 K measured 30 min after its preparation (first lower doublet: δ = 0.44 mm s^{-1}, ΔE_Q = 0.42 mm s^{-1}, $\Gamma_{left} = \Gamma_{right}$ = 0.37 mm s^{-1}; second upper doublet: δ = 0.43 mm s^{-1}, ΔE_Q = 1.10 mm s^{-1}, $\Gamma_{left} = \Gamma_{right}$ = 0.90 mm s^{-1}; relative area 0.85:1.03).

4 Conclusions

This PhD thesis represents a symbiotic model comprising environmental, catalytic chemistry and anticancer research. Synthesis and characterization of novel compounds were carried out in order to investigate their antiproliferative activity and catalytic properties. The benzaldehyde and benzoic acid derivatives, namely, methyl salicyl aldehyde and 3,4,5-trimethoxy benzoic acid were used, as starting compounds, in the synthesis. Those compounds have been ranked as model humic compounds due to their structural similarity to building blocks of humic substances.

In the first part of the thesis, a reaction pathway to L– and D–proline thiosemicarbazone conjugates, as well their copper(II) complexes, has been developed starting from methyl salicylaldehyde. The metal complexation behavior of L–proline conjugate, stoichiometry and thermodynamic stability of Fe(II), Fe(III), Cu(II) and Zn(II) complexes have been studied. The copper(II) and zinc(II) form mono–ligand complexes while mono– and bis–ligand complexes are built up with iron(II) and iron(III). The established coordination mode for copper(II) complexes via phenolate O and, N and S donors of thiosemicarbazide moiety. The carboxylic group of the proline moiety does not participate in the coordination, what is confirmed by X–ray diffraction and EPR studies. The cytotoxic potency of the conjugates, as well as their copper(II) complexes, has been investigated in two human cancer cell lines, namely colon (SW480) and ovarian (CH1) carcinoma. The conjugates showed only moderate cytotoxic potency, while their corresponding copper(II) complexes displayed a markedly increased cytotoxicity.

In the second part of the thesis, the two novel multinuclear iron complexes, a hexanuclear $[Fe_6(\mu_3\text{-}O)_2(\mu_4\text{-}O_2)L_{10}(OAc)_2(H_2O)_2]\cdot 2.625Et_2O\cdot 2.375H_2O$ and an undecanuclear $[Fe^{III}_{11}Cl(\mu_4\text{-}O)_3(\mu_3\text{-}O)_5L_{16}(dmf)_{2.5}(H_2O)_{0.5}]\cdot Et_2O\cdot 1.25dmf\cdot 3.8H_2O$, where HL = 3,4,5-trimethoxybenzoic acid, have been obtained, extending the small families of hexanuclear iron complexes, containing an almost planar μ_4–η^2:η^2 $\{Fe_4O_2\}^{10+}$ central peroxido unit, and undecanuclear clusters. Moreover, the undecanuclear iron(III) complex possesses unprecedented topology of the $\{Fe^{III}_{11}ClO_8\}^{16+}$ core unit, containing nine six–coordinate and two five–coordinate

ferric ions. Both complexes were synthesized starting from 3,4,5-trimethoxybenzoic acid and characterized by X–ray diffraction, optical and Mössbauer spectroscopy. The complexes act as catalyst precursors, in the system with pyrazinecarboxylic acid and H_2O_2, for the catalytic oxygenation of alkanes to alcohols and ketones.

Also, an overview of iron oxido carboxylate complexes, based on the number of iron atoms in the structure, was given, in order to systemize a permanently increasing family of polynuclear iron complexes.

Polynuclear iron complexes, and, in particular, hexa– and undecanuclear iron complexes prepared in this work do not show similarities with natural humic substances, but provide structural information for further investigation of iron–humic substances interactions. Additionally, they may play important role in catalytic processes in the environment.

5 Future Outlook

Elucidation of the structure of the species which act as catalyst in the oxidation of cyclohexane to cyclohexanol is of primary interest, since this can provide a basis for design and the synthesis of even more effective catalyst.

2-Hydroxy-3-methyl-(*S*)-pyrrolidine-2-carboxylate-5-methylbenzaldehyde thiosemicarbazone (L–Pro–STSC) is a water–soluble ligand and its cytotoxicity can be increased by introducing other functional groups.

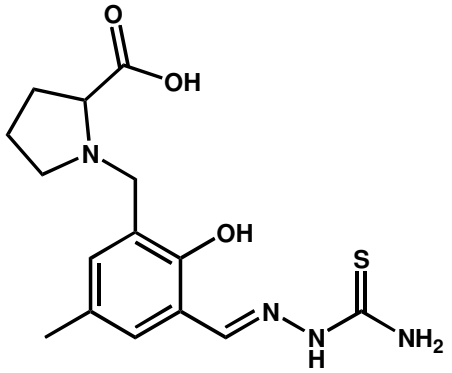

2-hydroxy-3-methyl-(S)-pyrrolidine-2-carboxylate-5-methylbenzaldehyd thiosemicarbazone

In particular, esterification of the carboxylic group can be performed. In addition, H–atoms of amino group of thisemicarbazone moiety can be substituted by aliphatic (dimethyl) and aromatic (phenyl, naphtyl) groups and/or a cyclic (pyrrolidyl) group and structure–activity relationships can be established.

Coordination of copper(II) to L–Pro–STSC increases the cytotoxic effect by 5 to 13 times resulting in IC_{50} values in micromolar concentration range. Further investigation of copper(II) complexes with L–Pro–STSC deserves to be performed to elucidate their mechanism of cytotoxic activity and their role as possible inhibitors of important enzymes such as ribonucleotide reductase and topoisomerase IIα.

By attachment of fluorescent groups at the end aminogroup of this class of bioconjugates can be prepared more lipophylic ligands and investigate their uptake by the cells and intracellular distribution by fluorescent microscopy.

In particular, we succeeded in obtaining of a fluorescent ligand by attachment of a naphtyl group to the terminal nitrogen atom of the thiosemicarbazide moiety of the esterified L–Pro–STSC.

The fluorescence is also observed upon coordination of this ligand to zinc(II). Both the ligand and its zinc(II) complex will be used to study the intracellular distribution of these potential anticancer drugs.

The iron(III) complexes of L–Pro–STSC, dimethyl–, pyrrolydyl–, phenyl–substituted thiosemicarbazone proline carboxylate as well as, N naphtyl–substituted thiosemicarbazone proline methyl ester have been synthesized and characterized in order to investigate the effect of iron(III) coordination and structural variations in the ligands on the antiproliferative activity in different cancer cell lines.

6 Curriculum Vitae

Personal Data

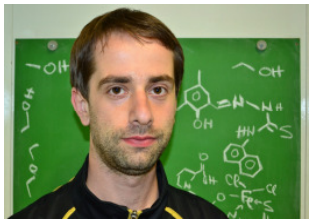

Name:	Miljan Milunović
Date of Birth:	18. 10. 1982
Place of Birth	Niš, Serbia
Nationality:	Serbian
Marital Status:	Single
Current Adress:	Bahnhofstrasse 2/2/11, 1140, Vienna, Austria
Working Adress:	Währinger strasse 42, Institute of Inorganic Chemistry, University of Vienna,
Contact Data:	Tel.: +43 680 1150468
	E-mail: miljan.milunovic@univie.ac.at
Spoken Languages:	Serbian, English, German, Bulgarian
Acad. Degree:	MSc (Dipl. Chem.)
Current Position:	PhD student and researcher, University of Vienna

Education History

1989 – 2001	Elementary/Secondary School, Niš, Serbia
2001 – 2006	Chemistry studies, Faculty of Sciences and Mathematics, University of Niš, Serbia
2006 – 2008	PhD student and scientific co-worker, Department of Chemistry, University of Niš, Serbia
2008 – to date	PhD student and scientific co-worker, Institute of Inorganic Chemistry, University of Vienna, Austria

Scientific Experience

1999	Participant in the scientific seminars of biomedicine, Research Station''Petnica'', Valjevo, Serbia
2007	Participant of symposium ''Novel technology and economic development'', Faculty of Technology, Leskovac, Serbia
2006 – 2008	Scientific co-worker of the Innovation ''VALETA-H_2O-92'', Serbia
2008	Participant of the international summer school of the mass spectrometry, Paris, France

2008 – to date	Scientific co-worker and researcher of the projects dealing with iron complexes of humic acid models and development of anticancer therapeutics
2011	Scientific collaboration, Department of Analytical Chemistry, University of Szeged, Hungary

Teaching Experience

2010	Assistant and tutor in practical inorganic chemistry courses, University of Vienna

Scholarships

2002 – 2003	Scholarship of the Serbian Ministry of Education
2007 – 2008	Scholarship of the Serbian ministry of Science

Other Interests

2002 – 2004	Head of Sport of the Students Union of Faculty of Sciences and Mathematics, University of Niš, Serbia
2004	Head of the Students Union of Faculty of Sciences and Mathematics, University of Niš, Serbia
2005	Student-vicedean of Faculty of Sciences and Mathematics, University of Niš, Serbia

Publications in Scientific Journals

Milunovic, M. N. M.; Enyedy, E. A.; Nagy, N. V.; Kiss, T.; Trondl, R.; Jakupec, M. A.; Keppler, B. K.; Krachler, R.; Novitchi, G.; Arion, V. B. *L*- and *D*-Proline Conjugates: Coordination Behaviour in Solution and the Effect of Copper(II) Coordination on Their Antiproliferative Acitivity. *Inorg. Chem.*, **2012**, *51*, 9309.

Milunovic, M. N. M.; Martins, L. M. D. R.; Alegria, E. C. B. A.; Pombeiro, A. J. L.; Krachler, R.; Trettenhahn, G.; Turta, C.; Shova, S.; Arion, V. B. Hexanuclear and Undecanuclear Iron(III) Carboxylates as Catalyst Precursors for Cyclohexane Oxidation. *Dalton Trans.,* **2013**, *42*, 14388–14401.